Analytical models to assess the potential of waste-based industrial plants in the energy transition: an application to the steelmaking sector

Department of Mechanics, Mathematics and Management
MECHANICAL AND MANAGEMENT ENGINEERING
Ph.D. Program
SSD: ING-IND/17–INDUSTRIAL SYSTEMS ENGINEERING

Final Dissertation

Analytical models to assess the potential of waste-based industrial plants in the energy transition: an application to the steelmaking sector

by
Micaela Vitti

Supervisors:

Prof. Francesco Facchini

Prof. Giorgio Mossa

Coordinator of Ph.D. Program:
Prof. Giuseppe Pompeo Demelio

Course n°36, 01/11/2020-31/10/2023

Department of Mechanics, Mathematics and Management
MECHANICAL AND MANAGEMENT ENGINEERING
Ph.D. Program
SSD: ING-IND/17–INDUSTRIAL SYSTEMS ENGINEERING

Final Dissertation

Analytical models to assess the potential of waste-based industrial plants in the energy transition: an application to the steelmaking sector

by
Micaela Vitti

Referees:

Prof. Luiz Fernando Rodrigues Pinto

Prof. Ferdinando Chiacchio

Supervisors:

Prof. Francesco Facchini

Prof. Giorgio Mossa

Coordinator of Ph.D. Program:
Prof. Giuseppe Pompeo Demelio

Course n°36, 01/11/2020-31/10/2023

Abstract

Human activities, such as fossil fuel combustion and deforestation, have led to increased greenhouse gas emissions and global warming. To mitigate these effects, countries have pledged to limit global warming to 1.5°C and achieve carbon neutrality by 2050. This requires a transition to renewable energy sources, including photovoltaic panels, wind turbines, hydrogen, and biomethane. While progress has been made in the context of the energy transition, additional actions are required to reach the goal of reducing greenhouse gas emissions to net-zero.

The steelmaking sector is particularly challenging to decarbonise due to its reliance on fossil fuels. However, the so-called secondary route, which involves melting recycled steel scrap in an electric arc furnace, offers a real decarbonisation potential. This route can be supported by the production of direct reduced iron, which can be produced using hydrogen instead of natural gas.

Waste valorisation, which involves converting waste into energy or other valuable products, can also play a role in the energy transition. Waste valorisation plants can indeed produce both electricity, hydrogen, and biomethane. However, current waste valorisation assessment methods lack consideration of their role in the ongoing energy transition.

Consistent with these gaps, the present work aims to develop analytical models to evaluate waste valorisation plants' economic and environmental performance within the context of the energy transition.

A cost and investment analysis carried out with respect to three waste-to-energy plants allowed to identify gasification as the best option to support the current energy transition, due to its high electricity output despite high operational costs. The application of the environmental analytical models developed to compare different waste valorisation alternatives from the anaerobic digestion of waste, showed that biomethane production is better than electricity production, while hydrogen production is better than biomethane production. Moreover, the application of an environmental analytical model to the EU 2020 and 2030 scenarios showed that waste-based hydrogen production routes offer significant decarbonization potential.

An economic model moreover showed that the secondary steelmaking route, supported by direct reduced iron production, prove to be profitable despite cost and carbon pricing

fluctuations. An environmental analytical model allowed to find that national energy mixes play a crucial role in enabling sector decarbonization. Finally, it was found that waste-based hydrogen routes can accelerate decarbonization in steelmaking, enabling low-emission steel production even before large-scale electrolyzer installation becomes viable.

These findings underscore the importance of incorporating energy transition considerations into waste valorisation assessments to optimize resource utilization and advance sustainable energy solutions.

Keywords: energy transition, decarbonisation, waste management, waste-to-energy, waste-to-hydrogen, biomethane production, analytical models.

Table of contents

List of figures

List of tables

List of abbreviations

Abbreviation	Meaning
H_2	Hydrogen
CE	Circular Economy
MSW	Municipal Solid Waste
GHG	Greenhouse gas
GWP	Global Warming Potential
CO_2	Carbon Dioxide
CH_4	Methane
GW	Global Warming
NZE	Net-zero emissions
EU	European Union
AD	Anaerobic Digestion
bio-CH_4	Biomethane
OW	Organic Waste
C	Carbon
OFMSW	Organic Fraction of Municipal Solid Waste
N	Nitrogen
O_2	Oxygen
P	Phosphorus
K	Potassium
Na	Sodium
Ca	Calcium
N_2	Nitrogen Gas
NH_3	Ammonia
DRM	Dry Methane Reforming

PBPT	Pay-back period time
NPV	Net Present Value
CCF	Cumulated Cash flow
DCF	Discounted Cash Flow
CDCF	Cumulated Discounted Cash flow
WWTP	Wastewater Treatment Plant
VS	Volatile Solids
PE	Population Equivalent
FME	Fugitive Methane Emissions
WtH_2	Waste-to-hydrogen
WtE	Waste-to-energy
LS	Liquid Steel
EAF	Electric Arc Furnace
BF	Blast Furnace
BOF	Basic Oxygen Furnace
LCA	Lifecycle Assessment
GESS	Green Energy Steel System
PEM	Proton Exchange Membrane
SC	Scenario
SS	Sewage Sludge
WWT	Wastewater Treatment
LHV	Lower Heating Value
IRENA	International Renewable Energy Agency
PES	Planned Energy Scenario

Introduction

Humanity, through its activities, is significantly altering the Earth's natural climatic balance. In this regard, during the last century, there has been an increase in temperatures equal to the increase occurred in the previous five thousand years. This phenomenon of anomalous rise in the Earth's temperature is called Global Warming (GW). The cause of GW are human-related emissions of so-called greenhouse gases (GHGs), which can trap received heat radiation and, in turn, radiate heat to the Earth's surface. The main GHGs are carbon dioxide (CO_2) and methane (CH_4); since 1750, the concentration of CO_2 and CH_4 in the atmosphere has risen by 149% and 262% respectively. The main sources of anthropogenic GHGs emissions are deforestation and the consumption of fossil fuels for energy production for all economic sectors (e.g., industry, transport, etc.). Emissions from the energy sector are estimated to constitute about 74% of global emissions. A continuation of the current trend of emissions generation is estimated to lead to irreversible consequences for our planet.

To reverse this trend, at the 2015 United Nations Climate Change Conference (COP) in Paris, an agreement known as the 'Paris Agreement' was signed, in which 196 countries of the world pledged to succeed in keeping global warming well below 2°C, or rather below 1.5°C. This value was identified by the Intergovernmental Panel on Climate Change as the limit value for not causing irreversible consequences on the Earth's climate system. Furthermore, as part of this agreement, states have agreed to achieve carbon neutrality by the middle of this century. Indeed, they committed to formulate and implement strategies to achieve a balanced condition between the amount of GHGs emitted and that sequestered by natural carbon sinks. However, during COP 27 in 2022, it was observed that, following all the policies stated by Paris Agreement Parties, the 1.5°C target could not be achieved. Consequently, the need to accelerate the

planning and implementation of actions to achieve the required carbon neutrality by the middle of this century and hence the 1.5°C target was stressed.

In this context lies the energy transition process, through which all countries are planning a transition from current carbon-intensive and low-efficiency energy systems to future deeply decarbonised, energy-efficient, and highly renewable solutions. As mentioned, the energy sector, being the main source of anthropogenic emissions, is crucial for reaching the 1.5°C target.

The first action to be implemented to decarbonise the energy sector is the large-scale installation of renewable energy conversion systems. In this regard, photovoltaic panels and wind turbines are expected to account for most of the new capacity installed globally. These technologies, indeed, allow to harness energy that is available in huge amounts on the whole globe and are mature enough to be cost-effective.

The second key element in the current energy transition is hydrogen (H_2). This gas has an energy density that is three times higher than that of gasoline and only water vapour is produced from its combustion. These aspects make H_2 a potentially clean fuel. In addition, H_2 can be used as an energy vector to cope with the discontinuity of energy production from renewable sources, as well as a fuel in the transport and buildings sector. Due to these very favourable characteristics from an environmental point of view, H_2 constitutes a key element in which most countries are investing to achieve carbon neutrality targets. However, the problem with H_2 relates to its production process. The only way to avoid emissions from a life-cycle perspective is to produce H_2 by using electrolysis powered by electricity from renewable sources. However, the electrolysis process is very energy intensive and there is currently not enough renewable energy available to meet the large-scale demand from this process.

A further key element in the current energy transition is biomethane (bio-CH_4). It is produced by upgrading biogas obtained through the anaerobic digestion (AD) of organic waste (OW). Bio-CH_4, which has almost the same Lower Heating Value (LHV) as CH_4, has its same applications. It can be established that the production of bio-CH_4 has a threefold environmental benefit; it is useful to reduce CO_2 emissions from the energy, industry and

transport sectors, it helps reducing the fugitive methane emissions (FMEs) generated from natural gas (NG) supply, and it helps reducing CH_4 emissions from waste and agriculture sectors.

Although, since the subscription of the Paris Agreement in 2015, many strategies have been planned and implemented to complete the energy transition process, it appeared that they are not sufficient to reach the 1.5°C target. Both regarding the production of energy from renewable sources, the production of clean H_2 and the use of bioenergy (including bio-CH_4), it has been observed that there is a significant gap between what is planned and what is needed to achieve global environmental goals.

For the achievement of carbon neutrality, the steelmaking sector is of utmost relevance. Indeed, it is one of the so-called hard-to-abate sectors. They are industrial sectors (e.g., iron and steel, cement and concrete, chemicals, etc.) characterised by high energy demand, high process heat needs, chemical process emissions, and other features that make them inherently difficult to decarbonise. Hard-to-abate sectors account for about 30% of global annual emissions. Among them, steelmaking generates the second largest energy demand and the largest share of emissions (i.e.,7% of global emissions). The negative environmental performance of this sector depends on the use of the so-called primary route, which generates 1.8 tCO_{2eq}/t liquid steel. In this regard, solutions for the decarbonisation of this sector need to be identified. The main solution for the decarbonisation of the steelmaking sector is the so-called secondary route. It consists of steel production by melting recycled iron scrap in an electric arc furnace (EAF). Although this solution is the best from an environmental point of view, the unpredictable availability of raw material makes it an unreliable alternative from an industrial point of view. To overcome this limitation, the production of Direct Reduced Iron (DRI) is used. This is a raw material that can be used, together with recycled scrap, to feed an EAF. DRI is produced using a reducing gas (consisting of carbon monoxide and H_2), which is generally obtained by reforming NG. However, it is possible to use only H_2 as a reducing gas. This alternative would generate a drastic reduction in emissions from the steelmaking process (i.e., the use of H_2 reduces direct emissions), but is subject to the issues on hydrogen production, which are amplified by the large volumes required by this sector.

In this context, urban waste management is a key topic. Due to phenomena such as urbanisation, population growth and economic growth, the amount of waste generated in the urban context is constantly increasing, resulting in huge emissions. In 2016, municipal waste management practices generated 5% of the globally emitted 1.6 billion tonnes of CO_{2eq}. Similarly, sewage sludge (SS), the main by-product of wastewater treatment operations, is growing in volume due to the implementation of policies to improve wastewater quality. Waste is a key element in achieving a CE condition. Indeed, waste can be used as a resource and can be kept in the economic cycle as long as possible. In this regard, the so-called waste hierarchy indicates the actions to be preferentially implemented to manage waste according to a CE perspective. The waste hierarchy states that, first of all, the production of waste should be avoided, then waste should be prepared for re-use or recycled. Finally, if all the previous actions are not possible, it is necessary to valorise the waste by recovering energy and/or valuable elements, and finally, as a last alternative, waste can be disposed of.

In this regard, three categories of waste treatment are of utmost relevance. The first are the so-called waste-to-energy (WtE) treatments. They consist of treating waste to obtain energy (i.e., electricity or heat). The second category of treatments are the so-called Waste-to-H2 (WtH_2) treatments. They consist of treating waste to obtain H_2 as a primary product. Finally, the treatment of AD enables the production of bio-CH_4. These treatments allow, on the one hand, to contribute to the acceleration of the current energy transition process and, on the other hand, to valorise waste in a CE perspective.

Although comparisons from an economic and environmental point of view of the different waste valorisation routes exist in scientific literature, there is a lack of methodologies to understand their potential with reference to the current energy transition.

In this regard, the aim of this work is to develop methodologies for evaluating and comparing the performance of waste valorisation plants to understand their potential in the current energy transition phase.

To achieve this objective, analytical models were developed that consider, on the basis of the material and energy flows exchanged within the plants

and with the external environment, the negative effects generated from an economic and environmental point of view (i.e., direct and indirect emissions, costs), as well as the positive ones (i.e., avoided emissions, profits).

The plants considered for the development of these models were divided into plants for energy production from waste, plants for H_2 production and plants for bio-CH_4 production. After analysing the plant configurations of the different alternatives and characterising the relevant flows, different analytical models were developed aimed at understanding different aspects of the contribution of waste valorisation alternatives to the current energy transition process.

To this end, an analytical economic model was first developed to compare the costs of WtE plants and an investment analysis was conducted over a 20-year time horizon, which was identified as being consistent with the objectives of the current energy transition. The cost model allow to estimate the total annual costs of WtE plants as a function of plant size, taking into account investment costs, operating costs, costs for expanding plant capacity and the generation of economies of scale, as well as a possible carbon tax. This cost model was the starting point for the investment analysis conducted in the case of the Metropolitan City of Bari, in Southern Italy.

Two environmental analytical models were then developed with the aim of comparing the emissions and environmental benefits of different waste valorisation alternatives from the AD treatment. The first developed model allowed to estimate the emissions associated with the production of electricity or bio-CH_4 depending on the characteristics of the treated SS. In this regard, the model was applied to the case of a Wastewater Treatment Plant (WWTP) located in Bari, Italy, to understand which valorisation alternative has the most advantages, as well as the sensitivity of the solutions obtained in scenarios of energy transition progress. The second model compares the emissions and environmental benefits of H_2 and bio-CH_4 production from AD treatment. The model was developed to consider the indirect and avoided emissions associated with each alternative. In the case of H_2 production, emissions were assessed under scenarios corresponding

to different global production mixes, evaluated according to the percentage of global H_2 volume produced by electrolysis.

Finally, an environmental analytical model was developed to compare the performance of different WtH_2 routes. The environmental model allows the emissions generated and avoided by each route to be estimated. Specifically, generated emissions were considered as direct and indirect emissions, while avoided emissions were considered as a beneficial effect generated by the non-disposal of waste. In addition, so-called counterfactual emissions were considered, which were defined as the emissions generated under alternative scenarios due to the use of a given WtH_2 route. This model was developed to understand the decarbonisation potential offered by WtH_2 in the current energy transition phase. Above all, it was intended to understand how investment in WtH_2 can help fill the gap that exists between the global H_2 production targets for reaching the 1.5°C target and the planned volumes. In this regard, the developed model was applied to two scenarios, corresponding to the situation of the European Union (EU) in 2020 and 2030, identified as two crucial years of the energy transition.

As mentioned above, the case of the steelmaking sector was explored. Following the previous scheme, the cost-effectiveness of the investment in decarbonised steelmaking routes was first assessed through the development of an economic model that considers the uncertainties of the market conditions for some variables. The cost model developed allows the investment and operating costs for the NG-DRI-EAF route to be assessed in the presence of variability in the purchase prices of raw materials (i.e., iron ores, scrap). Similarly, the uncertainty of the selling price of coils was considered. The application of the model to different scenarios allowed to build frequency distributions for some cost and profit items of the system considered.

Subsequently, an analytical model was developed to understand the environmental performance of a Green energy-Steel system (GESS) composed of a renewable energy production system and a DRI-EAF steelmaking plant fuelled in variable shares by scrap and DRI. The objective of the model is to understand which variables most influence the environmental performance of the entire system, and, above all, which make the installation of an H_2-based steelmaking plant environmentally

favourable. The model was applied by dividing the variables considered into two categories. Indeed, exogenous variables were considered, which were defined as variables that do not depend on the plant owner's choices, but which depend on the conditions of the market and the site where the system is installed. In addition, variables defined as endogenous, i.e., depending on the plant owner's choices, were considered. The application of the model in different scenarios defined by combinations of endogenous and exogenous variables allowed to identify the most critical variables for the abatement of emissions from the steelmaking process.

Finally, an environmental analytical model was developed to understand the decarbonisation potential offered by different WtH_2 routes to the steelmaking process. In this regard, the developed model considers direct, indirect and avoided emissions generated by the steelmaking route when supported by different H_2 production technologies. The application of the model in different scenarios allowed to understand the potential offered by the routes considered, as well as the prospects offered within the current energy transition phase.

The rest of the work is organised as follows. In the first chapter, the reference research context is explained. A literature review of sources dealing with waste-to-energy, WtH_2 and bio-CH_4 plants is also provided. In the second chapter, the plant configurations of the waste valorisation plants considered are first presented. Subsequently, in the same chapter, the development and application of the different analytical models developed is illustrated and the results obtained are discussed. In the third chapter, the decarbonisation of the steelmaking sector is firstly framed. Next, the development and application of the analytical models developed with reference to this sector is illustrated and the results obtained are discussed. Finally, the conclusions of the work summarise the overall results obtained and provide insights for future studies.

Chapter 1

Research context

The stability of the Earth's climatic conditions depends on the achievement of an energy balance in the Earth-Sun system, illustrated in detail in Figure 1.

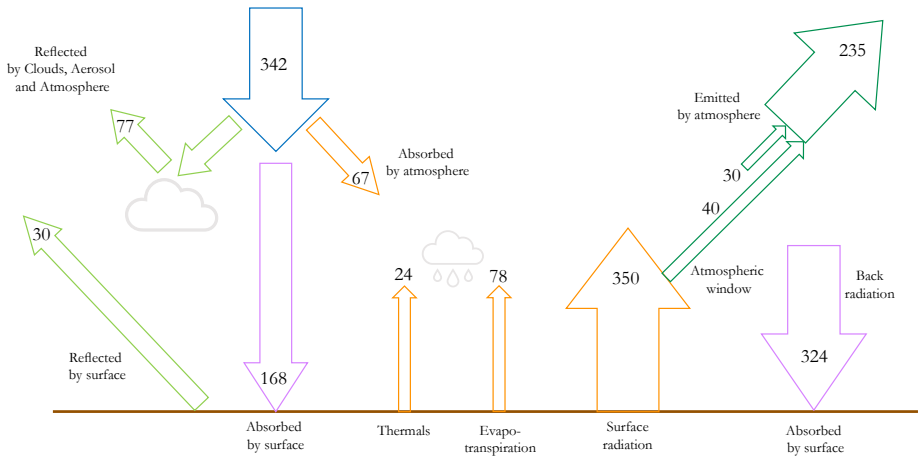

Figure 1. Schematic representation of the Earth's energy balance. All the values are expressed in W/m². Adapted from [1].

The Sun emits short-wave radiations that invest the Earth in the part above the atmosphere (about 342 W/m^2). About 30% of these radiations are reflected by bright surfaces like the atmosphere and the clouds (about 77 W/m^2) and directly by the Earth's surface (about 30 W/m^2). The remaining 70% is absorbed mainly by the Earth's surface (approx. 168 W/m^2) and partly also by the atmosphere (approx. 67 W/m^2). To balance the incoming energy input, the Earth's surface and the atmosphere re-emit energy to space in the form of long-wave radiations. In this respect, the Earth's surface emits heat into the atmosphere in the form of latent heat (approx. 78 W/m^2), sensible heat (approx. 24 W/m^2) and infrared radiations (approx. 390 W/m^2). Of the latter, a portion is emitted directly into space through the so-called atmospheric window (approx. 40 W/m^2). The amount of infrared radiations emitted from the surface into the atmosphere depends on the occurrence of the so-called "natural greenhouse effect". The heat emitted by the Earth's surface is retained by water vapour and other long-lived gases in the atmosphere, which are called greenhouse gases (GHGs) such as CO_2 and CH_4. The particles of these gases are themselves able to radiate heat in all directions. In this way, long-wave infrared radiations are generated from the top of the atmosphere towards space (235 W/m^2, obtained as the sum of radiation emitted from the atmosphere, 165 W/m^2, emissions through the atmospheric window, and emissions from clouds, 30 W/m^2). Similarly, emissions are generated from the atmosphere towards the earth's surface (about 324 W/m^2), which contribute to the establishment of a temperature suitable for life on the planet (about 15°C) [1], [2].

Although the Earth-Sun system is naturally in a state of equilibrium, since the Industrial Revolution and particularly in the last century, there has been an abnormal and rapid (approximately ten times faster than the ice-age-recovery warming [3]) increase in global temperatures. To this end, Figure 2 shows the trend of recorded anomalies in global land and ocean surface temperatures from 1880 to 2022.

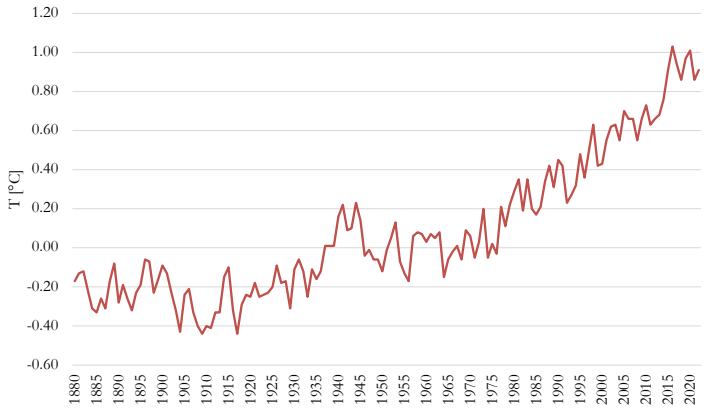

Figure 2. Annual anomalies in global land and ocean surface temperature. Adapted from [4].

As it can be noted, since 1980, the divergence of temperatures from the Earth's average has always been positive and increasing.

It is noteworthy that, during its history prior to the Industrial Revolution, the Earth's climate underwent variations that depended on natural causes, such as the variability of solar cycles and the Earth's orbit and volcanic eruptions, which alternately cooled (i.e., through the emission of reflective particles) or warmed (i.e., through the emission of GHGs) the global climate. These natural phenomena continue to occur, however, there is no direct correspondence between the magnitude of the recorded temperature increase and the observed natural phenomena. Indeed, climate models that only consider aerosols from volcanic eruptions and the variability of the Sun are able to fit global temperature observations until 1950. After that time, it is no longer possible to describe the Earth's climate situation without considering GHGs emissions generated by human activity [3]. Humanity, indeed, has caused the level of GHGs in the atmosphere to rise very rapidly through its activities; it is estimated that, since 1750, the concentration of CO_2 and CH_4 in the atmosphere has risen by 149% and 262% respectively [4]. The trend of GHGs emissions from 1990 to 2022 is illustrated in Figure 3.

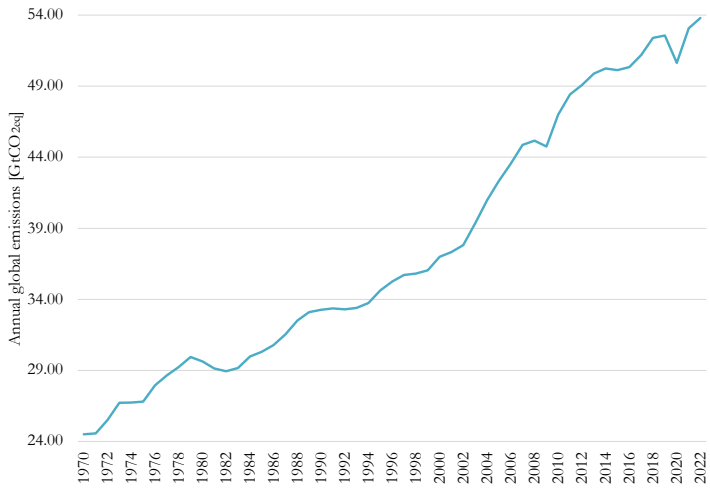

Figure 3. Trend of annual GHGs emissions from 1990 to 2022. Adapted from [4].

Given the trends shown in the previous figure, it is possible to understand how the greenhouse effect has become much more pronounced, resulting in a rise in global temperatures. This phenomenon is commonly referred to as Global Warming (GW) [5].

The causes directly ascribed to GW are [6]:

- Power generation: the generation of electricity and heat through the combustion of fossil fuels is the first cause of GW.
- Manufacturing of goods: manufacturing processes are among the main contributors to GW. Indeed, they generate significant emissions during specific processes in the production cycle, require the use of chemicals and consumables obtained from fossil fuels (e.g., coal, oil, etc.) and require a significant amount of electricity and heat, mainly obtained from fossil sources.
- Deforestation: the phenomenon of deforestation has a twofold negative effect on GW. Firstly, when trees are cut down, they release all the carbon they hold. Secondly, the removal of trees significantly decreases their ability to retain GHGs, which are released into the atmosphere.

- The transport sector: most vehicles such as cars, planes, trucks and ships use fossil fuels, generating a very significant amount of GHGs emissions.
- Food production: food production generates a significant amount of GHGs emissions due to deforestation, livestock digestion, fertiliser production and use, energy production to power farms and vehicles, as well as due to packaging production and distribution.
- The energy supply of buildings: residential and commercial buildings require ever increasing amounts of electricity and heat. To meet this demand, mainly fossil fuels are currently used, generating a significant amount of GHGs.
- Consumerism: the high consumption of goods, as well as the wasteful tendency of 1% of the global population, is responsible for the emissions of more than 50% of the poorest people.

The breakdown of total emissions in 2016 on a global scale can be observed in Figure 4. Through this representation, it is possible to identify the impact that each of the causes listed above has on GW.

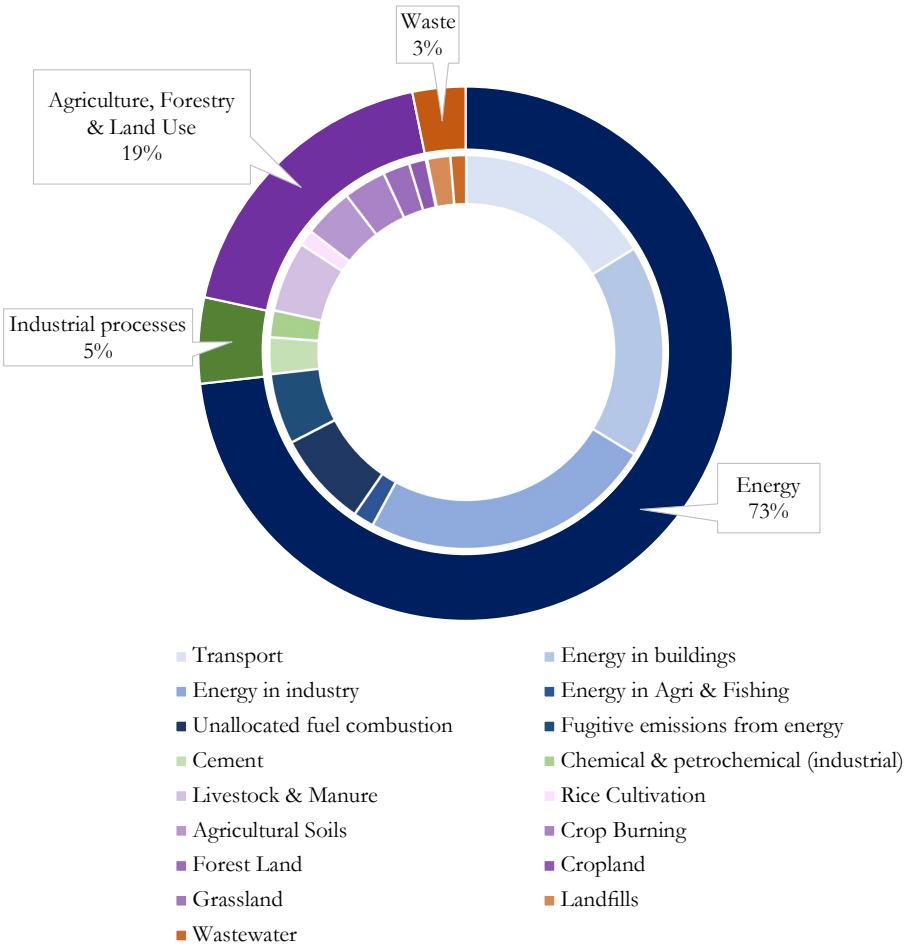

Figure 4. Breakdown of global GHGs emissions in 2016. Adapted from [7].

It can therefore be noted that the energy sector was responsible for the majority of global emissions (73.2%). Of this share, the largest share is energy use in industry (24.2%), followed by energy use in buildings (17.5%) and the transport sector (16.5%). The second most impactful sector is agriculture, forestry and land use, which accounted for 18.4% of global emissions. Emissions from this sector are related to deforestation (2.2%), as well as food production practices. Direct emissions from the industry sector, on the other hand, accounted for 5.2% of global emissions [7].

The generation of such significant amounts of GHGs is generating alterations on the entire climate system, producing a climate change phenomenon. So-called 'climate feedbacks', i.e., secondary climatic phenomena that, in turn, amplify GW are defined. [8]. The main climate feedbacks are related to [9]:

- Snow and ice: rising temperatures are melting the polar ice cap in the northern hemisphere. The consequence is that these areas, which used to reflect the sun's energy and thus lower temperatures, are now dark surfaces that absorb energy from the sun, generating an increase in global temperature.
- Water Vapour: water vapour is the most abundant GHG present in nature. In a normal condition, it evaporates from surfaces and enters the atmosphere, which is able to establish a balance between temperature and water vapour concentration. With rapidly rising temperatures, however, there is no way of knowing whether this equilibrium will be maintained, leading to even more rapid warming.
- Clouds: clouds, which act as both a reflecting surface and an energy-absorbing body, are generally divided into high clouds and low clouds. The former generate a rise in temperatures overall, as they retain a lot of energy due to their temperature and the low amount of water vapour at their atmospheric level. Low clouds, on the other hand, have no particular influence on temperature, as they can rely on the absorption of water vapour present above and, above all, often have the same temperature as the earth's surface. Current models estimate a reduction in the formation of low clouds, thus generating an increase in global temperatures.
- The carbon cycle: elements such as the oceans and the Earth's surface are able to absorb CO_2, thus reducing its content in the atmosphere. Similarly, through chlorophyll photosynthesis, plants absorb CO_2 for their growth. Given the current increase in anthropogenic CO_2 emissions, it is clear that the system will no longer be able to maintain an equilibrium, generating a significant increase in the CO_2 content of the atmosphere.
- Rising sea levels: rising sea levels, a direct consequence of melting ice and expanding warming sea water, will erode coasts and cause more frequent coastal flooding. As a result, some islands will

disappear. This is a problem, since about 10% of the population lives in vulnerable areas less than 10 meters above sea level. In this regard, Figure 5 shows the trend in ocean heat content from 1955 to 2022 (Fig. 5a) and the trend in sea level changes from 1993 to 2022 (Fig. 5b).

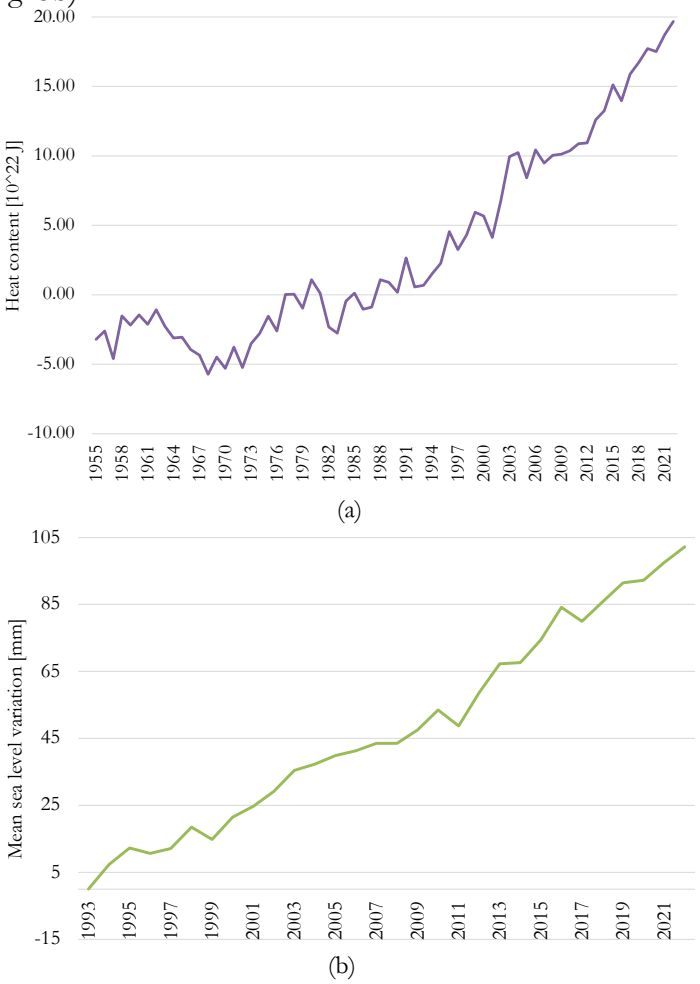

Figure 5. (a): Trend of the change in ocean's heat content from 1955 to 2022. Adapted from [4]. (b): Trend of the global mean sea level variation from 1993 to 2022. Adapted from [4].

As it can be observed in the figure above, there has been an ever-increasing increase in the heat content of the oceans since 1989. Similarly, it can be observed that the rise in sea level has been sudden and significant. It is noteworthy that the sea level recorded in January 2022 is 102.2 mm higher than that recorded in the same month in 1993. In fact, the sea level rose from 48.7 mm in 2011 to 102.2 mm in 2022, i.e., a much faster increase than the 3.4 mm average annual rise in previous years.

- Impacting ecosystems: GW is having a very significant effect on the balance of ecosystems coexisting in some climate zones. The growing season is getting longer, and spring is arriving earlier. This is causing an imbalance for migratory species, which must start foraging earlier, as well as for the balance of pollinator species such as bees, which risk having a lifecycle misaligned with the growth of flowers. This phenomenon, if amplified on a global scale, would cause a limited ability of plants and flowers to reproduce, also limiting the availability of food throughout the food chain. The current GW phenomenon is also generating migrations of some species towards the Pole, to find temperatures more conducive to survival. For those species that cannot migrate or adapt quickly to the changed climatic conditions, extinction is occurring. Furthermore, the human activities such as deforestation, fishing and unsustainable food production are contributing to an increasing risk of extinction for a growing number of species. In this regard, Figure 6 illustrates the outcome of the survey conducted by the UN Intergovernmental Science-Policy Platform on Biodiversity and Ecosystem Services on the extinction risk of major terrestrial species (i.e., 150,388 species).

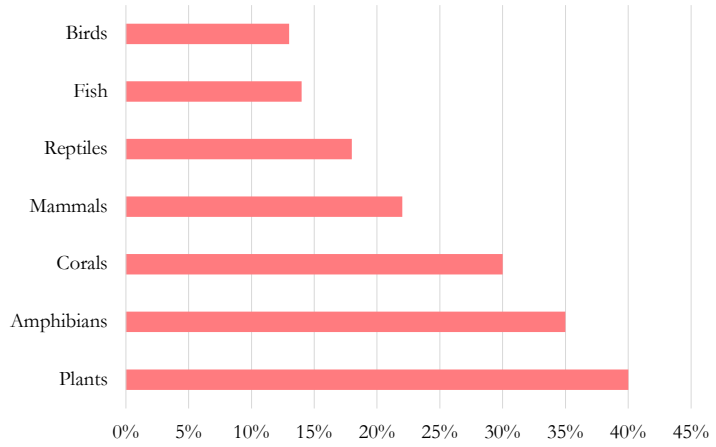

Figure 6. Percentage of the species at risk of extinction in 2022. Adapted from [10].

As it can be observed, the data on the risk of extinction are very significant. About 40% of the analysed plant species are at risk of extinction, followed by 35% of amphibian species and 30% of coral species. A total of 42,108 species were found to be at risk of extinction.

- Impacting people: current climate change will have direct consequences on human life. As mentioned, phenomena such as rising sea levels may make areas just above sea level no longer habitable. The GW will also produce an increase in temperatures in areas where there is already a torrid climate (e.g., Africa), thus making it difficult for poor sections of the population to adapt. Increased tropical climates will also lead to a greater spread of infections such as malaria, as well as extreme weather episodes such as hurricanes. Rising temperatures will also cause more and more fires, with a consequent worsening of air quality. The GW will also generate increasing droughts, resulting in long-term water shortages for the population.

In conclusion, human activity is generating very significant negative effects on the entire earth system. It is therefore necessary to take measures to limit these effects. In this regard, the agreement signed by 196 countries at the COP21 in Paris, on 12 December 2015, known as the 'Paris Agreement', is

of utmost relevance. The aim of the Agreement is to strengthen the global response to climate change, in the context of sustainable development and poverty eradication efforts [10]. To this end, the Parties agreed to implement key actions, which are:

- Keep the global average temperature increase well below 2°C compared to the pre-industrial level and make efforts to limit it to 1.5°C (threshold value identified by the Intergovernmental Panel on Climate Change [10]), recognising that this could significantly reduce the risks and impacts generated by climate change.
- Increasing adaptive capacity to adverse climatic conditions and fostering climate resilience and low GHG emissions development in ways that do not threaten food production.
- Making financial flows consistent with a low GHGs emissions and climate-resilient development path.

To achieve these goals, Parties have committed to reaching peak GHGs emissions as soon as possible, and then take rapid action to achieve a balance between anthropogenic emissions by sources and removals by natural sinks of GHGs in the second half of this century [11].

In this regard, all Parties were called upon to formulate and communicate, every five years, ambitious strategies for the achievement of the established goals, defined as Nationally Determined Contributions [12]. In accordance with the Paris Agreement, most countries have therefore defined strategies for achieving so-called Net-zero emissions (NZE) targets, i.e., targets for achieving the required carbon neutrality by 2050, starting in 2020 [13]. For example, the European Union (EU) has implemented the objectives of the Paris Agreement through the publication of the European Green Deal (2020). It aims to transform the EU into a modern, resource-efficient, and competitive economy by achieving carbon neutrality by 2050, decoupling growth from resource consumption, and taking into account the entire society in each member country [14]. In this regard, it was established that, by 2030, net GHGs emissions must be reduced by 55% compared to 1990 [15].

However, in the context of COP27 in 2022, critical issues emerged with respect to the progress achieved by Parties. Indeed, it was estimated that, considering the level of implementation of the published nationally

determined contributions up to 2022, GHGs emissions will fall by 0.3% in 2030 compared to 2019. This projection is of course not consistent with the GW limitation scenario below 1.5°C, which would require GHGs emissions to fall by 43% in 2030 compared to 2019. In this regard, the proceedings of the same conference highlighted the urgent need to plan and implement concrete actions to reach the set targets and to manage the expected transition phase to a net-zero World. This transition must include pathways that include energy, socioeconomic, and workforce dimensions [16].

This is the context of the global energy transition process, through which all countries are planning a transition from the current carbon-intensive and low-efficiency energy system to future profoundly decarbonised, energy-efficient and highly renewable solutions [17]. As highlighted, this process is crucial to achieving the targets set by the Paris Agreement since the energy sector represents the largest source of GHGs emissions globally and, consequently, makes the largest contribution to GW (Figure 4).

According to the International Renewable Energy Agency (IRENA), a radical and systematic transformation of the global energy system is needed over the next 30 years. This transformation must go beyond the decarbonisation of the energy supply and move strategically towards an energy system that cuts carbon emissions while supporting an inclusive and resilient economy. The three pillars for successful planning and execution of the energy transition process are: the development of a physical infrastructure to support a localised and decentralised energy system; the development of policies that facilitate the development, integration and exchange of renewable-based energy; and the development of skills and capacities to support the renewed energy system [18].

The main enabler of this transition process is the ever-increasing production of energy from renewable sources. The main sources of renewable energy are [19]:

- Solar energy: it is the most abundant of all energy resources and can constitute a significant share of the national energy mix in most countries of the world. The main devices that convert solar energy into electricity are photovoltaic panels and mirrors that concentrate solar radiation. Currently available solar energy conversion

technologies are capable of producing heat, cooling, electricity and fuels for a variety of applications. It is noteworthy that, the global weighted average levelised cost of electricity of newly commissioned utility-scale solar PV projects declined by 88% over the 12-year period from 2010 to 2021 [18]. This drastic cost reduction makes the installation of photovoltaic panels the main way to increase installed power from renewable sources in the future (Figure 7).

- Wind energy: wind energy is harnessed by turbines that convert the kinetic energy of wind into electrical energy. Also in this case, most areas globally have wind characteristics that make the installation of wind turbines favourable, although, at present, the greatest potential is offered by the installation of offshore wind turbines. In recent years, investments are being made to improve the efficiency of plants, as well as a drastic decrease in the levelised cost of electricity from this pathway for energy production (66% over the 2010-2021 period [18]). In this regard, wind energy is the second, after solar energy, on which investment is planned to increase the installation of power from renewable sources in the future (Figure 7).
- Geothermal energy: it harnesses thermal energy accessible from the earth's interior by means of wells or other means. Once they reach the earth's surface, fluids at various temperatures can be used to produce energy. Technologies for producing electricity from hydrothermal reserves are mature and have been in operation for a long time.
- Hydropower: hydropower generation harnesses the kinetic energy possessed by water flowing from higher to lower altitudes. Generally, water reservoirs are used, or the natural flow of rivers is exploited. Hydropower is currently the largest source of renewable energy in the electricity sector. Hydropower plants can have negative effects on the ecosystems in which they are located. Therefore, only small hydropower plants serving communities in remote locations are considered sustainable.
- Ocean energy: ocean energy is produced by technologies that harness the kinetic or thermal energy of seawater to produce heat

or electricity. Ocean energy systems are still at an early stage of development but have high potential for energy production.

- Bioenergy: bioenergy is obtained by processing a range of organic materials such as agricultural waste, biomass or energy crops specifically cultivated to produce electricity or heat. The production of energy from the combustion of biomass generates GHG emissions of biogenic origin, since the fuel is non-fossil. Energy production using specially cultivated energy crops, however, has a negative potential related to deforestation and land-use change.

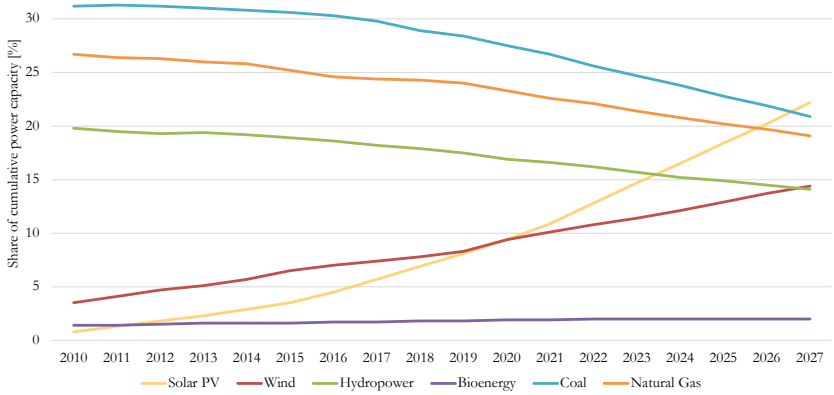

Figure 7. Trend of the global share of cumulative power capacity by renewable energy technology from 2010 to 2027. Adapted from [20].

In 2020, electricity production from renewable sources accounted for 28% of global gross electricity generation (i.e., 27000 TWh). According to the 1.5°C-compatible scenario established by IRENA, this percentage must rise to 91% in 2050 on an electricity generation that must triple (i.e., 90000 TWh). Renewable-based energy systems must therefore produce 81900 TWh of electricity in 2050 [18] (Figure 8).

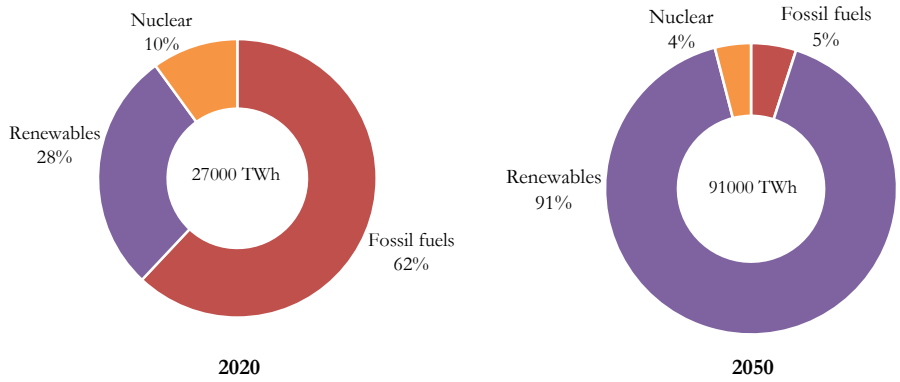

Figure 8. Shares of global gross electricity production in 2020 and 2050 (scenario compatible with the 1.5°C target). Adpated form [18].

Currently, the power sector has made good progress in terms of installed renewable capacity and generation. Renewables account for 83% of global capacity addition and installed power generation capacity reached 40% in 2022, with a total of 295 GW from renewables. In the scenario that considers the main global policies for reaching the NZE targets (so-called 'Planned Energy Scenario' (PES)), renewable energy capacity expands to 6773 GW by 2030 and 15835 GW by 2050. Renewables' share in generation scales up from 28% in 2020 to 46% in 2030, and to over 70% in 2050 [18]. However, as can be seen from Figure 9, these measures are insufficient to reach the 1.5°C target. In a scenario compatible with reaching the 1.5°C target, indeed, the power sector would reach 68% and 91% of renewable energy share in the total electricity generation in 2030 and 2050, respectively (Fig. 9a). Total installed renewable generation capacity would need to increase four-fold by 2030 (11 174 GW) and twelve-fold by 2050 (33 216 GW), over the 2020 level (Fig. 9b). This means annual average renewable energy capacity addition of approximately 1000 GW in the current decade, more than three times the installed renewable capacity addition in 2022 and close to 1 100 GW by 2050 [18].

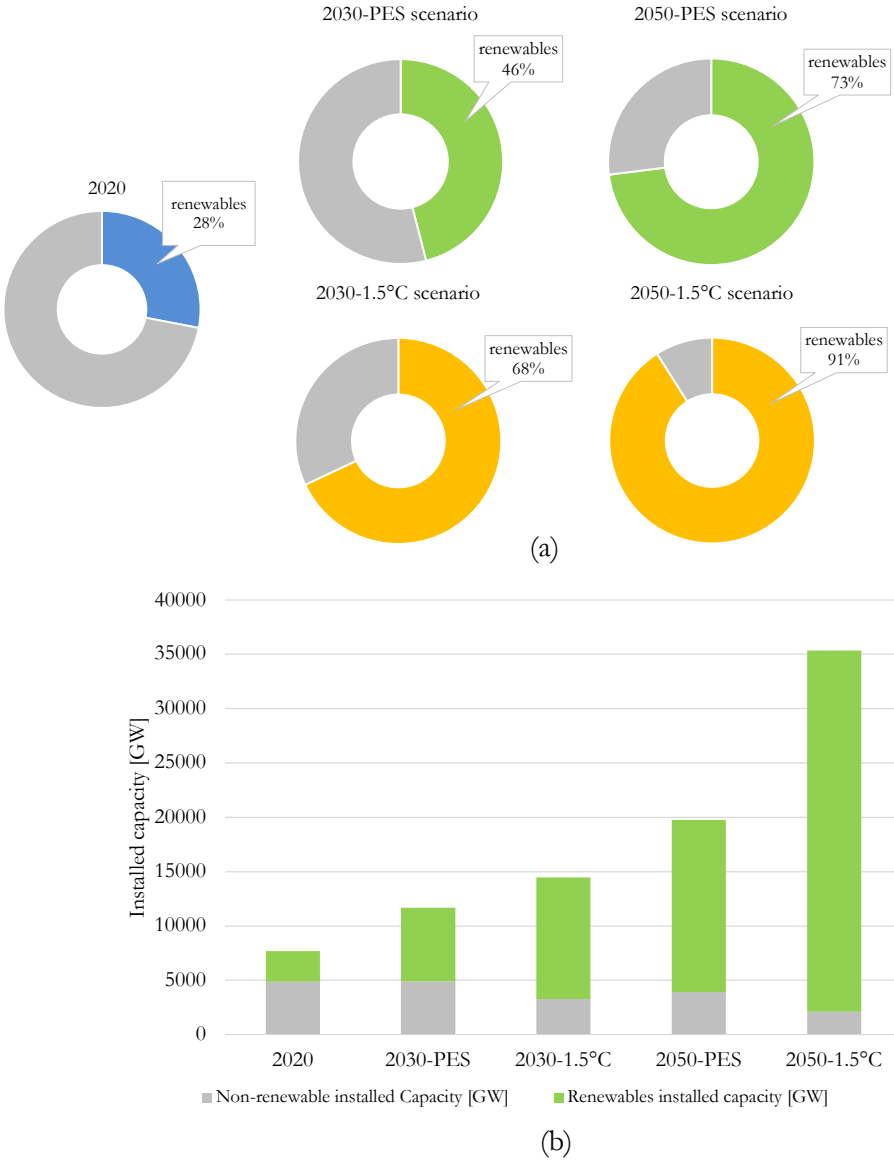

Figure 9. (a) Global power generation mix in 2030 and 2050, according to PES and 1.5°C scenarios. (b) Global installed capacity from renewables in 2030 and 2050, according to PES and 1.5°C scenarios. Adapted from [18].

Further key elements in the current energy transition phase are the so-called "green gases", i.e., H_2 and bio-CH_4.

First, H_2 is a key element in the current context of climate change tackling and energy crisis [21]. Its high energy density (about three times higher than gasoline [22]) and the generation of water vapor only from its combustion [23], make the H_2 a promising energy vector to be employed for several purposes [24]. Indeed, its large-scale production and use is crucial for achieving the NZE targets set worldwide to meet the Paris Agreement's 1.5°C global warming limit [25]. National H_2 strategies are therefore under increasing development. They include measures (e.g., political, economic, financial, policy, etc.) and initiatives to support H_2 development [26]. To this concern, the formulation of an early H_2 strategy in Japan (December 2017), catalyzed the attention of the Asian-Pacific region, resulting in strategy development in South Korea (January 2019) and Australia (November 2019). Similarly, in the European context, the publication of Germany's national H_2 strategy (June 2020) fostered the development of an EU H_2 strategy, published in July 2020 [26]. EU H_2 strategy is the most ambitious green H_2 strategy worldwide [27], and includes a roadmap for achieving the climate neutrality targets included in the European Green Deal [28]. Consistent with these goals, and thanks to COP 26 acting as a catalyst, most European countries have recently published or are working on their own H_2 strategy [29].

H_2 already finds applications in many industrial processes. Traditionally, it is used in crude oil refining sector (i.e., in hydrotreatment and hydrocracking process), upgrading of Fischer-Tropsch gas-to-liquid products and in the ammonia and urea production [24]. Due to its high versatility, H_2 is currently being considered in innovative applications. In this regard, applications of H_2 and H_2-based fuels are considered in the energy-intensive transport sector (e.g., aviation and shipping fuels), in the road transport sector (e.g., electric vehicles with H_2 fuel cells), in the building sector, and in the power generation sector [30]. H_2, most of all, represents a promising alternative for decarbonizing the so-called "hard-to-abate" sectors (e.g., iron and steel, cement and concrete, chemicals, etc.). They are characterized by high energy demand, high process heat needs and/or chemical process emissions, and other features that make them inherently difficult to decarbonize [31]. These aspects, combined with the

increasing investments fostered by H_2 strategies, will lead to an exponential growth in H_2 demand in the next future (Figure 10).

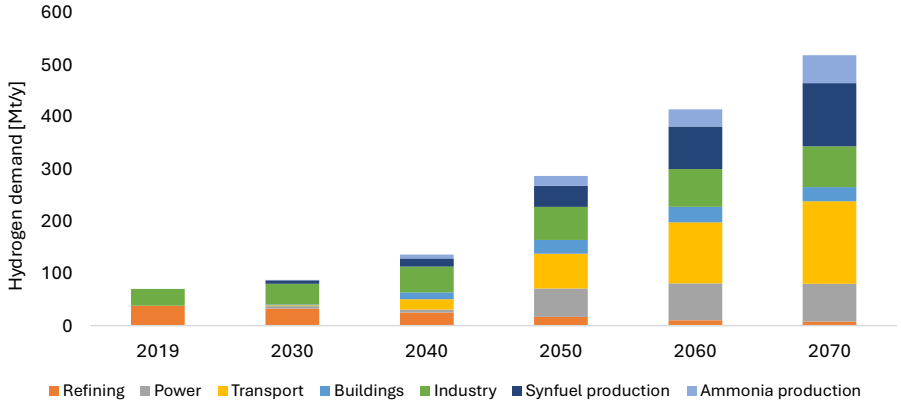

Figure 10. H_2 demand by sector from 2019 to 2070. Adapted from [32].

Global H_2 demand in 2019 was 75 Mt/y [32], and increased to 94 Mt in 2021/y [30]. In the future, a faster growth will occur, with global H_2 demand reaching 520 Mt/y by 2070 [32]. Almost the whole H_2 demand is currently coming from traditional sectors (e.g., refining sector). In the projected decarbonized scenario of 2070, this situation will change, with almost the entire H_2 demand coming from innovative sectors. Indeed, 30% of global H_2 demand will come from the transport sector for direct use for cars, trucks and ships, 20% will come from the production of synthetic fuels (e.g., synthetic kerosene for aviation), 10% for the conversion into ammonia as a fuel for the shipping sector, 15% from industrial sectors (e.g., iron and steel, and chemicals), 15% from the power sector to support flexible electricity generation, and 5% from the building sector (most in the form of pure hydrogen transported through a dedicated pipeline) (Figure 10) [32]. However, as it can be observed in Figure 11, environmental issues related to H_2 production arise.

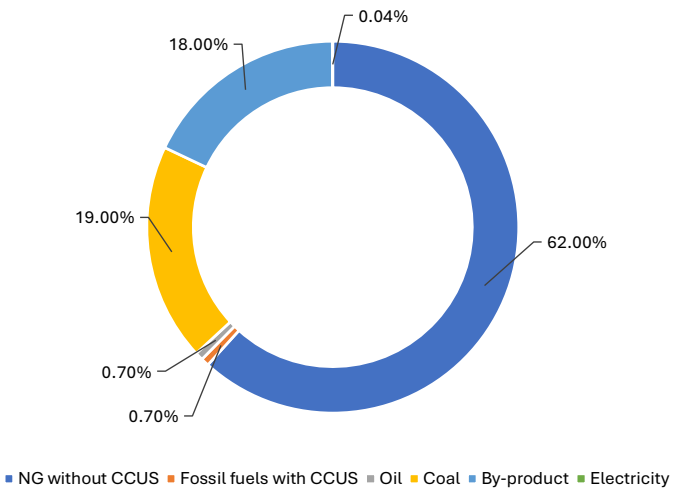

Figure 11. Global H_2 production mix in 2021. Adapted from [30].

Currently, almost all H_2 required is produced from unabated fossil fuels, generating 900 $MtCO_2/y$ [33]. Steam Methane Reforming (SMR) without Carbon Capture Utilization and Storage (CCUS), which totally relies on NG use, is the main H_2 Production Route (HPR). It accounted for 62% of H_2 production in 2021. In the same year, 18% of H_2 was produced as a by-product of the naphtha reforming process, and 18% came from coal processing. The minor sources of H_2 production were oil, which accounted for 0.7% of H_2 global production, and electricity, which accounted for 0.04% (i.e., 35 kt) [30]. To this concern, an urgent challenge consists of finding viable solutions to produce low-carbon H_2 [34]. If the growing demand for H_2 will indeed be met by employing the current production mix, an overall negative environmental effect would be generated, in contrast to the expected decarbonization function of H_2.

The most promising "green" HPR is water electrolysis fueled by renewable electricity [35]. This process is potentially zero-emission (without considering emissions from the life cycle of renewable energy conversion systems) [36]. However, the implementation of this technology on an industrial scale faces major barriers, both from an economic and environmental point of view. As for the environmental aspect, an electrolyzer has a high energy consumption (on average of 5 kWh/Nm^3H_2 [37]) and currently there is not enough renewable energy capacity to meet

the H_2 demand. Indeed, it is estimated that an electricity demand of 3600 TWh would be needed to meet the current H_2 demand, more than the total annual electricity generation of the EU [38]. This implies that an electrolyzer must also be powered by electricity produced from the grid, generating significant indirect emissions. From an economic point of view, the still high cost of renewable energy and the high cost of facilities make the installation of an electrolyzer expansive in terms of operating and investment costs [39]. For large-scale green H_2 production, therefore, a rapid and effective energy transition is needed. In the current transition phase, during which global efforts are in progress to increase the availability and reduce the cost of energy from renewable sources [40], it is therefore necessary to identify complementary HPRs that, on the one hand, ensure the growing demand for H_2 is met and, on the other hand, enable the production of low-carbon H_2 [41]. An alternative is the production of the so-called "blue H_2" via SMR with CCUS. This process allows the continued use of existing facilities, reducing emissions and pressure on the renewable energy production system. This HPR, however, is not fully in line with the decarbonization targets set in the mid-long term. Indeed, it relies entirely on the use of non-renewable sources and does not avoid CO_2 production [35].

Moreover, bio-CH_4, also known as "renewable natural gas", is a near-pure source of CH_4. It is generally produced by upgrading (i.e., by removing CO_2 and other contaminants) the biogas obtained from the AD of OWs, also the Organic Fraction of MSW (OFMSW), or biomasses [42]. Bio-CH_4 has almost the same LHV as fossil NG (around 36 MJ/m^3 [43]) and find its same several applications (e.g., electricity and heat production, and as a fuel in the transport sector) [44]. Most of all, Bio-CH_4 can be used with no changes in transmission and distribution infrastructure or end-user equipment with respect to the NG [43]. This green gas has therefore the potential for meeting the requirements of NG-based applications with the same effectiveness as the fossil fuel, but without the associated emissions. Emissions generated from the use of fossil NG for electricity and heat production were indeed 3.2 $GtCO_2$ in 2021 [45], a value not consistent with a decarbonized scenario. Moreover, bio-CH_4 could be helpful in reducing the emissions from the transport sector, which reached 7.7 $GtCO_2$ in 2021. Consistent with the "net-zero" scenario, indeed, emissions from this sector

must be reduced by 20% by 2030 [46]. It is noteworthy that also the main Bio-CH_4 production process, i.e., AD of organic wastes OWs, shows a great environmental potential. This process allows to valorise wastes, at the same time reducing CH_4 emissions mainly from OWs' decomposition and agriculture [47], which generated 1.49 $GtCO_{2eq}$ and 3.49 $GtCO_{2eq}$ in 2019, respectively [48]. CH_4 is indeed the second major greenhouse gas after CO_2. Although it persists in nature for fewer years than CO_2 (i.e., 12 years compared to centuries for CO_2), CH_4 has the capacity to absorb much more energy, generating 28-36 times more impact on global warming over a 100-year time horizon [49]. Consistently, CH_4 emissions reduction can provide significant climate benefits in the near-term [50]. It can be therefore stated that the production of bio-CH_4 has a threefold decarbonization potential; it is useful to reduce CO_2 emissions from the energy, industry and transport sectors, it helps reducing the FMEs generated from NG supply, and it helps reducing CH_4 emissions from waste and agriculture sectors. It is noteworthy that bioenergy in various forms, including biogas and bio-CH_4 production, will have to supply 22% of total primary energy in 2050, which is 2.5 times more than today. Furthermore, sustainable biofuels, including bio-CH4, will have to satisfy 13% of the final energy consumption of the transport sector in 2050. Therefore, the production of this green gas is crucial for the achievement of current environmental targets.

To understand the progress of the energy transition process, six indicators were chosen to be monitored over time. These indicators are [18]:

- The use of renewables for electricity generation, which includes the amount of electricity generated from renewable sources and the share of electricity from renewable sources in the total generated globally.
- The direct use of renewables, which includes the share of renewables in total global energy consumption and the amount of bioenergy consumed.
- Improvements in energy intensity.
- The level of electrification of the end-use sectors.
- The production of clean H_2 and derivative fuels (e.g. ammonia, kerosene, etc.).
- The amount of CO_2 captured and removed by various methods.

In this regard, Figure 12 shows the current values of these indicators and those expected under two scenarios defined by IRENA. The first is the so-called PES, which considers all the strategies declared by countries (especially the G20) in accordance with the requirements of the Paris Agreement. The second is the so-called '1.5°C scenario', which considers the achievement of the 1.5°C target in 2050 [18].

			2030		2050	
		2020	PES	1.5°C Scenario	PES	1.5°C Scenario
KPI.01 Renewables (Power)	Electricity generation (TWh/y)	7468	16504	27358	38118	82148
	Renewable energy share in electricity generation (%)	28%	46%	68%	73%	91%
KPI.02 Renewables (Direct Uses)	Renewable energy share in TFEC (%)	18%	23%	35%	33%	82%
	Modern use of bioenergy (EJ)	21	30	50	41	64
KPI.03 Energy intensity	Energy intensity improvement rate (%)	1.7%	1.8%	3.3%	2%	2.8%
KPI.04 Electrification in end-use sectors	Electrification rate in TFEC (%)	22%	23%	29%	28%	51%
KPI.05 Clean hydrogen and derivatives	Production of clean hydrogen (Mt)	0.7	2	125	21	523
KPI.06 CCS, BECCS and others	CO_2 captured from CCS, BECCS and other removals measures (Gt)	0.04	0.1	2.1	0.4	4.9

Figure 12. Key Performance Indicators for reaching the 1.5°C target in 2030 and 2050 according to PES and 1.5°C scenarios. Adapted from [18].

As it can be observed from the figure, there is a significant deviation between the PES and the 1.5°C scenario for the values of all indicators. For example, it can be observed that the planned energy production from renewable sources in 2050 is almost 54% lower than necessary to reach the 1.5°C target. Furthermore, energy production from renewable sources is planned to make-up 73% of global production, compared to the 91% needed. This value has a double negative meaning, if one considers the amount of energy produced to be less than necessary. The values for energy consumption from renewable sources and bioenergy consumption deviate significantly from those needed to reach the 1.5°C target. The most significant deviation occurs, however, regarding the production of so-called

'clean H_2' (i.e., includes green H_2 and blue H_2). The planned production of clean H_2 is indeed 21 Mt by 2050, compared to the 523 Mt needed to achieve the 1.5°C target.

It can therefore be established that strategies are needed to narrow the gap between what is planned and what is needed to complete the current energy transition process.

In this context of energy transition and the achievement of short-, medium- and long-term environmental goals, the issue of the management of waste produced in the urban context is of utmost relevance. Two main types of waste, i.e. Municipal Solid Waste (MSW) and SS, were considered in this work. The management of both types of waste represents a crucial issue for the achievement of fundamental environmental objectives and for the attainment of a CE condition. Furthermore, as illustrated below, waste management can support the current energy transition, as it is possible to process waste to obtain both electricity and green gases.

The current increase in MSW production is a direct consequence of population growth (at a yearly rate of 2.035% [51]), which is accelerating phenomena such as industrialization, urbanization, and economic development. The global production of MSW, equal to 2.01 billion tonnes in 2016, will grow to 2.56 billion in 2030 and will reach a level of 3.4 billion in 2050. As far as concern the correlation between MSW production and economic development, in 2016, about 34% (683 million tonnes) of the globally produced MSW was generated by high-income countries (i.e., countries with a gross national income per capita of 12,476 $/year or more), despite the same countries being populated by only the 16% of the global population [52].

MSW management shows criticalities both from an economic and an environmental perspective. MSW, indeed, represents one of the most significant sources of pollution at either a global, regional, or local scale [53]. To this concern, in 2016, the MSW management practices generated 5% of the globally emitted 1.6 billion tonnes of CO_{2eq} [52]. Furthermore, at a local and regional scale, the MSW management (e.g., collection, transport, treatment, and disposal) is generally operated in proximity to the urban centres, representing a significant pollution source, very close to citizenship.

From an economic point of view, MSW management is an expensive service for municipalities; in high-income countries, it accounts for 4% of the municipal budget, and of this expenditure, operating costs represent about 70% [54]. Therefore, identifying a solution to manage the increasing amount of MSW produced, accounting for both economic and environmental issues, is a worldwide highly perceived need.

The EU-27 countries are significantly involved in this issue since most of them are included in the high-income category. Several legislative measures have been enacted in the EU to promote sustainable MSW management. The most impactful is the Waste Framework Directive (WFD) 2008/98/EC [55], which can be considered the cornerstone of the European waste policy and regulation. The WFD introduced a waste hierarchy describing, in descending order of priority, the actions to be implemented to manage waste in an environmentally sustainable way, optimising resource efficiency and minimising the environmental consequences of waste management (Figure 13) [56].

Figure 13. Waste hierarchy pyramid. Adapted from [56].

According to the WFD, sustainable waste management can be ensured by minimising the generation of waste and hazardous substances, avoiding disposal practices and maximising the amount of recycled material [57]. The waste hierarchy identified is a crucial strategy for the transition of the EU economy towards a CE, allowing MSW management to achieve the best environmental performance [58]. According to CE's definition, waste

production should be minimized, maintaining resources as long as possible within the economic cycle [59]. To foster the achievement of a CE condition, a European target on recycling and landfilling rates of at least 65% and 10%, respectively, must be achieved within 2030 [60]. Currently, the percentage of landfilled and recycled MSW still remains equal to 23% and 48%, respectively, values far short of the target [61]. According to Chen *et al.* [53], despite the improvements achieved, a continuation of the current waste management trend is insufficient to reduce the pressure generated by MSW management and achieve a CE. In light of these considerations, identifying sustainable solutions for MSW management to support and accelerate the transition towards the achievement of the goals set at the EU level is necessary.

At the same time, Sewage Sludge (SS), i.e., the main by-product of wastewater treatment (WWT), is considered one of the most critical resources to be managed in the urban context for the transition towards a CE. Although it includes dangerous contaminants, both organic and inorganic, and pathogens (i.e., bacteria, viruses, protozoa, etc.) [62], it is rich in valuable nutrients like N and phosphorous (P). Indeed, SS contains, in dewatered condition, 50-70% of organic matter, 30-50% of mineral components, 3-4% of N, 0,5-0,25% of P, and significant amounts of the other useful nutrients [63]. It is noteworthy that P, that can be recovered by SS treatments, is classified as a Critical Raw Material [64], estimated to be exhausted in the next 50-100 years [63]; in other words, P is considered a strategic and relevant material from in economic perspective, with a high supply risk [64], [65]. Moreover, at 6% moisture content and 65% organic matter, the SS shows a LHV of about 13.5 kJ/kg [66]. Under this condition, the SS can be considered a solid fuel [67], since its LHV is comparable to traditional fuels' characteristic value, such as lignite and other biomasses. Currently, the global climate change and energy crises are forcing the valorization of the limited resources on earth. Under this perspective, the SS must be managed as a key resource. Therefore, it is recommended to adopt treatments to reduce the number of hazardous contaminants and, at the same time, recover energy and matter from this resource.

The SS production rate generated from WWT is growing day by day as the water demand, and thus the amount of wastewater produced, is on increase [68]. The rapid increase depends on two main factors. The first one is

strictly related to the increase in world population; the second one is the indirect consequence of the forced implementation of the European Council Wastewater Treatment Directive 97/271/EC, which requires a higher quality of the effluent treated with the unavoidable increase of the SS produced as a by-product of wastewater treatments [69]. Recent studies showed that, in the last fifteen years, the EU-12 annual production of the SS increased by almost 50%, from 9.8 million tons in 2005 to over 13 million tons in 2020. The lack of continuity among official reports and the relevant lack of data for the new Member States further complicate the study of this topic [70].

Also the SS management is regulated by the prescriptions of the "waste hierarchy". To take a further step towards achieving a circular approach, it is necessary, in addition to implementing the "4Rs" (i.e., reduction, reuse, recycle, and recovery), to apply a fifth "R" due to "rethink" of the process [65]. Therefore, a solution consistent with the CE approach and "nutrients-energy-water" paradigm is strictly required [65]. Rethinking the wastewater value chain means promoting a shift from the traditional concept of WWTP to that of wastewater resource recovery facilities [71]. According to Smol *et al.*, the traditional water value chain should be rethought, re-thinking how to use resources to create a sustainable economy, which is "free" of waste and emissions [72]. In other words, the authors consider as not sustainable a linear approach on the WWT, where the SS is considered waste. The authors, on the contrary, promote a "circular approach", where the SSs produced are resources for agriculture, pharmaceutical and personal care products, renewable energy production, and co-firing as construction materials.

Among the actions included in the waste hierarchy (Figure 13), a noticeable category of recovery options is the so-called WtE, including the treatments to convert waste into electricity. Although these options are at a lower level (i.e., less preferable) than prevention, reuse and recycling in the waste hierarchy, it can be stated that they are essential to ensure sustainable MSW and SS management and to support the CE transition [73]. WtE treatments, moreover, allow, in this transitional phase, to treat MSW that is not recycled and, simultaneously, to reduce the landfilling rate, consistent with the EU targets and a CE perspective. Once the goals are achieved, these treatments can still be helpful in treating not recyclable materials or perishable waste,

avoiding WtE plants' overcapacities. Consistently with these aspects, in the last years, an ever-increasing amount of waste has been processed by adopting WtE treatments [56].

Another category of waste treatments useful in this perspective are the so-called waste-to-H_2 (WtH_2) treatments. They consist of treating waste (e.g., MSW, wood, food waste) to obtain H_2 as a primary product. These HPRs have a twofold benefit: on the one hand, H_2 from alternative renewable sources is produced, and on the other hand, MSW is valorized.

Finally, as mentioned, AD treatment can be useful for producing bio-CH_4 and, therefore, should be considered among the waste valorisation treatments that contribute to the progress of the current energy transition.

In this regard, this work deals with the investigation of the performance of waste valorisation plants, since, as mentioned, they offer a dual benefit. On the one hand, they help to accelerate the energy transition process and reduce the gap between the current situation and the one needed to comply with the 1.5°C limit and, on the other hand, they enable the valorisation of resources in accordance with a CE perspective. Each solution, however, has its own characteristics from an economic and environmental point of view and, in this regard, it is necessary to make comparisons that take into account both the negative (e.g., costs, direct and indirect emissions) and positive (e.g., revenues, avoided emissions) effects associated with each alternative in order to understand their benefits in the current transition phase. A schematisation of the research context of this work is shown in Figure 14.

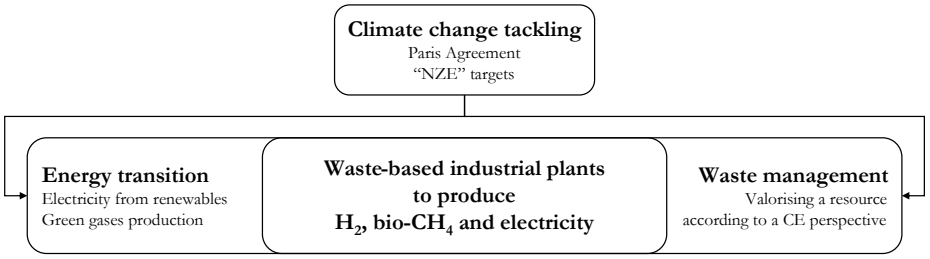

Figure 14. Schematization of the research context of the present work.

1.1 Literature review on waste-to-energy plants

The investigation on WtE plants is very relevant and, therefore, many sources can be found in the scientific literature on the subject. Wei Lu et al. [74] analysed incineration as a possible alternative for MSW management and proved its validity despite being an outdated technology. According to the authors, the choice of technology for MSW incineration depends on economic and environmental issues. Generally, the green aspects are affected by the high variability of MSW composition and the lack of reliable control systems. A Life Cycle Assessment (LCA) to evaluate the impact of refuse-derived fuel within the incineration process of the MSW instead of the coal was carried out by Havukainen et al. [75]. The results led to reduce the impact of the main environmental categories (i.e., global warming potential, acidification potential and eutrophication). Panepinto and Zanetti [76] adopted a multi-step approach for the economic and environmental evaluation of an incineration plant in Italy. They considered the capacity of the incinerator plant and possible connections with a district heating network for the use of the heat power produced. At a global and local level, an environmental balance and a cost analysis were carried out to evaluate the efficiency of a plant, including heat and electricity cogeneration. In this case, if, on the one hand, the installation of a cogeneration plant in a heating district minimises the environmental impacts, on the other hand, the configuration that provides only the electricity generation is more convenient from an economic perspective.

Similarly, in [77], an LCA was developed to evaluate the environmental impact generated by an incineration plant, including energy recovery in different operating conditions. The research shows that investing in technical improvements is convenient and, therefore, increases the electrical conversion efficiency in the case of a high-size plant. One of the recommended improvements consists of replacing the typical refractory bricks with phase-change material-based bricks in the reactor [78]. It is also shown that the recovery of the bottom ashes helps decrease indices' values in different impact categories [77]. Beylot et al. [79] analysed an LCA related to MSW incineration in France. The study identified a negative indicator for seven of the nine impact categories. In particular, the most significant benefit comes from the cogeneration of heat and electricity as well as from

the selective catalytic reduction for NOx abatement. In 2015, subsystems of the plant were modelled, adopting short-term stochastic planning to manage the energy produced by cogeneration [80]. It is noted that short-term stochastic planning increases net revenues and thermal efficiency instead of determinist short-term planning. In [81], the potential benefits in economic and environmental terms of an MSW management strategy based on the incineration and recycling of MSW for a Brazilian location were assessed. The technique consists in recycling 20% of the collected and selected waste and sending the remaining share to incineration. The results showed the potential of the adopted strategy from economic and environmental perspectives. A similar approach, based on the incineration treatment simulation models, was developed in [82] and [83].

Pyrolysis is another MSW treatment recently developed. It is described and detailed in [84], while Wang et al. [85] investigated the environmental feasibility of pyrolysis as an alternative for sustainable MSW management in North Carolina. The environmental impacts of the pyrolysis process were compared with the impact of incineration, anaerobic digestion and landfill. The results proved that fast pyrolysis is the best alternative from an environmental point of view while landfilling is the worst. In [86], the pyrolysis was compared with incineration, gasification and plasma treatment adopting multi-criteria decision-making methods. Li et al. [87] investigated catalytic pyrolysis. They established that if, on the one hand, the use of a catalyst allows a reduction of emissions due to the process, on the other hand, the refrigeration significantly increases the operating treatment costs.

Similarly, the performance of catalytic pyrolysis, if compared with thermal pyrolysis, is proved in [88], [89]. Wang et al. [90] investigated the potential of pyrolysis, combined with thermal or catalytic cracking, to produce syngas under certain operating conditions. In [91], the effects of moisture content and CaO on the product's composition derived from pyrolysis and syngas' Low Heating Value (LHV) were investigated. Song et al. [92] proposed the addition of iron ore and iron oxide to the treatment as an alternative to improve the efficiency and environmental impact due to the pyrolysis of MSW. According to the authors, iron ore and iron dioxide act as waste pyrolysis catalysts; they improve the efficiency and effectiveness of performance treatment.

In the last few years, an increasing interest can be observed in the MSW gasification treatment, which is a valid alternative to other technologies either from a social, economic, and environmental point of view [93]. Hameed *et al.* [94] proved the effectiveness of MSW gasification in reducing pollution and maximising the recovery of energy and material. In [95], the effectiveness of the MSW co-gasification with switchgrass was evaluated by considering LHV, the syngas' yield, and the gasifier and tar temperature. Cai et al. [96] investigated the refuse-derived fuels and straw mixtures' co-gasification performance. They identified a positive impact of the synergistic effects on the system's performance at low equivalent ratios (0.1-0.2) and high temperatures (800-900°C). Arena et al. [97] reported a technical analysis of the gasification of a recovered solid fuel obtained from MSW sorting. The report confirmed that adopting the syngas for energy applications was effective. From an economic point of view, the investment can be considered sustainable only if an incentive rate for the energy produced is provided. Kardani *et al.* [98] modelled the MSW gasification in a fluidised bed gasifier to predict treatment features, such as gas and product LHV, as well as syngas yield. Xu et al. [99] developed a thermodynamic model referring to a real case of MSW gasification. The model allowed to compare the composition of the produced gas using different gasifying agents to identify the best for the treatment's environmental performance improvement. A numerical model to compare different gasifying agents was developed in [100]. In [101], a system based on MSW gasification was proposed to simulate the production of electricity, hydrogen and methanol.

Similarly, the performance of a WtE multigeneration system was investigated in [102]. In [103], a biomass-driven cogeneration system was analysed, and the MSW gasification was evaluated. In [104], a thermodynamic model was developed to evaluate the feasibility of MSW gasification in Portugal. The optimal operating temperature of the treatment was identified at 900°C for an equivalent ratio of 0.25. The same approach evaluated the economic convenience of gasifier installation in Brazilian municipalities. The results showed a positive scale-up with increasing the population served, given by reducing the specific costs and increasing the plant's potential [105] Moreover, in previous works, a comparison has already been conducted between different alternatives for producing energy from MSW [106]–[109].

Many studies are moreover available in the scientific literature on the energy recovery technologies from SS. The first solution considered is the AD, a technological option producing biogas for heat and electric energy production. Li et al. compared the environmental performance of the different techniques adopted in AD (i.e., mesophilic and thermophilic AD, mesophilic and thermophilic high-solids AD and AD with thermal hydrolysis pre-treatment) consistently to this purpose, the LCA methodology was adopted [110]. With the aim of maximizing the biogas production, Gherghel et al. listed the possible pre-treatments which, in combination with AD, could increase biogas production by 21-31% [111]. Oladejo et al. provided a review on the SS-to-energy processes; the authors highlighted two limitations related to AD. The first one is the long duration of the process (from 7 days to 5 weeks); the second one is the low efficiency of conversion of organic matter [112]. They also considered thermochemical treatments such as combustion, pyrolysis, and gasification as alternatives to energy recovery. The low reaction time of these thermochemical treatments assures high treatment rates. However, thermochemical treatments require a SS with lower moisture content. In addition to the recovery of heat from combustion, the benefit due to further energy recovery treatments from the products of pyrolysis (i.e., pyrolytic oil, biochar, and non-condensable gases) and from the gas produced from gasification were evaluated [112]. Other thermal treatments such as incineration, pyrolysis, and gasification were discussed in [113], [114]. An overview of the SS thermal treatments in terms of sustainability was provided in [113]. The results showed that the SS incineration performance is better than pyrolysis and gasification treatments in terms of costs, energy efficiency, nutrient recovery, and flexibility of the feedstock dry matter content. To this concern, the authors showed that the pyrolysis ensures the best performance, considering the by-products' market value. Moreover, the treatment can be downscaled and adopted to small municipalities (i.e., 10000 inhabitants). In this context, the maximization of the syngas produced from pyrolysis was investigated in [115]. An overview on main SS-to-energy technologies adopted in industrial applications (i.e., pyrolysis, gasification, and incineration) was provided by Gao et al. [116]. Werle and Sobek defined the SS-to-energy solutions as a suitable strategy to comply with CE goals. Similarly, the gasification was identified as the most proper thermochemical treatment to improve the environmental performance in

SS management [117]. Similarly, the biochar production from SS and microalgae mixtures as well as the consequent energy recoveries due to co-digestion without SS organic wastes are described in [111], [118], [119]. The efficiency in energetic terms due to Hydrothermal carbonization process (i.e., a process where the SS are processed in an aqueous medium of subcritical water) are faced in different studies, most of available works conducted investigated on the energy recovery obtained from the treatment application in different part of the SS treatment. It is showed that energy efficiency significantly changes accordingly to the adopted treatments; in most cases, the choice depends on the quantity and typology of the SS to be treated [120], [121], [122], [123]. Finally, Singh et al. evaluated the potential for energy recovery by incineration and AD for India [124].

1.2 Literature review on waste-to-biomethane plants

Actions and strategies to foster the widespread use of bio-CH4 are subject of current studies. To this concern, in [125], starting from the economic and environmental potentials of Bio-CH_4, the opportunities and barriers for the implementation of a European Bio-CH_4 market are analyzed. In a previous study, starting from the experience of European countries, the large-scale development and drivers of biogas and Bio-CH_4 production are explored. At the same time, issues of future interest such as policy recommendations and supply chain risks are analyzed [126]. Similarly, by considering the Bio-CH_4 as a virtuous example of circular bioeconomy, in [127] a framework for evaluating Bio-CH_4 communities is proposed. As for the optimization of the bio-CH_4 production process, in [128] the integration of AD with hydrothermal gasification is proposed, in order to maximize the bio-CH_4 yield. In [129] the AD-based bio-CH_4 production process is analyzed in order to identify the operational variables that most affect the greenhouse gases emissions from the process. Similarly, in [130] the environmental impacts associated with bio-CH_4 production from AD are assessed through a LCA methodology. Process optimizations are also provided in [131]–[134]. The biomethane production alternative is currently generating an increasing interest, including from policymakers, who are incentivising the production of biomethane to be injected in the NG grid

and eventually be used as a fuel for the transportation sector [135]. Moreover, biomethane could be a CO2- negative source of energy, if the CO_2 produced during the upgrading process is stored underground [136]. Recent studies investigated the introduction of an upgrading unit into an existing anaerobic digestion plant to convert biogas to biomethane and found that it has a significant impact on the overall energy balance of the systems and that, moreover, a level of biomethane production exists that minimizes the emissions [137]. In [138] the feeding conditions of the AD process for maximizing biomethane production were investigated. In [139] a machine learning algorithm was developed to forecast biomethane production. In [140] the benefits generated by the production of biomethane were assessed by an economic perspective.

1.3 Literature review on waste-to-hydrogen plants

WtH_2 conversion methods can be split into thermochemical and biological techniques [141]. As for the thermochemical processes, in [142] a review of the biomass gasification process (including MSW gasification) for H_2 production is provided. In [143] a thermodynamic analysis of an integrated gasification based WtH_2 route is carried out. The analyzed system is composed of a gasifier for the treatment of dried unsorted MSW, followed by a catalytic reactor, a Water-gas Shift (WGS) unit and a Pressure Swing Adsorption (PSA) unit for pure H_2 separation. Results shows that it is possible to produce, under the operating conditions described, approximately 3 kgH_2/s. In [144] an exergetic analysis of the same system is provided, considering different types of biomasses. In [145] the results of an experimental study on biomass gasification for H_2 production are provided together with a kinetic model. The authors investigate different operating conditions and find that bio-H_2 yield is maximized at 0.2 equivalent ratio and 1000°C gasification temperature without steam addition. Similarly, in [146] an experimental study on an agricultural waste gasification system for H_2 production is carried out with CaO addition, and an increase in H_2 concentration and yield is observed. Xu *et al.* also proved the effectiveness of food-waste gasification for H_2 production from an exergetic, economic and environmental point of view [147]. Through a comparison with a system consisting of an electrolyzer powered by

photovoltaic panels or geothermal energy, Ishaq and Dincer find that the biomass gasification HPR has the highest energy and exergy efficiency [148]. In [149], the integration of gasification for H_2 production and incineration for electricity and heat production is investigated. The integrated system consists of treating a share of MSW in the incinerator to produce the thermal energy required in the gasification process and to serve a district heating. The remaining share of MSW is gasified for H_2 production. An integrated energy system is also modelled in [150]. Similarly, in [151] a multi-generation system based on waste gasification to produce H_2, power, heating-cooling and hot water is analyzed. As for the biological WtH_2 routes, in [152] a review of the biophotolysis, indirect photolysis, dark fermentation, photofermentation, and microbial electrolysis process is provided. In [153] a study focused on the dark fermentation process, in which substrates are converted by anaerobic bacteria grown in the dark, is provided. The authors investigate the most relevant operating parameter of the treatment. An interesting WtH_2 HPR is represented by the so-called Steam Biogas Reforming (SBR) route. It consists of producing H_2 from the reforming of the biogas obtained from the Anaerobic Digestion (AD) treatment of biomasses [154]. To this concern, in [155] the ecological, economic, and environmental effectiveness of the SBR route is provided. Similarly, in [156] SBR is identified as a promising low-carbon HPR, which allows for reducing overburden on NG. In [157], a simulation model of the SBR process on an industrial scale is proposed. Through the model, effect of change in biogas compositions on the performance of the SBR process are investigated.

In scientific literature, environmental comparisons between different WtH_2 routes are available. For example, in [158] a review of several renewable and non-renewable based HPRs is provided. The authors compare the alternatives based on the values of Global Warming Potential (GWP) and acidification potential (AP) indicators found in the literature. Similarly, in [159] an environmental, economic, energy and exergetic comparison is carried out between different HPRs and the GWP and AP values available in the literature are considered as indicators of the environmental performance of each process. The same indicators are used to perform an environmental comparison between different electricity-based HPRs in [160] and of different HPRs in [161], [162]. Through lifecycle assessment

methodology, different bio-H_2 routes are also compared to identify the best one in the UK contest. The authors highlight that there is a close correlation between the contribution offered by each alternative to tackling climate change and the national energy mix [163].

Chapter 2

Analytical models development and application

In this chapter, the analytical models developed to evaluate the performance of different waste-based plants for green gases or electricity production in the current energy transition phase are introduced.

First, the reference plant configurations for each alternative considered will be illustrated. Next, the analytical models developed, and the results obtained from their numerical application will be presented.

2.1 Plant configurations of waste-based plants

In this section, the plant configurations considered are illustrated with reference to the main flows (i.e., matter and energy) exchanged within the plant and with the outside environment. In addition, the main chemical reactions that are generated during treatment and that lead to the production of elements such as bio-CH_4 and H_2 are highlighted. The plants considered were divided into three categories, i.e., plants for electricity

production (section 2.1.1), plants for bio-CH_4 production (2.1.2) and plants for H_2 production (2.1.3). As will be observed in the following paragraphs, the most frequently employed WtE plants (e.g., AD, gasification) represent the starting basis in routes to produce green gases. In this regard, the description of the plant configurations will be carried out by considering, for each case under investigation, only the part that distinguishes it from an already described route.

2.1.1 Plant configurations of waste-based routes for electricity production

The plant configurations of the WtE routes considered are illustrated below. They are presented from the most common to the least common, i.e., from the most to the least commercially used. In this regard, incineration is the WtE treatment that has been available on the market for the longest time and is used in most cases to generate electricity from unsorted waste [164]. Next, the AD route is available on a commercial scale and is the most suitable for electricity production from OW [165]. Gasification, on the other hand, is a less common treatment than incineration, but is gaining increasing attention because of its performance (i.e., no combustion reaction occurs) and its versatility [166]. Finally, *flameless* oxy-combustion is a treatment still in the research and development phase, tested only in the case of pilot plants [167].

2.1.1.1 The incineration route for electricity production

The plant configuration considered for the incineration route is illustrated in Figure 15.

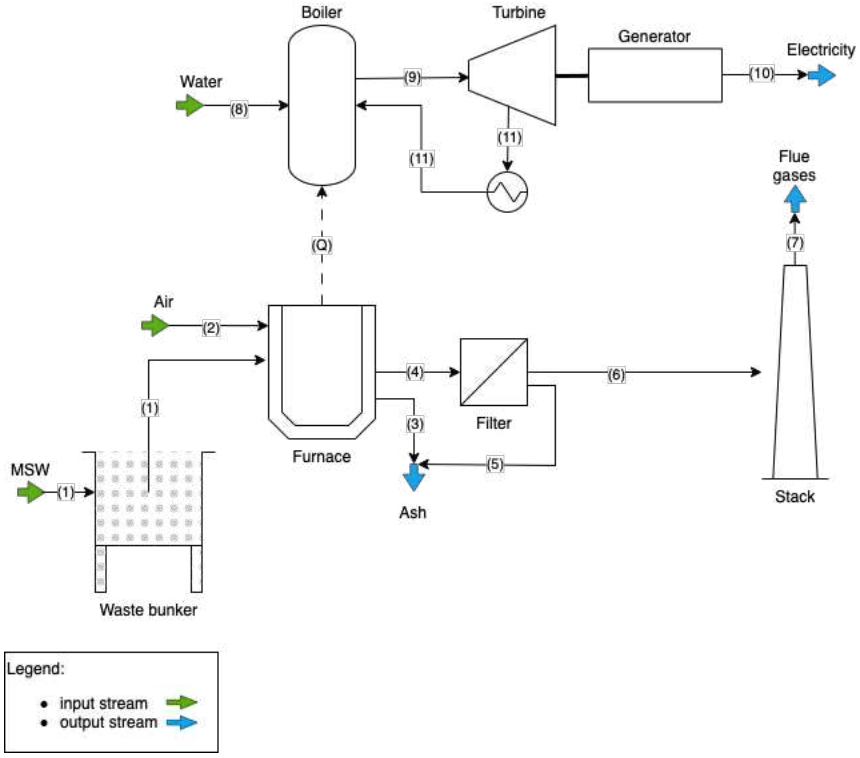

Figure 15. Plant configuration considered for the incineration route for electricity production.

As shown in Figure 15, the collected MSW (stream 1) is conveyed to a combustion chamber. Inside the reactor, the stored MSW are burnt with excess air (stream 2). Solid and gaseous by-products are generated from the combustion. The solid by-product consists of unburned products (so-called bottom ash) collected at the bottom of the reactor (stream 3). It is noteworthy that ash can be reused for different purposes, in accordance with a CE perspective (e.g., in the building sector) [168]. The gaseous by-product consists of flue gas at a temperature of 1000-1100°C [169]. The combustion flue gases are conveyed to a series of filters (stream 4) where specific additives (i.e., activated carbon, lime and sodium bicarbonate [60]) are added for dust abatement. The ashes recovered from this stage are collected along with the bottom ashes (stream 5). The purified exhaust gases are then conveyed to the stack (stream 6) and released into the atmosphere

(stream 7). Instead, the thermal energy from the flue gas is used to heat the water in a boiler (stream 8), producing steam. The steam produced (stream 9) powers a turbine connected to a current generator, which generates electricity (stream 10). Finally, after a condensation step, the steam leaving the turbine is fed back into the boiler (stream 11).

2.1.1.2 The anaerobic digestion route for electricity production

The plant configuration considered for the AD route is illustrated in Figure 16.

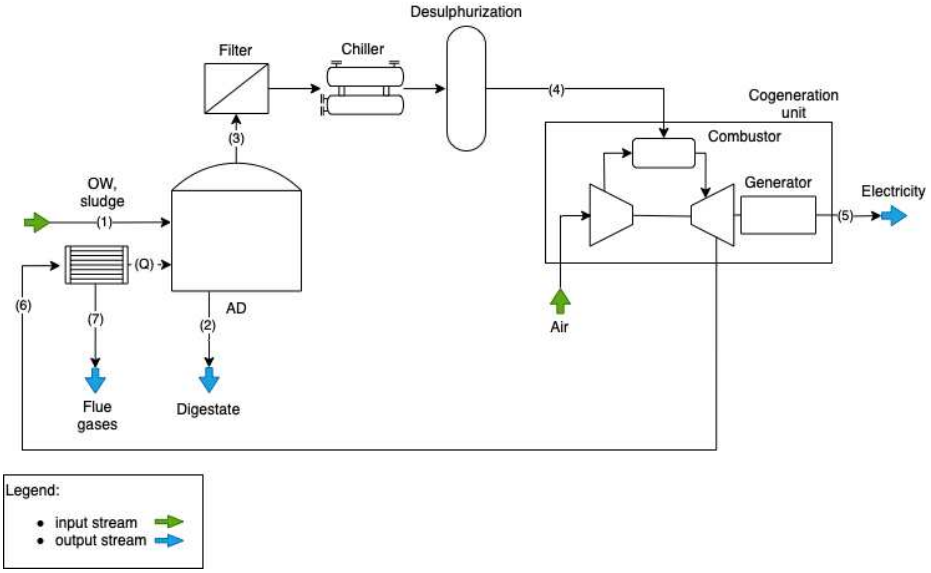

Figure 16. Plant configuration considered for the AD route for electricity production.

AD is a biological stabilisation treatment of organic matter using specific bacterial populations in an anoxic environment. For this reason, it is only possible to treat OW (including OFMSW) or biomasses, which can be viewed as a combination of carbohydrates (compounds of C, O_2, and H_2), proteins and amino acids (compounds of C, O_2, H_2, and N), and lipids (compounds of C, and H_2, with small proportions O_2) [170].

Once fed into the digester (stream 1), the waste is agitated and heated to a temperature of 40°C (i.e., to conduct a mesophilic AD process [171]). AD treatment can be seen as a sequential combination of fermentative processes. It is possible, therefore, to distinguish three phases that occur within the reactor:

- The hydrolysis phase: this phase aims to break down the complex substances within the organic matter to make them usable by the microorganisms involved in the AD process. To this concern, hydrolytic bacteria secrete extracellular enzymes that can convert carbohydrates, lipids, and proteins into sugars, long-chain fatty acids, and amino acids, respectively [172].
- The acidogenesis and acetogenesis phase: in this phase, intermediate volatile fatty acids and other compounds are produced due to the uptake of the products of the hydrolysis phase by acidogenic microorganisms [172]. To this concern, about 20% of the organic matter products are converted into acetate, 5% into H_2 and CO_2, and the remaining 75% into volatile fatty acids. Acetogenic microorganisms are responsible for further demolishing the volatile fatty acids to make more acetate and more H_2 and CO_2. They also produce the raw material to feed the homoacetogenic microorganisms, synthesising acetic acid from H_2 and CO_2 [170].
- The methanogenesis phase: in the last phase, acetoclastic methanogens convert acetate from the previous steps into CH_4 and CO_2, and hydrogenotrophic methanogens convert H_2 and CO_2 into CH_4 and H_2O [170].

The main reactions in the AD process can be expressed according to equations 1-6.

$$4H_2+CO_2 \rightarrow CH_2+H_2O \quad (1)$$

$$4HCOO^-+4H^+ \rightarrow CH_4+3CO_2+2H_2O \quad (2)$$

$$4CO+2H_2O \rightarrow CH_4+3CO_2 \quad (3)$$

$$4CH_3OH \rightarrow 3CH_4+CO_2+2H_2O \quad (4)$$

$$4(CH_3)_3N+H_2O \rightarrow 9CH_4+3CO_2+6H_2O+4NH_3 \quad (5)$$

$$CH_3COOH \rightarrow CH_4+CO_2 \quad (6)$$

At the end of the AD process, two by-products are obtained, one in the solid state and one in the gaseous state. The solid by-product, i.e., the digestate (stream 2), contains valuable elements such as C, N, P, K, Na, Ca, etc. For this reason, it can be valorised in a CE perspective, e.g., by subjecting it to thermochemical treatment for syngas production, subjecting it to further AD for biogas production, using it as a fertiliser or soil amendment, etc. [173]. Biogas, i.e., the gaseous by-product (stream 3), is almost totally composed of CH_4 and CO_2 and in smaller shares by H_2O, O_2, N_2, NH_3, and H_2 [174]. Once produced, biogas is stored in a gasometer at the top of the digester. After a purification treatment through a sand filter, a dehumidification and cooling step in a chiller and a desulphurisation treatment (useful to remove corrosive elements for the plant) [175], the biogas (stream 4) is conveyed to the cogeneration unit. It acts as fuel to produce electricity (stream 5) and heat (stream 6). The latter is used to maintain the temperature of the AD reactor, while the electricity produced is first employed to satisfy the demand of the plant (8.5-11% of the total electricity generated [175]).

2.1.1.3 The gasification route for electricity production

The configuration considered for the gasification route for electricity production is illustrated in Figure 17.

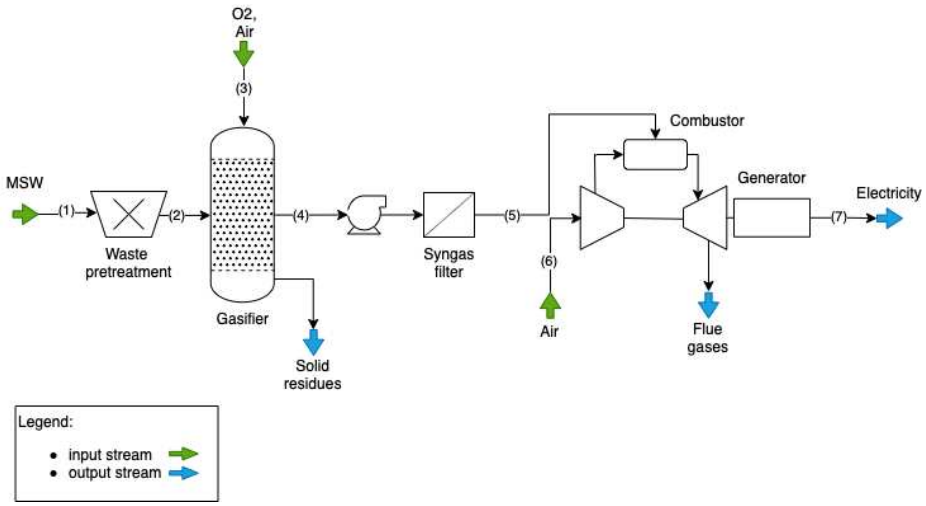

Figure 17. Plant configuration considered for the gasification route for electricity production.

The pre-treated waste (stream 1) is conveyed to the gasifier (stream 2). Chemical reactions occur within the reactor to obtain syngas, mainly composed of H_2, CO, CH_4, CO_2 and N_2 [176]. A direct gasification process, i.e., a process that employs an oxidising agent (e.g., oxygen, stream 3) that can partly oxidise the feedstock, was considered. Direct gasification is considered autothermal, i.e., the oxidation reactions produce the heat necessary for the progress of the process. For this reason, an external heat source is not required [177], [178]. The main steps in the gasification process are:

- Drying: at this stage (T=100-200°C [179]), the moisture content of MSWs evaporates without any decomposition reaction occurring.
- Pyrolysis (or devolatilization): at this stage (T=150-700°C [179]), the thermal decomposition of dried MSW takes place in the total absence of O_2. Pyrolysis reactions consist of thermal cracking, i.e., decomposition of high molecular weight hydrocarbons into lighter hydrocarbons (e.g., CH_4, H_2, CO_2, etc. [180]). The products of pyrolysis reactions are found in the liquid, solid, and gaseous state. One of the main products of the devolatilization step is tar, i.e., a complex mixture of condensable hydrocarbons that are found in

the gaseous state only due to the high temperature inside the reactor. Also, gases are produced, i.e., low molecular weight hydrocarbons and char, i.e., a solid matrix with a very high carbon content and porosity.

- Oxidation and reduction (T>700°C [180]): At this stage, the products of pyrolysis reactions result in different oxidation and reduction reactions, both homogeneous when they involve gases and heterogeneous when they involve compounds in different phases. The main products of oxidation reactions are CO_2, CO, and H_2O. The main products of the reduction reactions are H_2, CO, and CH_4 [179].

Although these phases are described and generally modelled serially, there is no clear boundary between them in a real gasification scenario, and they often occur simultaneously [179]. To this concern, the main reactions occurring inside the reactor are generally divided into char reduction reactions (equations 7-9), char oxidation reactions (equations 10-12), and gas phase reactions (equations 13-21).

$$C+H_2O \rightarrow CO+H_2 \quad (7)$$

$$C+CO_2 \rightarrow 2CO \quad (8)$$

$$C+2H_2 \rightarrow CH_4 \quad (9)$$

$$C+O_2 \rightarrow CO_2 \quad (10)$$

$$C+0.5\ O_2 \rightarrow CO \quad (11)$$

$$C+2H_2 \rightarrow CH_4 \quad (12)$$

$$CO+0.5\ O_2 \rightarrow CO_2 \quad (13)$$

$$CO+3H_2 \rightarrow CH_4+H_2O \quad (14)$$

$$2CO+2H_2 \rightarrow CH_4+CO_2 \quad (15)$$

$$CO+3H_2 \rightarrow CH_4+H_2O \quad (16)$$

$$CH_4+0.5\ O_2 \rightarrow CO+2H_2 \quad (17)$$

$$CH_4+2\ O_2 \rightarrow CO_2+H_2O \quad (18)$$

$$H_2+0.5\ O_2 \rightarrow H_2O \quad (19)$$

$$CH_4+H_2O \rightarrow CO+3H_2 \quad (20)$$

$$CO+H_2O \rightarrow CO_2+H_2 \quad (21)$$

Once obtained, the raw syngas (stream 4) is subjected to purification treatments to remove impurities and potentially corrosive compounds [181]. Subsequently, the purified syngas (stream 5) is used as fuel, together with excess air (stream 6), for electricity production (stream 7) through a gas turbine. Also in this case, the usable electricity is considered as net of plant demand.

2.1.1.4 The *flameless* oxy-combustion route for electricity production

The plant configuration considered for the *flameless* oxy-combustion route for electricity production is illustrated in Figure 18.

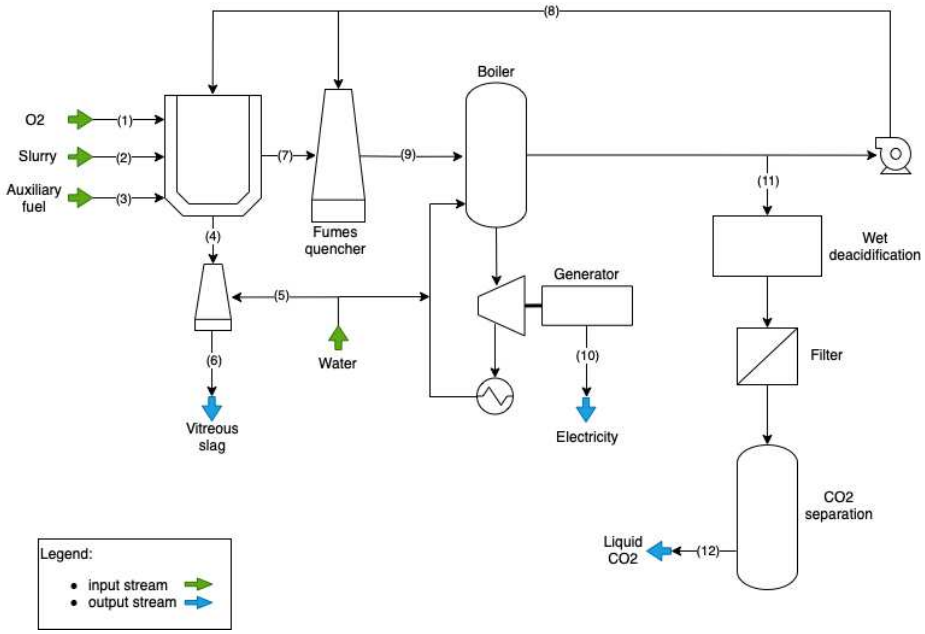

Figure 18. Plant configuration considered for the flameless oxy-combustion route for electricity production.

As it can be observed from Figure 18, the combustor feed consists of three elements: the technical O_2 of medium purity (88-94%) (stream 1), the mass of MSW pre-ground mixed in aqueous solution (i.e., slurry) (stream 2), and the auxiliary fuels (i.e., CH_4 and Very Low Sulfur Fuel Oil (VLSFO)) (stream 3). Inside the reactor, the so-called *flameless* oxy-combustion reaction occurs. It consists of a combustion reaction in which pure O_2 is used as an oxidiser instead of air [182]. This feature increases the process efficiency (the thermal efficiency of the oxy-combustion is in the range of 75-90%, with respect to the 25-60% efficiency of a traditional air-based combustion system) and reduces CO_2 emissions and NO_x formation. The *flameless* notation indicates the nature of the flame generated inside the combustion chamber. In a classic flame, indeed, the large temperature difference along the flame front is responsible for the formation of dangerous and undesirable compounds (dioxins, furans, etc). In a *flameless* combustion, the high, uniform and perfectly controllable temperature along the profile of the combustion chamber guarantees the absence of undesirable substances and compounds and the complete oxidation of the incoming carbon into CO_2, which is then recovered. *Flameless* combustion produces a transparent flame, confirming the absence of the production of dust and solid particles during the combustion process (typical instead of the traditional flame, which is non-transparent precisely because of the production of dust and solid particles during combustion and which are subsequently emitted into the atmosphere). The *flameless* oxy-combustion is favoured by the combustion chamber's pressure and high temperature (around 1300-1500°C) [183]. The MSW oxidation reactions produce two main by-products, at solid and gaseous state. The solid output (stream 6) consists of vitrified slag produced by the unburnt material in the molten state (stream 4) treated with cold water jets (stream 5). The resultant materials are inert pearls with a glassy structure, so-called vitreous slag, incorporating dangerous substances (not risky to human health and the environment [184]). The treated vitreous slag is potentially adoptable as an additive in concrete mixtures, cement raw materials, building materials, fluxes, and as a sintering additive [185]. The gaseous output consists of hot exhausts (around 1300-1500°C) (stream 7) and steam. If mixed in the fumes quencher (stream 9) with the cold fumes recovered from the blower and cooled at a temperature of 700-800°C, (stream 8) they can be used to produce electricity (stream 10) by a steam turbine. Cold fumes (at a

temperature of 200-250°C) in the output of the boiler (stream 11) are conveyed to an abatement system, including wet deacidification and a bag filter. The dedusted fumes, mainly CO_2, are then treated through a CO_2 separator and recovered as liquid CO_2 for industrial scopes (stream 12). It is noteworthy that part of the recycled flue gases is fed back into the furnace for temperature maintenance. As it can be observed, in this WtE treatment, the adoption of technical O_2 as an oxidizer allows almost all combustible material to be transformed into H_2O and CO_2. This reaction eliminates the concentration of pollutants in the flue gas [186]. Consequently, the obtained flue gas, with a high percentage of CO_2 [187], is generally purified, and the CO_2 is liquefied [188].

2.1.2 Plant configuration of the waste-based route for biomethane production

The only bio-CH_4 production route considered is based on AD treatment. However, two variants of this route were considered. The first, illustrated in Figure 19, assumes that a share of the biogas obtained is used to produce the electricity required by the plant. The second, illustrated in Figure 20, assumes that the entire volume of biogas obtained is used to produce bio-CH_4 and that, therefore, the plant's electricity demand is met through supply from the national grid.

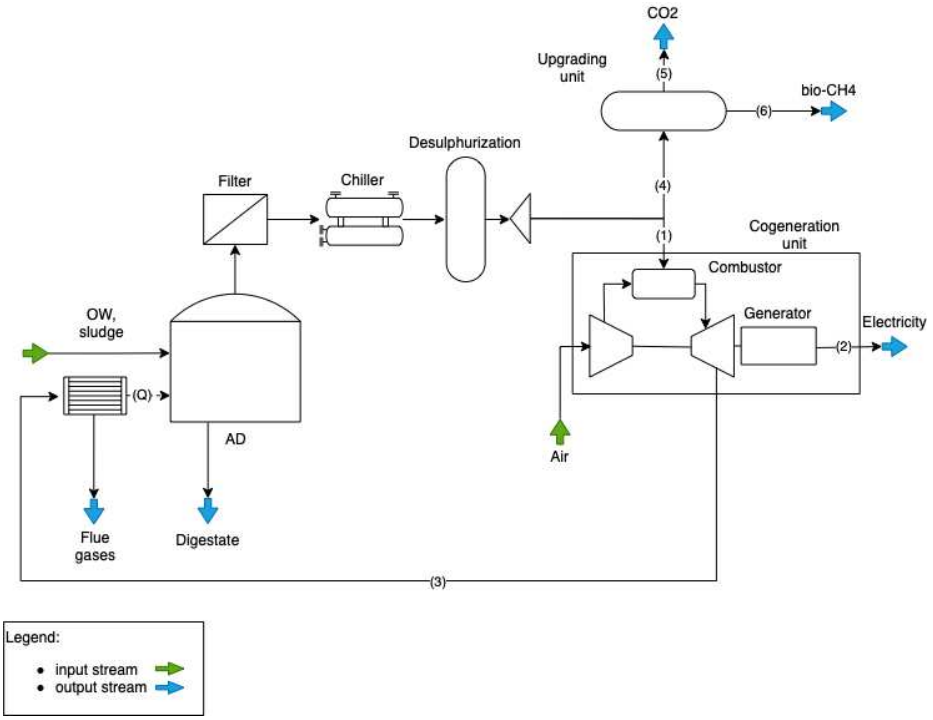

Figure 19. Plant configuration considered for the AD route for bio-CH_4 production in the case of self-production of the required electricity.

As it can be observed, the bio-CH_4 route considered coincides with the AD route for electricity production (Figure 16) up to the biogas purification stage. Subsequently, in accordance with the first considered solution (Figure 19), a share of the obtained biogas (stream 1) is used as fuel to produce electricity (stream 2) and heat (stream 3) in a cogeneration unit. The remaining share of biogas (stream 4) undergoes an upgrading treatment for CO_2 separation (the purified biogas is mainly composed of CH_4 and CO_2). In the analysed case, an upgrading step using multi-stage membrane separation treatment was considered. Membranes are generally made of CO_2-permeable materials. The biogas flow is therefore conveyed into the membranes, where the CO_2 is trapped (stream 5) and bio-CH_4, with a high degree of purity, is obtained (stream 6).

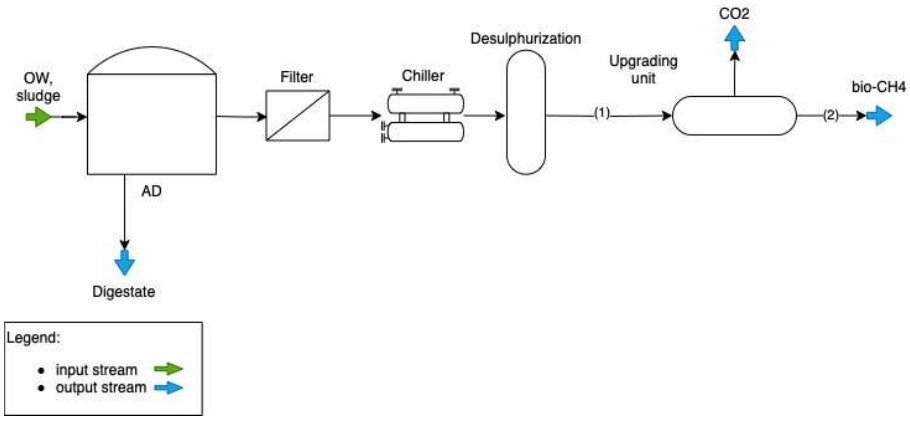

Figure 20. Plant configuration considered for the AD route for bio-CH_4 production in case all biogas obtained is used to produce bio-CH_4.

In the second case, as it can be observed from Figure 20, the entire biogas share (stream 1) is used to produce bio-CH_4 (stream 2) through the same membrane separation stage.

2.1.3 Plant configurations of waste-based routes for hydrogen production

In this section, the plant configurations of the waste-based H_2 production routes considered are illustrated. To this end, routes that are based on the main WtE treatments were analysed. Configurations of H_2 production routes based on incineration, gasification and AD will then be illustrated. It is noteworthy that while incineration is used as a WtE treatment (i.e., the electricity produced by the treatment is employed to produce H_2), in the case of gasification and AD, there is a specific treatment that allows syngas and biogas to be treated, respectively, to obtain H_2. Furthermore, two non-waste-based H_2 production routes, i.e., the SMR process and the electrolysis process, will be presented in this section. This description is necessary since these processes were considered as a reference for the performance analysis of waste-based alternatives. The SMR is indeed the most widespread fossil-based H_2 production route. The electrolysis route, as mentioned above, is the most promising route from an environmental point of view, but not yet developed on a large scale due to economic and environmental barriers.

2.1.3.1 The Steam Methane Reforming route for hydrogen production

The plant configuration considered for the SMR route is illustrated in Figure 21.

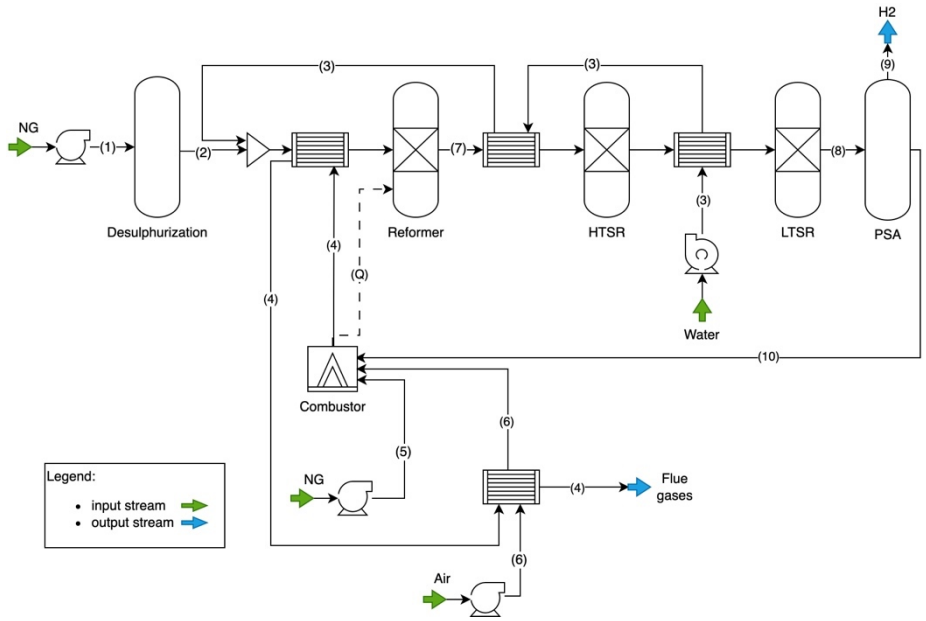

Figure 21. Plant configuration considered for the SMR route for H2 production.

As it can be observed (fig. 21), the NG (stream 1) first undergoes a desulfurization treatment via a zinc bed or hydrogenation stage, depending on the sulphur content of the feedstock. It is required because the catalysts used in the reformer and low-temperature shift reactor (LTSR) are very sensitive to this element [189]. Next, purified NG is conveyed to the reformer (stream 2) along with water vapour (stream 3) generated through heat recovered from the reformer and exhausted fumes from the combustor (stream 4). Inside the reactor, at a temperature of 700-900°C [190] and at a pressure of 10-30 bar [191], occurs the SMR reaction (eq. 20). The reforming reaction is strongly endothermic (ΔH=206.1 kJ/mol [192]). Additional NG is then burned to provide the necessary heat (stream 5) with

preheated air as the oxidiser (stream 6). Generally, reforming occurs inside tubes lined with a Ni-based catalyst [193], [194], accelerating the reaction between methane and water vapour. To increase the amount of H_2 produced, the syngas obtained (stream 7) is then sent to two reactors in series to let the carbon monoxide produced react with additional water vapour (stream 3) in the so-called Water-Gas Shift (WGS) reaction (eq. 21). The two reactors are called High-Temperature Shift Reactor (HTSR) and LTSR. The former operates at a temperature of 350-420°C and the latter at a temperature of 180-340°C [194]. The reason why reactors at different temperatures are used lies in the nature of the WGS reaction. In contrast to the steam reforming reaction, it is slightly exothermic (ΔH=-41.1 kJ/mol [193]). It is, therefore, favoured at low temperatures from a thermodynamic point of view, but it is disadvantaged from a kinetic point of view. The different operating temperatures thus serve to maximise the efficiency of H_2 production. The gas mixture (stream 8) obtained from the WGS treatment is then subjected to separation treatment by a Pressure Swing Adsorption (PSA) unit, and 99.99%vol pure H_2 is obtained (stream 9). Tail gas obtained from the separation process is fed back into the combustor as additional fuel (stream 10).

2.1.3.2 The electrolysis route for hydrogen production

Proton Exchange Membrane (PEM) technology was considered, as it is the only one currently available on a commercial scale along with alkaline technology [37]. This technology was developed to overcome the drawbacks of alkaline water electrolysis (e.g., the need for chemically aggressive hot aqueous solutions of potassium hydroxide as liquid electrolyte and operation at moderate current densities) [189], [195].

The system level of an electrolysis plant was chosen for flow assessment. Therefore, all supporting facilities for obtaining industrially usable H_2 were included (i.e., equipment for cooling and processing the H_2, converting the electricity input, and treating the water supply) [37]. A schematisation of the considered configuration can be observed in Figure 22.

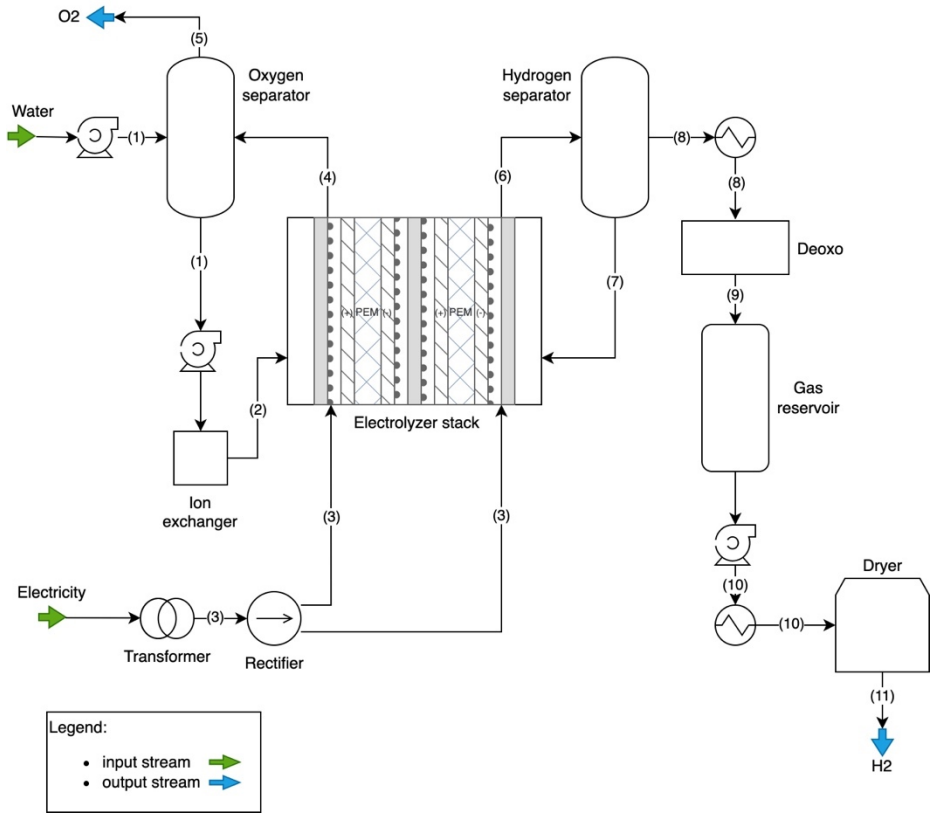

Figure 22. plant configuration considered for the electrolysis route for H2 production.

As it can be observed from Figure 22, purified water is fed into the system via circulating pumps (stream 1). Before reaching the stack, the water is conveyed to an ion exchanger to reduce its charge so as not to compromise the system's useful life [56]. Purified water (stream 2) is fed into the stack. It reaches the electrodes through two bipolar plates and a porous transport layer, distributing the flow and providing mechanical support [37]. Through the supply of an external direct current-generator (stream 3), the two electricity-driven non-spontaneous half reactions then occur, resulting in the splitting of water molecules and the generation of H_2. In this regard, the oxygen formation reaction takes place at the anode. It can be expressed according to the reaction in equation 22:

$$2H_2O \rightarrow O_2+4H^+ +4e^- \quad (22)$$

As observed, the oxidation reaction results in the formation of positive ions (i.e., H^+). They flow to the cathode through the solid membrane separating the electrodes. The membrane, generally consisting of a perfluorosulfonic acid polymer, serves to transport the ions formed, electrically isolate the electrodes, and keep the gas molecules formed separate [37]. The water-solvated protons then respond to the electric field set across the cell by the external electricity source and reach the cathode, where the H_2 formation reaction occurs [49]. It can be expressed according to equation 23 as:

$$4H^+ +4e^- \rightarrow 2H_2 \quad (23)$$

The gaseous oxygen formed at the anode is conveyed to a gravity gas separator (stream 4). The separator regulates water flow to the stack and separates the oxygen produced from the water [196]. Once separated, oxygen is removed from the system (stream 5). The H_2 gas formed is likewise conveyed to a gravity gas separator (stream 6), where the gas and water are separated. The water is subsequently fed back into the stack (stream 7), while the H_2 (stream 8), after a condensation stage, undergoes a deoxygenation treatment (stream 9) and is then conveyed to a drying stage (stream 10) after being compressed [37]. Pure H_2 at 99.99%vol is then obtained (stream 11).

2.1.3.3 The waste incineration-electrolysis route for hydrogen production

The plant configuration considered for the incineration-based H_2 production route is illustrated in Figure 23.

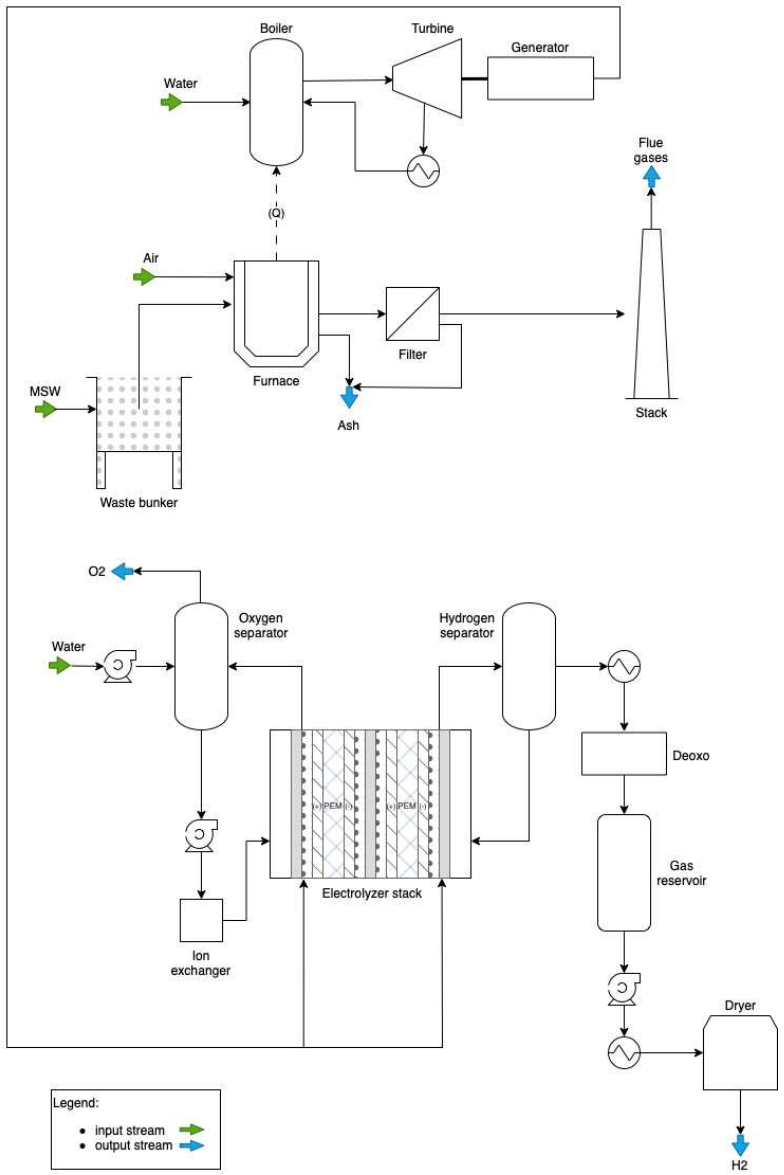

Figure 23. Plant configuration considered for the waste incineration-electrolysis route for H_2 production.

As it can be observed from the previous figure, the configuration of the present route results from the union of the two configurations considered in the case of the incineration route for electricity production (Figure 15) and in the case of the electrolysis route for H_2 production (Figure 22). Therefore, the electricity produced by the incineration treatment is used to power the electrolyser for H_2 production.

2.1.3.4 The waste gasification route for hydrogen production

The plant configuration considered for the waste gasification-based route for H_2 production is illustrated in Figure 24.

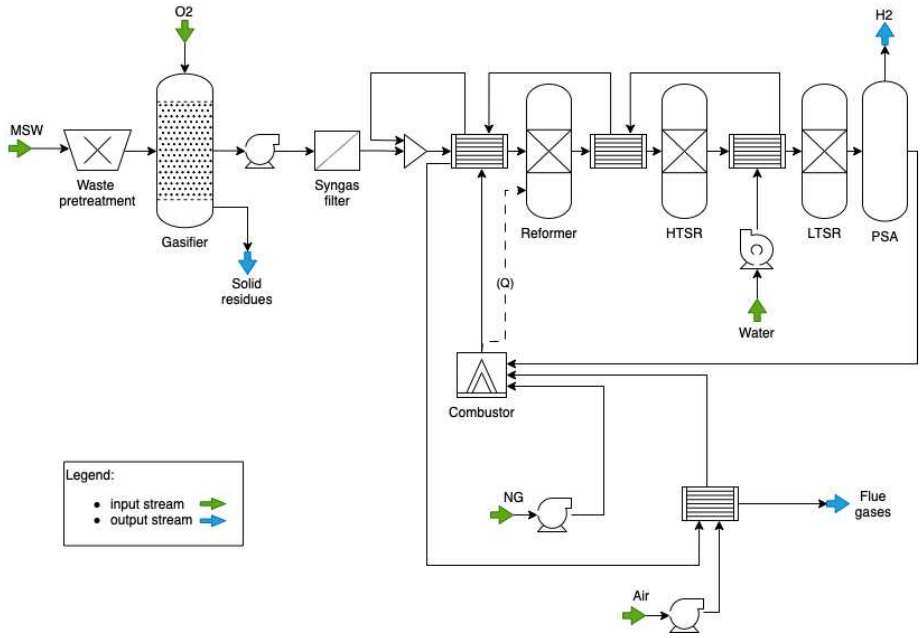

Figure 24. Plant configuration considered for the waste gasification route for H_2 production.

As it can be observed from the previous figure, this route coincides with the gasification route for electricity production up to the syngas purification stage, in accordance with Section 2.1.1.3. The purified syngas, is then subjected to a reforming process, replacing fossil NG. In this regard, the

description of the process through which H_2 is obtained can be found in Section 2.1.3.1.

2.1.3.5 The Steam Biogas Reforming route for hydrogen production

The plant configuration considered for the SBR route for H_2 production is illustrated in Figure 25.

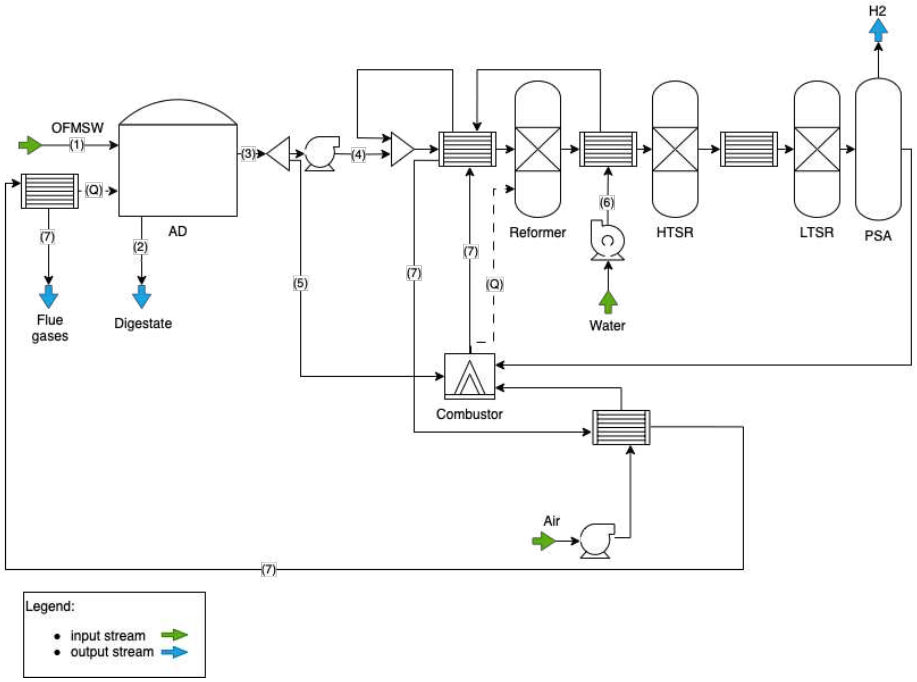

Figure 25. Plant configuration considered for the SBR route for H_2 production.

As it can be observed from the previous figure, the present route starts with the AD treatment of OW. To this concern, the treated waste (stream 1) is subjected to the AD treatment, and digestate (stream 2) and biogas (stream 3) are obtained (further information on the AD treatment can be found in Section x). Subsequently, a share of the obtained biogas is compressed and fed into the reformer (stream 4), and the remaining share is sent to the combustor to provide the necessary heat for maintaining the reforming process (stream 5). Since the biogas is mainly composed of CH_4 e CO_2,

unlike in the case of syngas, the SMR reaction (eq. 20) and the Dry Methane Reforming (DMR) reaction occur within the reformer, according to the reaction in equation 24:

$$CH_4+CO_2 \rightarrow 2CO+2H_2 \quad (24)$$

It is noteworthy that, unlike the traditional SMR process, excess water vapour (stream 6) is added to the reformer. This avoids the formation of coke during the DMR reaction and, consequently, the risk of deactivation of catalysts [197]. The H_2 production process then progresses similarly to the previous cases (i.e., WGS reactions and PSA), except for the flue gases from the combustor that are used to maintain the temperature in the AD reactor (stream 7) before being disposed into the environment.

2.2 A cost and investment analysis to compare waste-to-energy routes in the energy transition phase

In this section, the results of a cost and investment analysis carried out to identify the best WtE treatment to support the current transitional phase are illustrated. To this end, an overall yearly cost analysis was developed by varying local municipal requirements, including investment, operating, and carbon emissions costs. The overall yearly cost and the revenues, due to energy sales and tipping fees, allowed to evaluate the profitability of the investment in the plant lifetime (i.e., 20 years, according to global targets). Specifically, the investigated alternatives were incineration (Figure 15), gasification (Figure 17) and *flameless* oxy-combustion (Figure 18) treatments. A sensitivity analysis was performed to identify the most significant key drivers affecting the convenience of each considered option. The preliminary assessment allowed to identify the most sustainable WtE treatment for MSW management to support the transition phase when applied to the case study of southern Italy's the Metropolitan City of Bari.

2.2.1 Cost and investment analysis methodology

The proposed cost and investment analysis considers the environmental aspects as an operational cost to acquire emission rights through carbon pricing [198]. Consistent with this approach, the analysis doesn't consider the indirect emissions due to the procurement, extraction and transport of raw and auxiliary materials (Figure 26).

Similarly, the evaluations of indirect emissions, as well as the impact on public health due to energy supply, slag disposal, filtering systems recovery, etc., are out of the boundary of the system considered.

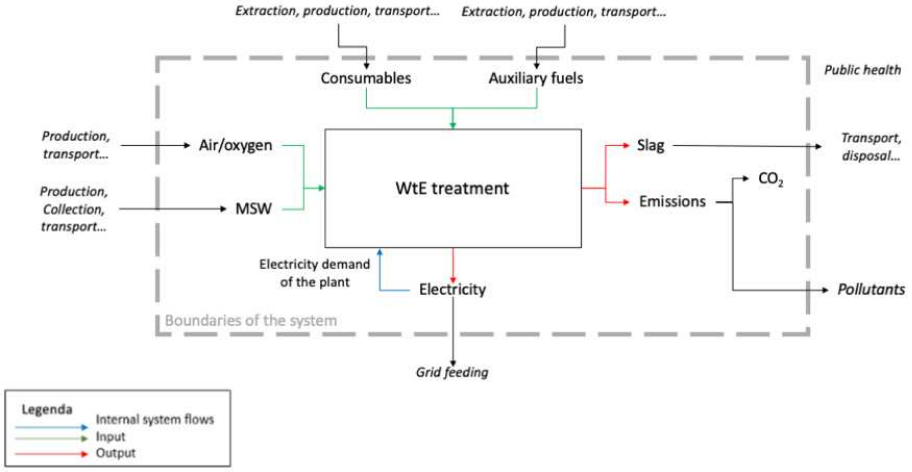

Figure 26. Boundaries of the considered system for the cost and investment analysis.

Concerning the pollutants in the flue gases, only CO_2 emissions *were considered*. Consistent with this assumption, it can be observed that in the WtE plants considered, the concentration of other pollutants and particulate matter is strongly reduced by adopting flue gas filtering and purification systems [199], [200], as shown in plant configurations (Figures 15,17,18).

As far as concerns the revenues from the CO_2 sale in the case of the flameless oxy-combustion plant, considering the amount of CO_2 produced, the related prices and the processing and storage costs required to handle the CO_2, the expected profit is negligible if compared to the profit generated from electricity sales (directly fed into the grid). Consistent with

this consideration, only the revenues from the sale of electricity have been included in the economic assessment.

Therefore, the approach proposed assumes a green-field investment on a stand-alone plant that provides to the decision-maker responsible for the installation and management of the WtE plant a preliminary evaluation on the profitability of the investment in the plant lifetime by varying local municipal requirements, including investment, operating, and carbon emissions costs.

The cost and investment analysis of the three proposed technologies consists of defining an overall yearly cost ($C_{tot}(q)$) including economic (i.e., investment, operation and maintenance costs) and carbon emissions costs. The MSW annual capacity to be treated (q [t_{MSW}/year]) depends on local municipal requirements. To this concern, a standard size (Q_{std} [t_{MSW}/year]) was set for each investigated WtE treatment. In other words, the Q_{std}-parameter defines the maximum annual capacity to treat MSW of a specific plant. The MSW annual capacity assumed is Q_{std}=1E5 [t_{MSW}/year] for all WtE treatments [201] [202]. In case the yearly amount of MSW to be treated exceeds the given Q_{std}, a significant investment is needed to face the installation of a new thermal utility (C_{ext}). The effect due to possible economies of scale was quantified by assuming a scaling k-coefficient equal to 0.6 [201]. Table 1 summarises the main items' costs with the corresponding notations.

Table 1. List of cost items included in the total cost function.

Cost item	Description	Cost type	Notation
Annual investment cost	Investment costs due to acquisition, construction and installation of industrial systems (greenfield project).	Fixed [€/year]	C_{inv}
Investment cost for plant size extension	Investment cost due to thermal facilities acquisition to increase the plant's annual capacity.	Fixed [€/year]	C_{ext}
Maintenance cost	Annual cost for the plant maintenance.	Fixed [€/year]	C_{m}

Consumables	Cost of additive materials required by the MSW treatments (e.g., oxygen, ammonia, auxiliary fuel, etc.).	Variable [€/t_{MSW}]	c_{cons}
Labour	Labour costs to manage the plant operations.	Variable [€/t_{MSW}]	c_{lab}
Solid by-product disposal	Cost due to disposal of solid by-products produced by MSW treatments (e.g. slag, ash, baking soda, etc.)	Variable [€/t_{MSW}]	c_{SbP}
CO_2 emissions	Cost due to CO_2 emitted (i.e., carbon tax).	Variable [€/t_{MSW}]	c_{em}

Fixed costs were evaluated considering the equipment depreciation period, assuming a given available capacity per year. Variable costs were assessed considering the materials needed to treat each tonne of MSW.

Assuming the items cost shown in Table 1, the WtE treatment $C_{tot}(q)$ ([€/year]) as a function of the annual capacity of the MSW (q) to be treated, is calculated by equation 25.

$$C_{tot}(q)=\alpha+\beta\left((n-1)\cdot Q_{std}\right)+C_{ext}(n-1)\sum_{i=1}^{n-1}k^i+\beta\left(q-(n-1)\cdot Q_{std}\right) \quad (25)$$

with n (n∈N; n≥1) that identifies the upper integer of the ratio between the MSW annual capacity and the maximum MSW annual capacity to be treated for a specific plant (eq. 26)

$$n=\left\lceil\frac{q}{Q_{std}}\right\rceil \text{ s.t. } q>0; \quad (26)$$

where α and β depend on equations 27 and 28, respectively.

$$\alpha=C_{inv}+C_m \ [€/year] \quad (27)$$

$$\beta=c_{cons}+c_{lab}+c_{SbP}+c_{em} \ [€/t_{MSW}] \quad (28)$$

Given C_{inv} and C_m, the other costs are estimated according to equations 29-31.

$$c_{cons}=q_{cons}p_{cons} \quad [€/t_{MSW}] \tag{29}$$

$$c_{SbP}=q_{SbP}p_{SbP} \quad [€/t_{MSW}] \tag{30}$$

$$c_{em}=q_{em}p_{em} \quad [€/t_{MSW}] \tag{31}$$

where q_{cons}, q_{SbP}, q_{em}, identify the amount of consumables, solid by-products, and CO_2 emissions, respectively, produced or needed to treat each MSW tonne . Similarly, p_{cons} and p_{SbP} identify the price of consumables and solid by-products disposal. The p_{em}-parameter represents the economic value assigned to the local carbon tax.

As an extended time period (i.e., twenty years) is considered, and a greenfield investment condition was assumed, the method of the Net Present Value (NPV)(eq. 32), was adopted to assess the investment profitability of each WtE treatment. In this case, considering the plant's entire lifetime, the NPV leads to identifying the investment's capability in WtE treatments to generate money-market liquidity.

$$NPV=\sum_{t=0}^{N}\frac{CF_t}{(1+r)^t} \quad [€] \tag{32}$$

Where:

- $t=0,1,\ldots,N$ [year] is the lifetime of the WtE plant.
- CF_t [€/year] is the cash flow generated at year *t* by choosing a WtE alternative.
- r [%] is the discount rate, i.e., the return value foregone by choosing a WtE alternative.

Similarly, the pay-back period time (PBPT) of the investment, corresponding to the time at which the investment starts to generate monetary liquidity, regarding the entire investment period, was estimated according to equation 33:

$$PBPT=t \in \{0,1,\ldots,N\} \ni \ | \quad \sum_{t=0}^{N}\frac{CF_t}{(1+r)^t}=0 \tag{33}$$

For all the considered WtE treatments, the initial investment outlay was assumed to be fully realised at t=0. The corresponding yearly costs were estimated according to equation 25.

As far as concerns the revenues generated by the WtE plants, the incomes from electricity sales (paid by the electricity supplier), and the tipping fee (paid by the municipality to treat MSW) were estimated according to equations 34 and 35.

$$r_e = q_e p_e q \ [€/year] \quad (34)$$

$$r_{t_{fee}} = t_{fee} q \ [€/year] \quad (35)$$

where q_e is the amount of electricity generated per each processed MSW tonne, and t_{fee} is the price paid by the municipality to treat one tonne of MSW.

2.2.2 Numerical application of the cost and investment analysis methodology

The most cost-effective WtE treatment to manage the MSW produced in the Metropolitan City of Bari was identified through the methodology presented in Section 2.2.1). The Metropolitan City of Bari is in the Apulia region in Southern Italy. In 2019, it had a population of 1.3 million inhabitants. MSW production for the same year was around 580000 t, with a per capita production of 463 [kg_{MSW}/(in*year)] [203]. The MSW production from 2011 to 2019 in this area decreased, from 650000 to 580000 t/year, showing a reduction of about 10% (fig. 27).

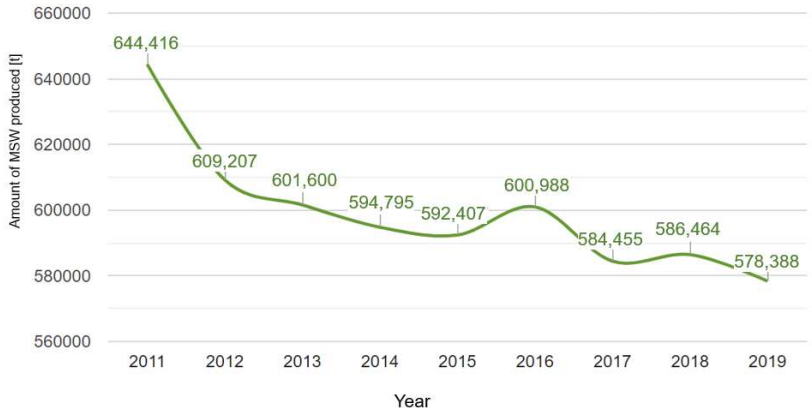

Figure 27. Production of yearly MSW for the Metropolitan City of Bari. Adapted from [203].

Considering the target on the percentage of separate collection and recycling of MSW set by the Legislative Decree no. 152/2006 issued by the Italian Government [204], the Metropolitan City of Bari would ensure a percentage of separate collection of 65% within 2012, December 31st. In 2019, the rate of separate collection for the province of Bari was 57.85% [203] (figure 28), which means about 10% less than the expected target. In 2012, about 20% of the separate collection was achieved.

Figure 28. Actual annual separate collection percentage data for the Metropolitan City of Bari. Adapted from [203].

Consistently with Directive 2008/98 of the European Commission, a local target of 55% of waste recycling within 2025 was set [60]. A share of 47% was currently achieved [203], which is a value far from the objectives set at the European level. Therefore, the amount of MSW that should be treated by adopting a WtE solution in the Metropolitan city of Bari is 53% of the total MSW produced, i.e., 306546 t/year.

The cost items corresponding to each of the three WtE alternatives were assumed according to data available in the scientific literature (Tables 2 and 3). In the case of the most innovative technology (i.e., *flameless* oxy-combustion), the investment estimation was identified, assuming an investment cost of 7.69 M€ per each MWe net produced [188], considering that a plant allows treating 1E5 [tMSW/year] of MSW, produces 10 Mwe [205]. Although, in this research, the *flameless* oxy-combustion is considered the most innovative technology, this kind of treatment is largely adopted to produce electricity and heat from coal and low-ranking fuel [206]. Therefore, no further costs due to technology immaturity have been considered. The investment costs for incineration and gasification plants can vary significantly from country to country. Therefore, the average values of the ranges given in [201] have been considered. The investment costs were estimated considering a useful plant life of twenty years and an interest rate of 3.5%.

Table 2. Yearly investment cost due to acquisition, construction and installation of industrial systems (greenfield project) and labour costs to manage the plant operations.

	Cost	**Incineration**	**Gasification**	***Flameless* oxy-combustion**
C_{inv}	M€/year	4.3 [201]	4.95 [201]	5.2 [188]
c_{lab}	€/t_{MSW}		8 [207]	

According to [207]' the annual cost for the plant maintenance (C_m) and the investment costs for plant size extension (C_{ext}) were identified to be used in equations 36 and 37.

$$C_m = 0.025 \cdot C_{inv} \text{ [€/year]} \quad (36)$$

$$C_{ext} = 0.55 \cdot C_{inv} \text{ [€/year]} \quad (37)$$

Table 3. Amount of consumable, solid by-products, emissions and electricity required/produced to treat 1 ton of MSW.

Amount required		Incineration	Gasification	Flameless oxy-combustion
q_{cons}	[t]	0.01 [208]	0.03 [208]	0.04 (CH_4) 0.01 (VLSFO) 0.5625 (O_2)
q_{SbP}	[t]	0.2 [209]	0.14 [209]	0.25
q_{em}	[t_{CO2}]	0.95 [208]	0.69 [210]	0 [186], [188]
q_e	[MWh]	0.544 [209]	0.685 [209]	0.70 [205]

Table 4 identifies the economic parameters to be used in equations 29-31. Their values allowed to identify the overall cost ($C_{tot}(q)$) coming from the treatment of one tonne of MSW for each WtE alternative technology. In the case of *flameless* oxy-combustion, the amount of consumables and solid by-products were assumed in accordance with available experimental data.

Table 4. The economic value of the parameters considered for the total cost assessment.

Parameter		Incineration	Gasification	Flameless oxy-combustion
p_{cons}	[€/t	800 [211]	800 [211]	300 (CH_4) 400 (VLSFO) 47 (O_2)
p_{SbP}	[€/t]		120	
p_{em}	[€/t_{CO2}]		42 [198]	

The variable costs associated with one tonne of MSW have been reported in Figure 29 for the three WtE alternatives.

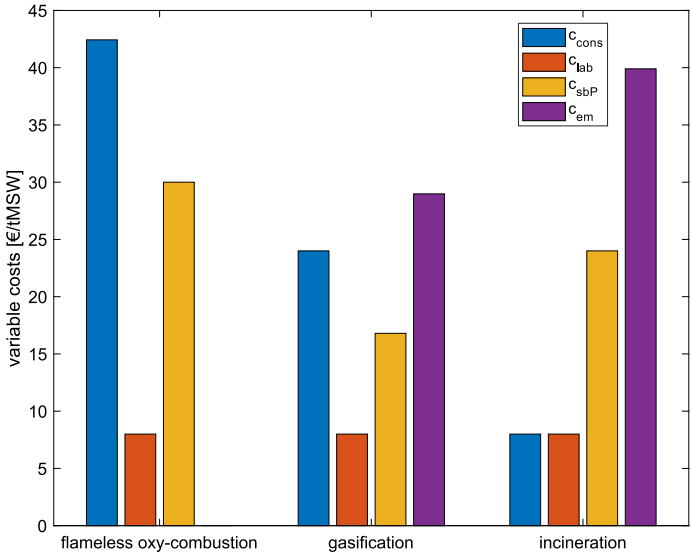

Figure 29. Values of the variable costs for the three considered WtE alternative technologies.

The values assumed in the case study to estimate the NPV in three WtE treatments are summarized in Table 5. The evaluation of the investment over a period of twenty years, i.e., a period equal to the useful lifetime of the plants, was assumed. Moreover, the time horizon identified depends on the current MSW management strategies that may be subjected to changes in the long period.

Table 5. Input parameters for investment evaluation

Parameter	Unit	Value
q	[t_{MSW}/year]	306,546
N	[year]	20
r	[%]	10%
p_e	[€/MWh]	84 [211]
t_{fee}	[€/t_{MSW}]	83 [212]
Income taxes	[%]	35%

The cash flow statements for the incineration, gasification and flameless oxy-combustion treatment are shown in Tables 6-8. For each period considered, the value of CF_t, cumulated cash flow (CCF), discounted cash flow (DCF) and cumulated discounted cash flow (CDCF) are provided. According to the performed analysis, the NPV identified for the gasification is equal to 21.7 M€, higher than 19.3 M€ for the flameless oxy-combustion and higher than 6.48 M€ for the incineration.

Although the most cost-effective treatment is incineration, looking at the highest NPV value, gasification is the most profitable both from an economical and environmental perspective. This result mainly depends on plant investment and revenue values. Therefore, it is possible to conclude that gasification is the most sustainable solution for the MSW management for the Metropolitan City of Bari, between the WtE alternatives.

Table 6. Cash flow statement of the incineration treatment [M€]

	t=0	t=1	t=2	t=3	t=4	t=5	t=6	t=7	t=8	t=9	t=10	t=11	t=12	t=13	t=14	t=15	t=16	t=17	t=18	t=19	t=20
Investment	-88.9	0.00	0.00	0.00	0.00	0.00	0.00	0.00	0.00	0.00	0.00	0.00	0.00	0.00	0.00	0.00	0.00	0.00	0.00	0.00	0.00
$\mathbf{r_e}$	0.00	14.0	14.0	14.0	14.0	14.0	14.0	14.0	14.0	14.0	14.0	14.0	14.0	14.0	14.0	14.0	14.0	14.0	14.0	14.0	14.0
$\mathbf{r_{t_{fee}}}$	0.00	25.4	25.4	25.4	25.4	25.4	25.4	25.4	25.4	25.4	25.4	25.4	25.4	25.4	25.4	25.4	25.4	25.4	25.4	25.4	25.4
$\mathbf{c_{lab}}$	0.00	-2.45	-2.45	-2.45	-2.45	-2.45	-2.45	-2.45	-2.45	-2.45	-2.45	-2.45	-2.45	-2.45	-2.45	-2.45	-2.45	-2.45	-2.45	-2.45	-2.45
$\mathbf{C_m}$	0.00	-0.111	-0.111	-0.111	-0.111	-0.111	-0.111	-0.111	-0.111	-0.111	-0.111	-0.111	-0.111	-0.111	-0.111	-0.111	-0.111	-0.111	-0.111	-0.111	-0.111
$\mathbf{c_{cons}}$	0.00	-2.45	-2.45	-2.45	-2.45	-2.45	-2.45	-2.45	-2.45	-2.45	-2.45	-2.45	-2.45	-2.45	-2.45	-2.45	-2.45	-2.45	-2.45	-2.45	-2.45
$\mathbf{c_{SbP}}$	0.00	-7.36	-7.36	-7.36	-7.36	-7.36	-7.36	-7.36	-7.36	-7.36	-7.36	-7.36	-7.36	-7.36	-7.36	-7.36	-7.36	-7.36	-7.36	-7.36	-7.36
$\mathbf{c_{em}}$	0.00	-12.2	-12.2	-12.2	-12.2	-12.2	-12.2	-12.2	-12.2	-12.2	-12.2	-12.2	-12.2	-12.2	-12.2	-12.2	-12.2	-12.2	-12.2	-12.2	-12.2
Depreciation	0.00	-4.45	-4.45	-4.45	-4.45	-4.45	-4.45	-4.45	-4.45	-4.45	-4.45	-4.45	-4.45	-4.45	-4.45	-4.45	-4.45	-4.45	-4.45	-4.45	-4.45
Gross profit	0.00	10.4	10.4	10.4	10.4	10.4	10.4	10.4	10.4	10.4	10.4	10.4	10.4	10.4	10.4	10.4	10.4	10.4	10.4	10.4	10.4
Net profit	0.00	6.76	6.76	6.76	6.76	6.76	6.76	6.76	6.76	6.76	6.76	6.76	6.76	6.76	6.76	6.76	6.76	6.76	6.76	6.76	6.76
Depreciation	0.00	4.45	4.45	4.45	4.45	4.45	4.45	4.45	4.45	4.45	4.45	4.45	4.45	4.45	4.45	4.45	4.45	4.45	4.45	4.45	4.45
CF	-88.9	11.2	11.2	11.2	11.2	11.2	11.2	11.2	11.2	11.2	11.2	11.2	11.2	11.2	11.2	11.2	11.2	11.2	11.2	11.2	11.2
CCF	-88.9	-77.7	-66.5	-55.3	-44.1	-32.9	-21.7	-10.5	0.727	11.9	23.1	34.3	45.6	56.8	68	79.2	90.4	102	113	124	135
DCF	-88.9	10.2	9.26	8.42	7.65	6.96	6.33	5.75	5.23	4.75	4.32	3.9	3.57	3.25	2.95	2.68	2.44	2.22	2.02	1.83	1.67
CDCF	-88.9	-78.7	-69.5	-61.1	-53.4	-46.4	-40.1	-34.4	-29.1	-24.4	-20.1	-16.1	-12.6	-9.32	-6.37	-3.69	-1.25	0.969	2.98	4.82	6.48

Table 7. Cash flow statement of the gasification treatment [M€]

	t=0	t=1	t=2	t=3	t=4	t=5	t=6	t=7	t=8	t=9	t=10	t=11	t=12	t=13	t=14	t=15	t=16	t=17	t=18	t=19	t=20
Investment	-98.8	0.00	0.00	0.00	0.00	0.00	0.00	0.00	0.00	0.00	0.00	0.00	0.00	0.00	0.00	0.00	0.00	0.00	0.00	0.00	0.00
$\mathbf{r_e}$	0.00	17.6	17.6	17.6	17.6	17.6	17.6	17.6	17.6	17.6	17.6	17.6	17.6	17.6	17.6	17.6	17.6	17.6	17.6	17.6	17.6
$\mathbf{r_{tfee}}$	0.00	25.4	25.4	25.4	25.4	25.4	25.4	25.4	25.4	25.4	25.4	25.4	25.4	25.4	25.4	25.4	25.4	25.4	25.4	25.4	25.4
$\mathbf{c_{lab}}$	0.00	-2.45	-2.45	-2.45	-2.45	-2.45	-2.45	-2.45	-2.45	-2.45	-2.45	-2.45	-2.45	-2.45	-2.45	-2.45	-2.45	-2.45	-2.45	-2.45	-2.45
$\mathbf{C_m}$	0.00	-0.124	-0.124	-0.124	-0.124	-0.124	-0.124	-0.124	-0.124	-0.124	-0.124	-0.124	-0.124	-0.124	-0.124	-0.124	-0.124	-0.124	-0.124	-0.124	-0.124
$\mathbf{c_{cons}}$	0.00	-7.36	-7.36	-7.36	-7.36	-7.36	-7.36	-7.36	-7.36	-7.36	-7.36	-7.36	-7.36	-7.36	-7.36	-7.36	-7.36	-7.36	-7.36	-7.36	-7.36
$\mathbf{c_{SbP}}$	0.00	-5.15	-5.15	-5.15	-5.15	-5.15	-5.15	-5.15	-5.15	-5.15	-5.15	-5.15	-5.15	-5.15	-5.15	-5.15	-5.15	-5.15	-5.15	-5.15	-5.15
$\mathbf{c_{em}}$	0.00	-8.88	-8.88	-8.88	-8.88	-8.88	-8.88	-8.88	-8.88	-8.88	-8.88	-8.88	-8.88	-8.88	-8.88	-8.88	-8.88	-8.88	-8.88	-8.88	-8.88
Depreciation	0.00	-4.94	-4.94	-4.94	-4.94	-4.94	-4.94	-4.94	-4.94	-4.94	-4.94	-4.94	-4.94	-4.94	-4.94	-4.94	-4.94	-4.94	-4.94	-4.94	-4.94
Gross profit	0.00	14.2	14.2	14.2	14.2	14.2	14.2	14.2	14.2	14.2	14.2	14.2	14.2	14.2	14.2	14.2	14.2	14.2	14.2	14.2	14.2
Net profit	0.00	9.21	9.21	9.21	9.21	9.21	9.21	9.21	9.21	9.21	9.21	9.21	9.21	9.21	9.21	9.21	9.21	9.21	9.21	9.21	9.21
Depreciation	0.00	4.94	4.94	4.94	4.94	4.94	4.94	4.94	4.94	4.94	4.94	4.94	4.94	4.94	4.94	4.94	4.94	4.94	4.94	4.94	4.94
CF	-98.8	14.2	14.2	14.2	14.2	14.2	14.2	14.2	14.2	14.2	14.2	14.2	14.2	14.2	14.2	14.2	14.2	14.2	14.2	14.2	14.2
CCF	-98.8	-84.7	-70.5	-56.3	-42.2	-28.00	-13.9	0.271	14.4	28.6	42.7	56.9	71.0	85.2	99.3	114	128	142	156	170	184
DCF	-98.8	12.9	11.7	10.6	9.67	8.79	7.99	7.26	6.60	6.00	5.46	4.96	4.51	4.10	3.73	3.39	3.08	2.80	2.55	2.31	2.10
CDCF	-98.8	-85.9	-74.2	-63.6	-53.9	-45.2	-37.2	-29.9	-23.3	-17.3	-11.8	-6.88	-2.37	1.73	5.46	8.85	11.9	14.7	17.3	19.6	21.7

Table 8. Cash flow statement of the *flameless* oxy-combustion treatment [M€]

	t=0	t=1	t=2	t=3	t=4	t=5	t=6	t=7	t=8	t=9	t=10	t=11	t=12	t=13	t=14	t=15	t=16	t=17	t=18	t=19	t=20
Investment	-98.8	0.00	0.00	0.00	0.00	0.00	0.00	0.00	0.00	0.00	0.00	0.00	0.00	0.00	0.00	0.00	0.00	0.00	0.00	0.00	0.00
$\mathbf{r_e}$	0.00	18	18	18	18	18	18	18	18	18	18	18	18	18	18	18	18	18	18	18	18
$\mathbf{r_{tfee}}$	0.00	25.4	25.4	25.4	25.4	25.4	25.4	25.4	25.4	25.4	25.4	25.4	25.4	25.4	25.4	25.4	25.4	25.4	25.4	25.4	25.4
$\mathbf{c_{lab}}$	0.00	-2.45	-2.45	-2.45	-2.45	-2.45	-2.45	-2.45	-2.45	-2.45	-2.45	-2.45	-2.45	-2.45	-2.45	-2.45	-2.45	-2.45	-2.45	-2.45	-2.45
$\mathbf{C_m}$	0.00	-0.124	-0.124	-0.124	-0.124	-0.124	-0.124	-0.124	-0.124	-0.124	-0.124	-0.124	-0.124	-0.124	-0.124	-0.124	-0.124	-0.124	-0.124	-0.124	-0.124
$\mathbf{c_{cons}}$	0.00	-13.0	-13.0	-13.0	-13.0	-13.0	-13.0	-13.0	-13.0	-13.0	-13.0	-13.0	-13.0	-13.0	-13.0	-13.0	-13.0	-13.0	-13.0	-13.0	-13.0
$\mathbf{c_{SbP}}$	0.00	-9.20	-9.20	-9.20	-9.20	-9.20	-9.20	-9.20	-9.20	-9.20	-9.20	-9.20	-9.20	-9.20	-9.20	-9.20	-9.20	-9.20	-9.20	-9.20	-9.20
$\mathbf{c_{em}}$	0.00	0.00	0.00	0.00	0.00	0.00	0.00	0.00	0.00	0.00	0.00	0.00	0.00	0.00	0.00	0.00	0.00	0.00	0.00	0.00	0.00
Depreciation	0.00	-4.94	-4.94	-4.94	-4.94	-4.94	-4.94	-4.94	-4.94	-4.94	-4.94	-4.94	-4.94	-4.94	-4.94	-4.94	-4.94	-4.94	-4.94	-4.94	-4.94
Gross profit	0.00	13.7	13.7	13.7	13.7	13.7	13.7	13.7	13.7	13.7	13.7	13.7	13.7	13.7	13.7	13.7	13.7	13.7	13.7	13.7	13.7
Net profit	0.00	8.94	8.94	8.94	8.94	8.94	8.94	8.94	8.94	8.94	8.94	8.94	8.94	8.94	8.94	8.94	8.94	8.94	8.94	8.94	8.94
Depreciation	0.00	4.94	4.94	4.94	4.94	4.94	4.94	4.94	4.94	4.94	4.94	4.94	4.94	4.94	4.94	4.94	4.94	4.94	4.94	4.94	4.94
CF	-98.8	13.9	13.9	13.9	13.9	13.9	13.9	13.9	13.9	13.9	13.9	13.9	13.9	13.9	13.9	13.9	13.9	13.9	13.9	13.9	13.9
CCF	-98.8	-84.9	-71.1	-57.2	-43.3	-29.4	-15.6	-1.68	12.2	26.1	39.9	53.8	67.7	81.6	95.5	109	123	137	151	165	179
DCF	-98.8	12.6	11.5	10.4	9.48	8.62	7.83	7.12	6.47	5.88	5.35	4.86	4.42	4.02	3.65	3.32	3.02	2.75	2.50	2.27	2.06
CDCF	-98.8	-86.2	-74.7	-64.3	-54.8	-46.2	-38.4	-31.3	-24.8	-18.9	-13.5	-8.68	-4.26	-0.244	3.41	6.73	9.75	12.5	15.0	17.3	19.3

The overall yearly cost of the three WtE treatments depending on the MSW annual capacity to be treated (q) is shown below (fig. 30). In case no waste is treated, total costs of about 4,410 k€/year, 5,070 k€/year, and 5,200 k€/year were estimated for the incineration, gasification, and *flameless* oxy-combustion, respectively. The total cost increases, according to a step function consistent with (eq. 25), when the treated MSW increase. If the MSW to be treated matches the maximum annual capacity of the plants (i.e., 400,000 t/year), a cost of about 39.070 M€/year, 39.279 M€/year, 40.735 M€/year was estimated for the incineration, gasification, and *flameless* oxy-combustion, respectively. An average increase of 714% of the overall cost was estimated compared to the zero-waste treatment condition.

The lowest costs due to plant extension were identified for incineration. They are lower than 13.2% and 20.9% compared to gasification and flameless oxy-combustion. The effect due to scale economies highlights a non-linear reduction of plant extension cost with increasing MSW to be treated.

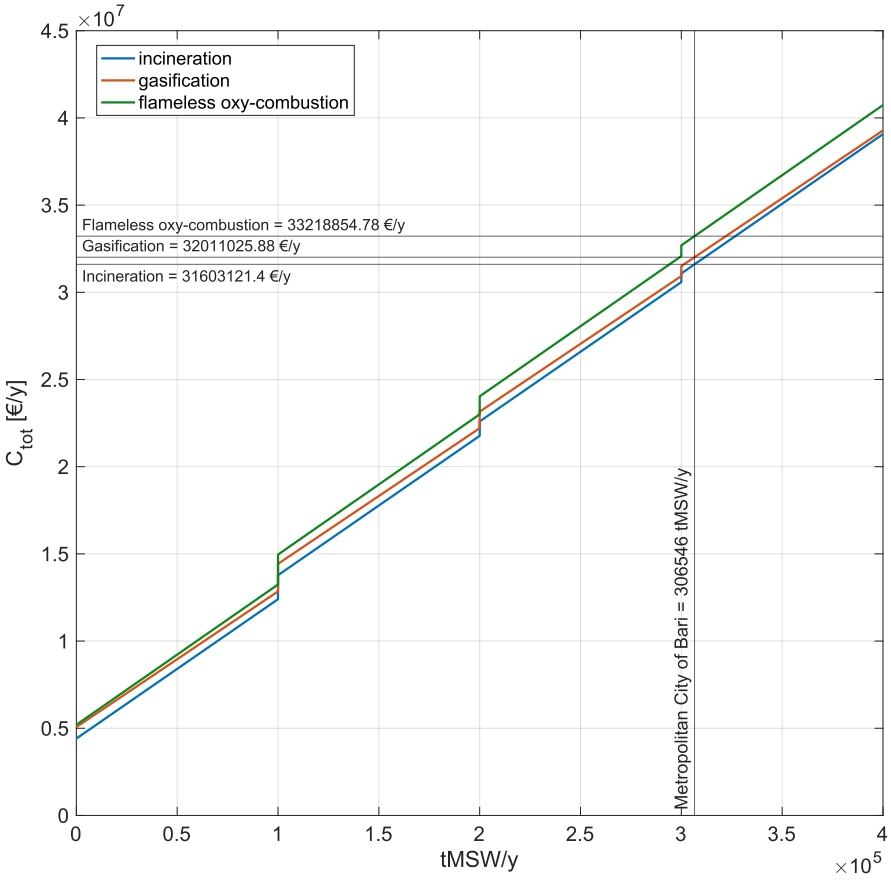

Figure 30. Overall yearly cost estimated by changing the annual capacity of the MSW to be treated.

The comparison among the slopes of the total cost functions represented in fig. 30 shows that the highest slope is identified for the *flameless* oxy-combustion case. The slope is related to the variable costs of each WtE alternative, depending on variable costs supported to manage the WtE plants. In this case, the variable costs estimated for the *flameless* oxy-combustion, incineration, and gasification amount to 80.43 €/t_{MSW}, 79.9 €/t_{MSW}, and 77.78 €/t_{MSW}, respectively. Although the variable costs of the *flameless* oxy-combustion are independent of the costs due to carbon emissions, the highest consumable costs lead to increasing the variable costs

of this WtE treatment compared to other alternatives (fig. 29). On the contrary, the highest emission value generated by the incineration treatment (i.e., 0.95 t_{CO2}/to_{MSW}) affected the variable cost of this WtE treatment. From this point of view, although gasification generates direct emissions, this alternative's lowest consumables cost leads to the lowest variable costs.

In the case of the Metropolitan City of Bari, the amount of MSW yearly produced is 306,546 t. Therefore, the overall yearly cost estimated for the incineration is lower than gasification and *flameless* oxy-combustion by around 1.3% and 5%, respectively. In this case, the revenues, due to energy sales and tipping fees, allowed to evaluate the profitability of the three investment options in the plant lifetime (fig. 31). The *flameless* oxy-combustion technology ensures the highest incomes due to the best efficiency in energy recovery. Nevertheless, the highest costs related to this WtE treatment reduce the profitability of the investment compared to gasification (i.e., 12.4%) and incineration (i.e., 64.5%).

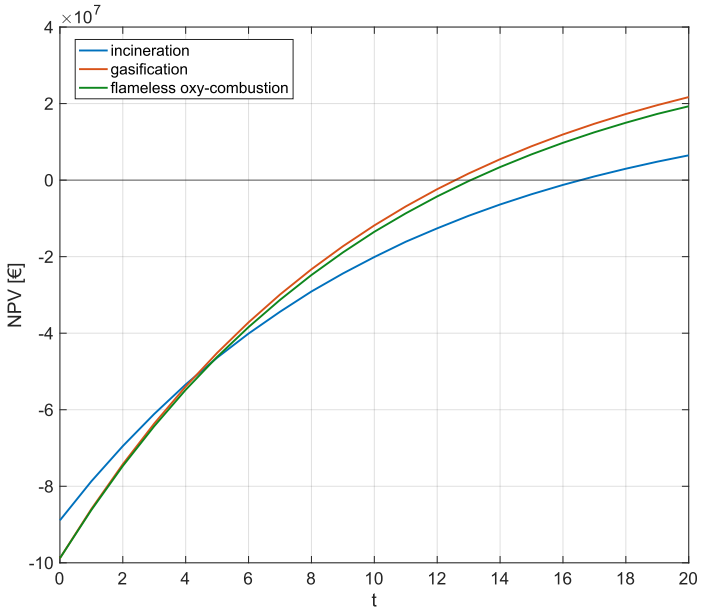

Figure 31. NPV of the three WtE alternatives evaluated in a lifetime period of 20 years.

The lowest PBPT was estimated for gasification (i.e., 13 years). The *flameless* oxy-combustion and incineration treatments show the highest PBPT

values, equal to 14 and 17 years, respectively. This means that the investment in a gasification plant allowed to generate money liquidity over the mid-life of the plant, while the incineration generates cash at more than 75% of the plant life.

A sensitivity analysis was carried out with respect to economic and environmental assessment. In the first case, the NPV trend was analysed by changing the electricity price for the three WtE treatments (fig. 32). As it can be observed, the investment in the gasification treatment is most profitable from an electricity price of about 30 €/MWh. The *flameless* oxy-combustion ensures the highest energy production, and, starting from an electricity price of about 44 €/MWh, it is more profitable than incineration. For the current electricity price (i.e., 84 €/MWh), gasification is most profitable than other WtE treatments. Nevertheless, the *flameless* oxy-combustion could be preferable for higher electricity prices (i.e., greater than 177 €/MWh). The increase of NPV by varying the p_e-values showed that the NPV of the flameless oxy-combustion increases more than the NPV of other WtE treatments for a given change of p_e-values. In other words, the electricity price mainly influences the profitability of the *flameless* oxy-combustion. This phenomenon depends on the greater capacity of this WtE treatment to produce electricity.

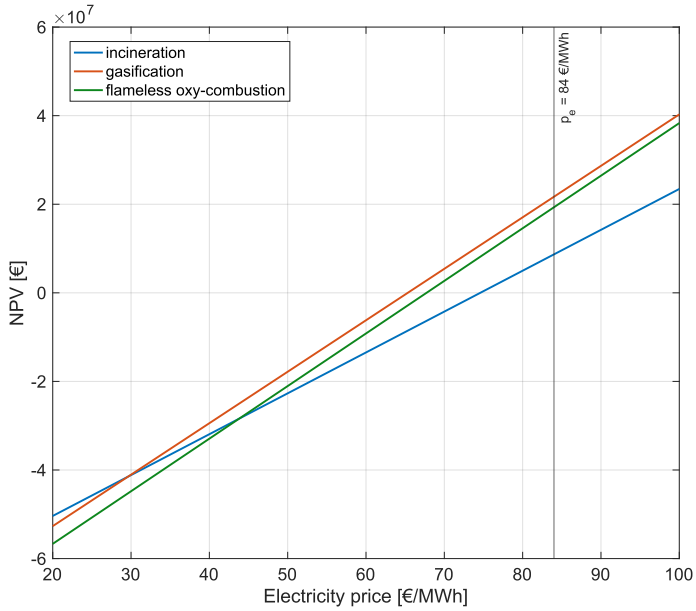

Figure 32. Profitability of the investment by varying the electricity price for each WtE treatment.

In a second case, the NPV trend was analysed by changing the costs due to carbon emissions produced by the plant for the three WtE treatments (fig. 33). Gasification is the most sustainable alternative, given the current carbon price [198]. It is more convenient than incineration for each carbon price. Unlike the previous case, the NPV of incineration and gasification treatment decreases when p_{em} value increases since it represents a cost item than a revenue. However, the NPV of the flameless oxy-combustion treatment is independent of the p_{em} variable since it is the only one that does not generate direct emissions into the atmosphere. It should be more profitable than incineration for a carbon price higher than 44 €/tCO2.

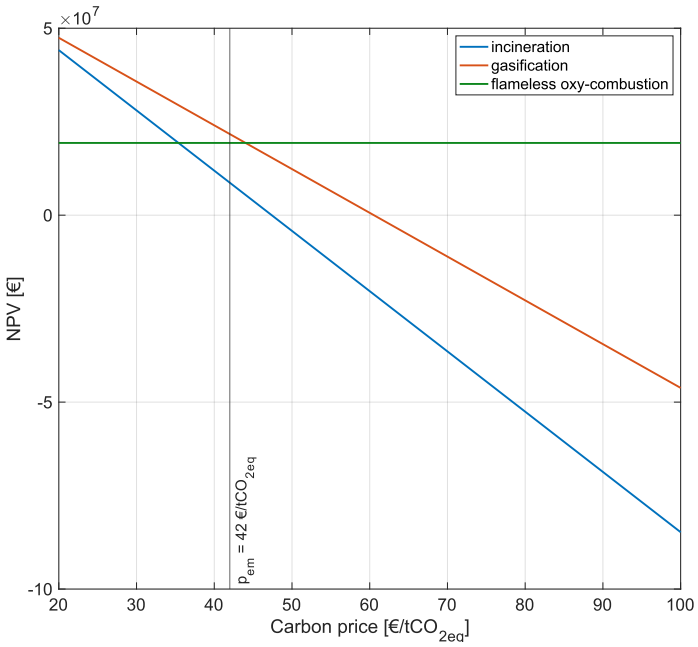

Figure 33. Profitability of the investment by varying the carbon price for each WtE treatment.

The NPV trend was analysed in a third case by changing the tipping fee amount for the three WtE treatments. In this case, it is observed that the results do not depend on the technology since each alternative's tipping fee has the same impact.

In conclusion, the cost and investment analysis carried out allowed to identify gasification as the best option to support the current transition phase. Although gasification, compared to incineration, showed the highest variable costs (mainly due to higher consumable costs), the convenience of this alternative is ensured by high profitability over time due to high revenues. In this regard, the conducted study showed a strong relationship between the carbon price, the electricity price and the investment profitability. In particular, a strong dependency on carbon price and NPV was observed; the *flameless* oxy-combustion could be preferable for slight price variations and, thus, in the next future this technology will gain an advantage over all the others when carbon price will increase over the actual price. Another parameter that will increase the oxy-combustion advantage

will be the selling of the extracted CO_2 which has been neglected in this work. On the contrary, the tipping fee does not affect the choice among the WtE treatments considered.

Similarly, it was proved that although the profitability of the three alternatives is strongly related to the MSW amount to be treated, the gasification ensures the highest profitability regardless of local municipal requirements. Therefore, in managing this transitional phase, gasification is the alternative that allows keeping a resource within the economic cycle for as long as possible, according to CE's definition, most efficiently, i.e., with the greatest benefits. It is noteworthy that the developed assessment is useful despite the current unstable situation in the energy market. Although in the last twelve months, there has been a 100% increase in the price of electricity for non-household consumers, the priority of preference among the three technologies analyzed does not change since, in all cases, revenue due to electricity sales it was considered.

2.3 Environmental comparisons of waste valorisation alternatives in the energy transition phase

This section presents the analytical models developed for the environmental comparison of different waste valorisation alternatives from AD treatment. Indeed, AD treatment offers the possibility of producing both electricity, H_2 and bio-CH_4 by exploiting different processes (see Figures 16,19,20,25). Each valorisation alternative has advantages but implies foregoing the other valorisation routes (e.g., producing electricity implies foregoing the production of H_2 or bio-CH_4). Therefore, models were developed that consider both the environmental benefits offered by each valorisation mode and the benefits foregone by not employing the other valorisation modes. The results obtained from the numerical application of these models are also presented. It is noteworthy that the numerical simulations conducted were aimed at understanding the potential offered by each valorisation method in the current energy transition phase.

2.3.1 Environmental comparison of waste-to-energy and waste-to-biomethane alternatives

This section discusses the development of an analytical model for comparing two waste valorization methods from AD treatment, i.e., electricity generation and bio-CH_4 production. Specifically, the model was developed considering the treatment of SS. Given the physic-chemical characteristics of the SS to be treated, the model predicts the composition of the obtainable biogas to identify the most sustainable recovery option in environmental terms. The model was applied to a real full-case study, considering one of the largest wastewater treatment plants (WWTPs) located in the metropolitan city of Bari (southern part of Italy).

2.3.1.1 Development of the analytical model for comparing the waste-to-energy and waste-to-biomethane alternatives

The considered system consists of an AD plant fed by SS with well-known physic-chemical characteristics. From the AD process, biogas with a specific composition is obtained. It can be employed in a generator for electricity production, or it can be treated within an upgrading unit to produce biomethane for feeding into the grid. The developed analytical model allows to identify the most environmentally sustainable among three biogas recovery options, assumed as three different scenarios:

- Scenario 1 (SC1): the entire amount of biogas produced is used to produce electricity. Firstly, the produced energy is adopted to meet the AD plant's energy demand and, if produced in excess, to feed the grid. In this scenario, the avoided emissions depend on the electricity surplus produced. The reference plant configuration for this scenario is reported in Figure 16.
- Scenario 2 (SC2): the entire amount of biogas produced is used to produce bio-CH_4 by adopting a dedicated upgrading unit. The produced biomethane is adopted to feed the grid. In this scenario, the national electricity grid generates emissions to meet the AD plant's electricity demand and the upgrading unit. The avoided emissions depend on the amount of biomethane produced. The

reference plant configuration for this scenario is reported in Figure 20.

- Scenario 3 (SC3) - the entire amount of biogas produced is used to produce biomethane and electricity. The electricity to meet the energy demand of the AD is produced. The excess biogas is sent to the upgrading unit to produce biomethane adopted to feed the grid. In this scenario, the avoided emissions depend on the amount of biomethane produced. No emission due national electricity grid is considered since the electricity demand of the AD plant and the upgrading unit is ensured by the same system. The reference plant configuration for this scenario is reported in Figure 19.

In all cases, the so-called "opportunity emissions" were considered. They are the loss of avoided emission corresponding to other scenarios when one scenario is chosen. For all scenarios, the emissions, expressed as [$kgCO_{2eq}$/day], were estimated, and the model suggests the scenario ensuring the lower emission value.

The total mass of SS (m_{ss}) feeding the AD treatment is estimated in equation 38.

$$m_{ss}=m_l+TS \left[\frac{g}{day}\right] \quad (38)$$

Where m_l [g/day] is the liquid content of the sludge mass, and TS [g/day] is the total solids content, identified in equation 39:

$$TS=VS+m_{in} \left[\frac{g}{day}\right] \quad (39)$$

Where VS [g/day] is the mass content of volatile solids (i.e., organic matter) and m_{in} [g/day] is the mass of inert matter in the SS (i.e., inorganic matter). It is assumed that VS is entirely composed of Carbon, Hydrogen, Oxygen, Nitrogen and Sulphur. Given the weight percentages of each element in the influent mass [%wt. VS] (i.e., C%, H%, O%, N% and S%), the molecular formula of the input organic matter is $C_aH_bO_cN_dS_e$ [mol], where the indexes (i.e., a, b, c, d, and e) can be estimated by equations 40-44, assuming the molar weight of each element (mol.wt. [g/mol]).

$$a=\frac{C\%}{\text{mol.wt. C}}\ [\text{mol}] \tag{40}$$

$$b=\frac{H\%}{\text{mol.wt.H}}\ [\text{mol}] \tag{41}$$

$$c=\frac{O\%}{\text{mol.wt.O}}\ [\text{mol}] \tag{42}$$

$$d=\frac{N\%}{\text{mol.wt.N}}\ [\text{mol}] \tag{43}$$

$$e=\frac{S\%}{\text{mol.wt.S}}\ [\text{mol}] \tag{44}$$

Given the composition of input organic matter, it is possible to estimate the biogas composition analytically using the Buswell model (eq. 45) [213]. This model assumes that the total mass of VS is biodegraded and that water is consumed.

$$C_aH_bO_cN_dS_e+n_{H_2O}H_2O \rightarrow n_{CO_2}CO_2+n_{CH_4}CH_4+n_{NH_3}NH_3+n_{H_2S}H_2S\ [\text{mol}] \tag{45}$$

Where the stoichiometric coefficients of H_2O, CO_2, CH_4, NH_3, and H_2S are estimated in equations 46-50, respectively.

$$n_{H_2O}=\frac{1}{4}\cdot(4a-b-2c+3d+2e)\ [\text{mol}] \tag{46}$$

$$n_{CO_2}=\frac{1}{8}\cdot(4a-b-2c+3d+2e)\ [\text{mol}] \tag{47}$$

$$n_{CH_4}=\frac{1}{8}\cdot(4a+b+2c-3d-2e)\ [\text{mol}] \tag{48}$$

$$n_{NH_3}=d\ [\text{mol}] \tag{49}$$

$$n_{H_2S}=e\ [\text{mol}] \tag{50}$$

According to the Buswell model's assumptions, the percentage of CH_4 and CO_2 ($\%CH_4$ and $\%CO_2$) theoretically obtainable in the biogas with a biodegradation efficiency η of 100% is provided by equations 51 and 52.

$$\%CH_4 = \frac{n_{CH_4}}{n_{CO_2} + n_{CH_4} + n_{NH_3} + n_{H_2S}} \quad (51)$$

$$\%CO_2 = \frac{n_{CO_2}}{n_{CO_2} + n_{CH_4} + n_{NH_3} + n_{H_2S}} \quad (52)$$

The AD process doesn't allow to degrade the whole mass of VS in the SS to be treated; it is necessary to assume a degradation efficiency of the organic carbon $\eta<100\%$, depending on the AD process parameters (e.g., temperature, pH, etc.). Therefore, under this condition, Banks claims that the predicted volume of methane (CH_{4_v}) depends on the application of the Buswell model with a carbon balance [214]. This approach makes it possible to identify the amount of carbon converted into biogas (C_{deg}) (eq. 53).

$$C_{deg} = \%C \cdot \eta \left[\frac{g}{day}\right] \quad (53)$$

Similarly, the amount of carbon converted into CH_4 ($C_{deg_{CH_4}}$) is shown in equation 54.

$$C_{deg_{CH_4}} = C_{deg} \cdot \%CH_4 \left[\frac{g}{day}\right] \quad (54)$$

The corresponding weight of methane (CH_{4_w}) and the stoichiometric coefficients (n_{CH_4}') assuming a degradation efficiency of the organic carbon $\eta<100\%$ are identified in equations 55 and 56, respectively.

$$CH_{4_w} = C_{deg_{CH_4}} \cdot \frac{\text{mol.wt. } CH_4}{\text{mol.wt. C}} \left[\frac{g}{day}\right] \quad (55)$$

$$n_{CH_4}' = \frac{CH_{4_w}}{\text{mol.wt.}CH_4} \text{ [mol]} \quad (56)$$

Assuming the molar volume of a gas under standard conditions (v_{STP} [L/mol]), it is possible to predict the volume of CH_4 obtained (CH_{4_v}) by the AD process and the corresponding biogas volume (v_{biogas}) (eqs. 57-58).

$$CH_{4_v} = n_{CH_4} \cdot v_{STP} \left[\frac{m^3_{STP}}{day}\right] \quad (57)$$

$$v_{biogas} = \frac{CH_{4_v}}{\%CH_4} \left[\frac{m^3_{STP}}{day}\right] \quad (58)$$

In SC1, given the lower heating value of CH_4 LHV [kWh/m^3_{STP}], and an electricity conversion efficiency η_{el}, it is possible to predict the amount of electricity produced by using the biogas entirely for electricity production (EL_{CH_4}), according to equation 59.

$$EL_{CH_4} = CH_{4_v} \cdot LHV \cdot \eta_{el} \left[\frac{kWh}{day}\right] \quad (59)$$

If, on the other hand, the amount of biogas produced is used to produce biomethane (SC2), it is necessary to predict the CO_2 amount in the biogas (CO_{2_v}), as shown in equation 60.

$$CO_{2_v} = v_{biogas} \cdot \%CO_2 \left[\frac{m^3_{STP}}{day}\right] \quad (60)$$

Therefore, in SC2, the CH_4 yield of the upgrading treatment ($v_{bio_{CH_4}}$) can be identified (eq. 61).

$$v_{bio_{CH_4}} = CH_{4_v} + \left(CO_{2_v} - CO_{2_v} \cdot \eta_{rem}\right) \left[\frac{m^3_{STP}}{day}\right] \quad (61)$$

Where η_{rem} is the CO_2 removal efficiency of the upgrading unit.

The daily electricity demand of the AD (EL_{AD} [kWh/day]) and the upgrading facilities (EL_{bio} [kWh/day), depend on the unit energy consumption due to AD el_{AD} [kWh/g] and upgrading facilities el_{bio} [kWh/g] per the total mass of SS (eq. 62) and biogas volume ($\mathbf{v_{biogas}}$) (eq. 63), respectively.

$$EL_{AD} = el_{AD} \cdot m_{ss} \left[\frac{kWh}{day}\right] \quad (62)$$

$$EL_{bio}=el_{bio}\cdot v_{biogas}\ \left[\frac{kWh}{day}\right] \quad (63)$$

In SC3, it is necessary to split the biogas volume produced in:

- Biogas required to meet the energy demand of the AD plant ($v_{biogas_{EL\text{-}AD}}$).
- Biogas to send to the upgrading unit to produce bio-CH_4 (v''_{biogas}).

In this respect, the volume of CH_4 needed to meet the energy demand from the AD plant ($CH_{4_{v,EL\text{-}AD}}$) was identified in equation 64).

$$CH_{4_{v,EL\text{-}AD}}=\frac{EL_{AD}}{LHV\cdot\eta_{el}}\ \left[\frac{m^3_{STP}}{day}\right] \quad (64)$$

Assuming the $\%CH_4$ (already defined in eq. 51), it is possible to predict the volume of biogas required to meet the energy demand of the AD plant (eq. 65).

$$v_{biogas_{EL\text{-}AD}}=\frac{CH_{4_{v,EL\text{-}AD}}\cdot 100}{\%CH_4}\ \left[\frac{m^3_{STP}}{day}\right] \quad (65)$$

Therefore, the theoretically volume of biogas to be send to the upgrading unit (v'_{biogas}) is provided in equation 66:

$$v'_{biogas}=v_{biogas}-v_{biogas_{EL\text{-}AD}}\ \left[\frac{m^3_{STP}}{day}\right] \quad (66)$$

To identify the actual volume of biogas to be sent to the upgrading unit (v''_{biogas}) is firstly necessary to calculate the electricity consumption for the v'_{biogas} upgrading $\left(EL'_{bio}\right)$ according to equation 67. Secondary, it is necessary to identify the CH_4 volume required to produce the electricity consumption for the v'_{biogas} $\left(CH_{4_{v,EL\text{-}bio}}\right)$ and the corresponding volume of biogas, showed in equations 68 and 69, respectively.

$$EL'_{bio} = el_{bio} \cdot v'_{biogas} \left[\frac{kWh}{day}\right] \quad (67)$$

$$CH_{4_{v,EL\text{-}bio}} = \frac{EL'_{bio}}{LHV \cdot \eta_{el}} \left[\frac{m^3_{STP}}{day}\right] \quad (68)$$

$$v_{biogas_{EL\text{-}bio}} = \frac{CH_{4_{v,EL\text{-}bio}} \cdot 100}{\%CH_4} \left[\frac{m^3_{STP}}{day}\right] \quad (69)$$

Therefore, the actual amount of biogas volume sent to the upgrading unit is (eq. 70):

$$v''_{biogas} = v'_{biogas} - v_{biogas_{EL\text{-}bio}} \left[\frac{m^3_{STP}}{day}\right] \quad (70)$$

To identify the amount of bio-CH_4 produced to be sent to the upgrading unit ($v''_{bio_{CH_4}}$), it is necessary estimate the updated values of CH_4 volume (CH''_{4_v}) and CO_2 (CO''_{2_v}), depending on v''_{biogas}, according to equations 71-73.

$$CH''_{4_v} = v''_{biogas} \cdot \%CH_4 \left[\frac{m^3_{STP}}{day}\right] \quad (71)$$

$$CO''_{2_v} = v''_{biogas} \cdot \%CO_2 \left[\frac{m^3_{STP}}{day}\right] \quad (72)$$

$$v''_{bio_{CH_4}} = CH''_{4_v} + \left(CO''_{2_v} - CO''_{2_v} \cdot \eta_{rem}\right) \left[\frac{m^3_{STP}}{day}\right] \quad (73)$$

Moreover, it is necessary to consider the amount of electricity that could be obtained from CH''_{4_v}, to calculate the opportunity emissions (eq. 74):

$$EL''_{CH_4} = CH''_{4_v} \cdot LHV \cdot \eta_{el} \left[\frac{kWh}{day}\right] \quad (74)$$

The emissions corresponding to each of the three scenarios (em_{SC1}, em_{SC2}, em_{SC3}) considered depend on the emission factors from the national electricity grid (f_{grid_e} [$kgCO_{2_{eq}}$/kWh]), and from the gas grid (representing indirect emissions from the supply of NG) ($f_{grid_{NG}}$ [$kgCO_{2_{eq}}/m^3_{STP}$]), according to equations 75-77.

$$em_{SC1}=\left(EL_{AD}-EL_{CH_4}\right)\cdot f_{grid_e}+v_{bio_{CH_4}}\cdot f_{grid_{NG}}\left[\frac{kgCO_{2_{eq}}}{day}\right] \quad (75)$$

$$em_{SC2}=(EL_{AD}+EL_{bio})\cdot f_{grid_e}+\left(EL_{CH_4}-EL_{AD}-EL_{bio}\right)\cdot f_{grid_e}+ \quad (76)$$
$$-v_{bio_{CH_4}}\cdot f_{grid_{NG}}\left[\frac{kgCO_{2_{eq}}}{day}\right]$$

$$em_{SC3}=-v''_{bio_{CH_4}}\cdot f_{grid_{NG}}+\left(v_{bio_{CH_4}}-v''_{bio_{CH_4}}\right)\cdot f_{grid_{NG}}+ \quad (77)$$
$$+EL_{CH_4}''\cdot f_{grid_e}\left[\frac{kgCO_{2_{eq}}}{day}\right]$$

The generated emissions have been assumed as positive contributions, while the avoided emissions have been assumed as negative contributions.

2.3.1.2 Numerical application of the analytical model for comparing the waste-to-energy and waste-to-biomethane alternatives

The developed model was applied to the real full-case study referred to the SS produced in the WWTP "Bari Ovest", located in the metropolitan city of Bari. It is one of the largest plants in Southern Italy. It has been recently redesigned to increase the capacity treatment from 240000 Population Equivalent (PE) to 360000 PE. In compliance with the national legislation, the SS treated in WWTP is stabilized by adopting AD. In the current plant configuration, the biogas produced is sent to a cogeneration plant to produce electricity and heat. The physic-chemical characteristics of the SS treated are summarized in Table 9.

Table 9. Physic-chemical characteristics of the SS assumed for the application of the analytical model to the "Bari Ovest" plant.

Variable	Unit of measurement	Value
m_{ss}	[g/day]	$75*10^6$ [215]
TS	[g/day]	$18*10^6$ [215]
VS	[g/day]	$12.96*10^6$ [215]
C%	[%wt. VS]	51 [216]
H%	[%wt. VS]	7.4 [217]
O%	[%wt. VS]	33 [217]
N%	[%wt. VS]	7.1 [217]
S%	[%wt. VS]	1.5 [217]
mol.wt. C	[g/mol]	12
mol.wt. H	[g/mol]	1
mol.wt. O	[g/mol]	16
mol.wt. N	[g/mol]	14
mol.wt. N	[g/mol]	32
mol.wt. CH_4	[g/mol]	16
η	[%]	52 [215]
v_{STP}	[L/mol]	22.4
η_{el}	[%]	38 [218]
LHV	[kWh/ m^3_{STP}]	10.69
η_{rem}	[%]	98 [219]
el_{AD}	[kWh/g]	0.000101 [219]
el_{bio}	[kWh/m^3_{STP}]	0.29 [219]
f_{grid_e}	[kgCO_{2eq}/kWh]	0.327 [220]
$f_{grid_{NG}}$	[kgCO_{2eq}/ m^3_{STP}]	1.98 [221]

The model was applied, and the results achieved for each scenario are shown below (Tab. 10)

Table 10. Results obtained by the application of the analytical model to the case study.

	SC1	**SC2**	**SC3**
$C_aH_bO_cN_dS_e$ [mol]	$C_{550800}H_{959040}O_{267300}N_{65726}S_{6075}$		
$\%CH_4$ [%]	70		
$\%CO_2$ [%]	18.45		
CH_{4_v} [m^3_{STP}/day]	4491		
v_{biogas} [m^3_{STP}/day]	6415.7		
$EL_{\text{-}CH_4}$ [kWh/day]	18243.34	-	-
$v_{bio_{CH_4}}$[kWh/day]	-	4514.67	-
EL_{AD} [kWh/day]	7575		-
EL_{bio} [kWh/day]	-	1860.55	-
$CH_{4_{v,EL\text{-}AD}}$[m^3_{STP}/day]	-	-	1864.75
$CH_{4_{v,EL\text{-}bio}}$[m^3_{STP}/day]	-	-	267.84
$v''_{bio_{CH_4}}$ [m^3_{STP}/day]	-	-	2367.9
$EL_{\text{-}CH_4}''$ [kWh/day]	-	-	9580.3
em_{SC1} [$kgCO_{2_{eq}}$/day]	5450.5	-	-
em_{SC2} [$kgCO_{2_{eq}}$/day]	-	-2973.5	-
em_{SC3} [$kgCO_{2_{eq}}$/day]	-	-	2694.96

The predicted composition of obtainable biogas includes 70% CH_4 and around 18% CO_2. The predicted v_{biogas} ensured by the plant is around 6500 [m^3_{STP}/day]; this value is consistent with data available in industries practices [215]. Moreover, the electricity produced in SC1 exceeds the energy demand of the AD plant; therefore, the electricity surplus will be sent to the grid.

The emissions corresponding to different scenarios are shown in Figure 34. It is possible to observe that only in SC2 emissions are generated (3085.42 $kgCO_{2eq}$/day). They depend on the supply of the AD plant and biogas upgrading unit from the national electricity grid. Nevertheless, SC2 is the scenario with the highest avoided emissions (-8939.05 $kgCO_{2eq}$/day). This effect depends on the emission factor of the gas grid $f_{grid_{NG}}$ (1.98

$kgCO_{2eq}/m^3_{STP}$); it is significantly higher than to emission factor of the national electricity grid f_{grid_e} (0.327 $kgCO_{2eq}$/kWh).

Consequently, the amount of avoided and opportunity emissions are strictly related to the amount of bio-CH_4 produced and sent into the grid. Consistent with this aspect, in the case of electricity production only (SC1), the highest amount of opportunity emissions are identified. It is results that, by comparing the avoided emissions of three scenarios, in SC2 are identified as the higher avoided emission than SC3 and SC1, respectively.

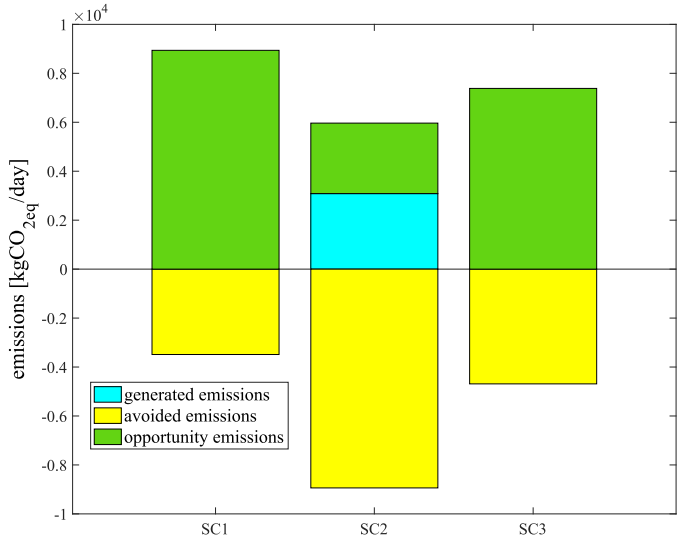

Figure 34. Predicted emissions in WWTP "Bari Ovest" for each scenario.

Therefore, SC2 is the best scenario from an environmental perspective; in this case, negative total emissions (-2973.5 $kgCO_{2eq}$/day) were predicted (fig. 35). This means that the avoided emissions of SC2 are greater than generated and opportunity emissions.

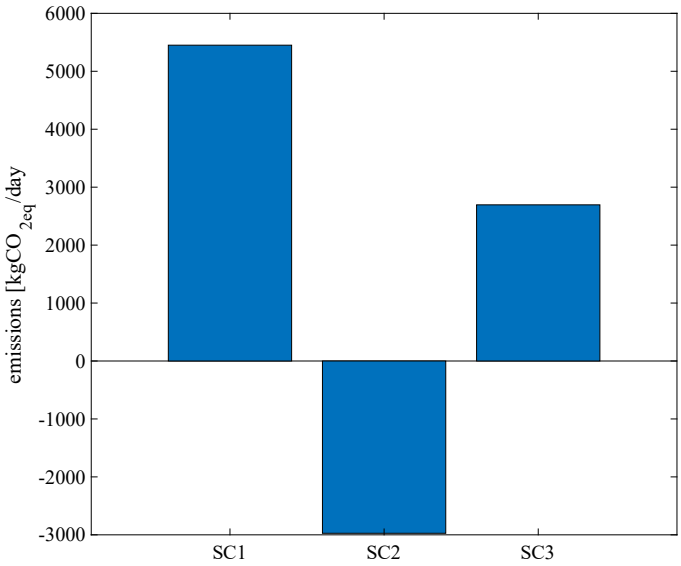

Figure 35. Predicted total emissions in WWTP "Bari Ovest" for each scenario.

The trend of the emission functions considered in the three scenarios (em_{SC1}, em_{SC2}, em_{SC3}) evaluated with respect to $f_{grid_{NG}}$ is shown in Figure 36. Three break-even points $f_{grid_{NG}}$ were identified. In the case of $f_{grid_{NG}}$ is lower than 0.66 $kgCO_{2eq}/m^3_{STP}$, the best environmental choice consists of using the entire amount of biogas to produce electricity (SC1). The recovery options based on electricity and bio-CH_4 production (SC3), and only-CH_4 (SC2), are less sustainable.

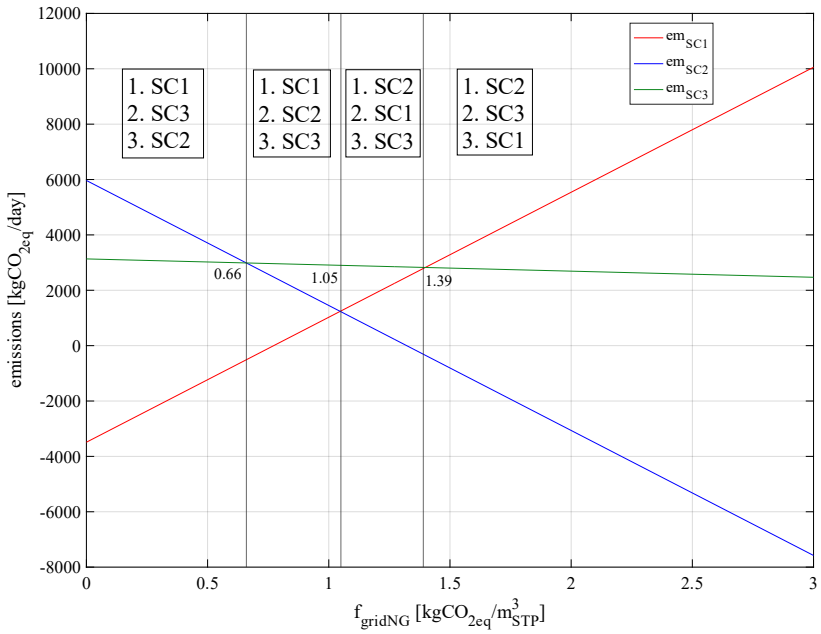

Figure 36. Trends of the emission functions by varying the emission factor from the gas grid for each scenario.

In the case of $f_{grid_{NG}}$ is included between 0.66 and 1.05 $kgCO_{2eq}/m^3_{STP}$, the best recovery option doesn't change (i.e., SC1), but the SC2 become preferable to SC3 in environmental terms.

In the case of $f_{grid_{NG}}$ is included between 1.05 and 1.39 $kgCO_{2eq}/m^3_{STP}$, the best environmental choice consists of producing only bio-CH_4 (SC2). The recovery options SC1 and SC3 are less sustainable.

In the case of $f_{grid_{NG}}$ is higher than 1.39, the best recovery option doesn't change (i.e., SC2), but the SC3 become preferable to SC1 in environmental terms. Therefore, under these assumptions, the recovery option of adopting the entire amount of biogas to produce bio-CH_4 and electricity is never preferable.

In conclusion, the results showed that the best alternative consists of producing only biomethane (SC2). It, indeed, ensures a negative global

emissions. Moreover, it was observed that the emission factor from the gas grid significantly affects the recovery option's choice. In most cases, the recovery options based on electricity and biomethane are not sustainable.

2.3.2 Environmental comparison of waste-to-hydrogen and waste-to-biomethane alternatives

This section discusses the development of an environmental analytical model for comparing two further waste valorization alternatives from AD treatment, i.e., H_2 production and bio-CH_4 production. The model was developed considering OW as a reference. The processes considered were AD followed by biogas upgrading for bio-CH_4 production (Figure 20) and the SBR route for H_2 production (Figure 25). They were referred to as the BG-bio-CH_4 and the BG-H_2 route, respectively. Numerical application of the model provided insight into the decarbonization potential of the two alteratives considered in the current energy transition phase.

2.3.2.1 Development of the analytical model for comparing the waste-to-hydrogen and waste-to-biomethane alternatives

The developed environmental analytical model allows to evaluate the total emissions associated with processing a ton of OW through the two considered routes. It is expressed according to equation 78.

$$\varphi\left[\mathrm{kgCO_{2_{eq}}/tOW}\right]=\varphi_{\mathrm{indirect}}-\varphi_{\mathrm{av}} \tag{78}$$

$\varphi_{\mathrm{indirect}}$ $[\mathrm{kgCO_{2_{eq}}/tOW}]$ are the emissions associated with electricity supply from the national grid (equation 79) and φ_{av} $[\mathrm{kgCO_{2_{eq}}/tOW}]$ are the avoided emissions provided by each green gas production route (equation 80). As it can be observed from equation 78, direct emissions were neglected. This is because both green gas routes generate biogenic emissions, which are considered to be carbon-neutral [222].

$$\varphi_{\mathrm{indirect}}\left[\mathrm{kgCO_{2_{eq}}/tOW}\right]=\mathrm{EL_{cons}}\cdot f_{\mathrm{grid}} \tag{79}$$

Indirect emissions were calculated as the product between the electricity consumption of the considered process (EL_{cons} [kWh/tOW]) and the national grid emission factor (f_{grid} [$kgCO_{2_{eq}}$/kWh]). It is noteworthy that the value of the f_{grid} variable directly reflects the composition of the national energy mix.

$$\varphi_{av}\left[kgCO_{2_{eq}}/tOW\right]=\varphi_{av_{CH_4}}+\varphi_{av_{H_2}} \quad (80)$$

Avoided emissions were calculated as the sum between avoided emissions from bio-CH_4 production ($\varphi_{av_{CH_4}}$ [$kgCO_{2_{eq}}$/tOW] and avoided emissions from H_2 production ($\varphi_{av_{H_2}}$[$kgCO_{2_{eq}}$/tOW]). They are expressed according to equations 81 and 82, respectively.

$$\varphi_{av_{CH_4}}\left[kgCO_{2_{eq}}/tOW\right]=\eta_{bio_{CH_4}}\cdot LHV_{CH_4}\cdot\eta_{pow}\cdot f_{pow} \quad (81)$$

Avoided emissions from bio-CH_4 production were considered as the emissions that would be generated from electricity production by employing fossil NG. They were calculated as the product between the bio-CH_4 yield of the process ($\eta_{bio_{CH_4}}$ [$kgCH_4$/tOW]), the lower heating value of NG (LHV_{CH_4} [kWh/$kgCH_4$]), the power efficiency of a NG power plant (η_{pow} [%]) and the emission factor of a NG-based power production process (f_{pow} [$kgCO_{2_{eq}}$/kWh]).

$$\varphi_{av_{H_2}}\left[kgCO_{2_{eq}}/tOW\right]=\varphi_{av_{SMR}}+\varphi_{av_{el}} \quad (82)$$

Avoided emissions from H_2 production were calculated as the sum between avoided emissions from fossil-based H_2 production ($\varphi_{av_{SMR}}$ [$kgCO_{2_{eq}}$/tOW]) and electrolysis based H_2 production (equation 84). The overall amount of H_2 produced by the BG-H_2 route (η_{H_2} [Nm^3H_2/tOW] is weighted according to the share of global H_2 production from electrolysis (α [%]). It is noteworthy that emissions from

the SMR process, i.e., currently the most widespread H_2 production route [223], were considered in the case of fossil-based production process. They are expressed according to equation 83.

$$\varphi_{av_{SMR}}\left[kgCO_{2_{eq}}/tOW\right] = \\ =(1-\alpha)\cdot\eta_{H_2}\cdot(\varphi_{d_{SMR}}+EL_{cons_{SMR}}\cdot f_{grid}+NG_{cons_{SMR}}\cdot FME\cdot GWP_{100}) \quad (83)$$

Emissions from the SMR process were calculated as the sum between direct emissions $\varphi_{d_{SMR}}[kgCO_{2_{eq}}/Nm^3H_2]$), indirect emissions from electricity supply ($EL_{cons_{SMR}}\cdot f_{grid}$ $[kgCO_{2_{eq}}/Nm^3H_2]$ and the FMEs generated from NG supply. They were calculated as the product between the NG consumption of the process ($NG_{cons_{SMR}}$ $[kgCH_4/Nm^3H_2]$), the factor which quantifies the amount of FMEs for each unit mass of CH_4 consumed (FME [#]) and the CH_4's impact factor on the GWP over a time horizon of 100 years (GWP_{100} $[kgCO_{2_{eq}}/kgCH_4]$.

$$\varphi_{av_{el}}\left[kgCO_{2_{eq}}/tOW\right] = \alpha\cdot\eta_{H_2}\cdot EL_{cons_{el}}\cdot f_{grid} \quad (84)$$

Emissions from electrolysis were finally calculated as the product between the electricity consumption of the process ($EL_{cons_{el}}[kWh/Nm^3H_2]$ and the national grid emission factor.

2.3.2.2 Numerical application of the analytical model for comparing the waste-to-hydrogen and waste-to-biomethane alternatives

The developed analytical model was then numerically applied to the current scenario. In this regard, the global average values of the grid emission factor and the share of H_2 production from electrolysis were employed. Table 11 shows the data used in the analysis.

Table 11. Data employed for the numerical application of the developed analytical model.

Variable	BG-bio-CH_4	BG-H_2
EL_{cons}	48.7 [224]	32.34 [225]
f_{grid}	0.342 [226]	
$\eta_{bio_{CH_4}}$	32.72 [224]	-
LHV_{CH_4}	13.9	-
η_{pow}	60 [227]	-
f_{pow}	0.506 [228]	-
FME	-	3.5% [229]
GWP_{100}	-	32 [230]
α	-	0.04 [223]
η_{H_2}	-	215.6 [225]
$\varphi_{d_{SMR}}$	-	0.91 [41]
$EL_{cons_{SMR}}$	-	0.12 [231]
$NG_{cons_{SMR}}$	-	0.3 [231]
$EL_{cons_{el}}$	-	6 [41]

The results obtained from the numerical application of the developed analytical model are illustrated in Figure 37.

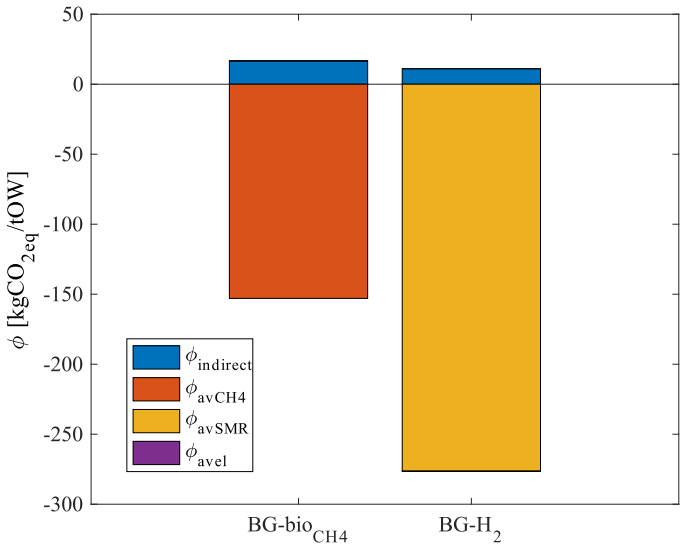

Figure 37. Total emissions for the BG-bio-CH_4 and BG-H_2 routes.

As it can be observed, both green gas production routes provide an environmental benefit, i.e., negative overall emissions. The alternative with a better overall balance is the BG-H_2 route. It has total emissions of -285.5 kgCO_{2eq}/tOW. This value is lower than the total emissions of BG-bio-CH_4 route (i.e., -136.32 kgCO_{2eq}/tOW). As for the BG-H_2 route, the major contribution is provided by avoided emissions from fossil-based H_2 production (φ_{avSMR} = -276.38 kgCO_{2eq}/tOW). In the BG-bio-CH_4 route, avoided emissions from power generation from fossil NG ($\varphi_{av_{CH_4}}$) are -153 kgCO_{2eq}/tOW, a value lower than avoided emissions from the BG-H_2 route. It is noteworthy that the contribution provided by avoided emissions from H_2 production by electrolysis ($\varphi_{av_{el}}$) is almost negligible. This is because this alternative is currently barely employed in the H_2 production mix (α=0.04%). It can be therefore concluded that, although H_2 yield (i.e., 19.38 kgH2/tOW) is lower than bio-CH_4 yield (i.e., 32.72 kgbio-CH_4/tOW) in the considered processes, BG-H_2 route currently shows a higher decarbonization potential.

Since, as pointed out, the major barrier to large-scale implementation of green H_2 relates to indirect emissions generated by the need of national grid

electricity supply, a sensitivity analysis of total emissions was conducted with respect to the f_{grid} and α variables. The objective was to jointly capture any effects caused by an energy transition (i.e., decreasing f_{grid} values) and changes in the H_2 production mix (i.e., increasing α values). The results obtained are represented in Figure 38.

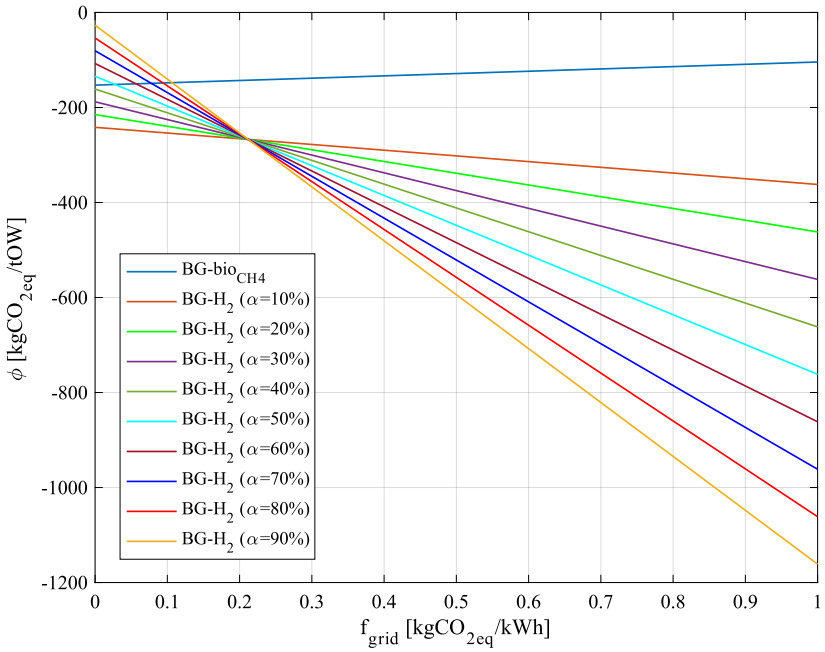

Figure 38. Sensitivity analysis with respect to the f_{grid} and α variables.

As it can be observed, as f_{grid} value increases, the total emission functions related to the two green gas production routes have an opposite trend. To this concern, the environmental benefit provided by the BG-bio-CH_4 route decreases as emissions from the national power grid increase. Indeed, the emissions generated by electricity consumption become greater than the avoided emissions. On the contrary, the environmental benefit provided by the BG-H_2 route increases as both the f_{grid} and α variables increase. It can also be observed that emissions from BG-H_2 route are equal for each value of α at f_{grid}=0.21[kgCO$_{2eq}$/kWh]. For lower values of f_{grid}, it is observed that the lowest emissions are recorded at minimum α (10%), and for higher

values the highest emissions are recorded at maximum α (90%). This result highlights the BG-H_2 route's high decarbonization potential in the current transition phase. Once decarbonization targets will be met, this environmental benefit will be reduced, given the advantage provided by the green electrolysis route. Finally, as it can be observed, for α values greater than 50% and f_{grid} values up to 0.11 kgCO2eq/kWh, there are intersections between the total emission curves relative to the two green gas production routes. This implies that, in a decarbonized scenario, also the BG-bio-CH_4 route will represent a viable alternative.

In conclusion, the results obtained from the numerical application of the model to the current scenario, showed that the BG-H_2 route offers the best decarbonization potential. Indeed, H_2 production from SBR process provides an environmental benefit of -285.5 $kgCO_{2eq}$/tOW, unlike the BG-bio-CH_4 route, which offers a benefit of -136.32 $kgCO_{2eq}$/tOW. As for the BG-H_2 process, the major contribution is provided by avoided emissions from fossil-based H_2 production. It is noteworthy that avoided emissions from the electrolysis process are almost negligible, due to the near absence of this route within the current H_2 production mix. A sensitivity analysis also allowed to understand that the decarbonization potential of the BG-H_2 route increases as emissions from the national power grid increase, in contrast to the BG-bio-CH_4 route. Moreover, it was possible to conclude that the BG-H_2 route offers a real decarbonization potential in the current energy transition phase, but this potential will be reduced when emissions from the grid will decrease, and electrolysis will turn out to be environmentally convenient. Finally, it was found that the BG-bio-CH_4 route could be effective in some decarbonized scenarios. Although the developed model is a useful tool for the evaluation of green gas production routes, the present work shows some limitations.

2.4 Environmental comparisons of waste-to-hydrogen routes

This section discusses the development of an analytical model to compare the environmental performance of different waste-based H_2 production routes (HPRs) in the current energy transition phase. To this concern, three

WtH2 routes were considered: a WtE plant coupled with an electrolyser (WtE+El) (Figure 23), an MSW gasification plant with a syngas treatment unit to produce H2 (Gas-H2) (Figure 24) and an SBR process based on AD of the Organic Fraction of Municipal Solid Waste (OFMSW) (Figure 25). Consistent with this end, the three WtH_2 routes were compared with the SMR process, i.e., the currently most employed HPR (Figure 21), and with water electrolysis (El), i.e., the most promising HPR from an environmental point of view (Figure 22). Notably, to reflect the current energy transition scenario, the El route is supposed to be fed from the national electricity grid. A schematic representation of the HPRs considered is provided in Figure 39.

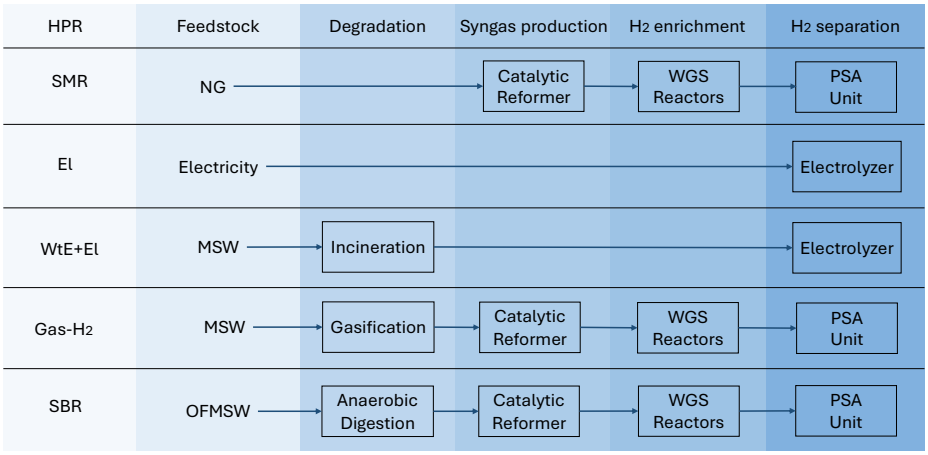

Figure 39. Schematization of the five HPRs considered with reference to the main phases of the H_2 production process.

The developed environmental analytical model allows to evaluate the GHGs emissions (i.e., direct, indirect, avoided, and counterfactual) associated with each HPR in two scenarios. The former describes the context of the EU in 2020, while the latter describes the same context in 2030. They were identified as the initial moment of the energy transition process and as a landmark year for achieving major environmental milestones from an EU and global perspective.

2.4.1 Development of the analytical model for comparing the waste-to-hydrogen routes

The developed analytical model allows to estimate the total emissions associated with the production of one Nm^3 of H_2 at 99.9% vol%. It can be expressed according to equation 85:

$$\varphi \left[\frac{kgCO_{2_{eq}}}{Nm^3H_2}\right] = \varphi_{direct} + \varphi_{indirect} - \varphi_{av} + \varphi_c \quad (85)$$

φ_{direct} $[kgCO_{2_{eq}}/Nm^3H_2]$ are the direct emissions generated by the plants during the H_2 production process. Notably, only the non-biogenic share of carbon emissions was evaluated since the biogenic one is considered carbon-neutral [222]. $\varphi_{indirect}$ $[kgCO_{2_{eq}}/Nm^3H_2]$ are the emissions associated with the supply of energy and fossil fuels (i.e., NG) required by the facilities. They are expressed according to Equation 86. φ_{av} $[kgCO_{2_{eq}}/Nm^3H_2]$ are the avoided emissions from MSW landfilling due to the adoption of valorisation treatments. They are expressed according to Equation 89. Finally, φ_c $[kgCO_{2_{eq}}/NM^3H_2]$, are the counterfactual emissions, i.e., the emissions generated for not adopting alternative methods of MSW valorisation. They are expressed according to Equation 90.

$$\varphi_{indirect} \left[\frac{kgCO_{2_{eq}}}{Nm^3H_2}\right] = \varphi_{EL} + \varphi_{NG} \quad (86)$$

$$\varphi_{EL} \left[\frac{kgCO_{2_{eq}}}{Nm^3H_2}\right] = EL_{cons} \cdot f_{grid} \quad (87)$$

$$\varphi_{NG} \left[\frac{kgCO_{2_{eq}}}{Nm^3H_2}\right] = NG_{cons} \cdot f_{FME} \cdot GWP_{100} \quad (88)$$

As it can be observed, indirect emissions were considered as the sum of two contributions, i.e., emissions from electricity supply φ_{EL} $[kgCO_{2_{eq}}/Nm^3H_2]$ and emissions from NG supply φ_{NG} $[kgCO_{2_{eq}}/Nm^3H_2]$. They are expressed according to Equations 87 and 88, respectively. As far as concerns emissions from electricity supply, they

were computed by assuming that the entire amount of electricity required by the process (EL_{cons} [kWh/Nm^3H_2]) is supplied by the national power grid, characterised by a specific emission factor (f_{grid} [$kgCO_{2_{eq}}/kWh$]). For the calculation of φ_{NG} (eq. 88) FMEs were considered. They are defined as methane emissions generated during the production, processing, and transportation of NG, and they are calculated as a percentage (f_{FME} [%]) of the total NG consumption of the process (NG_{cons} [$kgNG/Nm^3H_2$]) [232], weighted according to the methane's impact factor on the GWP over a time horizon of 100 years (GWP_{100} [$kgCO_{2_{eq}}/kgNG$]).

$$\varphi_{av}\left[\frac{kgCO_{2_{eq}}}{Nm^3H_2}\right]=MSW_{H_2}\cdot f_{disp_{MSW}} \tag{89}$$

As said, the avoided emissions were considered with respect to an MSW landfilling scenario. To this concern, they were computed by considering the amount of MSW processed to produce H_2 (MSW_{H_2} [$kgMSW/Nm^3H_2$]) and a waste landfilling emission factor f_{disp} [$kgCO_{2_{eq}}/kgMSW$]. This factor is mainly related to the GHGs generation during MSW decomposition when disposed of. The contribution related to avoided emissions was evaluated with a negative sign, thus highlighting the double benefit provided by WtH_2 HPRs.

$$\varphi_{c}\left[\frac{kgCO_{2_{eq}}}{Nm^3H_2}\right]=\alpha\cdot\varphi_{c_{EL}}+(1-\alpha)\cdot\varphi_{c_{NG}} \tag{90}$$

$$\varphi_{c_{EL}}\left[\frac{kgCO_{2_{eq}}}{Nm^3H_2}\right]=MSW_{H_2}\cdot\eta_{el}\cdot f_{grid} \tag{91}$$

$$\varphi_{c_{NG}}\left[\frac{kgCO_{2_{eq}}}{Nm^3H_2}\right]=MSW_{H_2}\cdot\eta_{CH_4}\cdot\left(f_{FME}\cdot GWP_{100}+LHV_{CH_4}\cdot\eta_{pow}\cdot f_{pow}\right) \tag{92}$$

Equation 90 shows the counterfactual emissions. They were defined as the emissions generated because alternative MSW valorisation routes are foregone. In the context of the present work, electricity and bio-CH_4 production were considered like counterfactual scenarios, being the main valorisation routes related to the MSW treatments considered. As it is well known, indeed, incineration, gasification and AD treatments are considered

among WtE technologies. They, therefore, allow producing electricity to be fed into the grid [233]. In this regard, counterfactual emissions from electricity production $\varphi_{c_{EL}}$ [$kgCO_{2_{eq}}/Nm^3H_2$] were considered by assuming that the electricity that could have been obtained from treating the amount of MSW used to produce H_2 ($MSW_{H_2} \cdot \eta_{el}$ [kWh/kgMSW]), should be produced by employing the current national energy mix (considered through the value of f_{grid})(eq. 91). AD also allows for bio-CH_4 production by upgrading the obtained biogas [224]. In this regard, counterfactual emissions ($\varphi_{c_{NG}}$ [$kgCO_{2_{eq}}/Nm^3H_2$]) were computed by considering the emissions from the production and use for energy purposes of the amount of bio-CH_4 the would be obtained (η_{CH_4} [kgNG/kgMSW]) by treating the amount of MSW used to produce H_2 (MSW_{H_2}). As for the emissions from bio-CH_4 production, they were calculated as FMEs (see eq. 88). The emissions from bio-CH_4 use for energy purposes were computed by considering the emissions generated by producing a kWh of electricity by employing a gas turbine characterised by an efficiency of η_{pow} [#] and a specific emission factor of f_{pow} [$kgCO_{2_{eq}}$/kWh]. Regarding the $\alpha \in [0,1]$ factor, it indicates the share of MSW not used to produce electricity. It, of course, assumes values different from 1 only in the case of the SBR route.

2.4.2 Numerical application of the analytical model for comparing the waste-to-hydrogen routes

The different HPRs considered were then compared through a numerical application of the developed model. To this concern, the data used for the comparison (shown in Table 12) are valid under the following basic assumptions:

- The LHV of MSW is 16 MJ/kg on a wet wt% basis.
- The moisture content of MSW is 15.70% on a wet wt% basis.
- The ash content of MSW is 16.52% on a wet wt% basis.
- The net electrical efficiency of the WtE plant is 25%.
- The gasification process is carried out at a high temperature (>1100 °C) with pure oxygen.

- The electrical consumption of the electrolyser is 5 kWh/Nm^3H_2 in the Wte+El route.
- The separation efficiency of the PSA unit is 85%.
- The biogas composition is 60% CH_4 and 35% CO_2.
- The LHV of biogas is 22 MJ/Nm^3.

Table 12. Data employed for the numerical application of the environmental analytical model.

Variable	El	SMR	WtE+El	Gas-H_2	SBR
φ_{direct}		0.91 [41]	3.9 [41]	0.94 [41]	0.5 [234]
EL_{cons}	6 [41]	0.12 [231]		0.74 [41]	0.15 [234]
f_{grid}			$0 \leq f_{grid} \leq 1$ [226]		
NG_{cons}		0.3 [231]	0.07 [41]	0.06 [41]	
f_{FME}			3.5 % [229]		
GWP_{100}			32 [230]		
MSW_{H_2}			4.64 [235]	1.09 [235]	4.6 [234]
$f_{disp_{MSW}}$				0.4 [236]	
α			1		$0 \leq \alpha \leq 1$
η_{el}			0.49 [209]	0.575 [209]	0.5 [234]
η_{CH_4}					0.033 [224]
LHV_{CH_4}					13.9
η_{pow}					0.5 [227]
f_{pow}					0.506 [228]

As mentioned, the developed analytical model aims to assess the decarbonisation potential offered by the WtH_2 routes considered in the current energy transition phase. For this purpose, two scenarios were constructed referring to the EU context in 2020 and 2030, respectively. The year 2020 was chosen as the start date of the energy transition process and, more generally, of a series of processes aimed at improving the environmental sustainability of the entire European system. Indeed, the publication of the EU H_2 strategy, in which the production of green H_2 is defined as strategic for achieving the NZE targets set for 2050, dates to 2020 [237]. Also from 2020 is the Circular Economy Action Plan, in which

relevant goals are set about MSW management [238]. The year 2030 was chosen because it is often identified as a time horizon to achieve many goals to enable the transition to a net-zero economy by 2050. It was therefore identified as an instant at which the transition process will be fully in progress. In this regard, the EU Green Deal has set a target to reduce net GHGs emissions by 55% by 2030 [239]. Within the EU H_2 strategy, a target is also set to produce 10 Mt of H_2 from renewable sources by 2030 [237]. As for waste management, 2030 is set as the deadline to achieve a 60% separate collection rate and reduce the amount of residual (non-recycled) MSW to half [238]. Thirty-five billion cubic meters of annual biomethane production by 2030 is also set in the REPowerEU plan [240]. Having examined the concerning contexts, i.e., H_2 production and MSW management, the variables chosen to describe the two scenarios are shown in Table 13.

Table 13. Variables employed to describe the 2020 and 2030 scenarios.

Variable	Unit of measurement	Meaning
f_{grid}	[$kgCO_{2_{eq}}$/kWh]	Specific emission factors from the national electricity grid
H_{2_y}	[Nm^3H_2/y]	Annual H_2 production required
Bio_{MSW}	[tMSW/y]	Annual biowaste availability (to be treated through SBR)
Res_{MSW}	[tMSW/y]	Annual residual MSW availability (to be treated through Gas-H_2)
$El_{installed}$	[GW/y]	Installed capacity from electrolysers

The values of the variables illustrated in the two scenarios are shown in Table 14.

Table 14. Values of the descriptive variables adopted for 2020 and 2030 scenarios.

Variable	2020	2030
f_{grid}	0.265 [241]	0.114 [241]
H_{2_y}	111,234,705,200 [237]	95,661,846,500 [242]
Bio_{MSW}	78,880,000 [243]	60,238,386.31 [240]
Res_{MSW}	113,000,000 [238]	56,000,000 [238]

$El_{installed}$	1 [242]	40 [237]

According to the objective of the investigation, a sensitivity analysis was first conducted to understand which WtH_2 route offers the lowest total emissions depending on the national electricity mix. To this concern, the performance of the total emission functions of all alternatives with respect to the f_{grid} variable was investigated. For the SBR route, in addition, the performance of the total emissions function was also investigated concerning the α variable.

Depending on the results obtained from the sensitivity analysis, the total emissions generated by H_2 production in the 2020 and 2030 scenarios were then calculated (Table 14), comparing both results in the scenario without WtH_2 technologies and with WtE technologies. Below are therefore presented and discussed the results obtained from the completed analysis.

Figure 40 shows the results obtained from the sensitivity analysis carried out on the total emission functions of the different WtH_2 routes with respect to f_{grid} and α variables.

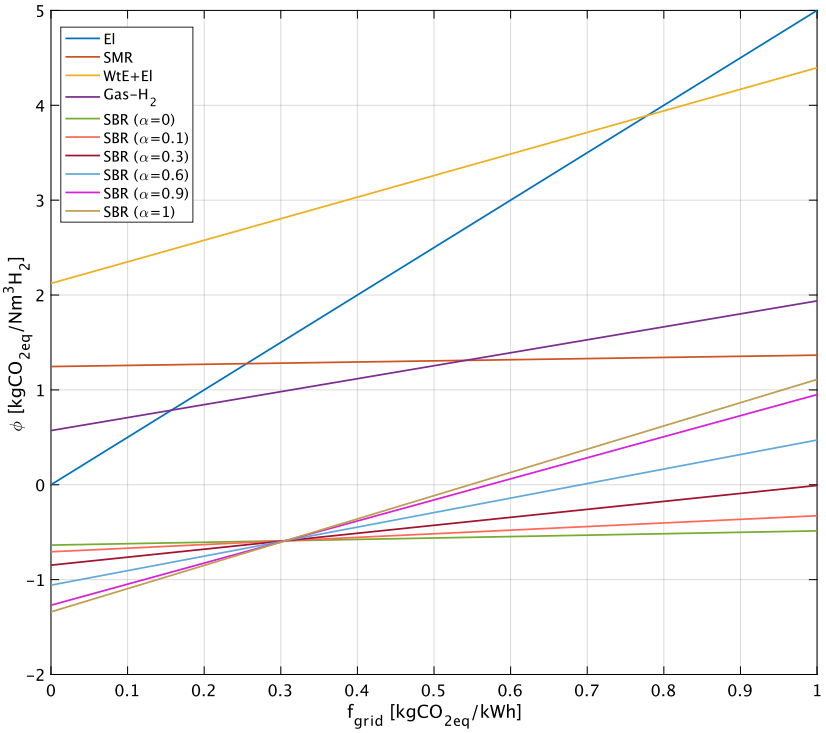

Figure 40. Results obtained from the sensitivity analysis on the total emissions functions with respect to the f_{grid} variable.

As expected, the total emissions functions of the different HPRs have an increasing trend as the f_{grid} value increases (Fig. 9). However, they show very different sensitivity to the considered variable, depending on the burden that emissions from electricity supply have on total emissions. To this concern, emissions from the El route increase from 0 [$kgCO_{2eq}/Nm^3H_2$] at f_{grid}= 0 [$kgCO_{2eq}$/kWh] to 5 [$kgCO_{2eq}/Nm^3H_2$] at f_{grid}= 1 [$kgCO_{2eq}$/kWh]. This is the most significant variation among those recorded. In the case of the El route, indeed, emissions from the electricity supply constitute the total emissions. In the same range, Gas-H_2 and WtE+El emissions increased by 239.28% and 197.36%, respectively. The route with the smallest variation is SMR, whose total emissions increased by 9.63%. This is because, for this route, emissions from electricity supply

have a minor impact on total emissions than, for example, direct emissions and emissions from NG consumption (see Table 12). Since, unlike the other HPRs, two counterfactual scenarios were considered, variation in emissions from the SBR also depends on α variable. Indeed, the maximum variation in its emissions occurs at α=1, and the minimum variation occurs at α=0. For the SBR route, the sensitivity analysis also allowed to identify the best counterfactual scenario (i.e., the preferable alternative use of biogas) depending on the national energy mix. To this concern, for f_{grid} values up to 0.31 [$kgCO_{2eq}$/kWh], emissions from the SBR route increase as α decreases (i.e., less electricity is produced). On the contrary, for higher f_{grid} values, emissions increase as α increases (i.e., more electricity is produced). This implies that, in the first interval, the alternative biogas use that generates the best environmental benefit is bio-CH_4 production. In contrast, electricity production ensures a lower impact in the second interval. Counterfactual emissions, indeed, in a scenario of electricity or bio-CH_4 production, would be considered as avoided emissions. In calculating emissions from H_2 production from SBR, it will therefore be necessary to consider as counterfactual emissions those with the greatest environmental benefit depending on the national energy mix (i.e., for f_{grid} values up to 0.31 [$kgCO_{2eq}$/kWh] bio-CH_4 production, and for f_{grid} higher values electricity production). The differences shown in the trends of the total emission functions result in five areas in the graph, each with a different order of preference among the HPRs considered. To this end, for f_{grid} values up to 0.16 [$kgCO_{2eq}$/kWh], the lowest emission HPR is the SBR, followed by the El route, the Gas-H_2 route, the SMR route, and finally, the WtE+El route. For f_{grid} values between 0.16 and 0.26 [$kgCO_{2eq}$/kWh], the order of preferences is unchanged, except that the Gas-H_2 route becomes preferable to the El route. For f_{grid} values between 0.26 and 0.54 [$kgCO_{2eq}$/kWh], there is no change in the best (i.e., SBR) and worst (i.e., WtE+El) route from an environmental point of view, but the SMR HPR becomes better than the El route. For f_{grid} values between 0.54 and 0.78 [$kgCO_{2eq}$/kWh], SMR becomes better than Gas-H_2, and finally, for f_{grid} values greater than 0.78 [$kgCO_{2eq}$/kWh], El becomes the route with the worst environmental performance. The results confirmed the main finding in the literature, i.e., that a radical energy transition pathway must be completed for the large-

scale implementation of water electrolysis for green H_2 production. For low values of the f_{grid} variable, it can be observed that El is the best alternative after the SBR route. At the same time, for very high values of f_{grid}, it results as the alternative with the worst environmental performance. The high decarbonisation potential offered by WtH_2 routes can also be observed (fig. 40). Indeed, the SBR is the only route that can offer negative total emissions. The Gas-H_2 route, on the other hand, is a valuable HPR in many scenarios characterised by intermediate f_{grid} values (i.e., 0.16÷0.54 [kgCO2eq/kWh]) and also in scenarios characterised by higher f_{grid} values, although it is not the preferable alternative. In scenarios characterised by higher f_{grid} values, it indeed offers far lower emissions than the El route and slightly higher than the SMR route.

The results obtained from the sensitivity analysis allowed the calculation of total emissions from H_2 production in the 2020 and 2030 scenarios. To this concern, Figures 41-42 show the contributions to emissions from H_2 production in the 2020 scenario with and without WtH_2 technologies, respectively.

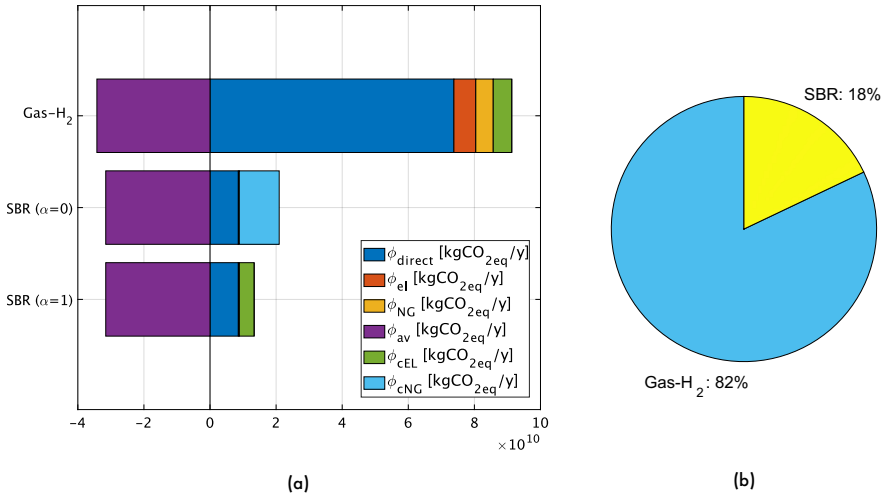

Figure 41. (a) Emissions from H_2 production in 2020 scenario with WtH_2 technologies. (b) H_2 production mix in 2020 scenario with WtH_2 technologies.

The 2020 scenario is characterised by a f_{grid} value of 0.265 [$kgCO_{2eq}$/kWh]. To this concern, the alternative with the best unit emissions is the SBR route, followed by the Gas-H_2, El, SMR and, finally, WtE+El routes (Fig. 40). Having considered the constraints on the availability of biowaste, residual MSW and installed capacity from the electrolysers (see Table 14), the total emissions from H_2 production are $4.6465 \cdot 10^{10}$ [$kgCO_{2eq}$/y] in the presence of WtH_2 technologies. It is noteworthy that, being the f_{grid} value lower than 0.31 [$kgCO_{2eq}$/kWh], bio-CH_4 production was considered the counterfactual scenario in calculating total emissions. With an amount of available biowaste (Bio_{MSW}) of $78.88 \cdot 10^6$ [tMSW/y], SBR offers total emissions of $-1.819 \cdot 10^{10}$ [$kgCO_{2eq}$/y] in case of $\alpha = 1$ and of $-1.0615 \cdot 10^{10}$ [$kgCO_{2eq}$/y] in case of $\alpha = 0$ (Fig. 41a). Given the availability of feedstock, a maximum of 18% of the H_2 required annually can be produced by the SBR route (Fig. 41b). The second alternative with the lowest unit emissions is in this scenario the Gas-H_2 route. With an amount of available residual MSW (Res_{MSW}) of $113 \cdot 10^6$ [tMSW/y], Gas-H_2 offers total emissions of $5.708 \cdot 10^{10}$ [$kgCO_{2eq}$/y]. As can be observed from Figure 41b, 82% of the annual H_2 demand can be produced from the Gas-H_2 route in the 2020 scenario with WtH_2 technologies. In conclusion, a total amount of waste was produced in 2020 that can fully meet the annual H_2 demand from WtH_2 technologies.

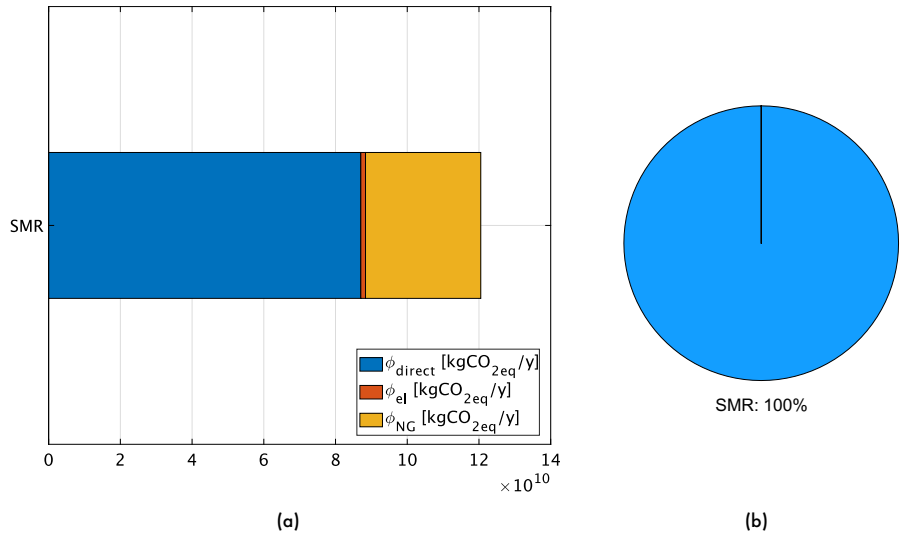

Figure 42. (a) Emissions from H_2 production in 2020 scenario without WtH_2 technologies. (b) H_2 production mix in 2020 scenario without WtH_2 technologies.

Figure 42 shows the contributions to total emissions from H_2 production in the 2020 scenario without the availability of WtH_2 technologies. In this case, given a f_{grid} value higher than 0.26 [$kgCO_{2eq}$/kWh], the best alternative from an environmental point of view is SMR (Fig. 40). Therefore, 100% of H_2 production occurs from this process (Fig. 42b). Emissions generated to meet the annual demand for H_2 are $1.2050 \cdot 10^{11}$ [$kgCO_{2eq}$/y]. Compared to the 2020 scenario with the availability of WtH_2 technologies, there is a 160% increase in total emissions. Therefore, it is possible to conclude that in 2020, using WtH_2 technologies, H_2 demand could have been met while generating significantly lower emissions.

Finally, Figures 43-44 show the contributions to emissions from H_2 production in the 2030 scenario with and without WtH_2 technologies, respectively.

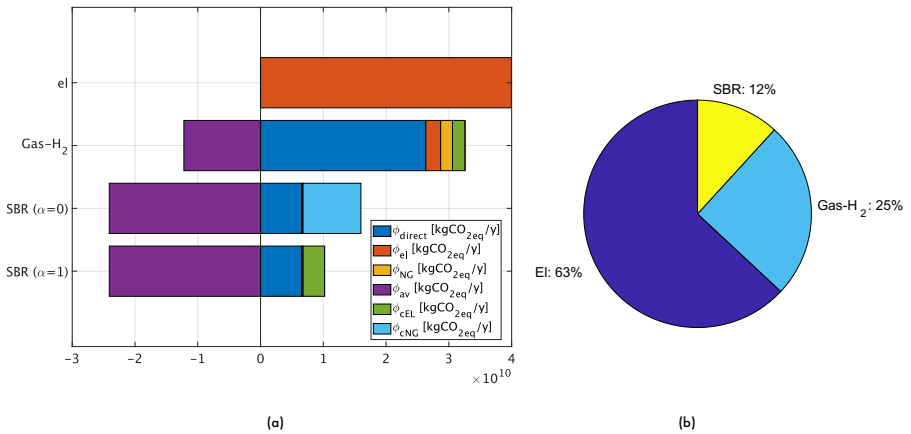

Figure 43. (a) Emissions from H_2 production in 2030 scenario with WtH_2 technologies. (b) H_2 production mix in 2030 scenario with WtH_2 technologies.

The 2030 scenario is characterised by a f_{grid} value of 0.114 [$kgCO_{2eq}$/kWh]. To this concern, the alternative with the best unit emissions is the SBR route, followed by the El, Gas-H_2, SMR and, finally, WtE+El routes (Fig. 40). Having considered the constraints on the availability of biowaste, residual MSW and installed capacity from the electrolysers (see Table 14), the total emissions from H_2 production are $5.2231 \cdot 10^{10}$ [$kgCO_{2eq}$/y] in the presence of WtH_2 technologies. Also, in this case, bio-CH_4 production was considered the counterfactual scenario in calculating total emissions. As can be observed in Table 14, in accordance with EU policies on green H_2 production and MSW management, in this scenario, there is a significant reduction in the availability of waste and an increase in H_2 demand and installed capacity by electrolysers. With an amount of available biowaste (Bio_{MSW}) of $60.24 \cdot 10^6$ [tMSW/y] (-31% with respect to the 2020 scenario), SBR offers total emissions of $-1.3890 \cdot 10^{10}$ [$kgCO_{2eq}$/y] in case of $\alpha = 1$ and of $-8.1066 \cdot 10^9$ [$kgCO_{2eq}$/y] in case of $\alpha = 0$ (Fig. 43a). Given the availability of feedstock, a maximum of 12% of the H_2 required annually can be produced by the SBR route (Fig. 43b). The second alternative with the lowest unit emissions is in this scenario the El route. As highlighted, the installed capacity of electrolysers is expected to increase forty-fold from 2020 ($El_{installed}$=40 GW/y). This enables the production of $70.128 \cdot 10^9$ [Nm^3H_2/y] with associated emissions of $3.99 \cdot 10^{10}$ [$kgCO_{2eq}$/y]. As can be

observed from Figure 43b, 63% of the H_2 annual demand can be satisfied by this process. Finally, with an amount of available residual MSW (Res_{MSW}) of $56 \cdot 10^6$ tMSW/y (-50% with respect to the 2020 scenario), Gas-H_2 offers total emissions of $2.0365 \cdot 10^{10}$ [$kgCO_{2eq}$/y]. As can be observed from Figure 43b, 25% of the annual H_2 demand can be produced from the Gas-H_2 route in the 2030 scenario with WtH_2 technologies.

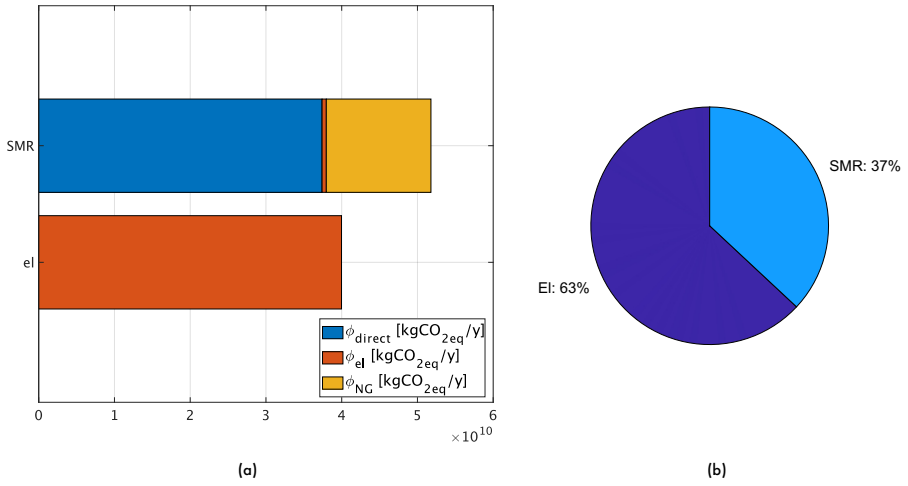

Figure 44. (a) Emissions from H_2 production in 2030 scenario without WtH_2 technologies. (b) H_2 production mix in 2030 scenario without WtH_2 technologies.

Finally, Figure 44 shows the contributions to total emissions from H_2 production in the 2030 scenario without the availability of WtH_2 technologies. In agreement with the results obtained from the sensitivity analysis, the order of preference among the HPRs routes considered involves the El route, followed by the SMR route (Fig. 40). Having considered the constraint on the installed capacity from the electrolysers, it results that the emissions from this process are $3.99 \cdot 10^{10}$ [$kgCO_{2eq}$/y] and that it is possible to produce 63% of the annual H_2 demand through this route (Fig. 44b). The remaining 37% of demand is in this case met by the SMR route (Fig. 44b), with emissions generated of $5.1781 \cdot 10^{10}$ [$kgCO_{2eq}$/y]. The total emissions generated under this scenario are $9.1754 \cdot 10^{10}$ [$kgCO_{2eq}$/y]. In this case, there is a 76% increase in total emissions compared to the 2030 scenario with WtH_2 technologies. Therefore, it is

possible to conclude that even in the 2030 scenario, where the energy transition process will already be at an advanced stage, WtH_2 technologies will be a valuable alternative for producing low-carbon H_2.

From the results obtained, it is possible to conclude that WtH_2 technologies offer real decarbonisation potential, even in scenarios characterised by intermediate energy mixes. Moreover, WtH_2 technologies allow for the simultaneous valorisation of waste, generating, in some scenarios, negative total emissions. These technologies' decarbonisation potential was observed to be very high in the actual transition phase. Consistent with this consideration, the comparison between the 2020 and 2030 contexts shows that the reduction in total emissions offered by WtH_2 technologies in 2020 is much higher than in the case of 2030. In 2030, the transition to more sustainable energy mixes and the capacity for production from electrolysers, together with the decreasing availability of waste, will make water electrolysis, as expected, the best HPR.

Chapter 3

Analytical models development for the steelmaking sector

In this chapter, the case of a crucial sector within the current energy transition, i.e., the steelmaking sector, is explored. It is indeed included among the "hard-to-abate" sectors. There are currently plant solutions for the decarbonisation of the steelmaking process that are mainly based on the use of NG, H_2 and energy from renewable sources. Although these solutions are promising, there are many limitations to their implementation on an industrial scale. In this regard, the following sections illustrate analytical models developed to understand the cost-effectiveness of investing in innovative steelmaking plants and the related decarbonisation potential. Furthermore, the development of an analytical model to assess the decarbonisation potential offered by WtH_2 routes to the steelmaking sector is illustrated.

3.1 Plants solutions for decarbonising the steelmaking sector

Energy transition and industrial emissions abatement are key issues to tackle climate change and achieve the NZE goal by 2050 [244]. To this concern, research efforts to investigate technological solutions enabling environmentally sustainable production are becoming mandatory. In this context, the steelmaking sector plays a key role [245]. Steelmaking is indeed one of the so-called "hard to abate" sectors. They are industrial sectors (e.g., iron and steel, cement and concrete, chemicals, etc.) characterized by high energy demand, high process heat needs, chemical process emissions, and other features that make them inherently difficult to decarbonise [246]. Hard-to-abate sectors account for about 30% of global annual emissions [247]. Among them, steelmaking generates the second largest energy demand and the largest share of emissions [248] (i.e.,7% of global emissions [249]). The negative steelmaking environmental performance depend on the adoption in most plants worldwide (73.2% in 2020 [250]) of the so-called Blast Furnace-Basic Oxygen Furnace (BF-BOF) route. This steelmaking route relies on the use of C-bearing materials for both energy and chemical requirements, resulting in emissions of about 1.8 tCO_{2eq}/t crude steel [251], and energy consumption of about 21 GJ/t crude steel [252]. As it can be observed in Figure 45, global steel production is expected to grow up to 2500 Mt/y by 2050, which would entail, following the current production process, the generation of 4500 tCO_2/y, a not consistent value with the achievement of the global decarbonisation targets [253].

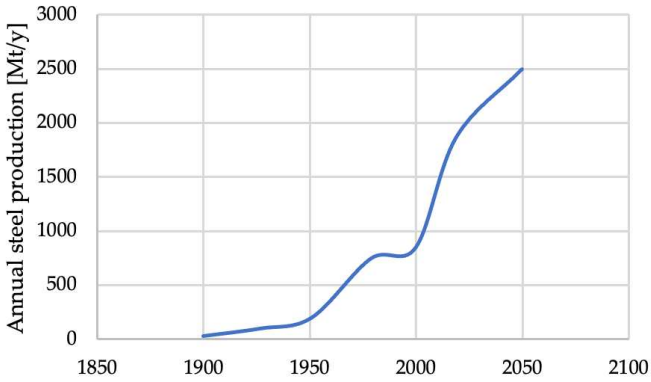

Figure 45. Annual global steel production from 1900 to 2050. Adapted from [253].

The identification of greener solutions for the steelmaking process is environmentally mandatory and is essential for the survival of most economic sectors. Steel is a feedstock for key economic sectors such as transport, construction, domestic appliances, electrical equipment, and machinery. The possibility of producing this raw material in an environmentally sustainable way would therefore allow the improvement of the whole economic system, according to a lifecycle approach [254]. The utmost relevance of this sector has been also confirmed at the 26th Conference of the Parties (COP26) on Climate Change, at which world leaders have signed an ambitious set of common targets, known as Glasgow Breakthrough, including actions for steel decarbonization. To this concern, countries have committed to promoting the production and exchange on global markets of steel produced at "near-zero" emissions by 2030 [255]. Although alternatives to reduce the environmental impact of the BF-BOF route have been investigated, (e.g., adopting a carbon capture utilization and storage system or employing biomass-based products instead of fossil coal [256]–[258]), it is necessary to find solutions that avoid the formation of pollutants and GHGs and reduce the energy consumption of the overall production system.

In the BF-BOF route, the hard coal is transformed into coke through the coke oven, which, together with the agglomerated iron ores (pelleted, sintered) and coal, feeds the BF to produce pig iron. The carbon content is subsequently reduced in the BOF, resulting in the production of liquid steel

(LS) (Figure 46). Table 15 shows the direct CO_2 emissions and direct energy consumption values by plants adopted in the production process.

Table 15. Direct CO_2 emissions and direct energy consumption from the BF-BOF route. Adapted from [259].

Plant	Direct emissions [tCO_2/t crude steel]	Direct energy consumption [GJ/t crude steel]
Coke Plant	0.794	6.539
Sinter plant	0.200	1.549
Pellet plant	0.057	0.901
BF	1.219	12.309
BOF	0.181	-0.853

As it can be observed, the main sources of CO_2 emissions and energy consumption are the coke plant and the BF.

The secondary steel production route (Figure 46) is the most promising alternative to produce steel and reduce CO_2 emissions. It consists of melting 100% of recycled steel scrap in an EAF. In this case, the direct CO_2 emissions and the energy consumption generated by the process would be only those related to the EAF [259]. This approach meets the objective of decarbonising the steelmaking process and enables the transition to a CE, as it does not involve the use of C-bearing virgin materials and allows end-of-life materials to be reintegrated into the production cycle. The average emissions and energy consumption of this process are 0.126 tCO_{2eq}/t crude steel [260] and 11 GJ/t crude steel [261], respectively, 93% lower in emissions and 48% lower in energy consumption than the BF–BOF route. This process, however, is critical because it is totally reliant on the availability of scrap on the market, which is not constant and not easily predictable. Although a break-even point between supply and demand for steel scraps is expected to be reached in the next ten years [262], it is estimated that 50% of steel production in 2050 will still come from the use of virgin material [263].

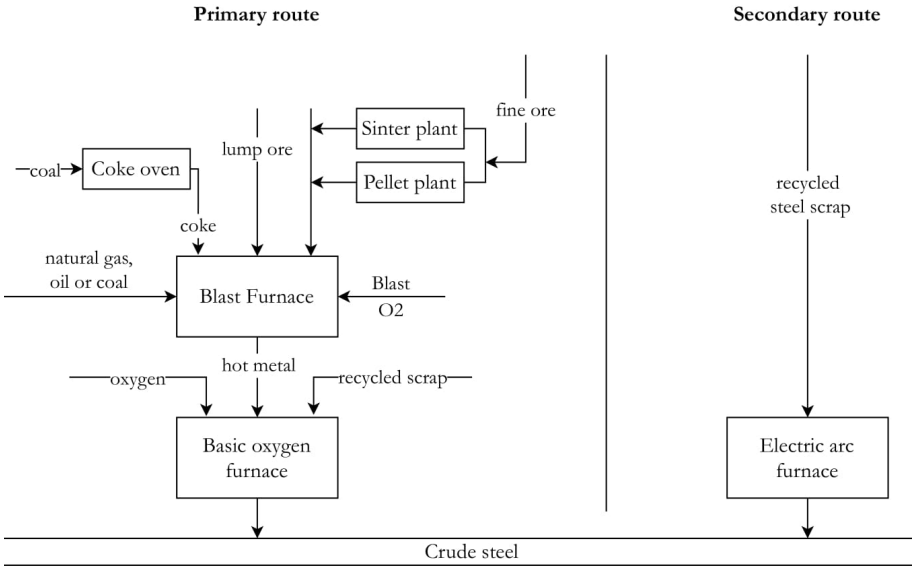

Figure 46. Primary and secondary routes for crude steel production. Adapted from [259].

To this concern, the DRI-EAF route (Figure 47) is identified as the solution which at the same time ensures the availability of feedstock and the reduction of emissions by about 34% compared to the BF-BOF route [264]. It consists of producing DRI, i.e., a virgin raw material, to feed the EAF together with recycled steel scrap. DRI is produced from the reaction between iron oxides at the solid-state (below the fusion temperature of pure iron, 1535°C), hydrocarbon gases, and/or carbon-bearing materials. DRI is a highly metallized solid (i.e., metallization degree around 90-95%) with a more porous structure compared to feedstock iron oxides [265].

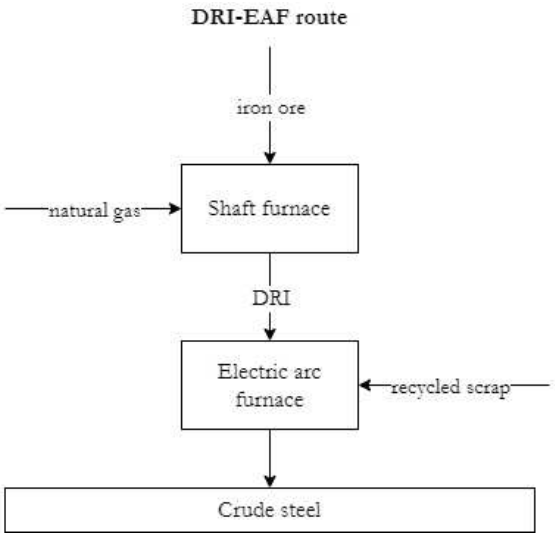

Figure 47. DRI-EAF route for crude steel production. Adapted from [259].

The DRI production processes can be classified as coal-based or hydrocarbon gas-based based on the adopted reducing agent. In the first case, the reducing agents are C-bearing materials (e.g., coal, gasified coal, coke breeze) [266]. In the second case, the reducing agents are hydrocarbon gases (e.g., H_2, carbon monoxide, and NG) [265]. According to [267], nowadays, the hydrocarbon gas-based processes (i.e., NG-based) ensure 92% of the total production of DRI. Specifically, DRI is generally produced through a reducing gas mixture consisting of CH_4 and H_2, mainly obtained from NG reforming. The NG-DRI route is characterized by lower direct emissions compared to the BF–BOF route, about 1.4 tCO_{2eq}/t crude steel [268], but higher energy consumption, about 30 GJ/t crude steel [259].

Although the NG-DRI-EAF route is the most promising alternative at commercial scale, further environmental improvements could be offered by employing the H_2-based DRI-EAF route. It consists of producing DRI by employing H_2 only as reducing gas. The use of pure H_2 in the DRI reducing shaft furnace allows to obtain almost exclusively water vapor as gaseous by-product, thus eliminating direct emissions. If H_2 is produced by electrolysis powered by renewable electricity (i.e., green H_2), indirect emissions are also abated, resulting in an emissions reduction by 95–100% compared to the BF–BOF route [269]. Although this steelmaking route is the most

environmentally favourable, it has a major drawback related to green H_2 production. The adoption of green water electrolysis on an industrial scale faces indeed major barriers, both from an economic and environmental point of view. It is noteworthy that electrolyzers have a high energy consumption (on average 5 kWh/Nm^3H_2 [270]) and large-scale green H_2 production would require an amount of renewable energy that is currently unavailable [271]. Assuming a need for 800 Nm^3/tDRI at 100% H_2 [272], about 40 GWh/y would be required for the production of 1 MtLS/y only for the electrolysis process. According to Vogl et al., indeed, two-thirds of the overall electricity consumption of an H_2-DRI-EAF route are represented by the energy demand of the electrolyser [273]. Similarly, in [274] it is found that the electrolyser efficiency is the most important factor affecting the system energy consumption, and thereby the amount of indirect emissions generated by the steelmaking process. This implies the need for electricity supply from the national power grid, which would result in high indirect emissions. As for the economic aspect, large-scale adoption of electrolysers is very expansive due to high costs for renewable energy production and facilities installation [270]. Moreover, it is noteworthy that the production of electricity from renewable sources is subject to many variations throughout the year and that significant areas are required to obtain an adequate amount of energy; the electricity obtainable through renewable energy conversion systems, above all, depends on the characteristics of the site where the steel is produced, such as global solar radiation and windiness.

Table 16 summarizes the strengths and weaknesses of the direct DRI production processes fuelled by NG and H_2.

Table 16. Strengths and weaknesses of DR processes fuelled with NG and H_2.

DRI production process	Strengths	Weaknesses
NG-DRI	Most developed at industrial scale	Carbon dependence
	Less energy-intensive process	CO_2 abatement potential of 34% compared to the primary route

	Low carbon dependency	Low developed at industrial scale
	CO_2 abatement potential of 95% compared to the primary route	Energy-intensive process
H_2-DRI		Increasing of operational costs by 35-100% compared to the primary route
		High dependence on electricity price
		Variability of available renewable energy

Since the reduction of emissions from the steelmaking process is an urgent issue, a viable solution could be represented by implementing the NG-DRI-EAF process with a gradual transition to the H_2 reduction process in the near future. The NG-DRI-EAF plant is flexible since it can also be used with an NG-H_2 mixture in variable share. Moreover, an energy transition is in progress to increase the availability and reduce the cost of energy from renewable sources [275]. This will allow large-scale installation of electrolysers with benefits both from an environmental and economic perspective (e.g., economies of scale will be generated). During this transition phase, it is needed to identify complementary H_2 production routes that enable the production of low-carbon H_2, thus accelerating the decarbonization process of hard-to-abate sectors.

Due to the scientific relevance of the topic, many studies deal with the investigation of solutions for the decarbonisation of the steelmaking sector. To this concern, in [276], a techno-economic evaluation of CO_2 emission reduction in the iron and steel industry with Carbon Capture and Storage (CCS) was conducted. The processes were assessed by using two indicators: the break-even price of CO_2 emission allowances for CCS and the impact of CCS on steel production cost. The first indicator showed that CO_2 break-even prices are very sensitive to several factors; in most cases, its value can be included in the range of 74 –158 €/t CO_2. Concerning the impact of CCS on steel production cost, the authors claim that CCS costs are heavily dependent not only on the characteristics of the facility and the operational

environment but also on the chosen system boundaries and assumptions. A numerical study on the economic and environmental impact of an integrated steelmaking plant, using surrogate, empirical and shortcut models, has been provided in [277]. In the case of oxygen BF operation, lower environmental emission and higher economic profit were estimated. On the contrary, the route NG-based has been considered most competitive in terms of emissions from the system.

About studies on energy conservation and carbon mitigation, four scenarios to analyse the utilization of CO_2 in the steelmaking process (i.e., BF-BOF, BF-BOF with waste heat and energy recovery, BF-BOF with CO_2 hydrogenation, and EAF) in China have been investigated. The results suggested that BF-BOF with CO_2 hydrogenation is most competitive in terms of energy consumption and under an economic perspective [278]. Recently, an economic comparison between alternatives for LS production with integrated electrolysers based on H_2 has been conducted by Krüger et al. (2020). The authors found that despite the electricity cost represents the main contributor to the cost of LS production using H_2, the low temperature needed for the electrolysis process reduces the overall cost, including investments and running costs [279].

A wide literature is available on technical-economic models on three ore-based steelmaking routes (i.e., BF-CCS route, H_2-DRI route, and Electrowinning (EW)) compared to the BF-BOF. The BF-CCS is based on a regular BF-BOF equipped with top gas recycling and CCS. H_2-DRI is a solid-state reduction process for iron ore using H_2 as a reducing gas. EW is a technology rather immature, based on electrolysis of iron ore in an alkaline solution of 110° C with subsequent refining in EAF. The models found that the H_2-DRI is the most attractive route in economic and environmental terms. Indeed, it was proved that this kind of technology is technically marketable and economically the most profitable investment choice [280][281].

The same steelmaking routes above described (i.e., BF-CCS, H_2-DRI, and EW) have been compared by a Multicriteria-Analysis including five different categories, i.e., technology, society and politics, economy, safety and vulnerability, and ecology. The analysis concludes that EW and, in particular, H_2-DRI, can be identified as the preferred future steelmaking

technology across different perspectives [282]. According to Vogl et al., the total production costs adopting H_2-DRI for fossil-free steelmaking are in the range of 361–640 EUR per ton of steel. The authors highlight a high sensitivity of total production cost to the electricity price and the amount of scrap used. In this regard, the study proved that H_2-DRI becomes cost-competitive with an integrated steel plant at a carbon emission price of 34–68 EUR per ton of CO_2 and electricity costs of 40 EUR/MWh [273].

Similarly, the cost analysis method of LCA has been adopted to analyse the environmental and economic impact of the steelmaking process in China industries. Quantitative analysis shows the cost of molten iron, accounting for 62%, and the total costs of scrap and oxygen, accounting for 10% and 13%, respectively, of the total cost per ton of steel produced. The total cost of auxiliary materials and labour is relatively small, accounting for 15% of the total cost. Therefore, optimizing the utilization of scrap steel and molten iron resources would significantly increase the process cost-saving in the steelmaking system [283]. On the one hand, the adoption of the scraps leads to advantages in economic and environmental terms.

On the other hand, the use of heterogeneous recycled scrap mixtures, not well characterized, increases the steelmaking process's uncertainties. The ferrous scrap stored for long periods in scrap yards can be affected by atmospheric corrosion that degrades its initial quality. An empirical methodology is proposed in [284] to quantify the economic impact of this degradation phenomenon on the EAF performance based on the value in use of the scrap adopted. The value in use includes, besides the purchasing cost, the additional costs associated with extra energy consumption and other additional material consumption (electrode, refractories, fluxes etc.) incurred due to the melting of non-metallic materials included in regular scrap.

Béchara et al. (2018) developed a multiscale (i.e., from the iron ore grains scale, measured in μm, to the shaft furnace scale, measured in hm) process model. They integrated it in a systemic plant-size model to optimize, from an environmental point of view, an NG-based DR process. By conducting different simulations with different inlet gas compositions, they found that NG consumption and CO_2 emissions could be reduced by the setting of ratios H_2/CO and $(H_2 + CO)/(H_2O+CO_2)$ at 1.23 and 12, respectively

[285]. The same authors solved an optimization problem aiming to identify the values of a DR-NG-based process operating parameters to minimize the emissions generated [286]. Sarkar et al. developed a DR-NG shaft thermochemical model to estimate the energy requirement and predict the emissions due to crude steel production, adopting an EAF. According to the model developed, the crude steel production route based on a DR-NG ensures lower CO_2 emissions (i.e., 1269 tCO_2/t crude steel) compared with the traditional BF-BOF route and coke oven gas/syngas route. Similar results were identified by comparing the net energy requirement by DR-NG (i.e., 18.54 GJ/t crude steel) with the net energy requirement by traditional BF-BOF (i.e., 18.56 GJ/t crude steel) [287]. In [288], a mathematical model was developed to estimate the performance of a DRI production plant fuelled with NG in terms of bustle gas temperature, reformer inlet temperature, metalisation degree, carbon content ratio (H_2/CO), reductants to oxidants ratio ((H_2 + CO)/(H_2O + CO_2)), and required compression energy. The influences of the input parameters on the system performance were evaluated to optimize the system's operating conditions. In a later work, the model was extended to describe the operating conditions of an EAF assessing the performance under an economic point of view [289]. Further mathematical models that simulate the reduction of the iron ores in the shaft furnace occur in [290], [291].

Rechberger et al. (2020) evaluate the CO_2 emissions and the electric energy required in systems fueled with NG-DR by varying the hydrogen percentage injected. The achieved result shows that starting from 453 kg CO_2/t DRI for the NG-DR case, the emissions could be reduced to a level of 40 kg CO_2/t DRI maximizing the hydrogen percentage injected. Moreover, the authors proved that, in this case, most CO_2 emissions depend on the electricity required for the electrolysis process. Therefore, increasing the hydrogen percentage injected in the system increases the electrical consumption of the electrolyser [260]. Bhaskar et al. (2020) compared the CO_2 emissions generated from a system based on a hydrogen direct reduction process coupled to an EAF with a traditional liquid steel production system (i.e., BF-BOF route). They found that the emissions of the hydrogen-based route were 1101 kgCO_2/t liquid steel, lower than 35% liquid steel of the traditional route. Both CO_2 emissions were evaluated

assuming a grid emission factor of 295 kgCO_2/MWh, corresponding to all EU countries' average CO_2 emission factor [292].

Similarly, Vogl et al. (2018) assessed the environmental impact of a H_2-based LS production system, adopting a mechanistic model. They evaluated the performance of the steelmaking process by varying the share of iron scrap used to fuel the EAF. They proved that increasing the share of iron scrap reduce the Specific Energy Consumption required by EAF. According to the authors, the lower energy requirement depends on two aspects. The first aspect is related to lower electric consumption of the electrolyser due to the low volume of DRI needed to process. The second aspect depends on a higher efficiency of EAF in steelmaking adopting scraps rather than DRI [273]. The H_2-based route was investigated in Béchara et al. (2018), adopting a shaft furnace mathematical model. The research aimed to compare the DRI production process adopting two different reducing agents (i.e., CO-H_2 mixture and 100% H_2). It emerged that in the case of 100% H_2, the complete metallization of ores could be achieved in a shorter time than to CO- H_2 mixture, thus allowing the utilization of smaller reactors. It was also highlighted that by adopting 100% H_2, the emissions could be reduced by 89-99% compared to the traditional process, assuming the utilization of only renewable or nuclear electricity was used to electrolysis step [293].

Chisalita et al. assessed the possibility of reducing emissions from the BF–BOF route by comparing the emissions generated in a scenario without CCS systems with one with CCS. Through a LCA, they found that integrating CCS into the steel production route decreases the global warming potential in the range of 47.98–75.74% [294]. In [295], the LCA method is employed to evaluate the possibility of reducing emissions from the BF–BOF by pelletizing biocarbon instead of traditional carbon coke. Similarly, in [296], the possibility of using biomass-based products in the primary steelmaking route is assessed and it is understood that it results in a maximum 43% reduction in CO_2 emissions.

3.2 An economic analytical model to assess the profitability of the investment in innovative steelmaking routes

In this section, the development and numerical application of an analytical model for assessing the profitability of investing in decarbonised steelmaking routes is presented. The profitability of the investment in innovative steelmaking routes is strongly related to the variability of some cost figures such as the cost of scraps, iron ore, and energy which are generally affected by market conditions. Therefore, the reliability of an economic evaluation depends on how main cost figures change over time. To this concern, a total cost function was identified to assess the economic convenience of investing in the steel production process through the NG-DRI-EAF route considering the variability of market conditions. A stochastic approach was adopted to identify the profitability of the investment in different scenarios by changing the independent variables' values and estimating the values assumed by dependent variables based on the historical data.

3.2.1 Development of an analytical model for assessing the profitability of the investment in innovative steelmaking routes

The cost breakdown employed to develop the total cost function with the respective cost components can be observed in Table 17.

Table 17. Cost components included in the total cost function.

Cost breakdown	Cost components
Investment	Investment costs for the acquisition of the main facilities of the production system.
Maintenance and operations	Maintenance and operation costs related to the main facilities of the production system.
Energy	Electricity and NG costs for the operation of the production system.
Labour	Labour cost related to the operation of the production system.

Raw materials	Raw materials cost for steel production through the system considered (i.e., iron ore pellets, lime, recycled steel scrap).
General expenditures	Rent, utilities, postage, supplies and computer equipment, etc.

The parameters and the corresponding notation, considered for the formulation of the total cost function, are shown in Table 18.

Table 18. Parameters included in the total cost function of the NG-DRI-EAF steelmaking process.

Parameters	**Notation**	**Unit of measurement**
Nominal plant capacity	P	[Mt/y]
Plant availability	A	[#]
Ratio between DRI and scrap stream to EAF and P	k_1	[#]
Ratio between iron ore stream to shaft furnace and DRI stream	k_2	[#]
Ratio between lime stream to EAF and P	k_3	[#]
Investment costs NG-DRI	C_{DR}	[M€]
Investment costs EAF	C_{EAF}	[M€]
Investment costs continuous casting	C_{CAST}	[M€]
Operations and maintenance costs for EAF, DRI and continuous casting	O&M	[M€/y]
Interest rate	r	[%]
Lifetime of facilities	n	[y]
Equivalent annual cost factor	i	[1/y]
Steel scrap price	φ_s	[€/t]
Iron ore pellets price	φ_{io}	[€/t]
Operating expenditures related to casting and rolling process	op_{cast}	[€/t]
Steel scrap percentage used in the process	α	[#]
Lime cost	c_l	[€/t]
Electricity cost	c_{el}	[€/kWh]
NG cost	c_{NG}	[€/GJ]

Electricity consumption NG-DRI	El_{DR}	[kWh/t]
NG consumption NG-DRI	NG_{DR}	[GJ/t]
Electricity consumption EAF	El_{EAF}	[kWh/t]
Labor cost	c_{lab}	[€/t]
General expenditures	G_{ex}	[M€/y]
Carbon tax	$CO2_{tax}$	[€/tCO_2]
Emission factor from DRI	$CO2_{DR}$	[tCO_2/t]
Emission factor from EAF	$CO2_{EAF}$	[tCO_2/t]
Grid emission factor	em_f	[tCO_2/kWh]

A synthetic representation of the process identifying the material flows considered for each phase is provided (fig. 48). It is possible to observe that the iron ore pellets (m_{io}), bought on the market at φ_{io}-price, is in input to NG-DRI process, where the DRI (m_{DRI}) produced is used, with the contribution of recycled steel scrap (m_s) and lime (m_{lime}), to feed the EAF. According to our assumptions, recycled steel scraps and lime are acquired on the market (φ_s, c_l). The price of the recycled steel scraps is assumed variable over time, and a percentage of scraps equal to 50% is considered to produce liquid steel (m_{ls}). Finally, casting and rolling operations have been adopted to transform liquid steel in hot-rolled coil (m_{HRC}). A residual part of unprocessed material flow is disposed of as slag (ms_{l1}, ms_{l2}).

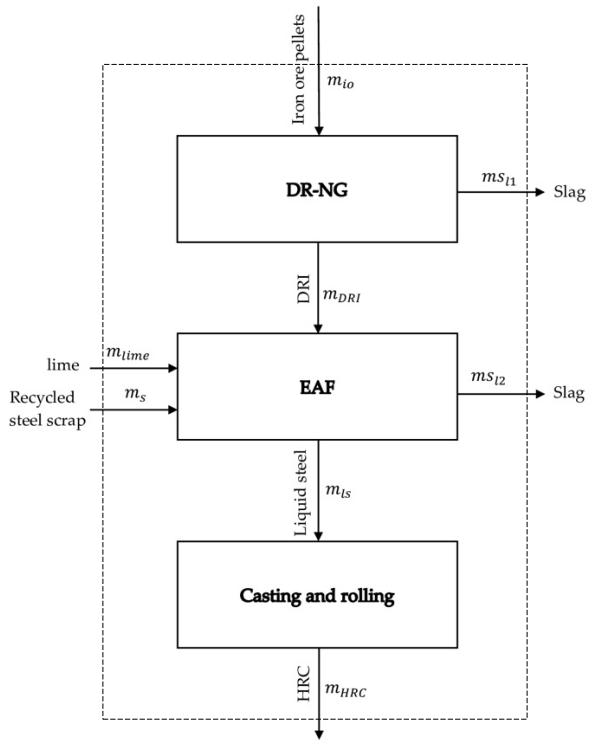

Figure 48. NG-DRI-EAF process with reference material flow considered for each step inside the system's boundaries, identified by the dotted line.

Consistently with the NG-DRI-EAF process above summarized, the price on the market of the iron ore pellets (φ_{io}) and the of the carbon tax ($CO2_{tax}$) represent the input parameters of the total cost function (i.e., independent variables). Observing the historical data, a strict dependency of cost of scarps (φ_s) and cost of hot-rolled coil (φ_{HRC}) on the price of iron ore pellets (φ_{io}) was observed. As possible to observe in Figure 51, the price variability (evaluated in the last 24 months) assumes the same trend over time. Therefore, the price of the iron ore pellets led to estimate the price of scarps (φ_s), and hot-rolled coil (φ_{HRC}) to be included in the cost total function. The total cost function (Φ) allows identifying the convenience of the investment, in terms of profitability (φ), by varying the input parameters' values (fig. 49).

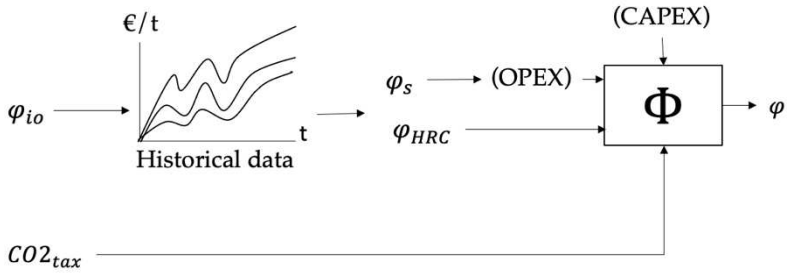

Figure 49. Input and output parameters of the total cost function. OPerating EXpense (OPEX) includes energy, labor, raw materials, general expenditures, maintenance, and operations; CAPital Expenditure (CAPEX) includes Investment costs.

The iron ore pellet price (φ_{io}) is subject to high uncertainty. A uniform probability density function was assumed to predict φ_{io}. Consequently, φ_s e φ_{HRC} are stochastic variables given by historical data relations (fig. X).

The representation of the frequency distribution of the unit profit (φ) has been identified, evaluating the economic convenience of the investment (eq. 93).

$$\varphi = \varphi_{HRC} - \varphi_u \left[\frac{€}{t}\right] \tag{93}$$

Where φ_u is the production cost per ton of hot-rolled coil, defined below (eq. 94), and the total cost function (Φ) has been modelled, according to equation 95, as a function of two independent variables (φ_{io}, $CO2_{tax}$).

$$\varphi_u = \frac{\Phi}{P \cdot A} \left[\frac{€}{t}\right] \tag{94}$$

$$\begin{aligned} \Phi \left[\frac{€}{y}\right] = {} & (C_{DR} + C_{EAF} + C_{CAST}) \cdot i + \text{O\&M} + \varphi_{io} \cdot \mathrm{m_{io}} + \varphi_S \cdot \mathrm{m_s} \\ & + c_l \cdot \mathrm{m_{lime}} + c_{el} \cdot El_{DR} \cdot \mathrm{m_{DRI}} + c_{el} \cdot El_{EAF} \\ & \cdot \mathrm{m_{ls}} + c_{NG} \cdot NG_{DR} \cdot \mathrm{m_{DRI}} + c_{lab} \cdot P + G_{ex} \\ & + op_{cast} \cdot \mathrm{m_{HRC}} + CO2_{tax} \\ & \cdot (CO2_{DR} \cdot m_{DRI} + CO2_{EAF} \cdot m_{ls}) + CO2_{tax} \\ & \cdot em_f (\mathrm{El_{DR}} \cdot \mathrm{m_{DRI}} + El_{EAF} \cdot \mathrm{m_{ls}}) \end{aligned} \tag{95}$$

Where the amount of the material flows considered are given by eqs. 96-103:

$$m_{io}\left[\frac{t}{y}\right]=k_1\cdot k_2\cdot P\cdot(1-\alpha)\cdot A \tag{96}$$

$$ms_{l1}\left[\frac{t}{y}\right]=k_1\cdot P\cdot(1-\alpha)\cdot A\cdot(k_2-1) \tag{97}$$

$$m_{DRI}\left[\frac{t}{y}\right]=k_1\cdot P\cdot(1-\alpha)\cdot A \tag{98}$$

$$m_{lime}\left[\frac{t}{y}\right]=k_3\cdot P\cdot A \tag{99}$$

$$msl_2\left[\frac{t}{y}\right]=P\cdot A\cdot(k_1\cdot(1-\alpha)+k_3+k_1-1) \tag{100}$$

$$m_s\left[\frac{t}{y}\right]=k_1\cdot P\cdot\alpha\cdot A \tag{101}$$

$$m_{ls}\left[\frac{t}{y}\right]=P\cdot A \tag{102}$$

$$m_{HRC}\left[\frac{t}{y}\right]=P\cdot A \tag{103}$$

3.2.2 Numerical application of the analytical model for assessing the profitability of the investment in innovative steelmaking routes

A numerical simulation was carried out to evaluate the profitability of the investment in the NG-DRI-EAF steelmaking process assuming different independent variables' values. In the first phase, the economic convenience was analysed by attributing random values to the independent variable φ_{io} and assuming a null value of the independent variable $CO2_{tax}$. In the second phase, the economic convenience has been analyzed considering the environmental costs in terms of the carbon tax ($CO2_{tax}$) and evaluating the investment profitability.

The total cost function has been applied by assigning different discrete values to input parameters and identifying, for each case, the corresponding profitability.

The system's boundaries are consistent with material flows included in the NG-DRI- EAF process (fig. 48). Therefore, only the emissions related to the operation (i.e., direct emissions) and the energy consumption (i.e., indirect emissions) of considered processes have been assessed. The investment costs were evaluated assuming a plan depreciation period of twenty years (n), including an i-utilization rate. A greenfield condition scenario was assumed for the investment evaluation.

The iron ore pellets price (φ_{io}) has been assumed as a uniform random variable U~[69,174]€/t, according to the probability distribution shown in Figure 50.

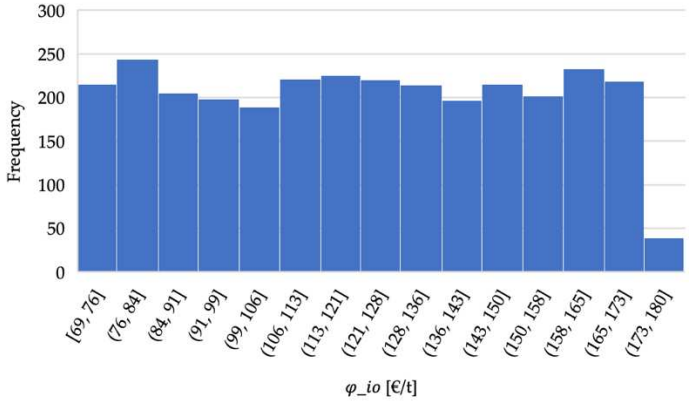

Figure 50. Frequency distribution of the independent variable φ_{io}

The steel scrap (φ_s) and hot-rolled coil (φ_{HRC}) prices, dependent on iron ore pellets price, were identified adopting continuous polynomial functions extracted by historical data of last 24 months (fig. 51).

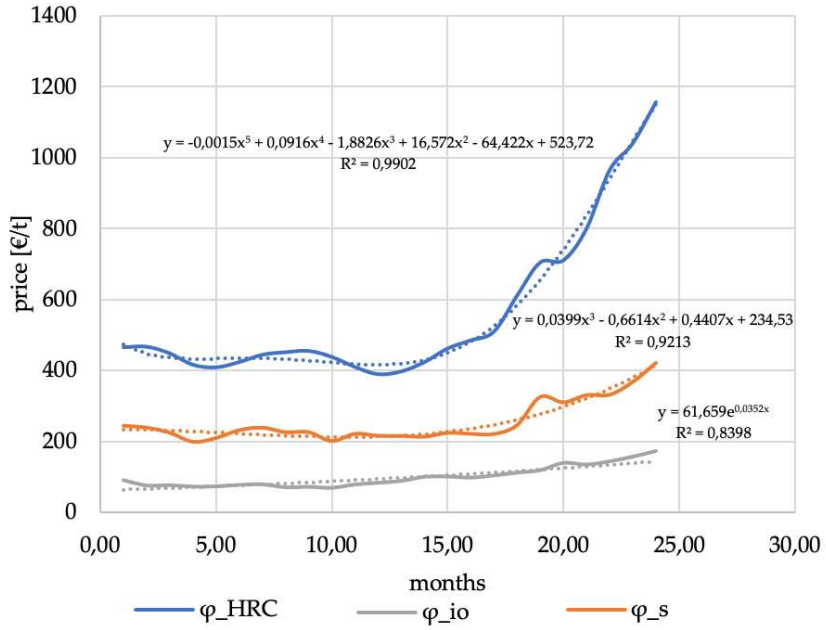

Figure 51. Historical data (from July 2019 to June 2021) referred to iron ore pellets (φ_{io}), steel scrap (φ_s) and hot-rolled coil (φ_{HRC}) prices fitted with continuous polynomial functions.

The summary of the model parameters' values assumed for the numerical simulation, with the corresponding sources, is shown in Table 19. In case data were not available in the scientific literature, they were estimated by interviewing a group of sector experts.

Table 19. Parameters adopted for the numerical simulation with the corresponding reference, classified according to independent variables (IV), dependent variables (V) and constant values (K).

Input	Unit of measurement	Value	Variable type	Source
φ_{io}	€/t	-	IV	[-]
$CO2_{tax}$	€/tCO_2	-	IV	[-]
φ_s	€/t	-	DV	[-]
φ_{HRC}	€/t	-	DV	[-]

P	Mt/y	2	K	Authors' assumption
A	[%]	90	K	Experts' opinion
k_1	[-]	1.15	K	Experts' opinion
k_2	[-]	1.4	K	Experts' opinion
k_3	[-]	0.05	K	Experts' opinion
C_{DR}	M€	237.28	K	Simbolotti and Tosato [297]
C_{EAF}	M€	200	K	Experts' opinion
C_{CAST}	M€	200	K	Experts' opinion
O&M	M€/y	3% of the investment costs	K	Vogl *et al.* [273]
r	%	5	K	Authors' assumption
n	y	20	K	Authors' assumption
i	1/y	0.08	K	Authors' assumption
op_{cast}	€/t	24	K	Experts' opinion
α	t	0,5	K	Authors' assumption
c_l	€/t	90	K	Vogl *et al.* [273]
c_{el}	€/kWh	0.042	K	Eurostat [298]
c_{NG}	€/GJ	3.8068	K	Eurostat [299]
El_{DR}	kWh/t	99	K	Experts' opinion
NG_{DR}	GJ/t	9.6	K	Experts' opinion
El_{EAF}	kWh/t	700	K	Vogl *et al.*[273]
c_{lab}	€/t	53.2	K	Vogl *et al.*[273]
G_{ex}	M€/y	5% of the overall annual cost	K	Experts' opinion
$CO2_{DR}$	tCO_2/t	0.453	K	Rechberger *et al.*[260]
$CO2_{EAF}$	tCO_2/t	0.123	K	Rechberger *et al.* [260]
em_f	tCO_2/kWh	0.0005357	K	ISPRA [300]

As explained, the economic convenience has been analysed by attributing random values to the independent variable φ_{io} and assuming a null value of the independent variable $CO2_{tax}$.

The numerical simulation led to identify the frequency distribution of the cost per ton of hot-rolled coil produced (φ_u) (eq. 93). As shown in Figure 52, in 33% of cases, the value of φ_u is included between 318 and 342 €/t (i.e., the lowest cost per ton of hot-rolled coil). The likelihood that φ_u is higher than 342 €/t decreases up to a relative frequency of 1.7%, corresponding to the maximum unit cost values (included between 630 and 654 €/t). Therefore, considering the variability of φ_{io} and the consequent values assumed by the dependent variable φ_s, it is shown that there is a high probability (33%) to support the minimum possible cost to produce one ton of hot-rolled coil.

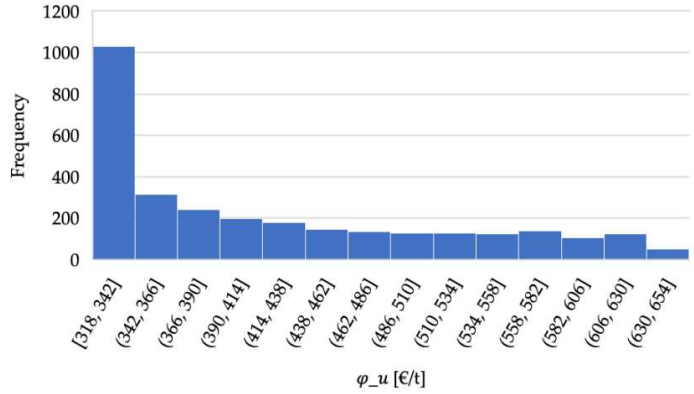

Figure 52. Frequency distribution of the cost per ton of hot-rolled coil produced φ_u

The frequency distribution of steel scrap price (φ_s) (fig. 53a) shows the same trend of φ_u. Therefore, it has been observed that in most cases (40%), the price of steel scrap assumes the lower values included between 212 and 247 €/t. The relative frequency of observations for higher price values decreases and reaches a value of 2.4% in correspondence with the maximum observed values (i.e., [667,702] €/t).

As for the frequency distribution of the dependent variable φ_{HRC} (fig. 53b), it was observed that in most cases (36.8%), the cost of the hot-rolled coil assumes the minimum values (i.e., [409,463] €/t). However, unlike in the previous case, in correspondence with the maximum price range identified

(i.e., [949,1003] €/t), a not negligible relative frequency (16%) has been estimated.

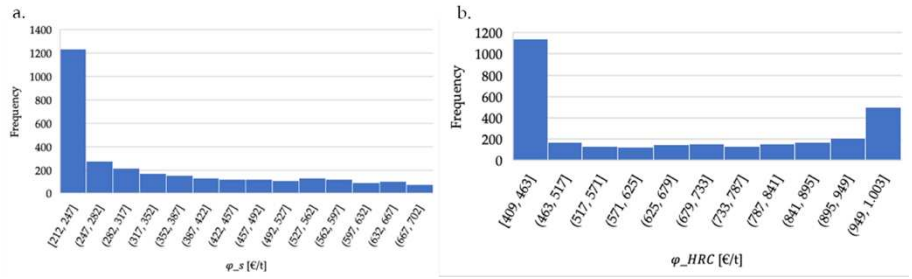

Figure 53. Frequency distributions of market cost of scraps (a) and price of hot-rolled coil (b).

Finally, the frequency distribution of the unit profit φ was estimated. As it can be observed in Figure 54, the numerical simulation didn't provide in any case negative profitability. Therefore, the risk of the investments can be considered very low. In most cases (around 45%), a profit between 75 and 149 €/t has been ensured. According to the economic assessment conducted, only in 0.02% of considered cases, the profitability can be lower than 75 €/t. On the contrary, a profit higher than 149 €/t has been estimated in 53.09% of cases.

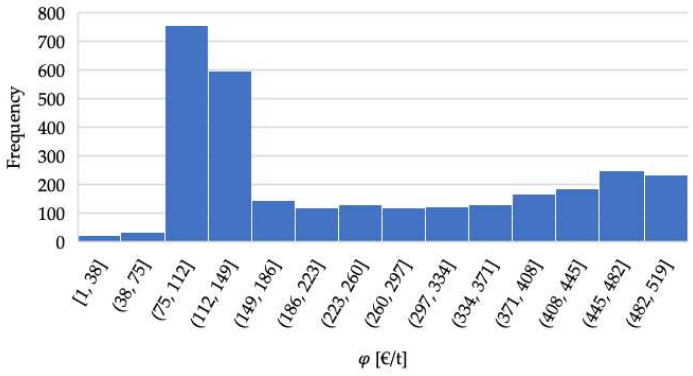

Figure 54. Frequency distribution related to the profitability estimated.

As for the environmental assessment, different values were attributed to the variable $CO2_{tax}$ (i.e., from 10 €/tCO_2 to 1300 €/ tCO_2) and the profitability

of the investment (φ) was assessed in three different scenarios. The variable φ_{io} assumed the minimum (#SC1), the average (#SC2) and the maximum values (#SC3), considering the dataset collected in the last 24 months (Figure 51). The values of the independent variable φ_{io} and the corresponding values assumed by dependent variables φ_s and φ_{HRC}, for each scenario, were summarized below (tab. 20).

Table 20. Values of the variables $\boldsymbol{\varphi_{io}}$, $\boldsymbol{\varphi_s}$ and $\boldsymbol{\varphi_{HRC}}$ adopted to environmental cost assessment.

ID Scenario	$\boldsymbol{\varphi_{io}}$ [€/t]	$\boldsymbol{\varphi_s}$ [€/t]	$\boldsymbol{\varphi_{HRC}}$ [€/t]
#SC1	69	230.4860	434.7010
#SC2	100	219.2060	413.9110
#SC3	174	415.7180	944.7470

Figure 55 shows the most significant results achieved. It is possible to observe that, in cases of carbon tax lower than 130 €/tCO_2, the investment is profitable in all hypothesised scenarios. In the case of $CO2_{tax}$-value corresponds to 130 €/tCO_2, a maximum profit (i.e., 394 €/t) was ensured in scenario 3.

Assuming a carbon tax of 150 €/tCO_2, the investment is not profitable in scenario 2, with an iron ore price (φ_{io}) equal to 100 €/t. In the case of $CO2_{tax}$-value equal to 210 €/tCO_2, a positive profit was estimated only in scenario 3, with an iron ore price (φ_{io}) of 174 €/t. Finally, it was observed that, in cases of carbon tax higher than 750 €/tCO_2, the investment results are not convenient in all scenarios considered.

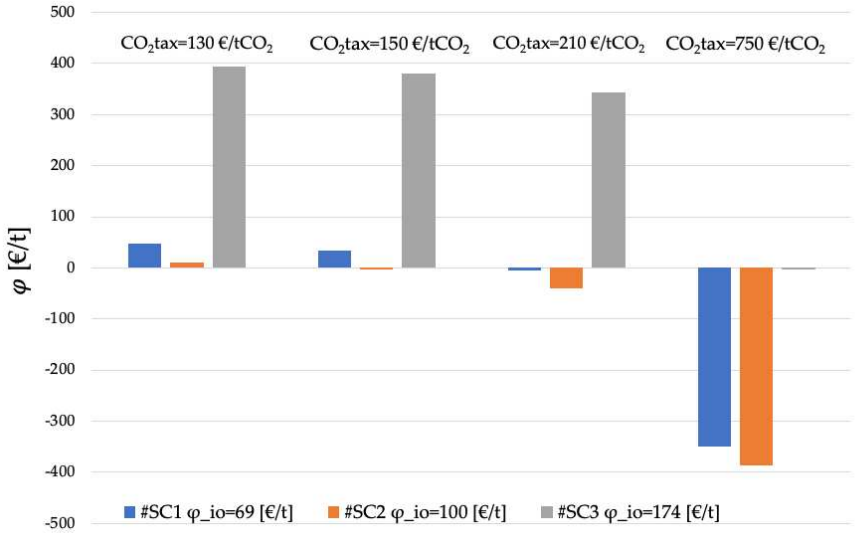

Figure 55. Investment profitability estimation in the different scenarios.

The conducted analysis proved that the environmental costs do not compromise investment convenience. Moreover, the highest carbon tax, currently assumed in European countries, is 116.33 €/tCO_2e (Sweden), more generally the average carbon tax, considering all EU countries, is about 30 €/ tCO_2e [301]. Therefore, it is possible to claim that, considering the market uncertainty of the steelmaking sector in the last 24 months and assuming a gradual increase of the carbon tax in the next years, the investment in the proposed process is profitable from an economic and environmental point of view.

3.3 An environmental analytical model to assess the minimum emission configuration of a green energy-steel system

This section illustrates the development of an analytical model for identifying the minimum emission configuration of a green energy–steel system (GESS) consisting of a secondary route supported by a DRI process and a renewable energy conversion system. The model allows to evaluate

the feasibility of the installation of a H_2-based steel plant considering the characteristics of the site where it is to be located as well as its technological characteristics. Previous studies have focused on the analytical modelling of different steelmaking routes, as well as on the identification of the optimal mix of renewable energies conversion systems for the supply of a H_2-DRI route, but have not considered both systems simultaneously and have not focused on the environmental optimization of a green steel system. The novelty of the proposed approach lies in the simultaneous modelling of an energy system and a steelmaking process, thus making the assessment of the critical availability of green H_2 an inherent part of the problem.

3.3.1 Development of the environmental analytical model to assess the minimum emission configuration of a GESS

Notations adopted in developing the analytical model are in Table 21. Assumed parameters' value or range of variability are provided in the table with corresponding references. In case no references are provided, values are discussed in the remainder of this section.

Table 21. Notations and parameters' values or ranges of variability assumed. The symbol [-] denotes adimensional parameters.

Notation	Unit Measure	Description	Value/Range
S	m^2	Total available area for the installation of renewable energy conversion systems or biomass cultivation.	-
P	tLS/y	Expected yearly production volume of LS.	-
ES_w	$\frac{kWh}{m^2 \cdot y}$	Producibility of electricity per unit installation area from wind turbines.	0÷400 [302]
δ	[-]	Installation area of wind turbines (share of S).	0÷1
ES_{pv}	$\frac{kWh}{m^2 \cdot y}$	Producibility of electricity per unit installation area from photovoltaic panels.	0÷400 [303]
β	[-]	Installation of photovoltaic panels (share of S).	0÷1
η_{bio}	$\frac{Nm^3H_2}{m^2 \cdot y}$	Yield per unit area of biomass culture in volume of hydrogen produced by indirect gasification.	0÷2 [304]

f_w	$\frac{kgCO_{2eq}}{kWh}$	Lifecycle emissions of wind turbines per unit of electricity produced.	0.025 [305]
f_{pv}	$\frac{kgCO_{2eq}}{kWh}$	Lifecycle emissions of photovoltaic panels per unit of electricity produced.	0.090 [306]
f_{bio}	$\frac{kgCO_{2eq}}{Nm^3H_2}$	Emissions from hydrogen production by indirect biomass gasification.	−1.315 [307]
γ	[-]	Biomass cultivation area (share of S).	0÷1
r	[-]	Volumetric share of hydrogen in the reducing gas mixture to produce 1 t of DRI.	0÷1
k	[-]	Ratio of 1 t LS to 1t DRI.	1.150 [308]
α	[-]	Share of scrap employed in EAF to produce 1 t of LS.	0÷1
$CH_4(r)$	$\frac{Nm^3CH_4}{tDRI}$	Methane requirement in the reducing gas mixture to produce 1 t of DRI.	33 ÷259 [272]
f_{CH4}	$\frac{kgCO_{2eq}}{Nm^3CH_4}$	Emissions generated by supplying 1 Nm^3 of methane from NG supply chain.	0.404 [309]
EL_{AUX}	$\frac{kWh}{tLS}$	Electrical consumption of DRI production process auxiliaries for producing 1 t LS.	100 [260]
$EL_{EAF_{DRI}}$	$\frac{kWh}{tLS}$	EAF electricity consumption for producing 1 t LS from DRI.	753 [308]
$EL_{EAF_{SCRAP}}$	$\frac{kWh}{tLS}$	EAF electricity consumption for producing 1 t of LS from scrap.	667 [308]
f_{grid}	$\frac{kgCO_{2eq}}{kWh}$	Emissions from the national grid for the supply of 1 kWh of electricity.	0÷1 [310]
$H_2(r)$	$\frac{Nm^3H_2}{tDRI}$	Hydrogen requirement in the reducing gas mixture to produce 1 t DRI.	0÷800 [272]
EL_{H2}	$\frac{kWh}{Nm^3H_2}$	Electricity demand of the electrolyzer to produce 1 Nm^3 of H_2.	4.8 [260]
$f_{DRI}(r)$	$\frac{kgCO_{2eq}}{tDRI}$	Direct emissions from DRI production process.	40÷450 [260]
$f_{EAF_{SCRAP}}$	$\frac{kgCO_{2eq}}{tLS}$	Direct emissions from EAF producing 1 t LS from scrap.	72 [260]
$f_{EAF_{DRI}}$	$\frac{kgCO_{2eq}}{tLS}$	Direct emissions from EAF producing 1 t LS from DRI.	180 [260]

The overall GESS under investigation consists of a green steel plant (Figure 56a) and an energy system (Figure 56b) operating an assigned site.

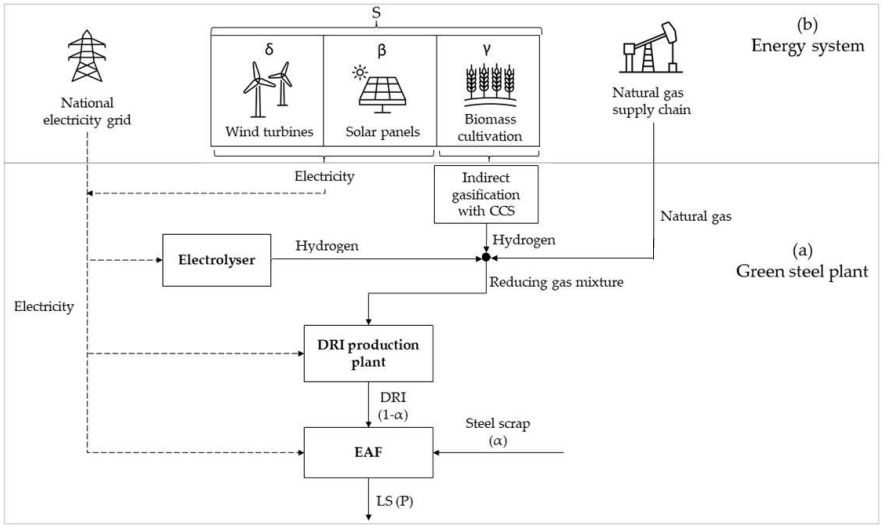

Figure 56. The green energy–steel system investigated: (a) green steel plant; (b) energy system.

The green steel plant (Figure 56a) consists of two main facilities: a DRI plant and an EAF to produce a yearly amount of liquid steel P [tLS/y]. Gas and electricity utilities feed both technological plants. A reducing gas mixture consisting of NG and H_2 is required to produce DRI. H_2 is produced by an electrolyser having an electricity consumption EL_{H2} [kWh/Nm^3H_2] and/or by a gasification unit. DRI is produced in variable share (α) of recycled steel scrap of the overall raw material flow, DRI-steel scraps, feeding the EAF. The DRI plant is fed with the NG–H_2 reducing gas mixture having a volume fraction of hydrogen, r. H_2 fraction depends on the environmental performance of the energy system, technology adopted for H_2 production, and steel scraps fraction (α). Electricity demand of the whole green steel plant is met primarily by energy produced by renewable energy conversion systems and integrated by the supply from the national electricity grid. Steemaking processes not adopting DRI as virgin material are not considered in the modelled green steel plant, as well as the type of steel to be produced.

The energy system (Figure 56b) consists of national electricity grid and a local renewable energy conversion system. The former system supplies

electric energy with almost unlimited capacity; it is characterized by a greenhouse gas emission factor, f_{grid} [$kgcO_{2eq}/kWh$], which depends on the mix of renewable/fossil energy sources of power plants feeding the national grid. The local renewable energy conversion system consists of a wind power plant and/or a photovoltaic plant; both power plants are limited in power capacity as they are installed in an area of limited extension S [m^2]. Wind and solar installations occupy a share of S, respectively, δ and β. In the same area, cultivated biomass, installed in a share γ of S is a feedstock for an indirect gasification process with CCS to produce H_2. Wind and photovoltaic power stations are characterized by an average yearly electricity production capacity per unit area and a lifecycle greenhouse gas emission factor per unit of electricity produced ES_w [$kWh/m^2 \cdot y$], f_w [$kgcO_{2eq}/kWh$] andES_{pv} [$kWh/m^2 \cdot y$], f_{pv} [$kgcO_{2eq}/kWh$], respectively. As far as the indirect gasification process is concerned, the H_2 production yield is referred here to the unit area of biomass cultivation, η_{bio} [$Nm^3H_2/m^2 \cdot y$], and a lifecycle emission factor per unit of H_2 produced, f_{bio} [$kgcO_{2eq}/Nm^3H_2$], is considered. An electrolysis unit powered by the electricity grid integrates H_2 required by the DRI production process. The energy system also includes a NG grid with almost unlimited capacity; NG integrates reducing gas required by the DRI production process. The NG supply chain is characterized by an emission factor, f_{CH4} [$kgCO_{2eq}/Nm^3CH_4$], which considers carbon emissions from gas extraction to transport and utilization. Electricity generated by renewable energy plants or made available by the grid, as well as H_2 produced by biomass or electrolyser, are utilities feeding the green steel plant.

The model proposed aims at identifying the minimum emission configuration of the energy system and of the green steel plant. Configuration is defined by values assumed by the variables considered in the analytical model (Table 21). Variables can be classified according to two categories (Figure 57):

- Exogenous variables: they are variables that cannot be influenced by the decision-maker because of the characteristics of the site where the GESS is expected to be located and the dynamic of the

raw materials market. In the context of the present work, the energy and H_2 producibility per unit area, the share of scrap employed to produce LS in EAF, the national grid emission factor, and the NG supply chain emission factor are considered in this category. The amount of energy and H_2 that can be produced per unit area by renewable energy conversion systems (i.e., wind turbines, and solar panels) depends on the characteristics of the installation site, such as windiness and global solar radiation, and the availability of steel scrap on the market cannot be influenced by the needs of a single plant and, finally, emissions from the electricity grid depend on the national energy mix.

- Endogenous variables: they are variables set by the decision-maker during the plant design phase. In the context of the present work, the total area of the energy system, the volumetric share of H_2 in the reducing gas of the DRI production process, the electrolyzer technology to be adopted, and the expected yearly production volume of LS are considered in this category since they are characteristic choices of a plant design.

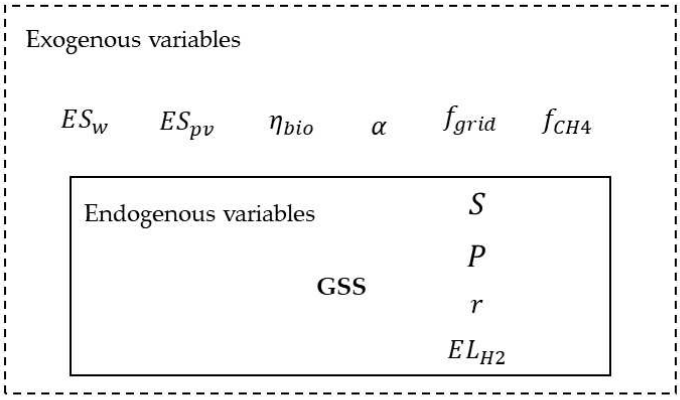

Figure 57. Exogenous and endogenous variables considered in the analytical model.

In accordance with the GHG protocol [311], the overall emissions of the system are expressed according to equation 104.

$$\varphi_{tot}\left[\frac{kgCO_{2eq}}{tLS}\right]=\varphi_{direct}+\varphi_{indirect} \quad (104)$$

Where:

- $\varphi_{direct}\ \left[\frac{kgCO_{2eq}}{tLS}\right]$: are direct emissions generated by the green steel plant. "Direct GHG emissions" are defined as GHG emissions generated in owned or controlled process equipment [311]. In the green steel plant, direct emissions are from DRI plant with an emission factor, $f_{DRI}(r)$, and from the EAF. Different EAF emission factors in case of scraps or DRI feeding it are considered ($f_{EAFSCRAP}$ and f_{EAFDRI}, respectively).
- $\varphi_{indirect}\ \left[\frac{kgCO_{2eq}}{tLS}\right]$: are the emissions generated by the production of electricity and the supply of NG to power the DRI process. As established by the GHG protocol [311], "electricity indirect emissions and other GHG emissions" are defined as emissions deriving from the production of electricity consumed by the plant and from activities that can be considered a consequence of the plant's activity, e.g., the extraction and transport of raw materials. The characteristic of indirect emissions is that, although they do not physically occur at the plant site, they have a significant influence on the total account of the emissions generated. In the case of the analysed system, lifecycle emissions related to renewable energy conversion systems to produce electricity and H_2, emissions related to the production of electricity fed into the national grid (f_{grid}), and emissions generated by the NG supply chain to power the DRI production process (f_{CH4}) were considered in this category. As far as emissions related to renewable energy and biomass conversion systems are considered, lifecycle emissions have been taken into reference as, on the one hand, all stages of the lifecycle of wind turbines and photovoltaic panels, from production to decommissioning, were considered (f_w, f_{pv}), while, on the other hand, consideration of the carbon sink associated with the growth of biomass was included (f_{bio}). In this work emissions due to iron ore extraction and scrap transport were not included in the model as they represent invariant variables in the optimization process.

Direct emissions (eq. 104) can be evaluated according to equation 105.

$$\varphi_{direct}\left[\frac{kgCO_{2eq}}{tLS}\right]=(1-\alpha)\cdot\left(\frac{f_{DRI}(r)}{k}+f_{EAF_{DRI}}\right)+\alpha\cdot f_{EAF_{SCRAP}} \quad (105)$$

Direct emissions include emissions from the DRI production process and EAF emissions, weighted on the share (α) of recycled steel scrap employed to produce LS. Direct emissions from the EAF have a different value, depending on whether recycled steel scrap ($f_{EAF_{SCRAP}}$) or DRI ($f_{EAF_{DRI}}$) feeds the furnace [308]. The direct emissions generated by the DRI production process were considered as a function of the volumetric share of H_2 in the reducing gas ($f_{DRI}(r)$).

Indirect emissions can be calculated according to equation 106.

$$\varphi_{indirect}\left[\frac{kgCO_{2eq}}{tLS}\right]=\varphi_{NG}+\varphi_{renewables}+\varphi_{grid} \quad (106)$$

$$\varphi_{NG}\left[\frac{kgCO_{2eq}}{tLS}\right]=(1-\alpha)\cdot\frac{CH_4(r)}{k}\cdot f_{CH4} \quad (107)$$

Equation 107 allows evaluating the indirect emissions generated by the supply of NG for the DRI production process. These emissions were accounted only for the DRI share employed to produce LS (1-α); moreover, the NG requirement was considered as function of the volumetric share of H_2 in the reducing gas ($CH_4(r)$).

$$\varphi_{renewables}\left[\frac{kgCO_{2eq}}{tLS}\right]=\frac{S\cdot(\delta\cdot ES_w\cdot f_w+\beta\cdot ES_{pv}\cdot f_{pv}+\gamma\cdot\eta_{bio}\cdot f_{bio})}{P} \quad (108)$$

In Equation 108, the indirect emissions generated by the energy system producing electricity and H_2 are computed. As it can be observed, global emissions mainly depend on the total area committed to the energy system (S) as well as on the shares of the area dedicated to the installation of the considered renewable energy conversion systems (δ,β) and the cultivation of biomass (γ). These indirect emissions also depend on the producibility of energy and H_2 per unit area for each of the alternatives considered (Es_w,Es_{pv},η_{bio}).

$$\varphi_{grid}\left[\frac{kgCO_{2eq}}{tLS}\right]=[E_{demand}-\frac{S\cdot(\delta\cdot ES_w+\beta\cdot ES_{pv})}{P}]\cdot f_{grid} \quad (109)$$

Equation 109 models the indirect emissions related to the supply of electricity from the national grid, with a characteristic emission factor f_{grid}. In eq. 109, the electricity supplied from the national grid is evaluated as the amount required by the steel system and not satisfied by the energy system. The more electricity produced by the energy system, therefore, the lower the emissions generated by the supply of electricity from the national grid.

Energy demand of the green steel plant is given in equation 110.

$$E_{demand}\left[\frac{kWh}{tLS}\right]=\begin{bmatrix}(1-\alpha)\cdot(EL_{AUX}+EL_{EAF_{DRI}})+\alpha\cdot EL_{EAF_{SCRAP}}+\\ \left((1-\alpha)\cdot\frac{H_2(r)}{k}-\frac{\gamma\cdot S\cdot\eta_{bio}}{P}\right)\cdot EL_{H2}\end{bmatrix} \quad (110)$$

The energy demand from the plant was also weighted according to the share of recycled steel scrap used for the production of liquid steel (α), and two different electricity consumptions of the EAF were considered ($EL_{EAF_{DRI}}$,$EL_{EAF_{SCRAP}}$), depending on whether DRI or scrap is processed. The H_2 requirement to supply the DRI production process was considered as a function of the volumetric share of H_2 used in the reducing gas ($H_2(r)$). The electrical requirement to produce H_2 from electrolyser was considered for the share of the total H_2 requirement not produced by indirect gasification of biomass.

As shown in Equation 106, indirect emissions of the system consist of three contributions: emissions due to NG supply chain as well as to grid and renewable sources operation to produce electricity or H_2. The more electricity that is produced by the renewable energy system, the lower the grid emissions are (eq. 109). For this reason, it is possible to compare the environmental effectiveness of renewable energy conversion and H_2 production systems on the basis of the avoided emissions. For this purpose, avoided emissions for each of the *i*-th renewable energy systems (*i* = wind, solar, biomass) are computed per unit installation area (Av_{em_i}) as the product of the *i*-th electricity yield (Es_i) and of the difference between the

grid emission factor (f_{grid}) and the lifecycle emissions factor of the *i*-th alternative (f_i) (Equation 111).

$$Av_{em_i}\left[\frac{kgCO_2}{m^2 \cdot y}\right] = ES_i \cdot f_{grid} - ES_i \cdot f_i = ES_i \cdot (f_{grid} - f_i) \quad (111)$$

In the case of H_2 production, the avoided emissions are calculated with reference to the production of H_2 from the electrolyser powered by the grid. Avoided emissions per unit area in case of the alternatives considered are in Equations 112-114:

$$Av_{em_w}\left[\frac{kgCO_2}{m^2 \cdot y}\right] = ES_w \cdot (f_{grid} - f_w) \quad (112)$$

$$Av_{em_{pv}}\left[\frac{kgCO_2}{m^2 \cdot y}\right] = ES_{pv} \cdot (f_{grid} - f_{pv}) \quad (113)$$

$$Av_{em_{bio}}\left[\frac{kgCO_2}{m^2 \cdot y}\right] = \eta_{bio} \cdot (EL_{H2} \cdot f_{grid} - f_{bio}) \quad (114)$$

Since f_{grid}, Es_w, Es_{pv}, and η_{bio} are exogenous variables, they are not subjected to optimization; their values depend on the GESS site location characteristics (e.g., average windiness, solar global radiation, cultivation yield) as well as on technology factors such as the electricity consumption of the electrolyser and the national grid emission factor.

For a given renewable energy system, avoided emissions differ at each location. For a given location, avoided emissions vary on the basis of the renewable energy system adopted:

$$ES_w \cdot (f_{grid} - f_w) \neq ES_{pv} \cdot (f_{grid} - f_{pv}) \neq \eta_{bio} \cdot (EL_{H2} \cdot f_{grid} - f_{bio}) \quad (115)$$

As an example, in case of

$$ES_w \cdot (f_{grid} - f_w) > ES_{pv} \cdot (f_{grid} - f_{pv}) > \eta_{bio} \cdot (EL_{H2} \cdot f_{grid} - f_{bio}) \quad (116)$$

Being

$$\delta + \beta + \gamma = 1 \text{ with } 0 \leq \delta, \beta, \gamma \leq 1 \quad (117)$$

then,

$$S \cdot ES_w \cdot (f_{grid} - f_w) \geq S \cdot \delta \cdot ES_w \cdot (f_{grid} - f_w) + S \cdot \beta \cdot ES_{pv} \cdot (f_{grid} - f_{pv}) + \\ + S \cdot \gamma \cdot \eta_{bio} \cdot (EL_{H2} \cdot f_{grid} - f_{bio}) \quad (118)$$

In this case, maximum avoided emissions are obtained with $\delta=1$, $\beta=0$, $\gamma=0$. Therefore, only one out of the three renewable energy system alternatives has to be considered as the best alternative from an environmental point of view for a specific site. In accordance, Equations 108-110 can be rearranged as:

$$\varphi_{renew} \left[\frac{kgCO_{2eq}}{tLS}\right] = e_{renew} \cdot f_{renew} + H_{2bio} \cdot f_{bio} \quad (119)$$

$$\varphi_{grid} \left[\frac{kgCO_{2eq}}{tLS}\right] = [E_{demand} - e_{renew}] \cdot f_{grid} \quad (120)$$

$$E_{demand} \left[\frac{kWh}{tLS}\right] = \left[\begin{array}{c} \left((1-\alpha) \cdot (EL_{AUX} + EL_{EAF_{DRI}}) + \alpha \cdot EL_{EAF_{SCRAP}}\right) + \\ \left((1-\alpha) \cdot \frac{H_2(r)}{k} - H2_{bio}\right) \cdot EL_{H2} \end{array}\right] \quad (121)$$

Where:

$$e_{renew} = \delta \cdot \frac{S \cdot ES_w}{P} + \beta \cdot \frac{S \cdot ES_{pv}}{P} \quad (122)$$

$$f_{renew} = \delta \cdot f_w + \beta \cdot f_{pv} \quad (123)$$

$$H_{2bio} = \gamma \cdot \frac{S \cdot \eta_{bio}}{P} \quad (124)$$

with $\delta,\beta,\gamma \in \{0;1\} \wedge \delta+\beta+\gamma=1$.

3.3.2 Numerical application of the environmental analytical model to assess the minimum emission configuration of a GESS

Figure 58 shows the procedure for applying the model in order to identify the minimum emission configuration of the GESS considered.

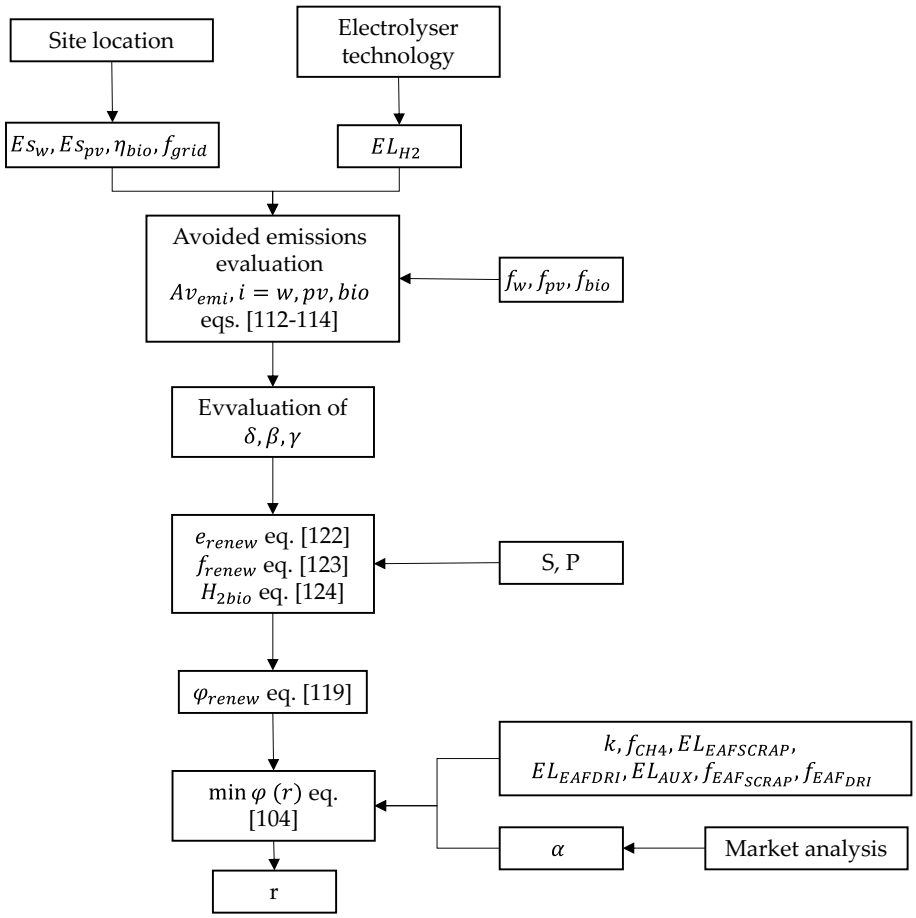

Figure 58. Procedure for applying numerically the developed analytical model.

Once the site location for the GESS's installation has been identified, the values of the variables ES_w, ES_{pv}, η_{bio}, f_{grid} can be obtained. It is also necessary to choose the electrolyser technology to be adopted (EL_{H2}).

From these data it is possible to evaluate the avoided emissions from the electricity grid for each of the renewable energy system alternatives considered (eq. 112-114), and to identify the one that provides the highest contribution. Depending on the specific context, therefore, it is possible to identify which one among the variables δ, β, γ should assume value 1, i.e., which one among the renewable energy conversion systems is to be installed. By choosing the liquid steel annual production capacity P, and the area S to be dedicated to the installation of the renewable energy conversion system identified, it is possible to calculate the values of e_{renew}, f_{renew}, H_{2bio} (eq. 122-124), and finally φ_{renew} (eq. 119). The share of available steel scrap with respect to annual requirements (α) can be obtained by market analysis. By assuming the values of the variables k, f_{CH4}, $EL_{EAF_{SCRAP}}$, $EL_{EAF_{DRI}}$, EL_{AUX}, $f_{EAFS_{SCRAP}}$, $f_{EAF_{DRI}}$, it is possible to calculate the value of the total emission function φ_{tot} (eq. 104) and to find the optimal value of the volumetric share of H_2 in the reducing gas mixture to be adopted in the DRI production process (r), minimizing emissions.

Figures 59 and 60 illustrate the results obtained from the numerical simulations carried out by calculating the avoided emissions in two scenarios corresponding to two different values of f_{grid} (corresponding to the 2019 Italian and French energy mix [220]). In both cases, avoided emissions were calculated for each of the energy system alternatives considered (eq. 122-124) by varying specific electricity/H_2 producibility values (ES_w, ES_{pv}, η_{bio}) with the aim of identifying the renewable energy conversion systems to be installed to maximize avoided emissions.

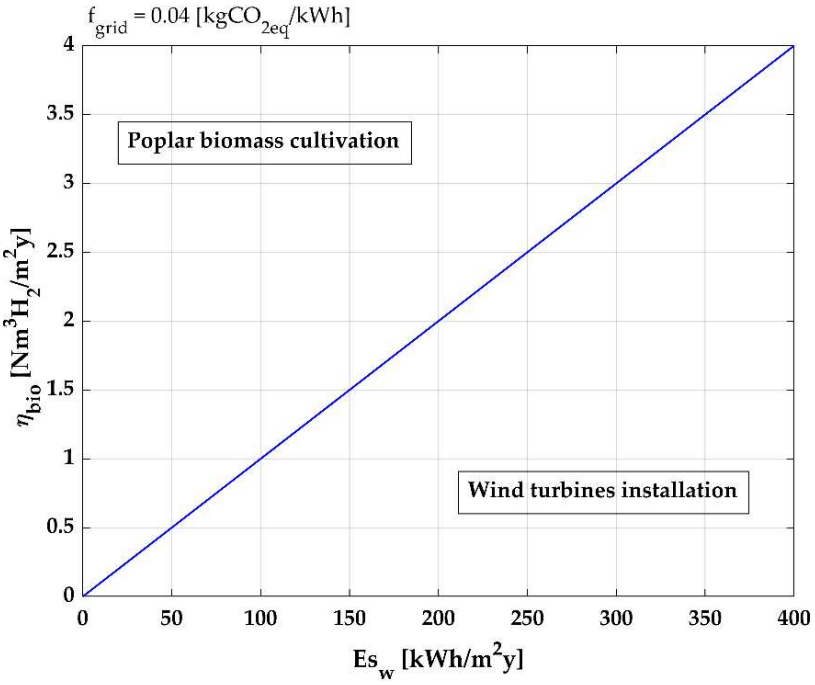

Figure 59. Results of the numerical simulation on avoided emissions in case of f_{grid}=0.04 $kgCO_{2eq}$/kWh.

Results obtained in the case of f_{grid}=0.04 $kgCO_{2eq}$/kWh are shown in Figure 59. As it can be observed, in this scenario, there are only two alternatives to choose from for the energy system configuration, i.e., wind turbines and poplar biomass cultivation (δ=1 or γ=1). In this scenario, installation of photovoltaic panels is never representative of the best alternative since photovoltaic emission factor (f_{pv}) is higher than the grid one (f_{grid}). For each site it possible to identify a point p $\left(ES_w,\eta_{bio}\right)$ located in a region of the plane characterized by an optimal solution, corresponding to the energy system configuration to be adopted. If the point p belongs to the line in the graph, the two energy conversion systems (wind, biomass) lead to the same environmental benefit.

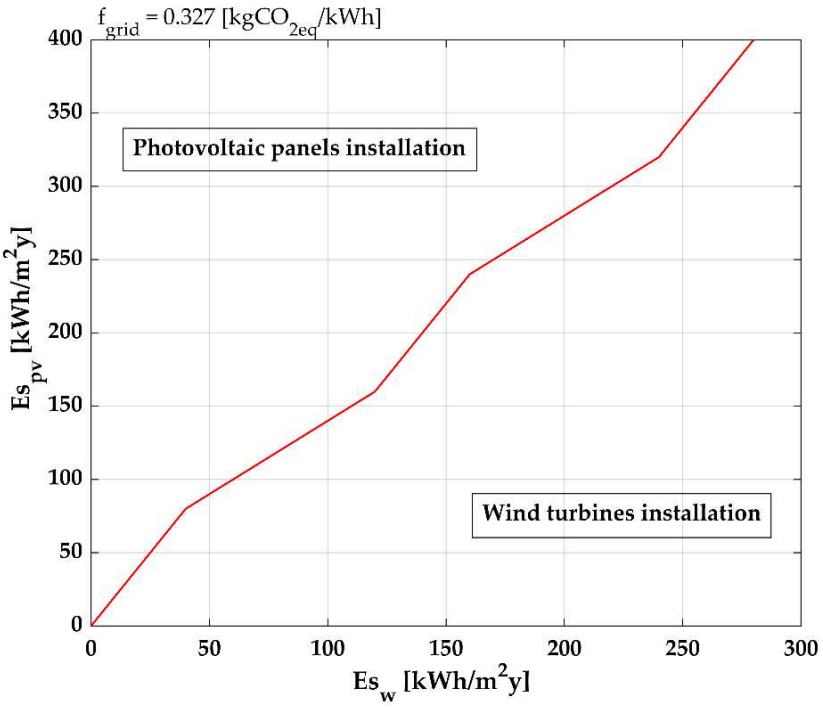

Figure 60. Results of the numerical simulation on avoided emissions in case of f_{grid}=0.327 $kgCO_{2eq}$/kWh.

Figure 60 shows the results obtained in case of f_{grid}=0.327 $kgCO_{2eq}$/kWh. Differently to the previous case, the two alternatives to choose from in this scenario are wind turbines and photovoltaic panels (δ=1 or β=1). Although biomass cultivation always offers positive avoided emissions (it has a negative characteristic emission factor f_{bio}), it never results as the best alternative since significant avoided emissions are from the production of electricity from energy conversion systems. Additionally, in this case, depending on the ES_w,ES_{pv}values of the site under analysis, it is possible to identify a point p of (Es_w,Es_{pv}) coordinates, located in a region of the plane characterized by an optimal solution, corresponding to the energy system configuration to be adopted.

According to the results obtained, it is noteworthy that the only scenario in which biomass cultivation could be the best alternative is the one

characterized by f_{grid}=0.04 $kgCO_{2eq}$/kWh. This implies that the starting condition represented by a particularly "green" national energy mix is required to trigger a mechanism of synergic relations between green steel production and the supporting public infrastructure. Once the best solution has been identified (eq. 112-114), and the values of S and P have been chosen, the values of e_{renew}, f_{renew}, H_{2bio} (eq.122-124), and φ_{renew} (eq. 119) are calculated (Figure 58). According to the results obtained (Figures 59 and 60), it is noteworthy that only in the scenario characterized by f_{grid}=0.04 $kgCO_{2eq}$/kWh, can the value of φ_{renew} be negative, with biomass cultivation being a possible best alternative.

Once the energy system has been optimally configured, it is possible to size the green steel plant. First, based on available market data, the maximum availability of recycled steel scrap must be identified (α). The more recycled steel scrap that can be used to feed the EAF (i.e., as close as possible to a theoretical secondary route), the more the sustainable steel production is considered from an environmental point of view. In this way, a valuable resource (scrap) can be placed back into the production cycle, avoiding the consumption of energy and raw materials associated with the production of DRI. Figure 61 shows the trend of total emissions φ_{tot} as a function of the α variable in different scenarios. The value of the remaining variables (i.e., k, f_{CH4}, $EL_{EAFSCRAP}$, EL_{EAFDRI}, EL_{AUX}, $f_{EAFSCRAP}$, f_{EAFDRI}) has been set according to Table 21.

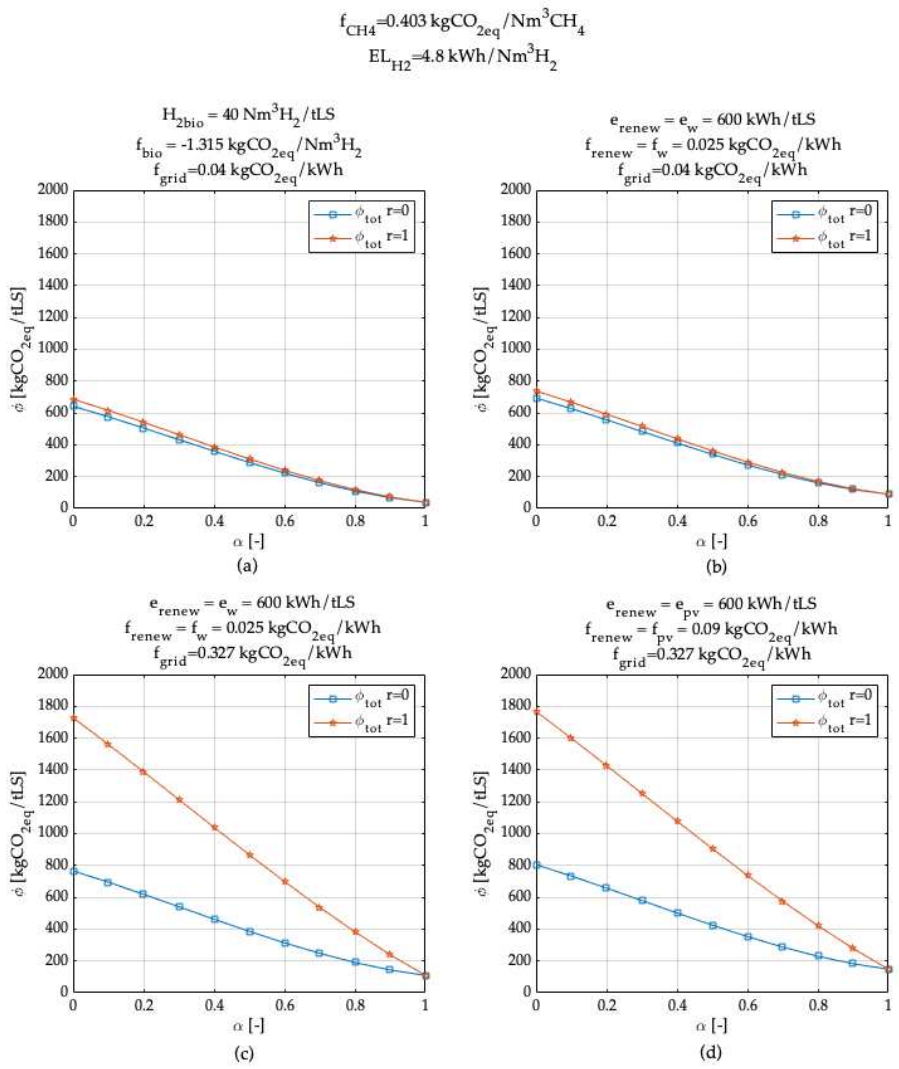

Figure 61. Trend of total emissions φ_{tot} as a function of the share of recycled steel scrap α in two scenarios characterised by different values of the volumetric share of H_2 in the DRI reducing gas mixture r. (a) H_2 production from biomass gasification and f_{grid}=0.04 $kgCO_{2eq}$/kWh. (b) Electricity production from wind turbines and f_{grid}=0.04 $kgCO_{2eq}$/kWh. (c) Electricity production from wind turbines and f_{grid}=0.327 $kgCO_{2eq}$/kWh. (d) Electricity production from solar panels and f_{grid}=0.327 $kgCO_{2eq}$/kWh.

The scenarios were built up according to the results obtained from the preview simulations. Electricity production from wind turbines (Figure 61b) and biomass cultivation (Figure 61a) were considered in the case of f_{grid}=0.04 $kgCO_{2eq}$/kWh, and electricity production from wind turbines (Figure 61c) or photovoltaic panels (Figure 61d) in the case of f_{grid}=0.327 $kgCO_{2eq}$/kWh. The trend of φ_{tot} was evaluated in the case of a reducing gas consisting of H_2 only (r=1) or NG (r=0). As itcan be observed, in all cases, φ_{tot} decreases as the value of α increases. For this reason, it is advisable to maximize the value of this variable as much as possible (consistently with market availability) when sizing the green steel plant. It can also be observed that, in the case of national "green" electricity production (f_{grid}=0.04 $kgCO_{2eq}$/kWh), the value of total emissions is significantly lower than in the case of f_{grid}=0.327 $kgCO_{2eq}$/kWh. Finally, it is noteworthy that, in the scenarios characterized by f_{grid}=0.327 $kgCO_{2eq}$/kWh, there is a significant gap between the emissions in the cases of r=1 and r=0. At α=0 and f_{grid}=0.327 $kgCO_{2eq}$/kWh, indeed, emissions at r=1 are about 125% higher than at r=0, while at α=0 and f_{grid}=0.04 $kgCO_{2eq}$/kWh, the difference is about 8%. This highlights the relevance of emissions generated by the supply of energy for H_2 production with respect to the GESS's total emissions. It is, therefore, possible to observe how, in the presence of favourable infrastructural conditions (i.e., low value of f_{grid}), synergies are generated and the production of steel using H_2 is favored.

After assigning (endogenous) or deriving (exogenous) values for all variables through the illustrated procedure (Figure 58), the objective is to identify the value of r that minimizes the total emissions function φ_{tot}. It is not possible to predict whether the value of this variable should be minimized or maximized (as in the case of α, which should be maximized in all cases), since increasing r generates the opposite effects in the contributions that constitute the total emissions function (Figure 62).

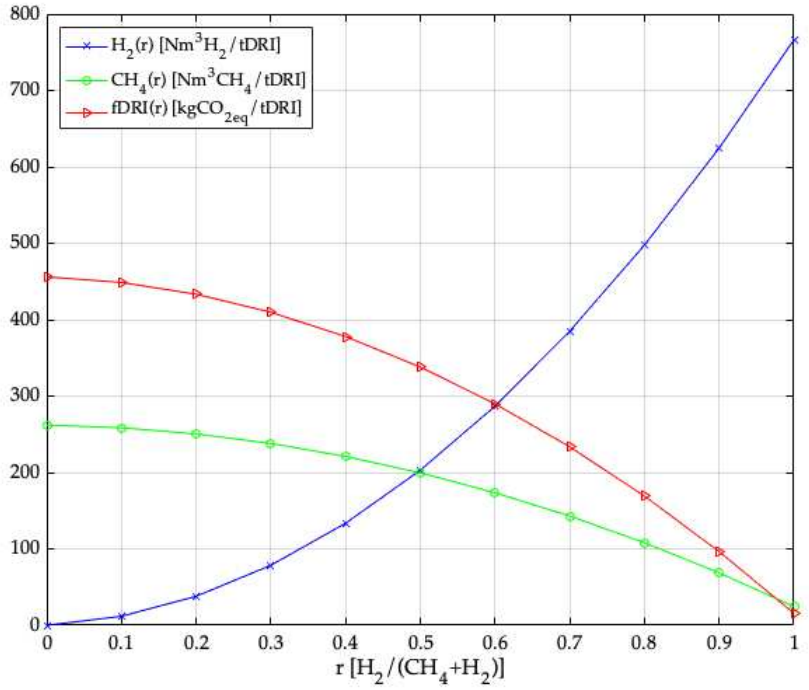

Figure 62. H_2 demand $H_2(r)$, NG demand $CH_4(r)$, and direct emissions $f_{DRI}(r)$ from the DRI production process as a function of r. Authors' elaboration of data in [272].

As it can be observed from Figure 62, the direct emissions from the DRI production plant ($f_{DRI}(r)$) and the demand of NG for the reducing gas ($CH_4(r)$) decrease as r increases, while the demand for H_2 ($H_2(r)$) increases. It is also possible to observe that the demand for H_2 and CH_4 reach the same value near to $r = 0.5$ and then the demand for H_2 increases more than the demand for CH_4 decreases. This is because H_2 has a lower reducing power compared to CH_4. To this concern, Figures 63 and 64 show the trend of φ_{tot} and its components (i.e., φ_{direct}, φ_{NG}, φ_{grid}, φ_{renew}) as functions of the r variable.

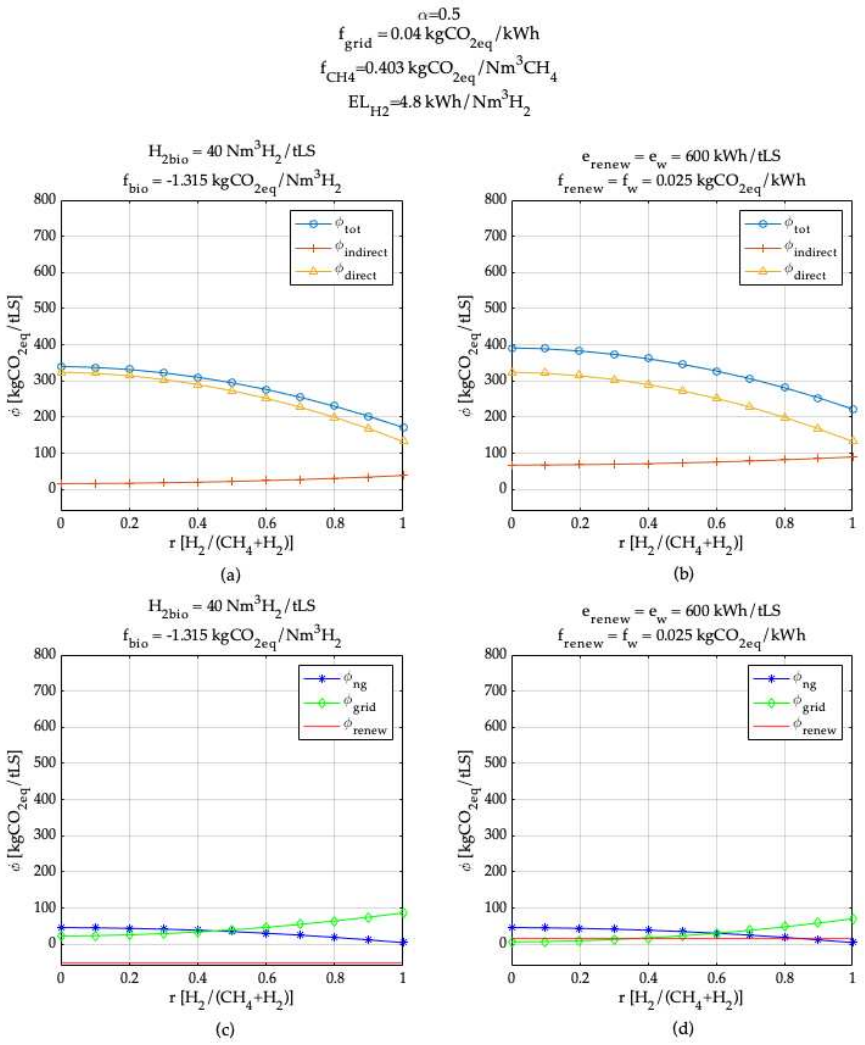

Figure 63. Trend of the total emissions φ_{tot} and its components (φ_{direct}, φ_{NG}, φ_{renew}, φ_{grid}) as a function of the r variable in different scenarios characterized by f_{grid}=0.04 $kgCO_{2eq}$/kWh. (a,c) H_2 production from biomass gasification. (b,d) Electricity production from wind turbines.

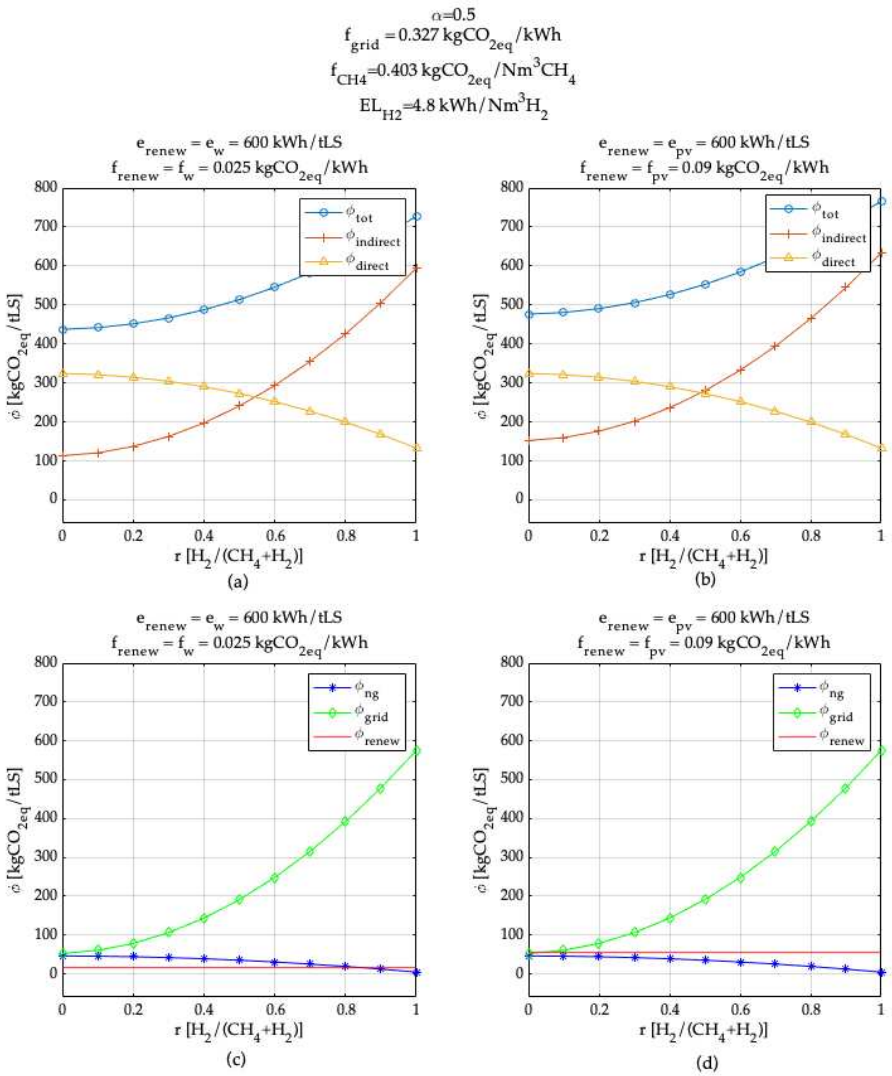

Figure 64. Trend of the total emissions φ_{tot} and its components (φ_{direct}, φ_{NG}, φ_{renew}, φ_{grid}) as a function of the r variable in different scenarios characterized by f_{grid}=0.327 $kgCO_{2eq}$/kWh. (a,c) Electricity production from wind turbines. (b,d) Electricity production from photovoltaic panels.

Also in this case, different scenarios were built up according to the results obtained from the preview simulations. Figure 63 shows the results

obtained in the case of f_{grid}=0.04 $kgCO_{2eq}$/kWh, and Figure 64 shows the results obtained in the case of f_{grid}=0.327 $kgCO_{2eq}$/kWh. Electricity production from wind turbines (Figure 63b,d) and biomass cultivation (Figure 63a,c) were considered in the case of f_{grid}=0.04 $kgCO_{2eq}$/kWh, and electricity production from wind turbines (Figure 64a,c) or photovoltaic panels (Figure 64b,d) in the case of f_{grid}=0.327 $kgCO_{2eq}$/kWh. As it can be observed, the φ_{tot} function decreases in scenarios with f_{grid}=0.04 $kgCO_{2eq}$/kWh (Figure 63), while it increases in scenarios with f_{grid}=0.327 $kgCO_{2eq}$/kWh (Figure 64). The values of emissions observed in the first case (Figure 63a,b) are significantly lower than those observed in the second case (Figure 64a,b). As far as concerns the contributions that constitute φ_{tot}, it is possible to observe that in all the scenarios considered (Figures 63 and 64), φ_{direct} and φ_{NG} decrease as r increases, while φ_{grid} increases. The most significant difference is observed in the latter contribution. In Figure 63c,d, the maximum value of φ_{grid}(at r=1) is slightly below 100 $kgCO_{2eq}$/tLS, while in Figure 64c,d, it is higher than 600 $kgCO_{2eq}$/tLS. This confirms that the emissions generated by electricity consumption for H_2 production are significant and that, consequently, sustainable energy production from the grid allows for green steel production.

Regarding the numerical simulations carried out to find the optimal value of r minimizing the overall emissions from the GESS by varying f_{grid}, it was found that, for any combination of values of the considered variables (Figure 65), overall emission function (φ_{tot}) does not admit a minimum for any r value.

For specific values of f_{grid}, indeed, the function has a monotonic trend; if it is monotonically increasing, minimum emissions are obtained in the case of r=0 (e.g., f_{grid}=0.22 $kgCO_{2eq}$/kWh); if it is monotonically decreasing, minimum emissions are obtained in the case of r=1 (e.g., f_{grid}=0.1 $kgCO_{2eq}$/kWh). When the function is not monotonic (e.g., f_{grid}=0.13 $kgCO_{2eq}$/kWh), it does not show a minimum, which confirms that for all f_{grid} values, minimum emissions are obtained in the cases of r=0

or r=1, and not in intermediate values (0<r<1). From the results obtained (Figure 65), it can be observed that the feasibility of installing a H_2-powered steel plant (r=1) is determined, from an environmental point of view, only by the f_{grid} value, i.e., by the way in which electricity is produced at national level. Also in this case, it can be observed that low f_{grid} values generate synergies in the GESS that allow the decrease of φ_{tot} as the share of H_2 produced increases (r). The other variables considered (e.g., α, e_{renew}, P, S, etc.) affect emissions in terms of absolute value, but do not influence the choice of DRI production mode (r=0 or r=1). At r=0, there is no significant difference between the φ_{tot} values recorded at the minimum and the maximum f_{grid} values considered. The situation is completely different at r=1, at which there is a very significant difference between the values of φ_{tot} at minimum f_{grid} and maximum f_{grid} considered. For example, in the case of electricity production from wind turbines (Figure 65b), at r=0, there is an increase of 13.18% from the φ_{tot} value at f_{grid}=0.01 $kgCO_{2eq}$/kWh, compared with f_{grid}=0.327 $kgCO_{2eq}$/kWh, while at r=1, the increase is 324.6%. This confirms that electricity consumption for H_2 production constitutes the most significant share of total emissions and that, therefore, it is necessary to assess the feasibility of GESS installation according to the reference context. However, the results showed that steel production with alternative route (DRI–EAF), regardless of the component of the DRI reducing gas (r), is environmentally favourable. At r=0, indeed, there is a significant reduction in emissions compared to the BF–BOF route in each scenario, which can even become more significant in contexts where it is convenient to produce with only H_2 (Figure 65). Referring to Figure 65b, it can be observed that φ_{tot} values at r=0 are around 400 $kgCO_{2eq}$/tLS, 83.34% less than the BF–BOF route, whereas at r=1, the minimum value recorded is 171 $kgCO_{2eq}$/tLS, 90.5% less than the conventional alternative. It is noteworthy that even at the worst scenario, i.e., f_{grid}=0.327 $kgCO_{2eq}$/kWh and r=1, the emissions are 726 $kgCO_{2eq}$/tLS, 59.6% less than the primary route, thus proving the effectiveness of the DRI–EAF route.

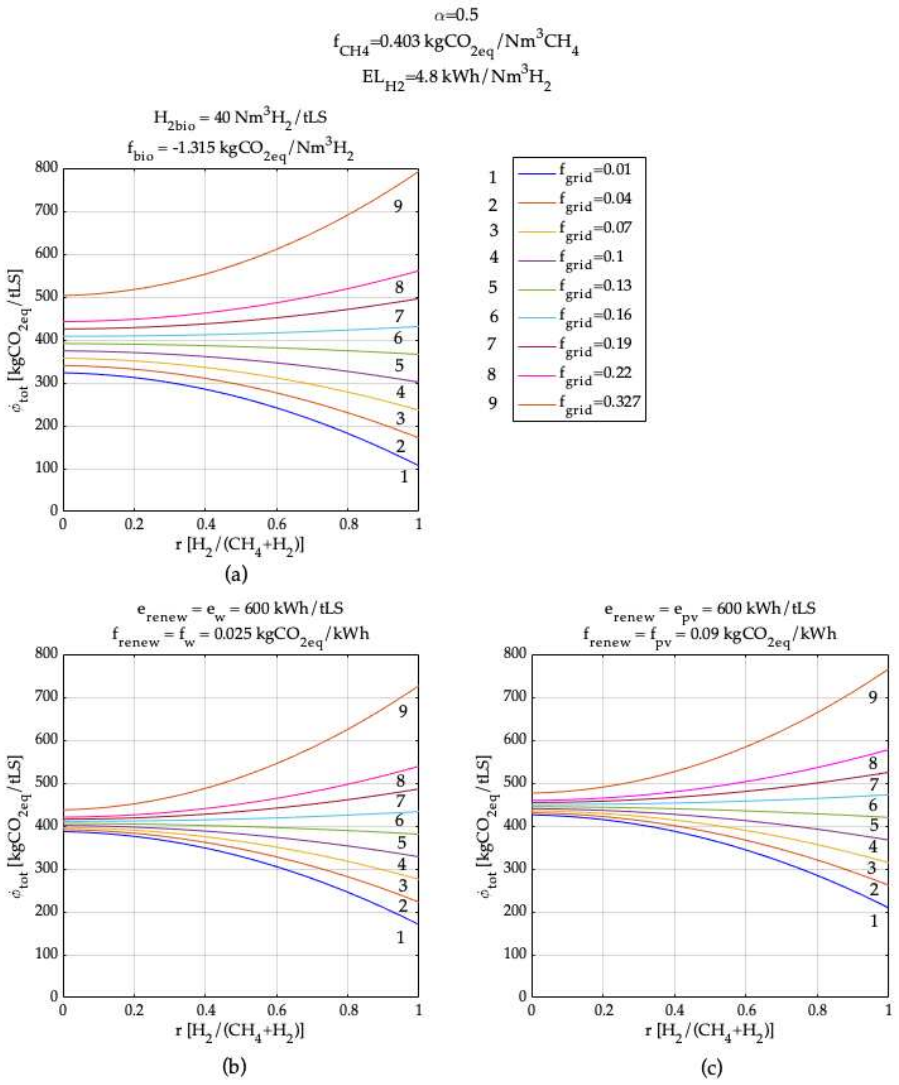

Figure 65. Trend of total emissions φ_{tot} as a function of the r variable in different scenarios characterized by different f_{grid}. (a) H_2 production from biomass gasification. (b) Electricity production from wind turbines. (c) Electricity production from photovoltaic panels.

From the observation made on the trend of φ_{tot} with respect to r (Figure 65), it was possible to calculate the value of f_{grid} that makes equal the value of φ_{tot} at r=0 and r=1, called f_{grid}". This is the maximum value of the grid emission factor at which it is environmentally convenient to install a H_2-powered steel plant (r=1). The analytical expression of f_{grid}" is in equation 125:

$$f_{grid}''(r)\left[\frac{kgCO_{2eq}}{kWh}\right]=\frac{\left(\varphi_{direct}(1)+\varphi_{NG}(1)\right)-(\varphi_{direct}(0)+\varphi_{NG}(0))}{(E_{demand}(0)-e_{renew})-(E_{demand}(0)-e_{renew})} \quad (125)$$

The expression in equation 125 is a function of the variables f_{CH4} and EL_{H2}. As the first variable is exogenous, the trend of f_{grid}" has been studied as a function of the only endogenous variable EL_{H2} (Figure 66).

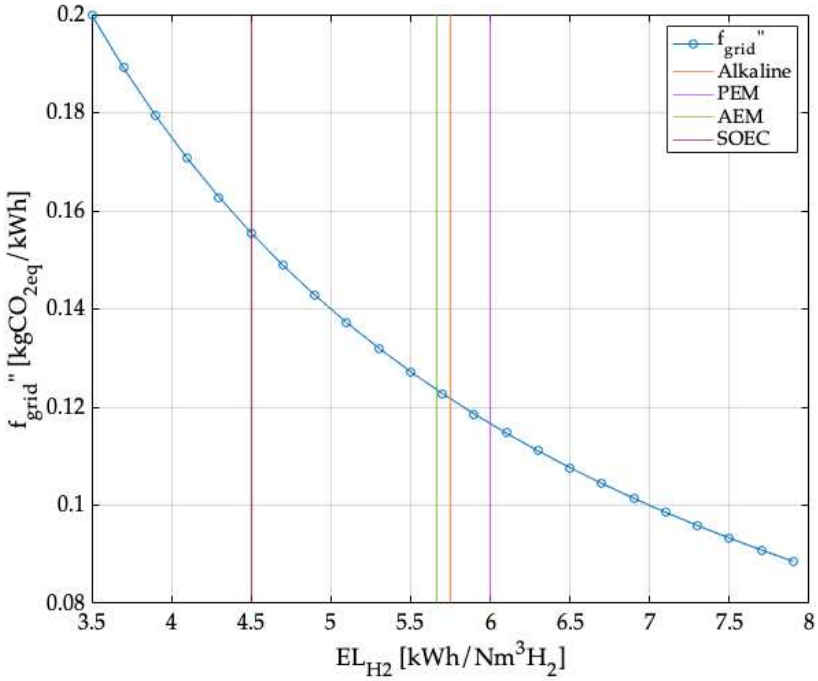

Figure 66. Trend of f_{grid}" as a function of EL_{H2}.

As it can be observed in Figure 66, f_{grid}" decreases as the electrical consumption of the electrolyser increases. In the figure, electricity consumption of the main electrolyzers' technologies is shown (vertical lines). To this concern, it is therefore possible to observe that for EL_{H2} characteristics of the solid oxide electrolyzer (SOEC) technology (4.5 kWh/Nm^3H_2 [312]), currently developed on a lab-scale, the maximum value of f_{grid} at which a H_2-powered steelmaking plant can be installed (f_{grid}") is 0.155 $kgCO_{2eq}/kWh$. For the alkaline and anion exchange membrane (AEM) technologies, which have very similar average electricity consumption (around 5.7 kWh/Nm^3H_2 [312]), the value of f_{grid}" decreases to approximately 0.122 $kgCO_{2eq}/kWh$. Finally, for the proton exchange membrane (PEM) technology (commercially available technology), which has the highest electricity consumption (6 kWh/Nm^3H_2 [312]), the value of further decreases to about 0.12 $kgCO_{2eq}/kWh$.

From the overall results obtained, therefore, it is possible to conclude that the installation of a H_2-powered steel plant (r=1) is only feasible if supported by both technological innovations and supporting infrastructure. The choice of an electrolyzer characterized by low energy consumption and a national energy mix with a low environmental impact represent favorable conditions for the installation of a H_2-powered steel plant, thus allowing the decarbonization of the steelmaking sector.

3.4 An environmental analytical model to assess the decarbonisation potential offered by waste-to-hydrogen routes to the steelmaking process

This section discusses the development and application of an environmental analytical model to assess the decarbonisation potential offered by waste-based H_2 production routes to the steelmaking sector. As mentioned, the use of H_2 currently represents the most promising alternative for decarbonising the steelmaking process. However, economic and environmental barriers to the implementation of electrolysis on a large scale make this route not easily applicable. For this reason, ana analytical

model was developed to evaluate how waste-based routes can help and accelerate the transition process towards large-scale green steel production. To this concern, the developed model allows to assess the decarbonization potential of different waste-based H_2 production routes with respect to the traditional H_2-based steelmaking route, i.e., electrolysis based DRI-EAF (El-DRI-EAF) route. The considered waste-based H_2 routes were MSW gasification followed by syngas reforming, MSW incineration to produce the electricity required by an electrolyzer, and SBR. A sensitivity analysis was also carried out to understand the benefit provided by each waste-based H_2 alternative in the current energy transition phase.

3.4.1 Development of the analytical model for assessing the decarbonisation potential offered by waste-to-hydrogen routes to the steelmaking process

The configuration considered for the El-DRI-EAF route is illustrated in Figure 67. It is adapted from [313].

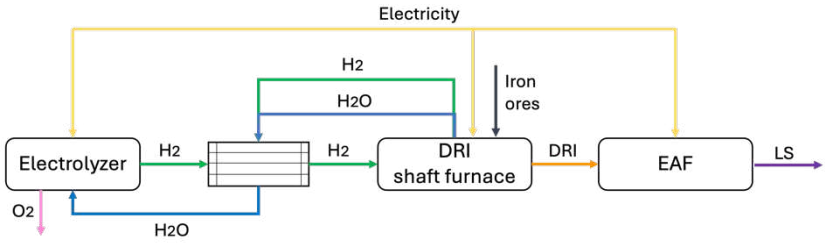

Figure 67. Plant configuration considered for the El-DRI-EAF route.

As it can be observed, the system consists of three main facilities: an electrolyzer for H_2 production, a shaft furnace for DRI production, and an EAF for LS production. The process starts with the production of H_2 by water electrolysis. To this end, by supplying electricity, the splitting of water molecules into H_2 and O_2 occurs at an assumed temperature of 70°C [313]. The produced H_2 is then heated within a condenser thanks to the heat recovered by the gases leaving the shaft furnace at a temperature between 275°C and 400 °C [314]. Through the condenser, it is also possible to separate the H_2 and water contained in the flue gases from the shaft furnace.

The separated water is recirculated to the electrolyzer. The heated H_2 is then conveyed to the shaft furnace, at the top of which preheated iron ores pellets are fed. In the shaft furnace, at an assumed temperature of 800°C, endothermic reduction reactions take place between the ores and the reducing gas. These solid-state reactions result in DRI with a minimum metallization degree of 94% [313]. The DRI is then melted within EAF, and LS is produced.

Figure 68 shows the plant configurations of the waste-based steelmaking routes considered. As it can be observed, the routes considered result from the combination of three of the WtH_2 routes considered with the traditional El-DRI-EAF route. To this end, the combination of the gasification-based route for H_2 production (Figure 68a) and the El-DRI-EAF route is referred to as the Gas-DRI-EAF route. The combination of the incineration-based route for H_2 production (Figure 68b) and the El-DRI-EAF route is referred to as the WtE-DRI-EAF route. Finally, the combination of the SBR route (Figure 68c) and the El-DRI-EAF route is referred to as the SBR-DRI-EAF route.

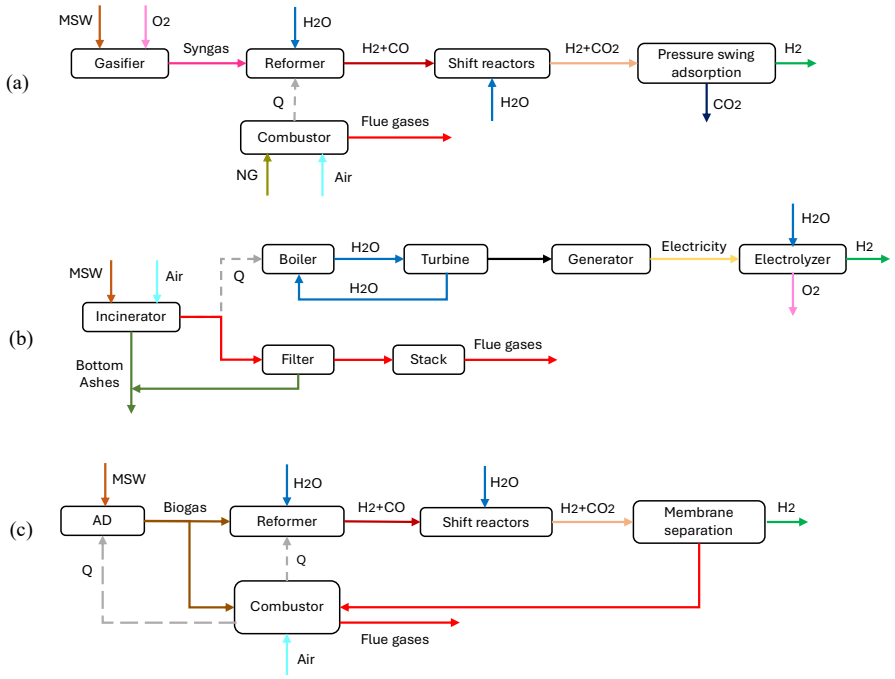

Figure 68. (a) Plant configuration considered for the Gas-DRI-EAF route; (b) Plant configuration considered for the WtE-DRI-EAF route; (c) Plant configuration considered for the SBR-DRI-EAF route.

The developed environmental analytical model aims to account for the total emissions associated with each steelmaking route. It can be expressed according to equation 126.

$$\varphi\ \left[\mathrm{kgCO_{2_{eq}}/tLS}\right] = \varphi_{steel} + \varphi_{H_2} \tag{126}$$

Where $\varphi_{steel}\ [\mathrm{kgCO_{2_{eq}}/tLS}]$ are the total emissions associated with the operation of the steelmaking facilities, i.e., the DRI shaft furnace and the EAF. $\varphi_{H_2}[\mathrm{kgCO_{2_{eq}}/tLS}]$ are the total emissions associated with the operation of the H_2 production facilities, depending on the considered route. They are expressed according to equations 127 and 130, respectively.

$$\varphi_{steel}\left[\mathrm{kgCO_{2_{eq}}/tLS}\right] = \varphi_{direct_{steel}} + \varphi_{indirect_{steel}} \tag{127}$$

Where $\varphi_{direct_{steel}}$ [$kgCO_{2_{eq}}$/tLS] are the direct emissions resulting from DRI shaft furnace and EAF operation. They are expressed according to equation 128. $\varphi_{indirect_{steel}}$ [$kgCO_{2_{eq}}$/tLS] are the emissions associated with the energy consumption of plants. In the case of the analysed steelmaking route, only electrical consumption was considered since no NG is used. Indirect emissions of the steelmaking plant are expressed according to equation 129.

$$\varphi_{direct_{steel}}\left[kgCO_{2_{eq}}/tLS\right] = \frac{f_{DRI}}{k} + f_{EAF} \quad (128)$$

Where f_{DRI} [$kgCO_{2_{eq}}$/tDRI] are the emissions generated by the shaft furnace to produce 1 ton of DRI. k [tLS/tDRI] represents the DRI need to produce 1 ton of LS. f_{EAF} [$kgCO_{2_{eq}}$/tLS] are the EAF direct emissions.

$$\varphi_{indirect_{steel}}\left[kgCO_{2_{eq}}/tLS\right] = \left(\frac{EL_{cons_{DRI}}}{k} + El_{cons_{EAF}}\right)\cdot f_{grid} \quad (129)$$

Where $EL_{cons_{DRI}}$[kWh/tDRI] and $El_{cons_{EAF}}$[kWh/tLS] are the electrical consumptions of the DRI plant and the EAF, respectively. f_{grid} [$kgCO_{2_{eq}}$/kWh] is the emission factor of the national electricity grid. Also in this case, this variable was chosen as an indicator of the progress of the current energy transition.

$$\varphi_{H_2}\left[kgCO_{2_{eq}}/tLS\right] = \varphi_{direct_{H_2}} + \varphi_{indirect_{H_2}} - \varphi_{avoided_{H_2}} \quad (130)$$

As it can be observed from equation 130, the total emissions associated with the production of H_2 were calculated as the sum between direct emissions, $\varphi_{direct_{H_2}}$[$kgCO_{2_{eq}}$/tLS], and indirect emissions, $\varphi_{indirect_{H_2}}$[$kgCO_{2_{eq}}$/tLS]. Avoided emissions $\varphi_{avoided_{H_2}}$[$kgCO_{2_{eq}}$/tLS] were subtracted from this amount. They are expressed according to equations 131-133.

$$\varphi_{direct_{H_2}}\left[kgCO_{2_{eq}}/tLS\right] = f_{H_2}\cdot H_{2_{LS}} \quad (131)$$

Where f_{H_2} [$kgCO_{2_{eq}}/Nm^3H_2$] are the direct emissions of the H_2 production facilities and $H_{2_{LS}}$ [Nm^3H_2/tLS] is the amount of H_2 required to produce 1 ton of LS. It is noteworthy that, according to the current guidelines, only non-biogenic CO_2 emissions were considered [222].

$$\varphi_{indirect_{H_2}}\left[kgCO_{2_{eq}}/tLS\right] = \\ =(El_{cons_{H_2}}\cdot f_{grid}+NG_{cons_{H_2}}\cdot f_{FME}\cdot GWP_{100})\cdot H_{2_{LS}} \quad (132)$$

Indirect emissions from H_2 production were considered as the sum of the emissions generated by electricity supply $El_{cons_{H_2}}$[kWh/Nm^3H_2] from the national grid and the emissions generated from NG supply, assumed as FMEs. Also in this case, FMEs are calculated as a percentage (f_{FME} [%]) of the total NG consumption of the process (NG_{cons} [$kgNG/Nm^3H_2$]) [232]. To assess these emissions' environmental impact, methane's impact factor on the Global Warming Potential was considered with a time horizon of 100 years (GWP_{100} [$kgCO_{2_{eq}}/kgNG$]).

$$\varphi_{avoided_{H_2}}\left[kgCO_{2_{eq}}/tLS\right] = MSW_{H_2}\cdot f_{disp_{MSW}}\cdot H_{2_{LS}} \quad (133)$$

Finally, avoided emissions from H_2 production through a waste-based route were considered as the emissions avoided from landfilling of the valorised waste. To this concern, the amount of MSW needed to produce H_2 MSW_{H_2}[$kgMSW/Nm^3H_2$] and the average emissions from the decomposition of 1 ton of MSW when landfilled $f_{disp_{MSW}}$ [$kgCO_{2_{eq}}/kgMSW$] were considered.

3.4.2 Numerical application of the analytical model for assessing the decarbonisation potential offered by waste-to-hydrogen routes to the steelmaking process

In Table 22 the data assumed for the numerical application of the developed model are illustrated

Table 22. Data assumed for the environmental analytical model application.

	f_{DRI}	k	f_{EAF}	$EL_{cons_{DRI}}$	$El_{cons_{EAF}}$	f_{grid}	f_{H_2}	$H_{2_{LS}}$	$El_{cons_{H_2}}$	$NG_{cons_{H_2}}$	f_{FME}	GWP_{100}	MSW_{H_2}	$f_{disp_{MSW}}$
El DRI EAF							-		6 [270]	-			-	-
WtE DRI EAF	40	1.15	180	100	753	0÷1	3.9 [315]	453	-	0.07 [41]	3.5 [229]	32 [230]	4.64 [235]	
Gas DRI EAF	[269]	[313]	[269]	[269]	[313]	[226]	0.94 [315]	[313]	0.74 [41]	0.06 [41]			1.09 [235]	0.302 [316]
SBR DRI EAF							-		0.15 [234]	-			4.6 [234]	

The results obtained from the numerical application of the model are reported in Figure 69. The total emissions of the different routes were evaluated in two scenarios (SCs) characterized by different energy mixes. To this concern, f_{grid} values of 0.08 $kgCO_{2eq}$/kWh (SC1) and 0.64 $kgCO_{2eq}$/kWh (SC2) were considered. These values were obtained as the average of the first and fourth quartiles, respectively, of the data available in [226]. They therefore represent the average emission factors of the 25% of countries with the best energy mixes and the 25% of countries with the worst energy mixes globally.

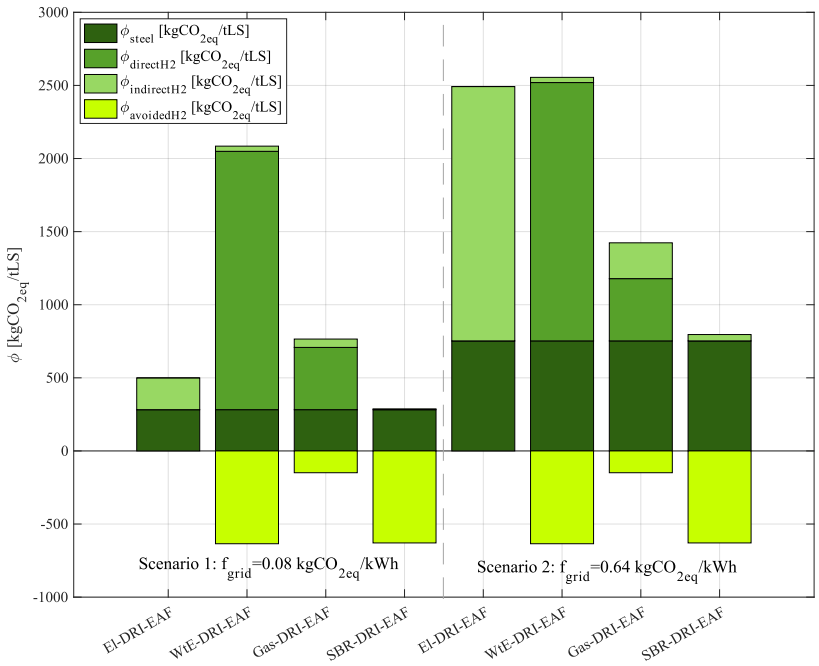

Figure 69. Results obtained from the application of the model to two scenarios characterized by f_{grid} values of 0.08 $kgCO_{2eq}$/kWh and 0.64 $kgCO_{2eq}$/kWh, respectively.

As far as concerns SC1, the route with the worst environmental performance is WtE-DRI-EAF. Although this route offers high avoided emissions (i.e., 635 $kgCO_{2eq}$/tLS), it has total emissions of 1450 $kgCO_{2eq}$/tLS. This value is higher than the estimated emissions for the NG-based DRI-EAF route (i.e., 1.4 tCO_{2eq}/tLS [264]). Therefore, this waste-

based H_2 production route does not support the decarbonization of the steelmaking sector. The second highest emissions in SC1 correspond to the Gas-DRI-EAF route (i.e., 616 $kgCO_{2eq}$/tLS,). This value is 57.5% lower than WtE-DRI-EAF route. This depends on the reduction of direct emissions (i.e., 426 $kgCO_{2eq}$/tLS vs 1767 $kgCO_{2eq}$/tLS). In the case of the Gas-DRI-EAF route, indeed, a complete combustion reaction does not take place, generating a high-value gas stream. In this scenario, the traditional El-DRI-EAF route is very promising from an environmental point of view. Indeed, the total emissions are about 500 $kgCO_{2eq}$/tLS, 65.5% and 64.4% lower than the total emissions of the WtE-DRI-EAF the NG-based DRI-EAF routes, respectively. These results confirm that renewable-based energy mixes enable the large-scale the implementation of water electrolysis. In SC1, the SBR-DRI-EAF route offers the best decarbonization potential. Indeed, this route is based on the valorisation of organic waste, avoiding non-biogenic carbon emissions. It also exploits the biogas produced to provide the necessary heat for the reforming reaction, not consuming fossil fuels. In addition, this route offers high avoided emissions, i.e., 629 $kgCO_{2eq}$/tLS. These features make the SBR-DRI-EAF route the only one that offers a negative emission balance, i.e., -342 $kgCO_{2eq}$/tLS. In SC2, an increase in the value of f_{grid}, generates a significant increase in total emissions in all cases. The main difference from the previous case is in the emissions of the El-DRI-EAF route. In SC2, indeed, the El-DRI-EAF route offers the worst environmental performance. The total emissions are 2492 $kgCO_{2eq}$/tLS, a higher value than the emissions of the BF-BOF route. On the contrary, the Gas-DRI-EAF and SBR-DRI-EAF routes offer a decarbonization potential even in this scenario. Therefore, the results obtained showed that waste-based H_2 production is a viable alternative for the decarbonization of the steelmaking process and that the current energy transition process is the condition for the implementation of large-scale electrolysis. To this concern, a sensitivity analysis was conducted to investigate the total emission function of each steelmaking route with respect to f_{grid}. This variable was chosen as representative of the progress of the energy transition. The results obtained from the sensitivity analysis are shown in Figure 70.

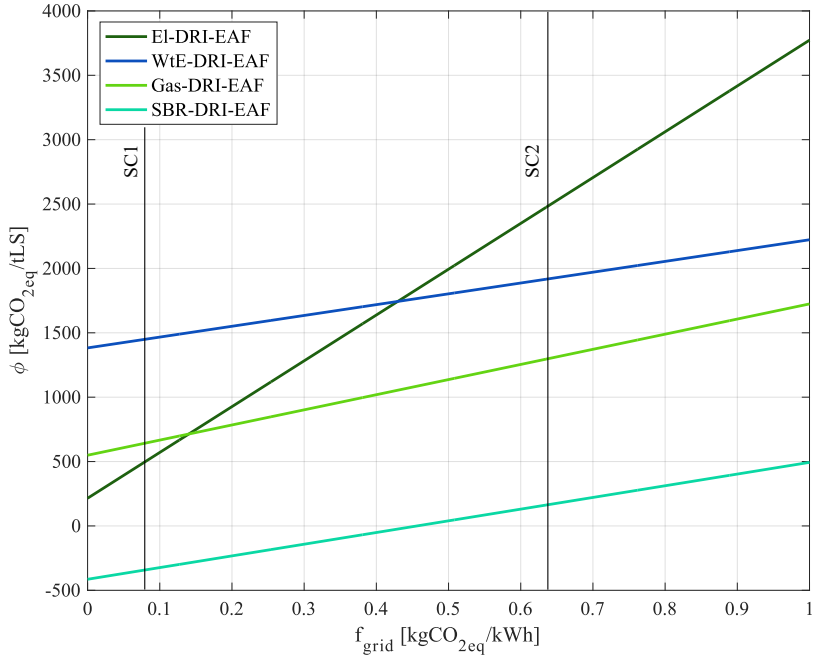

Figure 70. Results obtained from the sensitivity analysis conducted with respect to the f_{grid} variable.

As it can be observed, the trends of the functions at the two ends of the graph correspond to the results shown in Figure 70. To this concern, for f_{grid} values lower than 0.139 $kgCO_{2eq}$/kWh, the solution with the best environmental performance is the SBR-DRI-EAF route, followed by the El-DRI-EAF route and the Gas-DRI-EAF route. For f_{grid} values higher than 0.43 $kgCO_{2eq}$/kWh, the El-DRI-EAF route results in the worst environmental performance, followed by the WtE-DRI-EAF route and the Gas-DRI-EAF route. This sensitivity analysis was useful to understand the potential of the waste-based routes in the current energy transition phase. Indeed, as pointed out, in a scenario of energy production from renewable sources, the steelmaking process can have a negative overall emissions balance (i.e., adopting the SBR-DRI-EAF route). However, 75% of countries currently have an energy mix (i.e., a f_{grid} value) which makes steelmaking unfavorable from an environmental point of view. In this scenario, waste-based H_2 production routes represent a valuable alternative

for decarbonizing the process. Indeed, it is possible to observe how, for f_{grid} values between 0.139 and 0.44 $kgCO_{2eq}$/kWh, steelmaking process can offer negative overall emissions using the SBR-DRI-EAF route. For f_{grid} values higher than 0.44 $kgCO_{2eq}$/kWh, although no route achieves negative total emissions, waste-based H_2 routes offer high decarbonization potential, compared to both the El-DRI-EAF route and the NG-based DRI-EAF route.

Conclusions

The objective of this work was to develop methodologies for evaluating and comparing the performance of waste valorisation plants in order to understand their potential in the current energy transition.

To achieve this goal, analytical models were developed that consider, based on the material and energy flows exchanged within the systems and with the external environment, the negative effects generated from an economic and environmental point of view (i.e., GHGs emissions and costs), as well as the positive ones (i.e., avoided emissions and profits generated by the valorisation of resources).

In the current context of energy transition, the issue of decarbonisation of the steelmaking sector was also explored, through the development of analytical models aimed at understanding the cost-effectiveness of investing in innovative steelmaking routes, as well as the environmental performance of a GESS and the contribution of WtH_2 routes to the decarbonisation of this sector.

First, the cost and investment analysis of WtE plants showed that the gasification plant is the best option to support the current transition phase among the alternatives considered regardless of local municipal requirements. Moreover, the conducted analysis showed a strong relationship between the carbon price, the electricity price and the investment profitability. A strong dependency on carbon price and NPV was moreover observed.

As for the comparison between different waste valorisation alternatives, the development and application of the developed environmental analytical models allowed to understand how the production of bio-CH_4 has a greater decarbonisation potential than the production of electricity from AD.

Similarly, H_2 production is better from an environmental point of view than bio-CH_4 production. This result is in line with what emerges from the analysis of the state of progress of the energy transition. Indeed, H_2 production, which is very useful for the decarbonisation of the energy sector, suffers from the problems associated with the large-scale production of green H_2 and, in this context, the SBR route represents a supportive alternative.

The development and application of the analytical model for comparing different WtH_2 allowed to observe that WtH_2 technologies offer real decarbonisation potential, even in scenarios characterised by intermediate energy mixes. However, the most interesting results were observed in the scenario analysis conducted for 2020 and 2030 scenarios. Indeed, it was shown how investment in WtH_2 plants can effectively contribute to the decarbonisation of the H_2 production mix, accelerating the achievement of the environmental objectives set at European level.

As for the steelmaking sector, the analysis of the investment in the NG-DRI-EAF route allowed to understand its convenience in the presence of uncertain market conditions and also in the perspective of an increase in the carbon tax.

The development of an environmental analytical model for the estimation of the total emissions from the GEES then allowed to find some very relevant aspects regarding the environmental performance of the DRI-based steelmaking route. Indeed, it was shown that, regardless of the local availability of energy from renewable sources, the choice of electrolyser type, etc., the environmental convenience of installing an H_2-based steelmaking route only depend on the national energy mix and, therefore, will only be convenient when the energy transition will be accomplished. In this regard, the development of the model for the evaluation of the decarbonisation potential offered by the WtH_2 routes to the steelmaking process allowed to assess their effectiveness. WtH_2-based steelmaking routes demonstrated much lower emissions than the traditional NG-DRI-EAF route and seemed to be valid until the electrolysis becomes deployable on a large scale.

The developed models proved to be useful in the preliminary understanding of the performance of the analysed plants in view of an energy transition.

Each of the models developed, however, has limitations mainly related to unassessed cost or emission items, as well as the non-consideration of operational variables related to the plants considered. Furthermore, it can be stated that, in any comparison, it might be useful to include additional waste valorisation routes, such as, for example, biological processes for the production of H_2.

Future studies will certainly improve the individual models by including the currently neglected elements. The most significant development of this work, however, lies in the possibility of developing, from the individual models, an integrated methodology for evaluating the performance of waste valorisation plants. This methodology will allow to assess the performance of each alternative analysed in a specific reference contexts. Economic and environmental performance indicators could also be developed from the models to assess the contribution of each plant considered in view of current decarbonisation targets.

References

[1] Intergovernmental Panel on Climate Change, "Climate Change 2001: the scientific basis," 2001. [Online]. Available: https://www.ipcc.ch/site/assets/uploads/2018/03/WGI_TAR_full_report.pdf

[2] A. Berger and Ch. Tricot, "The greenhouse effect," *Surv Geophys*, vol. 13, no. 6, pp. 523–549, Nov. 1992, doi: 10.1007/BF01904998.

[3] NASA Earth Observatory, "Global Warming." [Online]. Available: https://earthobservatory.nasa.gov/features/GlobalWarming/page1.php

[4] Statista, "Global warming - statistics & facts," Sep. 2023. [Online]. Available: https://www.statista.com/topics/11239/global-warming/#topicOverview

[5] J. Houghton, "Global warming," *Reports on Progress in Physics*, vol. 68, no. 6, pp. 1343–1403, Jun. 2005, doi: 10.1088/0034-4885/68/6/R02.

[6] United Nations, "Causes and Effects of Climate Change." [Online]. Available: https://www.un.org/en/climatechange/science/causes-effects-climate-change

[7] Our World in Data, "Sector by sector: where do global greenhouse gas emissions come from?" [Online]. Available: Sector by sector: where do global greenhouse gas emissions come from?

[8] C. B. Field, D. B. Lobell, H. A. Peters, and N. R. Chiariello, "Feedbacks of Terrestrial Ecosystems to Climate Change," *Annu Rev Environ Resour*, vol. 32, no. 1, pp. 1–29, Nov. 2007, doi: 10.1146/annurev.energy.32.053006.141119.

[9] NASA, "Global Warming." [Online]. Available: https://earthobservatory.nasa.gov/features/GlobalWarming/page1.php

[10] Statista, "Threatened With Extinction." [Online]. Available: https://www.statista.com/chart/17914/he-share-of-plant-animal-species-at-risk-of-extinction-worldwide/

[11] United Nations Framework Convention on Climate Change, "The Paris Agreement." 2015. [Online]. Available: https://unfccc.int/sites/default/files/english_paris_agreement.pdf

[12] United Nations, "The Paris Agreement." [Online]. Available: https://unfccc.int/process-and-meetings/the-paris-agreement

[13] Climate Action Tracker, "Net Zero Targets." [Online]. Available: https://climateactiontracker.org/methodology/net-zero-targets/

[14] European Commission, "The European Green Deal", [Online]. Available: https://commission.europa.eu/strategy-and-policy/priorities-2019-2024/european-green-deal_en

[15] European Commission, "Delivering the European Green Deal", [Online]. Available: https://commission.europa.eu/strategy-and-policy/priorities-2019-2024/european-green-deal/delivering-european-green-deal_en

[16] United Nations Framework Convention on Climate Change, "Decision -/CMA.4 Sharm el-Sheikh Implementation Plan", [Online]. Available: https://unfccc.int/sites/default/files/resource/cma4_auv_2_cover_decision.pdf

[17] N. Zhao and F. You, "Can renewable generation, energy storage and energy efficient technologies enable carbon neutral energy transition?," *Appl Energy*, vol. 279, p. 115889, Dec. 2020, doi: 10.1016/j.apenergy.2020.115889.

[18] International Renewable Energy Agency, "World Energy Transitions Outlook 2023: 1.5°C Pathway," 2023. [Online]. Available: https://mc-cd8320d4-36a1-40ac-83cc-3389-cdn-endpoint.azureedge.net/-/media/Files/IRENA/Agency/Publication/2023/Jun/IRENA_World_energy_transitions_outlook_v1_2023.pdf?rev=cc4522ff897a4e26a47906447c74bca6

[19] United Nations, "What is renewable energy?" [Online]. Available: https://www.un.org/en/climatechange/what-is-renewable-energy

[20] International Energy Agency, "Solar PV", [Online]. Available: https://www.iea.org/energy-system/renewables/solar-pv

[21] I. - International Energy Agency, "Global Hydrogen Review 2022," 2022. [Online]. Available: www.iea.org/t&c/

[22] S. Griffiths, B. K. Sovacool, J. Kim, M. Bazilian, and J. M. Uratani, "Industrial decarbonization via hydrogen: A critical and systematic review of developments, socio-technical systems and policy options," *Energy Res Soc Sci*, vol. 80, p. 102208, Oct. 2021, doi: 10.1016/j.erss.2021.102208.

[23] M. Pal, R. Giri, and R. K. Sharma, "Production of biofuels in a microbial electrochemical reactor," in *Biofuels and Bioenergy*, Elsevier, 2022, pp. 303–319. doi: 10.1016/B978-0-323-85269-2.00010-1.

[24] Z. Abdin, A. Zafaranloo, A. Rafiee, W. Mérida, W. Lipiński, and K. R. Khalilpour, "Hydrogen as an energy vector," *Renewable and Sustainable Energy Reviews*, vol. 120, p. 109620, Mar. 2020, doi: 10.1016/j.rser.2019.109620.

[25] "Hydrogen for Net-Zero," 2021. [Online]. Available: www.hydrogencouncil.com

[26] "Working_Paper_-_National_Hydrogen_Strategies_-_September_2021".

[27] E. R. Sadik-Zada, "Political Economy of Green Hydrogen Rollout: A Global Perspective," *Sustainability*, vol. 13, no. 23, p. 13464, Dec. 2021, doi: 10.3390/su132313464.

[28] "COMMITTEE AND THE COMMITTEE OF THE REGIONS A hydrogen strategy for a climate-neutral Europe." [Online]. Available: https://www.eu2018.at/calendar-events/political-events/BMNT-

[29] E. R. Sadik-Zada, "Political Economy of Green Hydrogen Rollout: A Global Perspective," *Sustainability*, vol. 13, no. 23, p. 13464, Dec. 2021, doi: 10.3390/su132313464.

[30] International Energy Agency, "Global Hydrogen Review 2022," 2022. Accessed: May 04, 2023. [Online]. Available: https://www.iea.org/reports/global-hydrogen-review-2022

[31] C. G. F. Bataille, "Physical and policy pathways to net-zero emissions industry," *WIREs Climate Change*, vol. 11, no. 2, Mar. 2020, doi: 10.1002/wcc.633.

[32] International Energy Agency, "Energy Technology Perspectives 2020," 2020.

[33] International Energy Agency, "Hydrogen: energy system overview." Accessed: Jan. 17, 2023. [Online]. Available: https://www.iea.org/reports/hydrogen

[34] Hydrogen Council, "Path to hydrogen competitiveness A cost perspective," 2020. [Online]. Available: www.hydrogencouncil.com.

[35] International Renewable Energy Agency, "Green Hydrogen: a guide to policy making," 2020. Accessed: May 06, 2023. [Online]. Available: https://www.irena.org/-/media/Files/IRENA/Agency/Publication/2020/Nov/IRENA_Green_hydrogen_policy_2020.pdf?rev=c0cf115d8c724e4381343cc93e03e9e0

[36] A. Boretti, "There are hydrogen production pathways with better than green hydrogen economic and environmental costs," *Int J Hydrogen Energy*, vol. 46, no. 46, pp. 23988–23995, Jul. 2021, doi: 10.1016/j.ijhydene.2021.04.182.

[37] T. International Renewable Energy Agency, *GREEN HYDROGEN COST REDUCTION SCALING UP ELECTROLYSERS TO MEET THE 1.5°C CLIMATE GOAL H 2 O 2*. 2020. [Online]. Available: www.irena.org/publications

[38] International Energy Agency, "The future of hydrogen." Accessed: Jan. 17, 2023. [Online]. Available: https://www.iea.org/reports/the-future-of-hydrogen

[39] T. International Renewable Energy Agency, *GREEN HYDROGEN COST REDUCTION SCALING UP ELECTROLYSERS TO MEET THE 1.5°C CLIMATE GOAL H 2 O 2*. 2020. [Online]. Available: www.irena.org/publications

[40] United Nations, "ENERGY TRANSITION:TOWARDS THE ACHIEVEMENT OF SDG 7 AND NET-ZERO EMISSIONS," 2021. Accessed: May 07, 2023. [Online]. Available: https://www.un.org/sites/un2.un.org/files/2021-twg_2-062321.pdf

[41] A. Borgogna, G. Centi, G. Iaquaniello, S. Perathoner, G. Papanikolaou, and A. Salladini, "Assessment of hydrogen production from municipal solid wastes as competitive route to produce low-carbon H2," *Science of The Total Environment*, vol. 827, p. 154393, Jun. 2022, doi: 10.1016/j.scitotenv.2022.154393.

[42] F. Ardolino, G. F. Cardamone, F. Parrillo, and U. Arena, "Biogas-to-biomethane upgrading: A comparative review and assessment in a life cycle perspective," *Renewable and Sustainable Energy Reviews*, vol. 139, p. 110588, Apr. 2021, doi: 10.1016/j.rser.2020.110588.

[43] International Energy Agency, "Outlook for biogas and biomethane: prospects for organic growth," 2020.

[44] S. F. Ferreira, L. S. Buller, M. Berni, and T. Forster-Carneiro, "Environmental impact assessment of end-uses of biomethane," *J Clean Prod*, vol. 230, pp. 613–621, Sep. 2019, doi: 10.1016/j.jclepro.2019.05.034.

[45] International Energy Agency, "Global Energy Review: CO2 Emissions in 2021," 2021. [Online]. Available: www.iea.org/t&c/

[46] International Energy Agency, "Transport: Improving the sustainability of passenger and freight transport." Accessed: May 18, 2023. [Online]. Available: https://www.iea.org/topics/transport

[47] World Biogas Association, "Biogas:Pathways to 2030," 2021.

[48] Our World in data, "Methane Emissions, world." Accessed: May 18, 2023. [Online]. Available: https://ourworldindata.org/grapher/methane-emissions-by-sector

[49] International Energy Agency, "Methane Tracker 2021," 2021. Accessed: May 18, 2023. [Online]. Available: https://www.iea.org/reports/methane-tracker-2021

[50] S. Bakkaloglu, J. Cooper, and A. Hawkes, "Life cycle environmental impact assessment of methane emissions from the biowaste management strategy of the United Kingdom: Towards net zero emissions," *J Clean Prod*, vol. 376, p. 134229, Nov. 2022, doi: 10.1016/j.jclepro.2022.134229.

[51] H. Khandelwal, H. Dhar, A. K. Thalla, and S. Kumar, "Application of life cycle assessment in municipal solid waste management: A worldwide critical review," *Journal of Cleaner Production*, vol. 209. Elsevier Ltd, pp. 630–654, Feb. 01, 2019. doi: 10.1016/j.jclepro.2018.10.233.

[52] "What a Waste 2.0."

[53] D. M. C. Chen, B. L. Bodirsky, T. Krueger, A. Mishra, and A. Popp, "The world's growing municipal solid waste: trends and impacts," *Environmental Research Letters*, vol. 15, no. 7, Jul. 2020, doi: 10.1088/1748-9326/ab8659.

[54] G. Boskovic, N. Jovicic, S. Jovanovic, and V. Simovic, "Calculating the costs of waste collection: A methodological proposal," *Waste Management & Research: The Journal for a Sustainable Circular Economy*, vol. 34, no. 8, pp. 775–783, Aug. 2016, doi: 10.1177/0734242X16654980.

[55] "DIRECTIVE 2008/98/EC OF THE EUROPEAN PARLIAMENT AND OF THE COUNCIL of 19 November 2008 on waste and repealing certain Directives (Text with EEA relevance)."

[56] J. Van Caneghem, K. Van Acker, J. De Greef, G. Wauters, and C. Vandecasteele, "Waste-to-energy is compatible and complementary with recycling in the circular economy," *Clean Technologies and Environmental Policy*. Springer Verlag, 2019. doi: 10.1007/s10098-019-01686-0.

[57] F. Cucchiella, I. D'Adamo, and M. Gastaldi, "Sustainable waste management: Waste to energy plant as an alternative to landfill," *Energy Convers Manag*, vol. 131, pp. 18–31, Jan. 2017, doi: 10.1016/j.enconman.2016.11.012.

[58] A. Pires and G. Martinho, "Waste hierarchy index for circular economy in waste management," *Waste Management*, vol. 95, pp. 298–305, Jul. 2019, doi: 10.1016/j.wasman.2019.06.014.

[59] European Commission, "COMMUNICATION FROM THE COMMISSION TO THE EUROPEAN PARLIAMENT, THE COUNCIL, THE EUROPEAN ECONOMIC AND SOCIAL COMMITTEE AND THE COMMITTEE OF THE REGIONS:Closing the loop - An EU action plan for the Circular Economy," Brussels, Feb. 2015.

[60] J. M. Fernández-González, A. L. Grindlay, F. Serrano-Bernardo, M. I. Rodríguez-Rojas, and M. Zamorano, "Economic and environmental review of Waste-to-Energy systems for municipal solid waste management in medium and small municipalities," *Waste Management*, vol. 67, pp. 360–374, Sep. 2017, doi: 10.1016/j.wasman.2017.05.003.

[61] M. Abis *et al.*, "Assessment of the synergy between recycling and thermal treatments in municipal solid waste management in europe," *Energies (Basel)*, vol. 13, no. 23, Dec. 2020, doi: 10.3390/en13236412.

[62] A. Rorat, P. Courtois, F. Vandenbulcke, and S. Lemiere, "Sanitary and environmental aspects of sewage sludge management," *Industrial and Municipal Sludge: Emerging Concerns and Scope for Resource Recovery*, no. 1, pp. 155–180, 2019, doi: 10.1016/B978-0-12-815907-1.00008-8.

[63] A. Rorat, P. Courtois, F. Vandenbulcke, and S. Lemiere, "Sanitary and environmental aspects of sewage sludge management," in *Industrial and Municipal Sludge: Emerging Concerns and Scope for Resource Recovery*, 2019. doi: 10.1016/B978-0-12-815907-1.00008-8.

[64] EUROPEAN COMMISSION, *COMMITTEE AND THE COMMITTEE OF THE REGIONS on the 2017 list of Critical Raw Materials for the EU*. 2017.

[65] M. Smol, C. Adam, and M. Preisner, "Circular economy model framework in the European water and wastewater sector," *J Mater Cycles Waste Manag*, 2020, doi: 10.1007/s10163-019-00960-z.

[66] C. Karaca, S. Sözen, D. Orhon, and H. Okutan, "High temperature pyrolysis of sewage sludge as a sustainable process for energy recovery," *Waste Management*, vol. 78, pp. 217–226, 2018, doi: 10.1016/j.wasman.2018.05.034.

[67] J. Oladejo, K. Shi, X. Luo, G. Yang, and T. Wu, "A review of sludge-to-energy recovery methods," *Energies (Basel)*, vol. 12, no. 1, pp. 1–38, 2019, doi: 10.3390/en12010060.

[68] B. Use and C. Study, "energies The Enhancement of Energy E ffi ciency in a Wastewater Treatment Plant through Sustainable".

[69] K. Świechowski *et al.*, "Waste to energy: Solid fuel production from biogas plant digestate and sewage sludge by torrefaction-process kinetics, fuel properties, and energy balance," *Energies (Basel)*, vol. 13, no. 12, 2020, doi: 10.3390/en13123161.

[70] A. Kelessidis and A. S. Stasinakis, "Comparative study of the methods used for treatment and final disposal of sewage sludge in European countries," *Waste Management*, 2012, doi: 10.1016/j.wasman.2012.01.012.

[71] S. Sfez, S. De Meester, S. E. Vlaeminck, and J. Dewulf, "Improving the resource footprint evaluation of products recovered from wastewater: A discussion on appropriate allocation in the context of circular economy," *Resour Conserv Recycl*, vol. 148, no. October 2018, pp. 132–144, 2019, doi: 10.1016/j.resconrec.2019.03.029.

[72] M. Smol, C. Adam, and M. Preisner, "Circular economy model framework in the European water and wastewater sector," *J Mater Cycles Waste Manag*, 2020, doi: 10.1007/s10163-019-00960-z.

[73] F. Cucchiella, I. D'Adamo, and M. Gastaldi, "Sustainable waste management: Waste to energy plant as an alternative to landfill," *Energy Convers Manag*, vol. 131, pp. 18–31, Jan. 2017, doi: 10.1016/j.enconman.2016.11.012.

[74] J. W. Lu, S. Zhang, J. Hai, and M. Lei, "Status and perspectives of municipal solid waste incineration in China: A comparison with developed regions," *Waste Management*, vol. 69. Elsevier Ltd, pp. 170–186, Nov. 01, 2017. doi: 10.1016/j.wasman.2017.04.014.

[75] J. Havukainen *et al.*, "Environmental impact assessment of municipal solid waste management incorporating mechanical treatment of waste and incineration in Hangzhou, China," *J Clean Prod*, vol. 141, pp. 453–461, Jan. 2017, doi: 10.1016/j.jclepro.2016.09.146.

[76] D. Panepinto and M. C. Zanetti, "Municipal solid waste incineration plant: A multi-step approach to the evaluation of an energy-recovery configuration," *Waste Management*, vol. 73, pp. 332–341, Mar. 2018, doi: 10.1016/j.wasman.2017.07.036.

[77] L. Lombardi and E. A. Carnevale, "Evaluation of the environmental sustainability of different waste-to-energy plant configurations," *Waste Management*, vol. 73, pp. 232–246, Mar. 2018, doi: 10.1016/j.wasman.2017.07.006.

[78] F. Dal Magro, H. Xu, G. Nardin, and A. Romagnoli, "Application of high temperature phase change materials for improved efficiency in waste-to-energy plants," *Waste Management*, vol. 73, pp. 322–331, Mar. 2018, doi: 10.1016/j.wasman.2017.06.031.

[79] A. Beylot, S. Muller, M. Descat, Y. Ménard, and J. Villeneuve, "Life cycle assessment of the French municipal solid waste incineration sector," *Waste Management*, vol. 80, pp. 144–153, Oct. 2018, doi: 10.1016/j.wasman.2018.08.037.

[80] M. Touš, M. Pavlas, O. Putna, P. Stehlík, and L. Crha, "Combined heat and power production planning in a waste-to-energy plant on a short-term basis," *Energy*, vol. 90, pp. 137–147, Oct. 2015, doi: 10.1016/j.energy.2015.05.077.

[81] F. A. M. Lino and K. A. R. Ismail, "Evaluation of the treatment of municipal solid waste as renewable energy resource in Campinas, Brazil," *Sustainable Energy Technologies and Assessments*, vol. 29, pp. 19–25, Oct. 2018, doi: 10.1016/j.seta.2018.06.011.

[82] T. Gu, C. Yin, W. Ma, and G. Chen, "Municipal solid waste incineration in a packed bed: A comprehensive modeling study with experimental validation," *Appl Energy*, vol. 247, pp. 127–139, Aug. 2019, doi: 10.1016/j.apenergy.2019.04.014.

[83] F. Wissing, S. Wirtz, and V. Scherer, "Simulating municipal solid waste incineration with a DEM/CFD method – Influences of waste properties, grate and furnace design," *Fuel*, vol. 206, pp. 638–656, 2017, doi: 10.1016/j.fuel.2017.06.037.

[84] J. S. Lu, Y. Chang, C. S. Poon, and D. J. Lee, "Slow pyrolysis of municipal solid waste (MSW): A review," *Bioresource Technology*, vol. 312. Elsevier Ltd, Sep. 01, 2020. doi: 10.1016/j.biortech.2020.123615.

[85] H. Wang, L. Wang, and A. Shahbazi, "Life cycle assessment of fast pyrolysis of municipal solid waste in North Carolina of USA," *J Clean Prod*, vol. 87, Jan. 2015, doi: 10.1016/j.jclepro.2014.09.011.

[86] A. Shahnazari, M. Rafiee, A. Rohani, B. Bhushan Nagar, M. A. Ebrahiminik, and M. H. Aghkhani, "Identification of effective factors to select energy recovery technologies from municipal solid waste using multi-criteria decision making (MCDM): A review of thermochemical technologies," *Sustainable Energy Technologies and Assessments*, vol. 40, p. 100737, Aug. 2020, doi: 10.1016/J.SETA.2020.100737.

[87] Q. Li, A. Faramarzi, S. Zhang, Y. Wang, X. Hu, and M. Gholizadeh, "Progress in catalytic pyrolysis of municipal solid waste," *Energy Conversion and Management*, vol. 226. Elsevier Ltd, Dec. 15, 2020. doi: 10.1016/j.enconman.2020.113525.

[88] I. M. Gandidi, M. D. Susila, A. Mustofa, and N. A. Pambudi, "Thermal – Catalytic cracking of real MSW into Bio-Crude Oil," *Journal of the Energy Institute*, vol. 91, no. 2, pp. 304–310, Apr. 2018, doi: 10.1016/j.joei.2016.11.005.

[89] A. Veses, O. Sanahuja-Parejo, M. S. Callén, R. Murillo, and T. García, "A combined two-stage process of pyrolysis and catalytic cracking of municipal solid waste for the production of syngas and solid refuse-derived fuels," *Waste Management*, vol. 101, pp. 171–179, Jan. 2020, doi: 10.1016/j.wasman.2019.10.009.

[90] N. Wang, K. Qian, D. Chen, H. Zhao, and L. Yin, "Upgrading gas and oil products of the municipal solid waste pyrolysis process by exploiting in-situ interactions between the volatile compounds and the char," *Waste Management*, vol. 102, pp. 380–390, Feb. 2020, doi: 10.1016/j.wasman.2019.10.056.

[91] C. Chen, Y. Jin, and Y. Chi, "Effects of moisture content and CaO on municipal solid waste pyrolysis in a fixed bed reactor," *J Anal Appl Pyrolysis*, vol. 110, no. 1, pp. 108–112, 2014, doi: 10.1016/j.jaap.2014.08.009.

[92] Q. Song *et al.*, "Pyrolysis of municipal solid waste with iron-based additives: A study on the kinetic, product distribution and catalytic mechanisms," *J Clean Prod*, vol. 258, Jun. 2020, doi: 10.1016/j.jclepro.2020.120682.

[93] B. Vaish, B. Sharma, V. Srivastava, P. Singh, M. H. Ibrahim, and R. P. Singh, "Energy recovery potential and environmental impact of gasification for municipal solid waste," *Biofuels*, vol. 10, no. 1, pp. 87–100, Jan. 2019, doi: 10.1080/17597269.2017.1368061.

[94] Z. Hameed *et al.*, "Gasification of municipal solid waste blends with biomass for energy production and resources recovery: Current status, hybrid technologies and innovative prospects," *Renewable and Sustainable Energy Reviews*, vol. 136, Feb. 2021, doi: 10.1016/j.rser.2020.110375.

[95] P. R. Bhoi, R. L. Huhnke, A. Kumar, N. Indrawan, and S. Thapa, "Co-gasification of municipal solid waste and biomass in a commercial scale downdraft gasifier," *Energy*, vol. 163, pp. 513–518, Nov. 2018, doi: 10.1016/j.energy.2018.08.151.

[96] J. Cai *et al.*, "Synergistic effects of co-gasification of municipal solid waste and biomass in fixed-bed gasifier," *Process Safety and Environmental Protection*, vol. 148, pp. 1–12, Apr. 2021, doi: 10.1016/j.psep.2020.09.063.

[97] U. Arena, F. Di Gregorio, G. De Troia, and A. Saponaro, "A techno-economic evaluation of a small-scale fluidized bed gasifier for solid recovered fuel," *Fuel Processing Technology*, vol. 131, pp. 69–77, 2015, doi: 10.1016/j.fuproc.2014.11.003.

[98] N. Kardani, A. Zhou, M. Nazem, and X. Lin, "Modelling of municipal solid waste gasification using an optimised ensemble soft computing model," *Fuel*, vol. 289, Apr. 2021, doi: 10.1016/j.fuel.2020.119903.

[99] P. Xu, Y. Jin, and Y. Cheng, "Thermodynamic Analysis of the Gasification of Municipal Solid Waste," *Engineering*, vol. 3, no. 3, pp. 416–422, Jun. 2017, doi: 10.1016/J.ENG.2017.03.004.

[100] H. Gu, Y. Tang, J. Yao, and F. Chen, "Study on biomass gasification under various operating conditions," *Journal of the Energy Institute*, vol. 92, no. 5, pp. 1329–1336, Oct. 2019, doi: 10.1016/j.joei.2018.10.002.

[101] M. Mehrpooya, A. Ghorbani, S. M. Ali Moosavian, and Y. Amirhaeri, "Optimal design and economic analysis of a hybrid process of municipal solid waste plasma gasification, thermophotovoltaic power generation and hydrogen/liquid fuel production," *Sustainable Energy Technologies and Assessments*, vol. 49, p. 101717, Feb. 2022, doi: 10.1016/J.SETA.2021.101717.

[102] A. F. Sotoodeh, F. Ahmadi, Z. Ghaffarpour, M. Ebadollahi, H. Nasrollahi, and M. Amidpour, "Performance analyses of a waste-to-energy multigeneration system incorporated with thermoelectric generators," *Sustainable Energy Technologies and Assessments*, vol. 49, p. 101649, Feb. 2022, doi: 10.1016/J.SETA.2021.101649.

[103] H. Ding, J. Li, and D. Heydarian, "Energy, exergy, exergoeconomic, and environmental analysis of a new biomass-driven cogeneration system," *Sustainable Energy Technologies and Assessments*, vol. 45, p. 101044, Jun. 2021, doi: 10.1016/J.SETA.2021.101044.

[104] N. D. Couto, V. B. Silva, and A. Rouboa, "Thermodynamic Evaluation of Portuguese municipal solid waste gasification," *J Clean Prod*, vol. 139, pp. 622–635, 2016, doi: 10.1016/j.jclepro.2016.08.082.

[105] F. Mayer, R. Bhandari, and S. Gäth, "Critical review on life cycle assessment of conventional and innovative waste-to-energy technologies," *Science of The Total Environment*, vol. 672, May 2019, doi: 10.1016/j.scitotenv.2019.03.449.

[106] G. Li and M. Guo, "Current development of slag valorisation in China," *Waste Biomass Valorization*, vol. 5, no. 3, pp. 317–325, 2014, doi: 10.1007/s12649-014-9294-7.

[107] C. Mukherjee, J. Denney, E. G. Mbonimpa, J. Slagley, and R. Bhowmik, "A review on municipal solid waste-to-energy trends in the USA," *Renewable and Sustainable Energy Reviews*, vol. 119. Elsevier Ltd, May 2020. doi: 10.1016/j.rser.2019.109512.

[108] J. Dong, Y. Tang, A. Nzihou, Y. Chi, E. Weiss-Hortala, and M. Ni, "Life cycle assessment of pyrolysis, gasification and incineration waste-to-energy technologies: Theoretical analysis and case study of commercial plants," *Science of the Total Environment*, vol. 626, pp. 744–753, May 2018, doi: 10.1016/j.scitotenv.2018.01.151.

[109] M. Malavasi, C. Allouis, A. D. Anna, and R. Rse, "Flameless Technology for Particulate Emissions Suppression," 2009.

[110] H. Li, C. Jin, Z. Zhang, I. O'Hara, and S. Mundree, "Environmental and economic life cycle assessment of energy recovery from sewage sludge through different anaerobic digestion pathways," *Energy*, vol. 126, pp. 649–657, 2017, doi: 10.1016/j.energy.2017.03.068.

[111] A. Gherghel, C. Teodosiu, and S. De Gisi, "A review on wastewater sludge valorisation and its challenges in the context of circular economy," *J Clean Prod*, vol. 228, pp. 244–263, 2019, doi: 10.1016/j.jclepro.2019.04.240.

[112] J. Oladejo, K. Shi, X. Luo, G. Yang, and T. Wu, "A review of sludge-to-energy recovery methods," *Energies (Basel)*, vol. 12, no. 1, pp. 1–38, 2019, doi: 10.3390/en12010060.

[113] A. Tsybina and C. Wuensch, "ANALYSIS OF SEWAGE SLUDGE THERMAL TREATMENT METHODS IN THE CONTEXT OF CIRCULAR ECONOMY," *Detritus*, vol. 2, no. 1, p. 3, 2018, doi: 10.31025/2611-4135/2018.13668.

[114] J. D. Bień and B. Bień, "Sludge Thermal Utilization, and the Circular Economy," *Civil and Environmental Engineering Reports*, vol. 29, no. 4, pp. 157–175, Dec. 2019, doi: 10.2478/ceer-2019-0052.

[115] C. Karaca, S. Sözen, D. Orhon, and H. Okutan, "High temperature pyrolysis of sewage sludge as a sustainable process for energy recovery," *Waste Management*, vol. 78, pp. 217–226, Aug. 2018, doi: 10.1016/j.wasman.2018.05.034.

[116] N. Gao, K. Kamran, C. Quan, and P. T. Williams, "Thermochemical conversion of sewage sludge: A critical review," *Progress in Energy and Combustion Science*. 2020. doi: 10.1016/j.pecs.2020.100843.

[117] S. Werle and S. Sobek, "Gasification of sewage sludge within a circular economy perspective: a Polish case study," *Environmental Science and Pollution Research*, 2019, doi: 10.1007/s11356-019-05897-2.

[118] S. Bolognesi, G. Bernardi, A. Callegari, D. Dondi, and A. G. Capodaglio, "Biochar production from sewage sludge and microalgae mixtures: properties, sustainability and possible role in circular economy," *Biomass Convers Biorefin*, 2019, doi: 10.1007/s13399-019-00572-5.

[119] E. Thorin, J. Olsson, S. Schwede, and E. Nehrenheim, "Co-digestion of sewage sludge and microalgae – Biogas production investigations," *Appl Energy*, vol. 227, no. May, pp. 64–72, 2018, doi: 10.1016/j.apenergy.2017.08.085.

[120] R. Z. Gaur *et al.*, "Hydrothermal carbonization of sewage sludge coupled with anaerobic digestion: Integrated approach for sludge management and energy

recycling," *Energy Convers Manag*, vol. 224, no. June, p. 113353, 2020, doi: 10.1016/j.enconman.2020.113353.

[121] Y. Shen, C. He, X. Chen, A. A. Lapkin, W. Xiao, and C. H. Wang, "Nitrogen Removal and Energy Recovery from Sewage Sludge by Combined Hydrothermal Pretreatment and CO2 Gasification," *ACS Sustain Chem Eng*, vol. 6, no. 12, pp. 16629–16636, 2018, doi: 10.1021/acssuschemeng.8b03857.

[122] Y. Zhai *et al.*, "Hydrothermal carbonisation of sewage sludge for char production with different waste biomass: Effects of reaction temperature and energy recycling," *Energy*, vol. 127, pp. 167–174, 2017, doi: 10.1016/j.energy.2017.03.116.

[123] R. Wang, C. Wang, Z. Zhao, J. Jia, and Q. Jin, "Energy recovery from high-ash municipal sewage sludge by hydrothermal carbonization: Fuel characteristics of biosolid products," *Energy*, vol. 186, p. 115848, 2019, doi: 10.1016/j.energy.2019.07.178.

[124] V. Singh, H. C. Phuleria, and M. K. Chandel, "Estimation of energy recovery potential of sewage sludge in India: Waste to watt approach," *J Clean Prod*, vol. 276, p. 122538, 2020, doi: 10.1016/j.jclepro.2020.122538.

[125] P. Sulewski, W. Ignaciuk, M. Szymańska, and A. Wąs, "Development of the Biomethane Market in Europe," *Energies 2023, Vol. 16, Page 2001*, vol. 16, no. 4, p. 2001, Feb. 2023, doi: 10.3390/EN16042001.

[126] T. Zhu, J. Curtis, and M. Clancy, "Promoting agricultural biogas and biomethane production: Lessons from cross-country studies," *Renewable and Sustainable Energy Reviews*, vol. 114, p. 109332, Oct. 2019, doi: 10.1016/j.rser.2019.109332.

[127] I. D'Adamo and C. Sassanelli, "Biomethane Community: A Research Agenda towards Sustainability," *Sustainability*, vol. 14, no. 8, p. 4735, Apr. 2022, doi: 10.3390/su14084735.

[128] I. Sharma *et al.*, "Exploring the potential for biomethane production by the hybrid anaerobic digestion and hydrothermal gasification process: A review," *J Clean Prod*, vol. 362, p. 132507, Aug. 2022, doi: 10.1016/j.jclepro.2022.132507.

[129] P. W. R. Adams and M. C. McManus, "Characterisation and variability of greenhouse gas emissions from biomethane production via anaerobic digestion of maize," *J Clean Prod*, vol. 218, pp. 529–542, May 2019, doi: 10.1016/j.jclepro.2018.12.232.

[130] M. Adelt, D. Wolf, and A. Vogel, "LCA of biomethane," *J Nat Gas Sci Eng*, vol. 3, no. 5, pp. 646–650, Oct. 2011, doi: 10.1016/j.jngse.2011.07.003.

[131] S. Croce, Q. Wei, G. D'Imporzano, R. Dong, and F. Adani, "Anaerobic digestion of straw and corn stover: The effect of biological process optimization and pre-treatment on total bio-methane yield and energy performance," *Biotechnol Adv*, vol. 34, no. 8, pp. 1289–1304, Dec. 2016, doi: 10.1016/j.biotechadv.2016.09.004.

[132] M. Saghouri, R. Abdi, M. Ebrahimi-Nik, A. Rohani, and M. Maysami, "Modeling and optimization of biomethane production from solid-state anaerobic co-digestion of organic fraction municipal solid waste and other co-substrates," *Energy Sources, Part A: Recovery, Utilization, and Environmental Effects*, pp. 1–17, May 2020, doi: 10.1080/15567036.2020.1767728.

[133] D. Lu, X. Liu, O. G. Apul, L. Zhang, D. K. Ryan, and X. Zhang, "Optimization of biomethane production from anaerobic Co-digestion of microalgae and septic tank sludge," *Biomass Bioenergy*, vol. 127, p. 105266, Aug. 2019, doi: 10.1016/j.biombioe.2019.105266.

[134] Y. R. Ouahabi, K. Bensadok, and A. Ouahabi, "Optimization of the Biomethane Production Process by Anaerobic Digestion of Wheat Straw Using Chemical Pretreatments Coupled with Ultrasonic Disintegration," *Sustainability*, vol. 13, no. 13, p. 7202, Jun. 2021, doi: 10.3390/su13137202.

[135] I. D'Adamo, P. M. Falcone, and F. Ferella, "A socio-economic analysis of biomethane in the transport sector: The case of Italy," *Waste Management*, vol. 95, no. March 2018, pp. 102–115, 2019, doi: 10.1016/j.wasman.2019.06.005.

[136] International Energy Agency, "Report extract. An introduction to biogas and biomethan."

[137] G. Caposciutti, A. Baccioli, L. Ferrari, and U. Desideri, "Biogas from anaerobic digestion: Power generation or biomethane production?," *Energies (Basel)*, vol. 13, no. 3, 2020, doi: 10.3390/en13030743.

[138] E. S. Salama *et al.*, "Enhanced anaerobic co-digestion of fat, oil, and grease by calcium addition: Boost of biomethane production and microbial community shift," *Bioresour Technol*, vol. 296, no. October 2019, p. 122353, 2020, doi: 10.1016/j.biortech.2019.122353.

[139] D. De Clercq, Z. Wen, F. Fei, L. Caicedo, K. Yuan, and R. Shang, "Interpretable machine learning for predicting biomethane production in industrial-scale anaerobic co-digestion," *Science of the Total Environment*, vol. 712, p. 134574, 2020, doi: 10.1016/j.scitotenv.2019.134574.

[140] F. Cucchiella, I. D'Adamo, and M. Gastaldi, "An economic analysis of biogas-biomethane chain from animal residues in Italy," *J Clean Prod*, vol. 230, pp. 888–897, 2019, doi: 10.1016/j.jclepro.2019.05.116.

[141] J. Lui, W.-H. Chen, D. C. W. Tsang, and S. You, "A critical review on the principles, applications, and challenges of waste-to-hydrogen technologies," *Renewable and Sustainable Energy Reviews*, vol. 134, p. 110365, Dec. 2020, doi: 10.1016/j.rser.2020.110365.

[142] M. A. Salam, K. Ahmed, N. Akter, T. Hossain, and B. Abdullah, "A review of hydrogen production via biomass gasification and its prospect in Bangladesh," *Int*

J Hydrogen Energy, vol. 43, no. 32, pp. 14944–14973, Aug. 2018, doi: 10.1016/j.ijhydene.2018.06.043.

[143] M. Ozturk and I. Dincer, "An integrated system for clean hydrogen production from municipal solid wastes," *Int J Hydrogen Energy*, vol. 46, no. 9, pp. 6251–6261, Feb. 2021, doi: 10.1016/j.ijhydene.2020.11.145.

[144] Y. Zhang, P. Xu, S. Liang, B. Liu, Y. Shuai, and B. Li, "Exergy analysis of hydrogen production from steam gasification of biomass: A review," *Int J Hydrogen Energy*, vol. 44, no. 28, pp. 14290–14302, May 2019, doi: 10.1016/j.ijhydene.2019.02.064.

[145] A. C. C. Chang, H.-F. Chang, F.-J. Lin, K.-H. Lin, and C.-H. Chen, "Biomass gasification for hydrogen production," *Int J Hydrogen Energy*, vol. 36, no. 21, pp. 14252–14260, Oct. 2011, doi: 10.1016/j.ijhydene.2011.05.105.

[146] B. Li, H. Yang, L. Wei, J. Shao, X. Wang, and H. Chen, "Hydrogen production from agricultural biomass wastes gasification in a fluidized bed with calcium oxide enhancing," *Int J Hydrogen Energy*, vol. 42, no. 8, pp. 4832–4839, Feb. 2017, doi: 10.1016/j.ijhydene.2017.01.138.

[147] Z. Xu *et al.*, "Modeling and comprehensive analysis of food waste gasification process for hydrogen production," *Energy Convers Manag*, vol. 258, p. 115509, Apr. 2022, doi: 10.1016/j.enconman.2022.115509.

[148] H. Ishaq and I. Dincer, "Comparative assessment of renewable energy-based hydrogen production methods," *Renewable and Sustainable Energy Reviews*, vol. 135, p. 110192, Jan. 2021, doi: 10.1016/j.rser.2020.110192.

[149] S. Rudra and Y. K. Tesfagaber, "Future district heating plant integrated with municipal solid waste (MSW) gasification for hydrogen production," *Energy*, vol. 180, pp. 881–892, Aug. 2019, doi: 10.1016/j.energy.2019.05.125.

[150] H. Ishaq and I. Dincer, "A new energy system based on biomass gasification for hydrogen and power production," *Energy Reports*, vol. 6, pp. 771–781, Nov. 2020, doi: 10.1016/j.egyr.2020.02.019.

[151] Y. E. Yuksel, M. Ozturk, and I. Dincer, "Energy and exergy analyses of an integrated system using waste material gasification for hydrogen production and liquefaction," *Energy Convers Manag*, vol. 185, pp. 718–729, Apr. 2019, doi: 10.1016/j.enconman.2019.02.033.

[152] R. Sivaramakrishnan *et al.*, "Insights on biological hydrogen production routes and potential microorganisms for high hydrogen yield," *Fuel*, vol. 291, p. 120136, May 2021, doi: 10.1016/j.fuel.2021.120136.

[153] R. Łukajtis *et al.*, "Hydrogen production from biomass using dark fermentation," *Renewable and Sustainable Energy Reviews*, vol. 91, pp. 665–694, Aug. 2018, doi: 10.1016/j.rser.2018.04.043.

[154] D. Pham Minh *et al.*, "Hydrogen Production From Biogas Reforming: An Overview of Steam Reforming, Dry Reforming, Dual Reforming, and Tri-Reforming of Methane," in *Hydrogen Supply Chains*, Elsevier, 2018, pp. 111–166. doi: 10.1016/B978-0-12-811197-0.00004-X.

[155] L. B. Braga, J. L. Silveira, M. E. da Silva, C. E. Tuna, E. B. Machin, and D. T. Pedroso, "Hydrogen production by biogas steam reforming: A technical, economic and ecological analysis," *Renewable and Sustainable Energy Reviews*, vol. 28, pp. 166–173, Dec. 2013, doi: 10.1016/j.rser.2013.07.060.

[156] R. Kumar, A. Kumar, and A. Pal, "Overview of hydrogen production from biogas reforming: Technological advancement," *Int J Hydrogen Energy*, vol. 47, no. 82, pp. 34831–34855, Sep. 2022, doi: 10.1016/j.ijhydene.2022.08.059.

[157] K. Chouhan, S. Sinha, S. Kumar, and S. Kumar, "Simulation of steam reforming of biogas in an industrial reformer for hydrogen production," *Int J Hydrogen Energy*, vol. 46, no. 53, pp. 26809–26824, Aug. 2021, doi: 10.1016/j.ijhydene.2021.05.152.

[158] M. Ji and J. Wang, "Review and comparison of various hydrogen production methods based on costs and life cycle impact assessment indicators," *Int J Hydrogen Energy*, vol. 46, no. 78, pp. 38612–38635, Nov. 2021, doi: 10.1016/j.ijhydene.2021.09.142.

[159] I. Dincer and C. Acar, "Review and evaluation of hydrogen production methods for better sustainability," *Int J Hydrogen Energy*, vol. 40, no. 34, pp. 11094–11111, Sep. 2015, doi: 10.1016/j.ijhydene.2014.12.035.

[160] R. S. El-Emam and H. Özcan, "Comprehensive review on the techno-economics of sustainable large-scale clean hydrogen production," *J Clean Prod*, vol. 220, pp. 593–609, May 2019, doi: 10.1016/j.jclepro.2019.01.309.

[161] X. Xu, Q. Zhou, and D. Yu, "The future of hydrogen energy: Bio-hydrogen production technology," *Int J Hydrogen Energy*, vol. 47, no. 79, pp. 33677–33698, Sep. 2022, doi: 10.1016/j.ijhydene.2022.07.261.

[162] C. Acar and I. Dincer, "Impact assessment and efficiency evaluation of hydrogen production methods," *Int J Energy Res*, vol. 39, no. 13, pp. 1757–1768, Oct. 2015, doi: 10.1002/er.3302.

[163] G. Amaya-Santos, S. Chari, A. Sebastiani, F. Grimaldi, P. Lettieri, and M. Materazzi, "Biohydrogen: A life cycle assessment and comparison with alternative low-carbon production routes in UK," *J Clean Prod*, vol. 319, p. 128886, Oct. 2021, doi: 10.1016/j.jclepro.2021.128886.

[164] J. Dong, Y. Tang, A. Nzihou, Y. Chi, E. Weiss-Hortala, and M. Ni, "Life cycle assessment of pyrolysis, gasification and incineration waste-to-energy technologies: Theoretical analysis and case study of commercial plants," *Science of The Total Environment*, vol. 626, pp. 744–753, Jun. 2018, doi: 10.1016/j.scitotenv.2018.01.151.

[165] C. Jin *et al.*, "Anaerobic digestion: An alternative resource treatment option for food waste in China," *Science of The Total Environment*, vol. 779, p. 146397, Jul. 2021, doi: 10.1016/j.scitotenv.2021.146397.

[166] Y. Sun, Z. Qin, Y. Tang, T. Huang, S. Ding, and X. Ma, "Techno-environmental-economic evaluation on municipal solid waste (MSW) to power/fuel by gasification-based and incineration-based routes," *J Environ Chem Eng*, vol. 9, no. 5, p. 106108, Oct. 2021, doi: 10.1016/j.jece.2021.106108.

[167] M. Malavasi, C. Allouis, A. D. Anna, and R. Rse, "Flameless Technology for Particulate Emissions Suppression Flameless Technology for Particulate Emissions Suppression," 2009.

[168] N. Poranek, B. Łaźniewska-Piekarczyk, A. Czajkowski, and K. Pikoń, "Circular Economy for Municipal Solid Waste Incineration Bottom Ash (MSWIBA) Management in Mortars with CSA and CEM I, MSWIBA Glassy Phase, and DTG," *Energies (Basel)*, vol. 15, no. 1, p. 135, Dec. 2021, doi: 10.3390/en15010135.

[169] E. N. Kalogirou, *Waste-to-Energy Technologies and Global Applications*. Boca Raton, FL : CRC Press, 2018.: CRC Press, 2017. doi: 10.1201/9781315269061.

[170] M. A. Rosato, *Managing Biogas Plants A Practical Guide*, 1 Press. CRC Press.

[171] M. Albanna, "Anaerobic digestion of the organic fraction of municipal solid waste," in *Management of Microbial Resources in the Environment*, vol. 9789400759312, Springer Netherlands, 2013, pp. 313–340. doi: 10.1007/978-94-007-5931-2_12.

[172] J. N. Meegoda, B. Li, K. Patel, and L. B. Wang, "A review of the processes, parameters, and optimization of anaerobic digestion," *International Journal of Environmental Research and Public Health*, vol. 15, no. 10. MDPI AG, Oct. 11, 2018. doi: 10.3390/ijerph15102224.

[173] W. Wang and D.-J. Lee, "Valorization of anaerobic digestion digestate: A prospect review," *Bioresour Technol*, vol. 323, p. 124626, Mar. 2021, doi: 10.1016/j.biortech.2020.124626.

[174] "Anaerobic Digestion-Making Biogas-Making Energy."

[175] A. Fusi, J. Bacenetti, M. Fiala, and A. Azapagic, "Life Cycle Environmental Impacts of Electricity from Biogas Produced by Anaerobic Digestion," *Front Bioeng Biotechnol*, vol. 4, Mar. 2016, doi: 10.3389/fbioe.2016.00026.

[176] N. Couto, A. Rouboa, V. Silva, E. Monteiro, and K. Bouziane, "Influence of the Biomass Gasification Processes on the Final Composition of Syngas," *Energy Procedia*, vol. 36, pp. 596–606, 2013, doi: 10.1016/j.egypro.2013.07.068.

[177] T. Bhaskar, B. Balagurumurthy, R. Singh, and M. K. Poddar, "Thermochemical Route for Biohydrogen Production," in *Biohydrogen*, Elsevier, 2013, pp. 285–316. doi: 10.1016/B978-0-444-59555-3.00012-X.

[178] D. T. Pio, L. A. C. Tarelho, and M. A. A. Matos, "Characteristics of the gas produced during biomass direct gasification in an autothermal pilot-scale bubbling fluidized bed reactor," *Energy*, vol. 120, pp. 915–928, Feb. 2017, doi: 10.1016/j.energy.2016.11.145.

[179] S. Ferreira, E. Monteiro, P. Brito, and C. Vilarinho, "A Holistic Review on Biomass Gasification Modified Equilibrium Models," *Energies (Basel)*, vol. 12, no. 1, p. 160, Jan. 2019, doi: 10.3390/en12010160.

[180] *Biomass Gasification and Pyrolysis*. Elsevier, 2010. doi: 10.1016/C2009-0-20099-7.

[181] Y. Richardson, J. Blin, and A. Julbe, "A short overview on purification and conditioning of syngas produced by biomass gasification: Catalytic strategies, process intensification and new concepts," *Prog Energy Combust Sci*, vol. 38, no. 6, pp. 765–781, Dec. 2012, doi: 10.1016/j.pecs.2011.12.001.

[182] B. Raho, G. Colangelo, M. Milanese, and A. de Risi, "A Critical Analysis of the Oxy-Combustion Process: From Mathematical Models to Combustion Product Analysis," *Energies (Basel)*, vol. 15, no. 18, May 2022, doi: 10.3390/en15186514.

[183] W. Blasiak and J. von Schéele, "'Flameless' oxyfuel combustion development for process improvement, emission reduction in furnaces and incinerators," in *Waste Management and the Environment III*, Southampton, UK: WIT Press, Jun. 2006, pp. 247–256. doi: 10.2495/WM060271.

[184] M. Malavasi, C. Allouis, A. D. Anna, and R. Rse, "Flameless Technology for Particulate Emissions Suppression," 2009.

[185] G. Li and M. Guo, "Current development of slag valorisation in China," *Waste Biomass Valorization*, vol. 5, no. 3, pp. 317–325, 2014, doi: 10.1007/s12649-014-9294-7.

[186] M. Malavasi, "A flameless oxycombustion route to lower cost CCS?" [Online]. Available: https://www.modernpowersystems.com/features/featurea-flameless-oxycombustion-route-to-lower-cost-ccs-4300064/

[187] B. Raho, G. Colangelo, M. Milanese, and A. de Risi, "A Critical Analysis of the Oxy-Combustion Process: From Mathematical Models to Combustion Product Analysis," *Energies (Basel)*, vol. 15, no. 18, Sep. 2022, doi: 10.3390/en15186514.

[188] J. M. Schmitt, "PRE-PROJECT PLANNING FOR A FLAMELESS PRESSURIZED OXY-COMBUSTION PILOT PLANT," 2016.

[189] *Compendium of Hydrogen Energy*. Elsevier, 2015. doi: 10.1016/C2014-0-02671-8.

[190] A. Basile, F. Dalena, J. Tong, and T. Nejat Vezirogl, "IET ENERGY ENGINEERING SERIES 89 Hydrogen Production, Separation and Purification for Energy."

[191] *Advances in Hydrogen Production, Storage and Distribution*. Elsevier, 2014. doi: 10.1016/C2013-0-16359-3.

[192] M. B. Syed, "Technologies for renewable hydrogen production," in *Bioenergy Resources and Technologies*, Elsevier, 2021, pp. 157–198. doi: 10.1016/B978-0-12-822525-7.00013-5.

[193] M. A. Nieva, M. M. Villaverde, A. Monzón, T. F. Garetto, and A. J. Marchi, "Steam-methane reforming at low temperature on nickel-based catalysts," *Chemical Engineering Journal*, vol. 235, pp. 158–166, Jan. 2014, doi: 10.1016/j.cej.2013.09.030.

[194] A. Basile, S. Liguori, and A. Iulianelli, "Membrane reactors for methane steam reforming (MSR)," in *Membrane Reactors for Energy Applications and Basic Chemical Production*, Elsevier, 2015, pp. 31–59. doi: 10.1016/B978-1-78242-223-5.00002-9.

[195] S. Shiva Kumar and V. Himabindu, "Hydrogen production by PEM water electrolysis – A review," *Mater Sci Energy Technol*, vol. 2, no. 3, pp. 442–454, Dec. 2019, doi: 10.1016/j.mset.2019.03.002.

[196] J. J. C. Mancera, F. S. Manzano, J. M. Andújar, F. J. Vivas, and A. J. Calderón, "An optimized balance of plant for a medium-size PEM electrolyzer. Design, control and physical implementation," *Electronics (Switzerland)*, vol. 9, no. 5, May 2020, doi: 10.3390/electronics9050871.

[197] N. Hajjaji, S. Martinez, E. Trably, J.-P. Steyer, and A. Helias, "Life cycle assessment of hydrogen production from biogas reforming," *Int J Hydrogen Energy*, vol. 41, no. 14, pp. 6064–6075, Apr. 2016, doi: 10.1016/j.ijhydene.2016.03.006.

[198] International Monetary Fund., *Fiscal monitor : how to mitigate climate change*.

[199] Z. Wen, J. Di, S. Liu, J. Han, and J. C. K. Lee, "Evaluation of flue-gas treatment technologies for municipal waste incineration: A case study in Changzhou, China," *J Clean Prod*, vol. 184, May 2018, doi: 10.1016/j.jclepro.2018.02.282.

[200] W. P. Chan *et al.*, "A hot syngas purification system integrated with downdraft gasification of municipal solid waste," *Appl Energy*, vol. 237, pp. 227–240, Mar. 2019, doi: 10.1016/j.apenergy.2019.01.031.

[201] P. Mckendry, "Costs of Incineration and Non-Incineration Energy from Waste Technologies Energy from Wastes View project WEM Diploma Course notes View project," 2008, doi: 10.13140/RG.2.2.30993.12649.

[202] G. Figini, Gianfranco, Di Salvia, "La flameless combustion per il trattamento di rifiuti industriali anche a basso LHV."

[203] ISPRA, *Rapporto Rifiuti Urbani*, vol. 53, no. 9. 2013.

[204] "President of the Italian Republic, Legislative Decree 152/2006 'Norms Concerning the Environment.'"

[205] Itea S.p.A, "Itea flameless technologies." [Online]. Available: https://www.iteaspa.it/

[206] J. Schmitt, B. Ridens, and M. Malavasi, "System Modelling of a 50MWth Demonstration Flameless Pressurized Oxy-Combustion Pilot Plant," *SSRN Electronic Journal*, 2019, doi: 10.2139/ssrn.3365705.

[207] X. gang Zhao, G. wu Jiang, A. Li, and L. Wang, "Economic analysis of waste-to-energy industry in China," *Waste Management*, vol. 48, pp. 604–618, Feb. 2016, doi: 10.1016/j.wasman.2015.10.014.

[208] "Waste and resources assessment tool for the environment (WRATE) LCA model."

[209] J. Dong, Y. Tang, A. Nzihou, Y. Chi, E. Weiss-Hortala, and M. Ni, "Life cycle assessment of pyrolysis, gasification and incineration waste-to-energy technologies: Theoretical analysis and case study of commercial plants," *Science of the Total Environment*, vol. 626, pp. 744–753, Jun. 2018, doi: 10.1016/j.scitotenv.2018.01.151.

[210] N. Indrawan, B. Simkins, A. Kumar, and R. L. Huhnke, "Economics of Distributed Power Generation via Gasification of Biomass and Municipal Solid Waste," *Energies (Basel)*, vol. 13, no. 14, Jul. 2020, doi: 10.3390/en13143703.

[211] R. Voss, R. P. Lee, L. Seidl, F. Keller, and M. Fröhling, "Global warming potential and economic performance of gasification-based chemical recycling and incineration pathways for residual municipal solid waste treatment in Germany," *Waste Management*, vol. 134, pp. 206–219, Oct. 2021, doi: 10.1016/j.wasman.2021.07.040.

[212] V. Iaboni, P. De Stefanis, and (ENEA), "Aspetti economici del recupero di energia da rifiuti urbani," 2007.

[213] C. Liu, J. Wang, X. Ji, H. Qian, L. Huang, and X. Lu, "The biomethane producing potential in China: A theoretical and practical estimation," *Chin J Chem Eng*, vol. 24, no. 7, pp. 920–928, 2016, doi: 10.1016/j.cjche.2015.12.025.

[214] C. Banks, "Anaerobic digestion and energy," *Valorgas Seventh Framework Programme*, p. 41, 2009.

[215] Comune di Bari, "PIANO DI AZIONE del Piano Energetico Ambientale (PEAC) 2005," 2005.

[216] G. D. Gebreeyessus and P. Jenicek, "Thermophilic versus mesophilic anaerobic digestion of sewage sludge: A comparative review," *Bioengineering*, vol. 3, no. 2, pp. 1–14, 2016, doi: 10.3390/bioengineering3020015.

[217] G. D. Gebreeyessus and P. Jenicek, "Thermophilic versus mesophilic anaerobic digestion of sewage sludge: A comparative review," *Bioengineering*, vol. 3, no. 2, pp. 1–14, 2016, doi: 10.3390/bioengineering3020015.

[218] F. Ardolino, F. Parrillo, and U. Arena, "Biowaste-to-biomethane or biowaste-to-energy? An LCA study on anaerobic digestion of organic waste," *J Clean Prod*, vol. 174, pp. 462–476, 2018, doi: 10.1016/j.jclepro.2017.10.320.

[219] F. Ardolino, F. Parrillo, and U. Arena, "Biowaste-to-biomethane or biowaste-to-energy? An LCA study on anaerobic digestion of organic waste," *J Clean Prod*, vol. 174, pp. 462–476, 2018, doi: 10.1016/j.jclepro.2017.10.320.

[220] Carbon Footprint, "Carbon Footprint, Country specific Electricity Factors," no. June, pp. 1–10, 2019.

[221] ISPRA, "Italian Greenhouse Gas Inventory 1990-2019, National Inventory Report 2021."

[222] L. Rosa, D. L. Sanchez, and M. Mazzotti, "Assessment of carbon dioxide removal potential via BECCS in a carbon-neutral Europe," *Energy Environ Sci*, vol. 14, no. 5, pp. 3086–3097, 2021, doi: 10.1039/D1EE00642H.

[223] I. E. Agency, "Global Hydrogen Review 2022." 2022. [Online]. Available: https://www.iea.org/reports/global-hydrogen-review-2022

[224] F. Ardolino, F. Parrillo, and U. Arena, "Biowaste-to-biomethane or biowaste-to-energy? An LCA study on anaerobic digestion of organic waste," *J Clean Prod*, vol. 174, pp. 462–476, Feb. 2018, doi: 10.1016/j.jclepro.2017.10.320.

[225] N. Hajjaji, S. Martinez, E. Trably, J.-P. Steyer, and A. Helias, "Life cycle assessment of hydrogen production from biogas reforming," *Int J Hydrogen Energy*, vol. 41, no. 14, pp. 6064–6075, May 2016, doi: 10.1016/j.ijhydene.2016.03.006.

[226] "CARBON FOOTPRINT COUNTRY SPECIFIC ELECTRICITY GRID GREENHOUSE GAS EMISSION FACTORS." [Online]. Available: www.carbonfootprint.com

[227] B. RUKES, "Status and perspectives of fossil power generation," *Energy*, vol. 29, no. 12–15, pp. 1853–1874, Dec. 2004, doi: 10.1016/j.energy.2004.03.053.

[228] R. Gupta, R. Miller, W. Sloan, and S. You, "Economic and environmental assessment of organic waste to biomethane conversion," *Bioresour Technol*, vol. 345, p. 126500, Feb. 2022, doi: 10.1016/j.biortech.2021.126500.

[229] G. U. Ingale *et al.*, "Assessment of Greenhouse Gas Emissions from Hydrogen Production Processes: Turquoise Hydrogen vs. Steam Methane Reforming," *Energies (Basel)*, vol. 15, no. 22, Nov. 2022, doi: 10.3390/en15228679.

[230] IEA, "Methane and Climate Change." Accessed: Jan. 09, 2023. [Online]. Available: https://www.iea.org/reports/methane-tracker-2021/methane-and-climate-change

[231] A. Susmozas, D. Iribarren, and J. Dufour, "Life-cycle performance of indirect biomass gasification as a green alternative to steam methane reforming for

hydrogen production," *Int J Hydrogen Energy*, vol. 38, no. 24, Aug. 2013, doi: 10.1016/j.ijhydene.2013.06.012.

[232] G. U. Ingale *et al.*, "Assessment of Greenhouse Gas Emissions from Hydrogen Production Processes: Turquoise Hydrogen vs. Steam Methane Reforming," *Energies (Basel)*, vol. 15, no. 22, Nov. 2022, doi: 10.3390/en15228679.

[233] Z. Wang, J. Ren, M. E. Goodsite, and G. Xu, "Waste-to-energy, municipal solid waste treatment, and best available technology: Comprehensive evaluation by an interval-valued fuzzy multi-criteria decision making method," *J Clean Prod*, vol. 172, pp. 887–899, May 2018, doi: 10.1016/j.jclepro.2017.10.184.

[234] N. Hajjaji, S. Martinez, E. Trably, J.-P. Steyer, and A. Helias, "Life cycle assessment of hydrogen production from biogas reforming," *Int J Hydrogen Energy*, vol. 41, no. 14, pp. 6064–6075, Apr. 2016, doi: 10.1016/j.ijhydene.2016.03.006.

[235] A. Borgogna, G. Centi, G. Iaquaniello, S. Perathoner, G. Papanikolaou, and A. Salladini, "Assessment of hydrogen production from municipal solid wastes as competitive route to produce low-carbon H2," *Science of The Total Environment*, vol. 827, Jun. 2022, doi: 10.1016/j.scitotenv.2022.154393.

[236] S. L. Nordahl *et al.*, "Life-Cycle Greenhouse Gas Emissions and Human Health Trade-Offs of Organic Waste Management Strategies," *Environ Sci Technol*, vol. 54, no. 15, pp. 9200–9209, Aug. 2020, doi: 10.1021/acs.est.0c00364.

[237] European Commission, "Hydrogen." Accessed: Jul. 05, 2023. [Online]. Available: https://energy.ec.europa.eu/topics/energy-systems-integration/hydrogen_en

[238] European Environment Agency, "Reaching 2030's residual municipal waste target — why recycling is not enough," 2023. Accessed: Jul. 05, 2023. [Online]. Available: https://www.eea.europa.eu/publications/reaching-2030s-residual-municipal-waste

[239] European Commission, "A European Green Deal." Accessed: Jul. 05, 2023. [Online]. Available: https://commission.europa.eu/strategy-and-policy/priorities-2019-2024/european-green-deal_en

[240] Guidehouse, "Biomethane production potentials in the EU," 2022. Accessed: Jul. 05, 2023. [Online]. Available: https://www.europeanbiogas.eu/wp-content/uploads/2022/07/GfC_national-biomethane-potentials_070722.pdf

[241] European Environment Agency, "Greenhouse gas emission intensity of electricity generation in Europe." Accessed: Jul. 05, 2023. [Online]. Available: https://www.eea.europa.eu/ims/greenhouse-gas-emission-intensity-of-1

[242] Fuel Cells and Hydrogen Observatory, "Chapter 2: hydrogen supply and demand," 2021. Accessed: Jul. 05, 2023. [Online]. Available: https://www.fchobservatory.eu/sites/default/files/reports/Chapter%202%20Hydrogen%20Supply%20and%20Demand%202021.pdf

[243] Eurostat, "Generation of waste by waste category, hazardousness and NACE Rev. 2 activity," 2023. Accessed: Jul. 05, 2023. [Online]. Available: https://ec.europa.eu/eurostat/databrowser/view/ENV_WASGEN/default/table?lang=en

[244] E. Union *et al.*, "PE-CONS 27/21 TREE.1.A MFG/NC/fh," vol. 2021, no. 401, 2021.

[245] International Energy Agency, "Iron and Steel." Accessed: May 29, 2023. [Online]. Available: https://www.iea.org/reports/iron-and-steel

[246] C. G. F. Bataille, "Physical and policy pathways to net-zero emissions industry," *WIREs Climate Change*, vol. 11, no. 2, May 2020, doi: 10.1002/wcc.633.

[247] A. H. Azadnia, C. McDaid, A. M. Andwari, and S. E. Hosseini, "Green hydrogen supply chain risk analysis: A european hard-to-abate sectors perspective," *Renewable and Sustainable Energy Reviews*, vol. 182, p. 113371, Aug. 2023, doi: 10.1016/j.rser.2023.113371.

[248] International Energy Agency, "Driving Energy Efficiency in Heavy Industries." [Online]. Available: https://www.iea.org/articles/driving-energy-efficiency-in-heavy-industries

[249] Our World in Data, "Emissions by sector." [Online]. Available: https://ourworldindata.org/emissions-by-sector

[250] W. Association, "World Steel in Figures Report," 2021.

[251] W. S. Association, "STEEL ' S CONTRIBUTION TO A LOW CARBON FUTURE AND CLIMATE RESILIENT SOCIETIES worldsteel position paper," *World Steel Association*, pp. 1–6, 2020.

[252] N. Pardo, J. A. Moya, K. Vatopoulos, N. Pardo, J. A. Moya, and K. Vatopoulos, *Prospective Scenarios on Energy Efficiency and CO 2 Emissions in the EU Iron & Steel Industry*. 2012. doi: 10.2790/64264.

[253] L. Holappa, "A general vision for reduction of energy consumption and CO2 emissions from the steel industry," *Metals (Basel)*, 2020, doi: 10.3390/met10091117.

[254] World Steel Association, "STEEL ' S CONTRIBUTION TO A LOW CARBON FUTURE AND CLIMATE RESILIENT SOCIETIES worldsteel position paper," *World Steel Association*, pp. 1–6, 2020.

[255] U. C. C. Conference, "the Glasgow," p. 28, 2021.

[256] D. A. Chisalita, L. Petrescu, P. Cobden, H. A. J. (Eric) van Dijk, A. M. Cormos, and C. C. Cormos, "Assessing the environmental impact of an integrated steel mill with post-combustion CO2 capture and storage using the LCA methodology," *J Clean Prod*, vol. 211, pp. 1015–1025, 2019, doi: 10.1016/j.jclepro.2018.11.256.

[257] E. Gul *et al.*, "Substitution of coke with pelletized biocarbon in the European and Chinese steel industries: An LCA analysis," *Appl Energy*, vol. 304, no. June, 2021, doi: 10.1016/j.apenergy.2021.117644.

[258] C. M. Nwachukwu, C. Wang, and E. Wetterlund, "Exploring the role of forest biomass in abating fossil CO2 emissions in the iron and steel industry – The case of Sweden," *Appl Energy*, vol. 288, no. January, p. 116558, 2021, doi: 10.1016/j.apenergy.2021.116558.

[259] N. Pardo, J. A. Moya, K. Vatopoulos, N. Pardo, J. A. Moya, and K. Vatopoulos, *Prospective Scenarios on Energy Efficiency and CO 2 Emissions in the EU Iron & Steel Industry*. 2012. doi: 10.2790/64264.

[260] K. Rechberger, A. Spanlang, A. Sasiain Conde, H. Wolfmeir, and C. Harris, "Green Hydrogen-Based Direct Reduction for Low-Carbon Steelmaking," *Steel Res Int*, vol. 91, no. 11, 2020, doi: 10.1002/srin.202000110.

[261] N. Pardo, J. A. Moya, K. Vatopoulos, N. Pardo, J. A. Moya, and K. Vatopoulos, *Prospective Scenarios on Energy Efficiency and CO 2 Emissions in the EU Iron & Steel Industry*. 2012. doi: 10.2790/64264.

[262] G. Tosini, "Analisi Strategica del Mercato Italiano Degli Acciai Speciali. Dimensioni e Prospettive.," 2020. Accessed: May 30, 2023. [Online]. Available: https://www.siderweb.com/filter/original/GTosini_webinar_12.10.2020_def.pdf

[263] J. Morfeldt, W. Nijs, and S. Silveira, "The impact of climate targets on future steel production - An analysis based on a global energy system model," *J Clean Prod*, vol. 103, pp. 469–482, 2015, doi: 10.1016/j.jclepro.2014.04.045.

[264] T. Eprs and E. Parliamentary, *Carbon-free steel production*, no. April. 2021.

[265] B. Anameric and S. K. Kawatra, "Mineral Processing and Extractive Metallurgy Review : An International Journal PROPERTIES AND FEATURES OF," no. May 2014, pp. 37–41, doi: 10.1080/08827500600835576.

[266] B. Anameric and S. K. Kawatra, "Mineral Processing and Extractive Metallurgy Review : An International Journal PROPERTIES AND FEATURES OF," no. May 2014, pp. 37–41, doi: 10.1080/08827500600835576.

[267] R. Remus, M. A. Aguado-monsonet, S. Roudier, and L. D. Sancho, *JRC REFERENCE REPORT Best Available Techniques (BAT) Reference Document for Iron and Steel Production (Integrated Pollution Prevention and Control)*. 2013. doi: 10.2791/97469.

[268] T. Eprs and E. Parliamentary, *Carbon-free steel production*, no. April. 2021.

[269] K. Rechberger, A. Spanlang, A. S. Conde, H. Wolfmeir, and C. Harris, "Green Hydrogen-Based Direct Reduction for Low-Carbon Steelmaking," *Steel Res Int*, vol. 91, no. 11, 2020, doi: 10.1002/srin.202000110.

[270] T. I. R. E. Agency, *GREEN HYDROGEN COST REDUCTION SCALING UP ELECTROLYSERS TO MEET THE 1.5°C CLIMATE GOAL H 2 O 2*. 2020. [Online]. Available: www.irena.org/publications

[271] I. E. Agency, "The future of hydrogen." [Online]. Available: https://www.iea.org/reports/the-future-of-hydrogen

[272] K. Rechberger, A. Spanlang, A. Sasiain Conde, H. Wolfmeir, and C. Harris, "Green Hydrogen-Based Direct Reduction for Low-Carbon Steelmaking," *Steel Res Int*, vol. 91, no. 11, 2020, doi: 10.1002/srin.202000110.

[273] V. Vogl, M. Åhman, and L. J. Nilsson, "Assessment of hydrogen direct reduction for fossil-free steelmaking," *J Clean Prod*, 2018, doi: 10.1016/j.jclepro.2018.08.279.

[274] A. Bhaskar, M. Assadi, and H. N. Somehsaraei, "Decarbonization of the iron and steel industry with direct reduction of iron ore with green hydrogen," *Energies (Basel)*, vol. 13, no. 3, pp. 1–23, 2020, doi: 10.3390/en13030758.

[275] U. Nations, "ENERGY TRANSITION:TOWARDS THE ACHIEVEMENT OF SDG 7 AND NET-ZERO EMISSIONS." 2021. [Online]. Available: https://www.un.org/sites/un2.un.org/files/2021-twg_2-062321.pdf

[276] A. Arasto, *Techno-economic evaluation of significant CO2 emission reductions in the iron and steel industry with CCS*, vol. 111. 2015.

[277] H. Ghanbari, F. Pettersson, and H. Saxén, "Sustainable development of primary steelmaking under novel blast furnace operation and injection of different reducing agents," *Chem Eng Sci*, vol. 129, 2015, doi: 10.1016/j.ces.2015.01.069.

[278] Q. Chen, Y. Gu, Z. Tang, W. Wei, and Y. Sun, "Assessment of low-carbon iron and steel production with CO2 recycling and utilization technologies: A case study in China," *Appl Energy*, vol. 220, 2018, doi: 10.1016/j.apenergy.2018.03.043.

[279] A. Krüger, J. Andersson, S. Grönkvist, and A. Cornell, "Integration of water electrolysis for fossil-free steel production," *Int J Hydrogen Energy*, vol. 45, no. 55, 2020, doi: 10.1016/j.ijhydene.2020.08.116.

[280] D. R. R. Gonçalves, W. C. Fontes, J. C. Mendes, G. J. B. Silva, and R. A. F. Peixoto, "Evaluation of the economic feasibility of a processing plant for steelmaking slag," *Waste Management and Research*, vol. 34, no. 2, 2016, doi: 10.1177/0734242X15615955.

[281] M. Fischedick, J. Marzinkowski, P. Winzer, and M. Weigel, "Techno-economic evaluation of innovative steel production technologies," *J Clean Prod*, vol. 84, no. 1, 2014, doi: 10.1016/j.jclepro.2014.05.063.

[282] M. Weigel, M. Fischedick, J. Marzinkowski, and P. Winzer, "Multicriteria analysis of primary steelmaking technologies," *J Clean Prod*, vol. 112, 2016, doi: 10.1016/j.jclepro.2015.07.132.

[283] H. Liu, Q. Li, R. Ding, and G. Li, "Environmental and economic impact assessment of converter steelmaking based on life cycle assessment," *International Journal of Innovative Computing, Information and Control*, vol. 17, no. 2, 2021, doi: 10.24507/ijicic.17.02.499.

[284] A. Vicente, A. Picon, and E. Barco, "New method for estimating the economic penalties of ferrous scraps in the steelmaking industry due to material degradation during its storage in scrap yards," *Ironmaking and Steelmaking*, vol. 47, no. 5. 2020. doi: 10.1080/03019233.2020.1748433.

[285] R. Béchara, H. Hamadeh, O. Mirgaux, and F. Patisson, "Optimization of the iron ore direct reduction process through multiscale process modeling," *Materials*, 2018, doi: 10.3390/ma11071094.

[286] R. Béchara, H. Hamadeh, O. Mirgaux, and F. Patisson, "Carbon impact mitigation of the iron ore direct reduction process through computer-aided optimization and design changes," *Metals (Basel)*, 2020, doi: 10.3390/met10030367.

[287] S. Sarkar, R. Bhattacharya, G. G. Roy, and P. K. Sen, "Modeling MIDREX Based Process Configurations for Energy and Emission Analysis," *Steel Res Int*, 2018, doi: 10.1002/srin.201700248.

[288] K. Alhumaizi, A. Ajbar, and M. Soliman, "Modelling the complex interactions between reformer and reduction furnace in a midrex-based iron plant," *Canadian Journal of Chemical Engineering*, 2012, doi: 10.1002/cjce.20596.

[289] A. Ajbar, K. Alhumaizi, M. A. Soliman, and E. Ali, "Model-based energy analysis of an integrated midrex-based iron/steel plant," *Chem Eng Commun*, vol. 201, no. 11, pp. 1686–1704, 2014, doi: 10.1080/00986445.2013.825835.

[290] A. Shams and F. Moazeni, "Modeling and Simulation of the MIDREX Shaft Furnace: Reduction, Transition and Cooling Zones," *JOM*, 2015, doi: 10.1007/s11837-015-1588-0.

[291] H. Hamadeh, O. Mirgaux, and F. Patisson, "Detailed modeling of the direct reduction of iron ore in a shaft furnace," *Materials*, 2018, doi: 10.3390/ma11101865.

[292] A. Bhaskar, M. Assadi, and H. N. Somehsaraei, "Decarbonization of the iron and steel industry with direct reduction of iron ore with green hydrogen," *Energies (Basel)*, vol. 13, no. 3, pp. 1–23, 2020, doi: 10.3390/en13030758.

[293] R. Béchara, H. Hamadeh, O. Mirgaux, and F. Patisson, "Optimization of the iron ore direct reduction process through multiscale process modeling," *Materials*, 2018, doi: 10.3390/ma11071094.

[294] D. A. Chisalita, L. Petrescu, P. Cobden, H. A. J. (Eric) van Dijk, A. M. Cormos, and C. C. Cormos, "Assessing the environmental impact of an integrated steel mill

with post-combustion CO2 capture and storage using the LCA methodology," *J Clean Prod*, vol. 211, pp. 1015–1025, 2019, doi: 10.1016/j.jclepro.2018.11.256.

[295] E. Gul *et al.*, "Substitution of coke with pelletized biocarbon in the European and Chinese steel industries: An LCA analysis," *Appl Energy*, vol. 304, no. June, 2021, doi: 10.1016/j.apenergy.2021.117644.

[296] C. M. Nwachukwu, C. Wang, and E. Wetterlund, "Exploring the role of forest biomass in abating fossil CO2 emissions in the iron and steel industry – The case of Sweden," *Appl Energy*, vol. 288, no. January, p. 116558, 2021, doi: 10.1016/j.apenergy.2021.116558.

[297] G. Simbolotti and G. Tosato, "Iron and Steel - Technology Brief I02," no. May, p. 6, 2010.

[298] Eurostat, "Electricity prices for non-household consumers - bi-annual data."

[299] Eurostat, "Gas prices for non-household consumers - bi-annual data."

[300] L. Mas *et al.*, *Fattori di emissione atmosferica di gas serra nel settore elettrico nazionale e nei principali Paesi Europei*, vol. 53, no. 9. 2015.

[301] World Bank, "Carbon Pricing Dashboard."

[302] "Global Wind Atlas." [Online]. Available: https://globalwindatlas.info

[303] "Global Solar Atlas."

[304] R. Testa, A. M. Di Trapani, M. Foderà, F. Sgroi, and S. Tudisca, "Economic evaluation of introduction of poplar as biomass crop in Italy," *Renewable and Sustainable Energy Reviews*, vol. 38, no. 2014, pp. 775–780, 2014, doi: 10.1016/j.rser.2014.07.054.

[305] K. Li, H. Bian, C. Liu, D. Zhang, and Y. Yang, "Comparison of geothermal with solar and wind power generation systems," *Renewable and Sustainable Energy Reviews*. 2015. doi: 10.1016/j.rser.2014.10.049.

[306] K. Li, H. Bian, C. Liu, D. Zhang, and Y. Yang, "Comparison of geothermal with solar and wind power generation systems," *Renewable and Sustainable Energy Reviews*. 2015. doi: 10.1016/j.rser.2014.10.049.

[307] A. Susmozas, D. Iribarren, P. Zapp, J. Linβen, and J. Dufour, "Life-cycle performance of hydrogen production via indirect biomass gasification with CO2 capture," *Int J Hydrogen Energy*, vol. 41, no. 42, pp. 19484–19491, 2016, doi: 10.1016/j.ijhydene.2016.02.053.

[308] V. Vogl, M. Åhman, and L. J. Nilsson, "Assessment of hydrogen direct reduction for fossil-free steelmaking," *J Clean Prod*, vol. 203, pp. 736–745, 2018, doi: 10.1016/j.jclepro.2018.08.279.

[309] P. Balcombe, K. Anderson, J. Speirs, N. Brandon, and A. Hawkes, "The Natural Gas Supply Chain: The Importance of Methane and Carbon Dioxide Emissions," *ACS Sustainable Chemistry and Engineering*. 2017. doi: 10.1021/acssuschemeng.6b00144.

[310] Carbon Footprint, "Carbon Footprint, Country specific Electricity Factors," no. June, pp. 1–10, 2019.

[311] World Resources Institute World Business Council for Sustainable Development, "The Greenhouse Gas Protocol."

[312] IRENA, *Green Hydrogen Cost Reduction*. 2020.

[313] V. Vogl, M. Åhman, and L. J. Nilsson, "Assessment of hydrogen direct reduction for fossil-free steelmaking," *J Clean Prod*, 2018, doi: 10.1016/j.jclepro.2018.08.279.

[314] A. Bhaskar, M. Assadi, and H. N. Somehsaraei, "Decarbonization of the iron and steel industry with direct reduction of iron ore with green hydrogen," *Energies (Basel)*, vol. 13, no. 3, pp. 1–23, 2020, doi: 10.3390/en13030758.

[315] A. Borgogna, G. Centi, G. Iaquaniello, S. Perathoner, G. Papanikolaou, and A. Salladini, "Assessment of hydrogen production from municipal solid wastes as competitive route to produce low-carbon H2," *Science of The Total Environment*, vol. 827, May 2022, doi: 10.1016/j.scitotenv.2022.154393.

[316] E. A. Mohareb, H. L. MacLean, and C. A. Kennedy, "Greenhouse Gas Emissions from Waste Management—Assessment of Quantification Methods," *J Air Waste Manage Assoc*, vol. 61, no. 5, pp. 480–493, May 2011, doi: 10.3155/1047-3289.61.5.480.